Electrospun Poly(Caprolactone) and Strontium-Substituted Bioactive Glass for Bone Tissue Engineering

Martin Eduardo Santocildes Romero

MEng (Hons)

Submitted for the degree of Doctor of Philosophy

School of Clinical Dentistry

The University of Sheffield

April 2014

Contents

Acknowledgments

First of all, I would like to thank my supervisors, Dr Cheryl Miller, Prof Paul Hatton and Prof Ian Reaney, for their continuous support and guidance throughout the PhD. This has been an exciting learning experience that would not have been possible without them.

I also would like to thank Dr Rebecca Goodchild for her willingness to help every time I came to her with all kinds of questions and doubts. At the School of Clinical dentistry I would also like to thank Dr Felora Merkavoly for her help and companionship, Dr Aileen Crawford for her guidance in the experiments involving mesenchymal stem cells, Ms Kirsty Franklin for all her teaching and patience in the cell culture laboratory, Dr Robert Moorehead for his technical support and good humour, and Mrs Brenka McCabe for her instruction in molecular biology. At the Department of Materials Science and Engineering I would like to thank Mr Ian Watts for his assistance during glass melting; Mr Andrew Mould for his training and guidance in glass milling; Dr Nick Reeves-McLaren for his instruction on XRD; and Ms Beverly Lane for her help with the particle size analyses. Finally, I would like to thank the staff at the Sorby Nano Investigation Centre, whose training and assistance were essential for this project to be completed.

All my friends, who made this an even more unforgettable experience, need to be remembered as well. Your support has been very important for me. As there are too many of you to mention by name, I will shout out a massive thank you to all from these pages.

I am very grateful to the EPSRC and the School of Clinical Dentistry of the University of Sheffield for providing the funding that made this project a reality.

Finally, I must mention my parents, Eduardo Ismael and Maria Cristina, who were exceptionally supportive during my education and always tried to help in any way possible, even with the limitations that the distance between us created. I will always be grateful for all you have done for me.

Abstract

Electrospinning is a technique which has been widely studied to fabricate fibrous polymeric membranes. More recent work has demonstrated the preparation of composite fibres by incorporation of ceramic or glass particles in the spinning process. However, the incorporation of strontium-substituted bioactive glasses (Sr-BGs) into electrospun membranes has not yet been studied with detail. This is perhaps surprising, as Sr-BGs have been reported to exhibit superior osteogenic activity compared to conventional bioactive glasses. Therefore, the aim of this project was to fabricate electrospun composite materials combining poly(caprolactone) (PCL) and Sr-BG particles, and to study their potential use as scaffolds for bone tissue engineering. Here, three Sr-BGs in which calcium was substituted by strontium in molar proportions of 0, 50 and 100% were prepared and characterised. Glass particles with sizes <45 μm were prepared by milling and sieving, and added to PCL solutions before electrospinning. The resulting composite materials were then examined using scanning electron microscopy, energy dispersive X-ray spectroscopy (EDS), and by performing solubility and cytotoxicity studies. Two methods to add Sr-BG particles to the surface of the fibres were also investigated. The effect of Sr-BG dissolution on mesenchymal stromal cells (MSCs) was studied by assessing cytotoxicity and the expression of six genes associated with osteoblastic differentiation. Strontium substitution resulted in a reduction of glass transition temperature, increased density and increased solubility of the glasses. EDS confirmed the presence of Sr-BG particles within the electrospun fibres. Solubility studies suggested an accelerated degradation of PCL due to Sr-BG dissolution in the composite fibres, with an apparent effect on medium pH. All the materials generally presented good levels of *in vitro* biocompatibility, although the addition of particles to the surface of the fibres increased their apparent cytotoxicity in some cases. Sr-BG dissolution was associated with an up-regulation of genes involved in the process of osteoblastic differentiation. It was concluded that Sr-BGs may indeed enhance osteogenic differentiation in MSC populations, and electrospun PCL/Sr-BG showed great potential for use as a versatile medical device or scaffold for bone tissue regeneration.

Table of abbreviations

αMEM	Minimum essential medium Eagle's medium – α modification
β-GP	β-Glycerophosphate
AA	Ascorbic acid
Alpl	Alkaline phosphatase gene (liver/bone/kidney)
Bglap	Bone γ-carboxyglutamate (gla) protein gene
Bmp2	Bone morphogenetic protein 2 gene
BO	Bridging oxygen
Col1a1	Collagen type I gene, Alpha I
DCM	Dichloromethane
DEX	Dexamethasone
DMEM	Dulbecco's modified Eagle's medium
DMF	Dimethylformamide
DMSO	Dimethylsulfoxide
DTA	Differential thermal analysis
EDS	Energy dispersive X-ray spectroscopy
FCS	Foetal calf serum
Gapdh	Glyceraldehyde-3-phosphate dehydrogenase gene
HA	Hydroxyapatite
HCA	Hydroxy-carbonate apatite
I_b	Index of bioactivity
Mol%	Molar percentage
MSC	Mesenchymal stromal cell
NBO	Non-bridging oxygen
NC	Network connectivity
PBS	Phosphate buffered saline
PCL	Poly(caprolactone)
qFCS	MSC qualified foetal calf serum
ROS	Rat osteosarcoma
rpm	Revolutions per minute
RT-qPCR	Reverse transcription quantitative polymerase chain reaction
Runx2	Runt-related transcription factor 2 gene
sd	Standard deviation
SEM	Scanning electron microscopy
Spp1	Secreted phosphoprotein 1 gene

T_c	Onset of crystallisation temperature
TCP	Tricalcium phosphate
T_g	Glass transition temperature
T_p	Peak crystallisation temperature
Wt%	Weight percentage
XRD	X-ray diffraction

1 Introduction

The regenerative capacity of bone tissue means that many injuries are able to heal without the need of surgical intervention. However, large defects may lack the conditions required for the regeneration process to occur and, if left untreated, may cause pain, loss of function, disability and disfigurement, affecting the quality of life of patients worldwide (Bueno and Glowacki, 2011). Therefore, these injuries will necessitate medical treatment to support the healing process, especially in older patients.

The 'gold standard' treatment for those defects is the transplantation of autogenous bone grafts obtained from other sites in the skeleton. This method generally presents good clinical outcomes due to the good integration of the graft into the defect site and virtually non-existent risks of rejection and disease transmission compared to grafts obtained from other sources. However, severe limitations in the amount of bone which can be harvested from the patient and increased risks of morbidity and pain in the donor sites led to the pursuit of suitable alternatives (Moore, 2001; Myeroff and Archdeacon, 2011).

Historically, a wide range of biomaterials have been investigated as potential substitutes for bone grafts, with varying degrees of success (Hench and Polak, 2002). Bioinert materials, such as steel alloys, were initially selected due to showing good mechanical properties and biocompatibility, and because they elicited minimal reactions from the body. However, this biological inertness meant that the materials were unrecognised by the body and did not bond with the surrounding tissues, leading to encapsulation, isolation and final deterioration of the implant.

Degradable and bioactive materials later received considerable attention due to their improved biological properties. Degradable materials, such as bioresorbable polymers (Pulapura and Kohn, 1992; Middleton and Tipton, 2001), exhibit controlled degradation and resorption in the body, eliminating the need of a second surgical intervention to remove the implant. Bioactive materials, such as bioactive glasses (Hench, 1998; Jones, 2013), are able to

stimulate specific cellular responses that may encourage the production of new bone tissue and will result in generally stronger biomaterial-tissue interfaces. Additionally, the composition of both degradable and bioactive materials may be tailored to modify their properties. For example, co-polymerisation may be used to modify the degradation rates of bioresorbable polymers. It is also possible to substitute certain chemical elements in the composition of bioactive glasses in order to alter their physical properties and bioactivity. Strontium is a particular element which has received attention in the last few years as it has been reported to encourage the formation of new bone tissue, both as a component of the drug strontium ranelate (Marie *et al.*, 2001; Marie, 2005; Bonnelye *et al.*, 2008) and as part of bioactive glasses (Lao *et al.*, 2009; Gentleman *et al.*, 2010; Gorustovich *et al.*, 2010; O'Donnell *et al.*, 2010; Isaac *et al.*, 2011). Finally, novel alternative approaches to bone grafts have been developed which combine the concepts of degradable and bioactive materials in order to elicit specific responses at the molecular level.

Bone tissue engineering is a discipline that aims to create healing responses in precise anatomic regions of the skeleton to encourage the formation of new bone tissue that is structurally integrated with the surrounding tissues and which is durable and effective (Langer and Vacanti, 1993; Kakar and Einhorn, 2005). For this purpose porous scaffolds with the appropriate characteristics to support the development of the new tissues need to be designed and fabricated. Various biomaterials have been investigated for the production of these scaffolds, including demineralised bone matrix, natural and synthetic polymers, ceramics and bioactive glasses. However, as no single material is able to fulfil all the requirements for bone tissue engineering applications, the use of composite biomaterials that attempt to mimic the composite nature of bone tissue have been explored because they offer the possibility of combining the material and biological properties of the different components into a single structure (Barone *et al.,* 2010).

Several manufacturing methods have been historically employed to process biomaterials into porous structures to be used as scaffolds (Chan and Leong; 2008; Moroni *et al.*, 2008). Among them, electrospinning has been widely

investigated due to its versatility and ease of use. Electrospun fibres with diameters of a few micrometres down to tens of nanometres may be produced from a polymer solution through the application of electrostatic forces, resulting in the fabrication of non-woven porous membranes after the fibres are deposited on a collecting plate (Doshi and Reneker, 1995; Huang *et al*., 2003; Martins *et al*., 2008). Composite materials may also be fabricated using this technique by adding particles of a different biomaterial, such as ceramics or glasses, to the initial polymer solution. This particulate will then be incorporated within the electrospun fibres, creating a structure that may present enhanced properties compared to the non-composite fibres (Holzwarth and Ma, 2011).

To summarise, the incorporation of bioactive glass particles into electrospun membranes is technically feasible and it is possible that a strontium-substituted bioactive glass may stimulate the formation of new bone tissue, if incorporated into this structure. Surprisingly, relatively little work studying this topic has been reported. Therefore, the aim of this research was to investigate the development of novel electrospun composite materials combining poly(caprolactone), a bioresorbable polymer, and particles of strontium-substituted bioactive glass, and to investigate their potential use as a scaffold for bone tissue engineering. Additionally, the materials may be used as fillers of bone voids in non-load bearing sites of the skeleton or as bioresorbable components in barrier membranes for guided bone regeneration applications, where it may encourage bone growth in structures affected by periodontal disease.

The relevant scientific literature and principles supporting this project will be reviewed in the following section of this report, before presenting the research work performed and the conclusions drawn from it.

2 Literature review

2.1 Biomaterials and bone tissue

The use of materials to replace missing or damaged parts of the body can be traced to centuries ago. For example, the Mayans used artificial teeth made of nacre obtained from sea shells and ancient Greek literature mentions the use of metallic sutures (Ratner, 2013). However, it was only after the development of aseptic surgical techniques and of an adequate understanding of the immune system that their use became more frequent and efficient. Previous to that, surgical procedures involving implanted materials were generally unsuccessful due to infection and to the presence of a region created by the implant which was inaccessible to the immune system.

2.1.1 Classification of biomaterials

A biomaterial can be defined as a 'nonviable material used in a medical device, intended to interact with biological systems' (Ratner *et al*., 2013). Hench and Polak (2002) outlined three generations in the historical development of modern biomaterials.

Initially, the principle applied to select a biomaterial was its biological inertness in order to minimise the response of the immune system to the presence of the implanted material. Although this approach proved to be very successful, enhancing the quality of life of many patients worldwide, the biological inertness of the implant meant that it would be unrecognised by the body and would not bond with the surrounding tissues, leading to their isolation from the host by encapsulation in fibrous connective tissue and chronic inflammation. This process may also lead to material deterioration, loosening of the implant and final clinical failure (Barone *et al*., 2010). In response to this, second generation biomaterials were developed. The focus shifted towards creating implants that could elicit controlled reactions in the physiological environment using bioactive components and that, therefore, would improve the interface between the implant and the surrounding tissues. Additionally, degradable materials exhibiting controlled chemical

degradation and resorption in the body and which would be eventually replaced by the regenerating tissues were investigated. Examples of second generation biomaterials are bioactive glasses, ceramics, glass-ceramics, bioresorbable polymers and composites, which were soon successfully used in a wide variety of clinical applications. Finally, third generation biomaterials emerged as a result of the convergence of bioactive and degradable biomaterials, in such a way that 'bioactive materials are being made resorbable and resorbable polymers are being made bioactive', as Hench and Polak (2002) described it.

Two alternative routes to repair damaged tissues arose from this convergence: tissue engineering and *in situ* tissue regeneration. The main advantage offered by these two is the potential to elicit specific cellular responses at the molecular level that will stimulate cell differentiation or the activation of certain genes (Hench and Polak, 2002; Hench and Thompson, 2010). For example, it has been reported that bioactive glasses are able to upregulate seven families of genes in primary human osteoblasts after their exposition to the glass ionic dissolution products (Xynos *et al*., 2001; Hench, 2009). There is growing scientific evidence supporting the use of these advanced biomaterials and approaches in the regeneration of damaged tissues, exhibiting promising results and many potential benefits, especially for an ageing population.

The success of an implanted biomaterial will depend on its biocompatibility and its ability to achieve a stable attachment to the surrounding tissues. Biocompatibility can be defined as 'the ability of a material to perform with an appropriate host response in a specific application' (Ratner *et al*., 2013). Depending on the type of host response elicited, four categories of biomaterials have been described (Hench *et al.*, 2013; Woesz and Best, 2008):

1) Bioinert materials are those that elicit minimal interaction and minimal chemical reactions at the biomaterial-tissue interface. This results in the production of a fibrous capsule covering the implant in order to prevent further interactions with the host.

2) Bioresorbable materials are those that are either dissolved or resorbed by the body, in such a way that the implant can be eventually replaced by the surrounding tissues.
3) Bioactive materials are those that can trigger a chemical reaction with the environment, undergoing time-dependent changes as a consequence. These changes result in the formation of a layer of hydroxy-carbonate apatite on the surface of the implant, providing binding sites for cells and tissues.
4) Toxic materials are those that cause cellular death due to their composition, locally or remotely.

The mechanism of attachment is directly related to the type of host response at the implant-tissue interface (Hench and Best, 2013). In the case of bioinert materials, which do not bond chemically or biologically to tissues, the thickness of the fibrous capsule will vary depending on the nature of the material and on the motion and fit at the implant-tissue interface. The presence of movement will usually lead to an eventual deterioration of the implant, possibly requiring additional surgery to remove it. On the other hand, bioresorbable and bioactive materials are more suitable alternatives for the fabrication of implants because bioresorbable materials can be replaced by the surrounding tissues as they degrade, resulting in thin or nonexistant interfacial regions, and bioactive materials are able to elicit specific biological responses at the implant-tissue interface that may result in the formation of stronger bonds with the surrounding tissues.

2.1.2 Bone tissue structure and biology

A bone is a complex organ which fulfils important functions in the body, including the protection of internal organs from damage, the provision of structural support for soft tissues and of attachment points for muscles and ligaments, and the storage of minerals and energy in the form of fat. Depending on their shape, bones can be classified into five categories: long, short, flat, irregular and sesamoid bones (Table 2.1).

Table 2.1. Types of bone by shape, functions and examples.

Type of bone	Function	Example
Long	Movement of body	Femur
Short	Shock absorption	Carpals
Flat	Protection of internal organs	Cranium
Irregular	Support and protection	Vertebrae
Sesamoid	Protection of tendons	Patella

The anatomy of a bone can be analysed by considering the parts that form a long bone such as the humerus (Figure 2.1). The external parts are the diaphysis, forming the main body of the bone; the epiphyses, which are the distal and proximal ends of the bone; the metaphyses, which are the regions in a mature bone where the diaphysis joins the epiphyses; the articular cartilage, formed by a thin layer of hyaline cartilage where the bone forms an articulation; and the periosteum, which is a cover of connective tissue surrounding the whole bone, except on the cartilaginous surfaces. The internal parts are the medullary cavity, which is the space within the diaphysis containing the bone marrow; and the endosteum, formed by a thin membrane of connective tissue lining the medullary cavity.

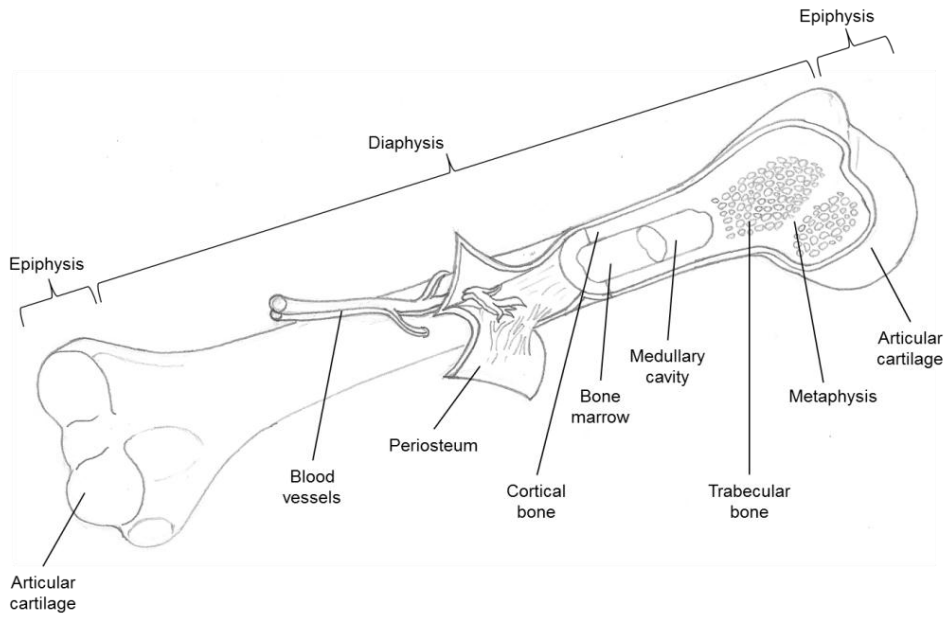

Figure 2.1. Schematic diagram of a humerus, identifying the main parts that form it.

The main tissue in bone is osseous (bone) tissue, which can be described as a composite material made of a matrix possessing an organic and an inorganic component (Boskey, 2005). The organic component of the matrix

represents approximately 30% of the total bone tissue and is mainly composed by proteins, of which type I collagen is the most abundant. The collagen fibres assemble in an organised manner parallel to the long axis of bone, creating bone calcification sites in a region known as the 'hole zone' (Figure 2.2). Other organic molecules are present in the organic phase, participating in signalling processes related to tissue remodelling, mineralization and turnover. These include structural and biologically active proteins, proteoglycans, glycoproteins, peptides, lipids and adsorbed serum proteins (Bueno and Glowacki, 2011). The inorganic component of the matrix provides strength and rigidity to bone tissue and is mainly composed of an analog of the mineral hydroxyapatite (HA) with chemical composition $Ca_{10}(PO_4)_6(OH)_2$ and a Ca:P molar ratio ranging from 1.3:1 to 1.9:1. The size of the HA crystals are in the range of 2 to 7 nm in thickness, 15 to 200 nm in length and 10 to 80 nm in width (Katsanevakis *et al*., 2012), and are deposited parallel to the collagen fibres and in direct contact with them. This occurs through a cell-mediated process of nucleation: ions or ion clusters in solution collide to generate a stable nucleus from which the crystal grows as more ions or ion clusters are added over time (Boskey, 2005; Bueno and Glowacki, 2011).

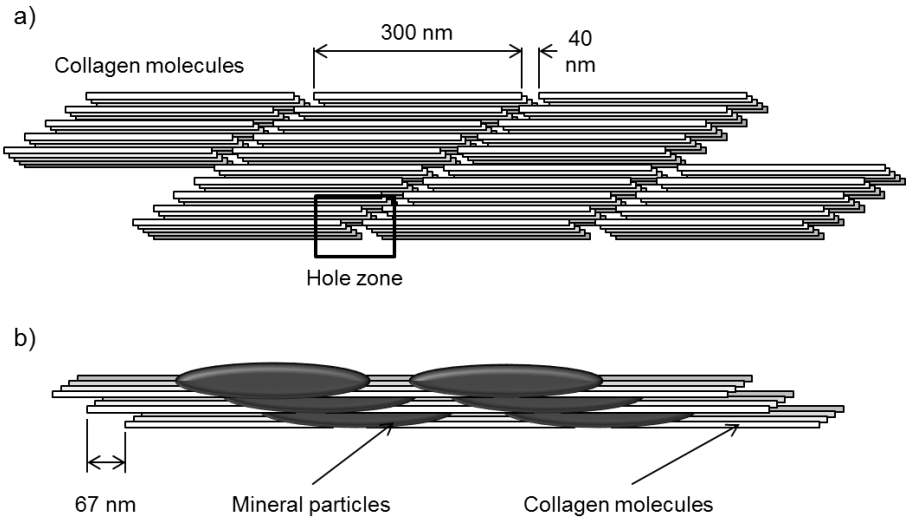

Figure 2.2. Schematic diagram of a) the microstructure of bone, showing the arrangement of collagen molecules creating 'hole zones' where hydroxyapatite crystals are nucleated; and of b) the lowest level of the hierarchical structure of bone, showing the parallel alignment and elongation of the mineral particles formed with hydroxyapatite crystals. Adapted from Katsanevakis *et al*. (2012).

The way in which the mineral is deposited maximises the resistance to external mechanical forces applied to the bone. The HA crystals provide high strength and fracture toughness while the collagen fibres maintain its load-bearing and viscoelasticity, allowing bone tissue to absorb shock (Safadi *et al*., 2009; Katsanevakis *et al*., 2012). When the collagen fibres are abnormally produced, as it occurs in osteogenesis imperfecta, the HA crystals are smaller in size and may be deposited apart from the collagen fibres, resulting in a weaker bone matrix and a reduced ability to withstand mechanical forces (Boskey, 2005).

Macroscopically, bone tissue can be organised in two different architectures: cortical (lamellar) bone and trabecular (woven) bone. Cortical bone represents approximately 80% of the total mass of the skeleton. It is a dense structure made up by circumferential lamellae, woven tissue or plexiform tissue. The circumferential lamellae are arranged parallel to the bone surface. Located within these are osteons (Haversian systems) with an average diameter of 200 μm and enclosing a central cavity (Haversian canal) which contains blood and lymphatic vessels. The external boundary of each osteon is the cement line, which separates it from the surrounding interstitial tissues. Woven tissue and plexiform tissue are usually found in the bones of large or fast growing animals, and may also be formed at fracture healing sites. Also within cortical bone are cavities known as lacunae, where the osteocytes are located. Trabecular bone, making up the remaining 20% of the total mass of the skeleton, is found in the metaphysis, epiphyses and medullary cavity of long bones. It consists of an interconnected lattice of trabeculae with approximate thickness of 200 μm (Wang *et al*., 2010).

The main cell types present in bone tissue are osteoblasts, osteocytes and osteoclasts (Table 2.2; Figure 2.3). Bones in the axial and appendicular skeleton are formed by one of two processes: intramembranous bone formation or endochondral bone formation. In intramembranous bone formation the osteoprogenitor cells in the mesenchyme aggregate in the areas where a new bone is to be formed and differentiate into osteoblasts, which will then synthesise new bone matrix. Growth occurs by the deposition of new bone tissue by osteoblasts on previously existing bone. On the other

hand, endochondral bone formation involves the initial formation of cartilage tissue through the differentiation of mesenchymal cells into chondrocytes and its subsequent replacement by bone tissue through a process of chondrocyte hypertrophy, invasion of the cartilage by blood vessels, chondrocyte apoptosis, and final differentiation of osteoprogenitor cells into osteoblasts, which will deposit new bone matrix on the cartilage remains (Safadi *et al*., 2009).

Table 2.2. Main cell types present in bone tissue, including their origin, location and function. Adapted from Boskey (2005), Safadi *et al*. (2009) and Wang *et al*. (2010).

Cell type	Origin	Location	Function
Osteoblasts	Mesenchymal stromal cells	Line bone surfaces at sites of active bone formation.	Production of type I collagen; Mineralisation of matrix by deposition of calcium and phosphate.
Osteocytes	Osteoblasts trapped within bone matrix	In cavities within the bone matrix known as lacunae.	Extend long cellular processes through canaliculi, joined by gap junctions to enable cellular communication, possibly to maintain bone metabolism.
Osteoclasts	Multinucleated cells created by the fusion of several monocytes	In pits or cavities of active bone resorption known as Howship's lacunae.	Bone resorption during bone remodelling.

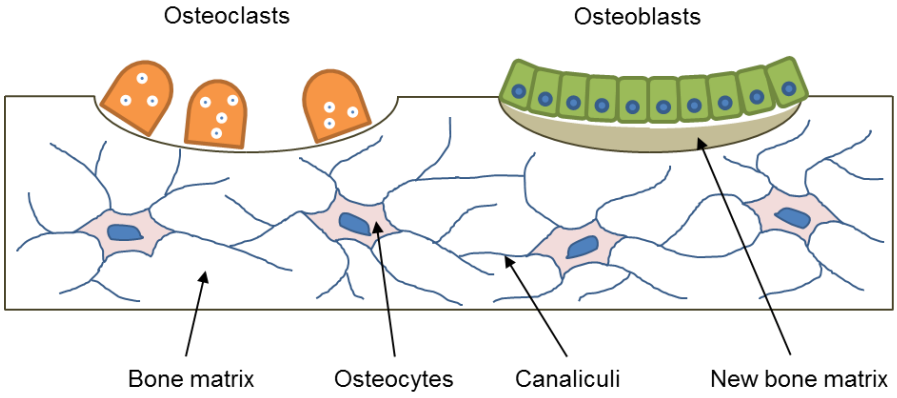

Figure 2.3. Schematic diagram of bone tissue structure at a cellular level, showing the main cell types present in bone tissue. Adapted from Jang *et al*. (2009).

An important characteristic of bone tissue is that it has the ability to remodel itself (e.g. in response to external mechanical forces) and to repair itself after injury. The remodelling of bone tissue is a process which occurs in temporary locations known as basic multicellular units (BMU). An active BMU consists

of a leading front of osteoclasts, which will resorb the bone tissue and form a defect. Reversal cells will follow the osteoclasts, covering the defect and preparing it for the deposition of new bone tissue. Osteoblasts will then occupy the area and deposit new unmineralised bone matrix, directing its formation into lamellar bone. Following mineralisation, osteoblasts will become embedded into the new matrix and differentiate into osteocytes (Raggatt and Partridge, 2010).

The mechanical properties of bone tissue have generally been well documented, using various approaches to measure them at the micro and macroscopic levels (Rho *et al*., 1998; Currey, 2009; Wang *et al*., 2010). Cortical bone shows a high degree of anisotropy and the measured values of different mechanical properties may vary depending on the species, age, health, location in the bone and testing conditions. The case of trabecular bone is more complex due to the small dimensions of the individual trabeculae. Table 2.3 presents typical values for some mechanical properties of human cortical and trabecular bone.

Table 2.3. Values of the mechanical properties of human cortical and trabecular bone. Adapted from Katsanevakis *et al* (2012).

Bone	Mechanical property	Value
Cortical	Yield stress (Tension)	78-151 MPa
	Yield stress (Compression)	131-224 MPa
	Elasticity modulus	17-20 GPa
Trabecular	Yield stress	5-10 MPa
	Elasticity modulus	50-100 MPa

2.1.3 Response of bone tissue to injury

Bone tissue usually fails when the loads applied to a bone exceed the range of forces to which it has adapted. Fractures are then formed, resulting in the disruption of the continuity of the tissue and affecting cellular viability, vascular connections and the structural integrity of the bone. In the strict clinical sense, the term includes a whole range of potential defects affecting bone, from microscopic fractures to the rupture of a bone into many fragments (McRae and Esser, 2008; Bueno and Glowacki, 2011)

As any other material, cyclic loading may lead to the failure of bone tissue through a process known as fatigue. This involves the accumulation of microstructural cracks, also known as microdamage, resulting in an increase in bone fragility (Schaffler, 2003; Bueno and Glowacki, 2011). These defects were first described by Frost in human rib samples as small cracks with linear morphology and lengths between 30 and 100 μm, and he was also the first to propose that these cracks may be targeted by the remodelling process of bone tissue in order to maintain the mechanical integrity of the skeleton (Schaffler, 2003). Since then, this idea has been supported by significant experimental studies. For example, Mashiba *et al.* (2001) reported an increase in the number of microstructural cracks and decreased mechanical properties in the bones of dogs treated with drugs that suppressed the remodelling process. There is also evidence that the presence of the cracks can initiate targeted remodelling of bone tissue, as reviewed by Burr (2002). Verborgt *et al.* (2000) reported that microdamage is translated into osteocyte death through apoptosis, which may then play a significant role in the remodelling process due to the strong associations that exist between osteocyte apoptosis and subsequent bone remodelling. In summary, this continuous cycle of microdamage due to wear and tear and bone tissue remodelling has the benefit of providing bone the ability to regenerate and heal injuries. Most other tissues lack a similar regenerative capacity and usually heal by scar formation (Bueno and Glowacki, 2011).

The causes of larger fractures are varied. Trauma is the most frequent cause and it may occur both directly and indirectly. Fatigue fractures may develop due to excessive cyclic loading of a bone, generating damage at a faster rate than the healing process and leading to eventual failure. Pathological fractures occur in abnormal or diseased bone, where a particular condition weakens the tissue and the force required to produce the fracture is reduced (McRae and Esser, 2008). Fractures may also be classified depending on the mechanism of injury, the strength of the force causing them, the direction of the fracture lines and the degree of associated soft tissue damage (Bueno and Glowacki, 2011).

In order for proper healing to occur in bone there must be enough vascularity and viable cells available to facilitate each phase of the repair process. This may occur by one of two mechanisms: primary healing or secondary healing. Primary healing occurs in fractures which are partial or stable and that are aligned so that the surfaces are very closely positioned. Osteons close to the fracture will die due to the lack of blood supply and then osteoclasts will begin to cut cones at the ends of the Haversian canals, resorbing the bone and allowing for the expansion of the capillary network around the fracture site. Osteoblasts then will follow the osteoclasts, depositing new woven bone tissue and creating osteons that connect with the other surface (Bueno and Glowacki, 2011). Secondary healing is a more complex mechanism, involving four stages: inflammation, soft callus formation, hard callus formation and remodelling. These are summarised in Table 2.4.

Table 2.4. Description of the four stages in the secondary healing mechanism in bone tissue. Adapted from Bueno and Glowacki (2011).

Stage	Length	Actions
Inflammation	3 – 4 days	Formation of hematoma and fibrin clot; Arrival on immune, mesenchymal and osteoprogenitor cells; Bone at the edges become necrotic and degrades due to release of lysosomal enzymes by osteocytes; Macrophages phagocytose debris and osteoclasts resorb fragments of necrotic bone.
Soft callus formation	3 – 4 weeks	Rapid proliferation of osteoprogenitor cells in the periosteum; Differentiation into chondrocytes and osteoblasts; Formation of cartilaginous callus, immobilising fracture fragments.
Hard callus formation	3 – 4 months	Vascularisation of soft callus and replacement with woven bone, through endochondral bone formation and intramembranous bone formation; Osteoclasts continue resorbing dead bone.
Remodelling	Several years	Reorganisation of woven bone into lamellar bone and formation of medullary cavity

2.1.4 Bone graft substitutes

Although many fractures have the ability to regenerate without the need of surgical intervention, there may be situations when the results of the healing process may not be optimal due to systemic problems, such as poor health or advanced age; diseases, such as diabetes; and the use of medications, such as glucocorticoids. Poor results can also occur due to issues associated with the defect site, such as the fracture of bone tissue into many

fragments, infection, inadequate immobilisation and anatomical problems (Bueno and Glowacki, 2011).

Bone grafts are generally used to promote bone formation in defect sites derived from congenital or acquired conditions (Bueno and Glowacki, 2011). Currently, the transplantation of autogenous bone grafts obtained from non-load bearing sites in the skeleton is the treatment that presents the best clinical outcomes in the replacement of damaged bone tissue. The iliac crest is the most commonly used donor site, although alternatives such as the proximal part of the tibia, the distal end of the radius or the greater trochanter have also been investigated (Myeroff and Archdeacon, 2011). The transplanted bone tissue tends to integrate well into the defect site and the risks of immune rejection and disease transmission are practically eliminated, in contrast to what may occur with grafts obtained from other donors (allografts) or from animal sources (xenografts). Despite these benefits, autogenous bone grafts present important challenges such as the limited amount of bone which can be obtained and the variable quality of the grafts depending on the conditions of the patient. There are also associated issues such as increased risks of bleeding, hematoma, infection, chronic pain and morbidity in the donor sites (Moore, 2001; Myeroff and Archdeacon, 2011).

A wide range of materials have been investigated as alternatives for bone grafts: metals, ceramics and polymers of synthetic and natural origin (Table 2.5). Metals have usually been used in orthopaedic and dental applications due to their good mechanical properties. However, as they are bioinert materials, metals will form a bond with bone which is simply mechanical and cannot adapt to varying conditions, potentially leading to a loosening of the implant. An approach used to improve their performance is to coat the metallic surface with a bioactive material such as HA, which may promote the formation of a strong bond with bone. However, this presents certain limitations, such as potential chemical reactions occurring between the metal and the coating which may weaken the implant at the proximity of the interface and may reduce the strength of the coated system (Barone *et al.*, 2010).

Table 2.5. Materials investigated to be used as bone substitutes and their potential applications Adapted from Barone *et al.* (2010) and Bohner (2010).

Type of material	Material	Applications
Metals	Stainless steel Titanium Titanium alloys	Joint replacement Bone plates Dental implants
Ceramics	Alumina Zirconia Calcium sulphates Calcium carbonates Calcium phosphates Hydroxyapatite Bioactive glasses Bioactive glass-ceramics	Joint replacement Dental implants Bone screws Maxillofacial reconstruction Ossicular bone substitutes Kerato-prostheses
Polymers	Poly(lactic acid) Poly(glycolic acid) Poly(caprolactone) Cellulose Hyaluronic acid Fibrin Collagen Chitosan	Joint replacements Bone fixation devices Drug delivery systems

Ceramics were proposed as bone graft substitutes due to good resistance to corrosion, good biocompatibility levels, low friction, high resistance to wear, and stability in physiological environments (Barone *et al.*, 2010). Alumina (Al_2O_3) was the first ceramic widely used clinically with great success, usually in dental applications and in total joint prostheses. Zirconia (ZrO_2) has also been successfully used in total joint prostheses due to high fracture toughness and tensile stress values. However, both alumina and zirconia are bioinert and only form a mechanical bond with bone.

Polymers are very attractive materials to be used as bone graft substitutes because their composition and structure can be tailored to suit specific needs depending on the method of polymerisation, processing and functionalization, making it possible to create devices with predictable chemical and physical characteristics (Barone *et al.* 2010). A group of polymers which has received considerable attention for this purpose is the family of poly(α-hydroxy esters). These polymers can be processed using a wide range of techniques, including electrospinning, exhibit good levels of biocompatibility and are bioresorbable. Bioresorbable polymers are those that will degrade after implantation, usually through a non-biological process

such as hydrolysis, and will be safely removed from the body through cellular activity (Treiser *et al.*, 2013). The most frequently used poly(α-hydroxy esters) for tissue regeneration applications are poly(glycolic acid) (PGA), poly(lactic acid) (PLA) and poly(caprolactone) (PCL). The properties of these polymers, as well as their mechanisms of degradation and resorption, will be discussed with detail in the following sections of this Literature Review. However, despite these advantageous characteristics, polymers are preferentially used in non-load bearing sites in the skeleton due to their weak mechanical properties compared to metals and ceramics.

A common characteristic of most of the previously mentioned materials is that they are bioinert. However, bioactive materials offer the potential to improve the attachment between the implant and bone tissue as a result of a series of physical and chemical reactions that occur at the implant-tissue interface. Bioactive ceramics, such as hydroxyapatite and tricalcium phosphate, have been used in several clinical applications because they are biocompatible, biodegradable, osteoconductive and can bond directly to bone. Bioactive glasses, capable of forming a layer of hydroxy-carbonate apatite which leads to the formation of a bond with soft and hard tissues, have been used in prostheses, bone fillers and scaffolds. Bioactive glass-ceramics, made through the application of appropriate thermal treatments to glass that result in the growth of crystal phases within the amorphous vitreous matrix, have shown improved mechanical properties and moderate bioactivity compared with the bioactive glass compositions from which they were derived. One of the most clinically successful glass-ceramic compositions is the denominated A/W, constituted by two crystalline phases (i.e. an apatite phase and a wollastonite phase) and a residual vitreous phase (De Aza *et al*., 2007). Despite the beneficial characteristics of bioactive materials, they do not usually provide good support in load-bearing applications and it may be difficult to process them into specific shapes for particular clinical applications (Barone *et al.*, 2010).

Finally, an approach which has received considerable attention is the production of composite bone graft substitutes through the combination of two or more biomaterials. This has usually been achieved by embedding a

ceramic or bioactive glass within a polymer matrix, creating structures which may retain key characteristics of both biomaterials. For example, it may be possible to mould structures with shapes fitting specific bone defects using polymers presenting resorption rates that match the rate of new bone tissue formation (Barone *et al*., 2010). Additionally, it may be possible to mimic the composite nature of bone matrix by adding ceramics which may enhance the mechanical properties of the polymer. Bonfield (1988) reported that a composite material made of synthetic HA embedded within a matrix of polyethylene presented mechanical properties comparable to those of bone. The addition of 45S5 bioglass particles to a poly(lactic-co-glycolic acid) (PLGA) matrix by Lu *et al.* (2003) resulted in the creation of structures with higher compressive modulus than the polymer on its own and which supported the growth and mineralisation of osteoblast-like cells *in vitro*.

The most frequent polymers chosen for the fabrication of composite materials are poly(α-hydroxy esters), mainly due to their bioresorbability. These polymers generate acidic degradation by-products as they degrade, reducing the local pH and potentially affecting negatively the surrounding tissues after implantation. It has been proposed that the alkalinity produced by the dissolution of embedded bioactive glass particles may be used to buffer the acidic effect of the polymer degradation (Suggs *et al.*, 2007; Jones, 2013). Another concern is the potential loss of structural integrity as the new bone tissue grows. Ideally, the composite biomaterial should maintain its structure for as long as necessary while the regeneration occurs. However, the potentially different rates of degradation of each phase may result in an unstable construct and an increased risk of some particles migrating within the body after implantation (Jones, 2013).

2.1.5 Commercial bone graft substitutes

About half a million bone graft operations are performed in the United States and around 300000 in Europe every year. The majority of those procedures involve the treatment of bone defects caused by trauma, the removal of tumours and non-union of fractures using a temporary template composed by the patient's own bone (Jones, 2011). However, as previously discussed,

there are major issues associated with the use of autogenous bone grafts which will have a significant impact in the patient's quality of life. Bone graft substitutes with appropriate characteristics may have a beneficial effect as the patient would require a smaller number of operations and may be able to return to a normal life more rapidly. From an economic perspective, bone graft substitutes may also reduce the costs involved in the operations. It is estimated that the market of bone graft substitutes is worth US$ 2 billion/year (Jones, 2011) and has been in continuous growth for several years. Many companies have produced their own designs and have commercialised them after strict control and approval by regulatory bodies such as the FDA and the EU. Table 2.6 and Table 2.7 present a summarised list of commercial products approved to be used as bone graft substitutes in the United States and Europe.

Table 2.6. Summarised list of commercial products approved to be used as bone graft substitutes in the United States and Europe. Adapted from Finkemeier (2002) and Jones (2011).

Product	Company	Source	Type
Grafton DBM	Osteotech	Human	Demineralised bone matrix
DynaGraft	GenSci Regeneration Sciences	Human	Demineralised bone matrix
OrthoBlast	GenSci Regeneration Sciences	Human	Demineralised bone matrix and allograft cancellous bone
Osteofil	Sofamor Danek	Human	Demineralised bone matrix with gelatin carrier and water
Opteform	Exactech	Human	Compacted corticocancellous bone chips mixed with the same material as Osteofil
DBX	Synthes	Human	Demineralised bone matrix
Allomatrix	Wright Medical Technology	Human/Synthetic	Demineralised bone matrix in an Osteoset medium
Endobon	Merck KGaA	Animal	Sintered bovine cancellous bone
Bio-Oss	Osteohealth	Animal	Bovine bone
Interpore	Interpore International Inc	Animal	Coralline hydroxyapatite
Pro-Osteon	Interpore International Inc	Animal	Coralline hydroxyapatite
Collagraft	Zimmer	Animal/Synthetic	Bovine collagen, hydroxyapatite, tricalcium phosphate

Table 2.7. (Continuation) Summarised list of commercial products approved to be used as bone graft substitutes in the United States and Europe. Adapted from Finkemeier (2002) and Jones (2011).

Product	Company	Source	Type
NovaBone	NovaBone Products LLC	Synthetic	Bioactive glass
PerioGlas	NovaBone Products LLC	Synthetic	Bioactive glass
BonAlive	BonAlive Biomaterials Ltd	Synthetic	Bioactive glass
StronBone	RepRegen Ltd	Synthetic	Bioactive glass
Osteoset	Wright Medical Technology	Synthetic	Calcium sulphate
ApaPore	Apatech Ltd	Synthetic	Hydroxyapatite
Vitoss	Orthovita	Synthetic	Ultraporous β-tricalcium phosphate
SRS	Norian	Synthetic	Calcium phosphate injectable cement

2.2 Bone tissue engineering

Two main approaches currently exist for the repair and regeneration of damaged tissues, driven by a desire to prevent the issues associated with the replacement of damaged tissues using grafts: tissue engineering and *in situ* tissue regeneration (Hench and Polak, 2002).

Tissue engineering involves the isolation of specific cells and their seeding on a scaffold *in vitro* under controlled conditions that would encourage the synthesis of new extracellular matrix. The overall aim is to engineer a biological construct which may be implanted into a defect site in order to support the regeneration of the damaged tissues. Langer and Vacanti (1993) proposed that tissue engineering may be defined as: ‘an interdisciplinary field that applies the principles of engineering and the life sciences toward the development of biological substitutes that restore, maintain, or improve tissue function’. *In situ* tissue regeneration involves the implantation of cell-free biomaterials into a defect site in order to stimulate and guide local cells in the surrounding tissues to repair the defect *in vivo*. Various bioactive materials and growth factors may be used to encourage the activation and recruitment of cells, which in turn would produce additional growth factors and would stimulate multiple generations of cells to form the new tissues. Figure 2.4 shows a schematic representation of both approaches.

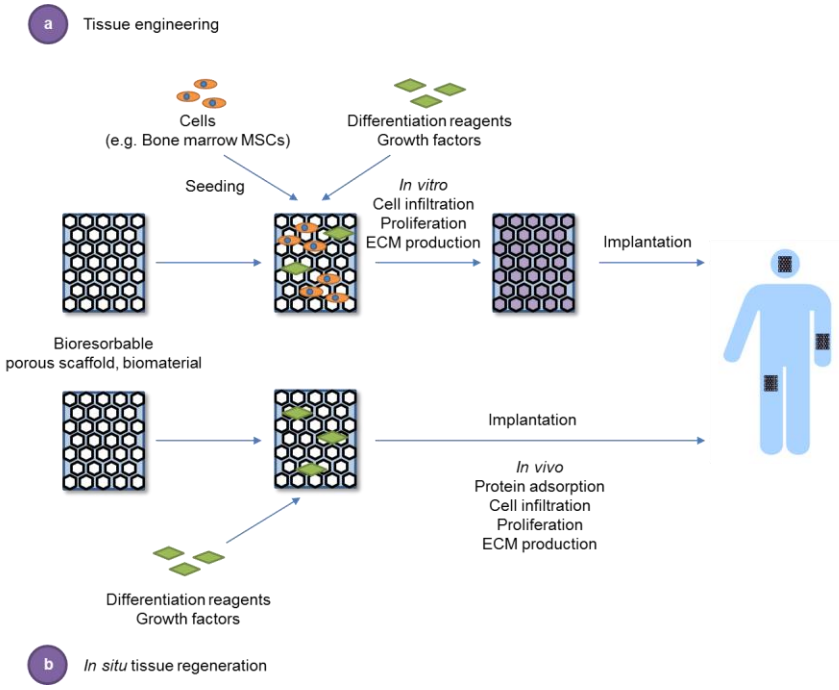

Figure 2.4. Schematic diagram of two alternative approaches for tissue regeneration: a) Tissue engineering, involving the i*n vitro* seeding of a porous scaffold, cellular infiltration, proliferation and production of extracellular matrix (ECM), followed by the implantation of the construct into a defect site; and b) *in situ* tissue regeneration, involving the implantation of a cell-free biomaterial into a defect site, followed by *in vivo* protein adsorption on the implant's surface, cellular infiltration, proliferation and production of extracellular matrix.

The main advantage of tissue engineering is the potential to deliver cells which are already differentiated and are capable of sustaining the regeneration process, directly into the defect site. Although *in situ* tissue regeneration is based on a similar fundamental idea, encouraging the surrounding cells to repair the defect, this approach may prove ineffective if the gap to be filled is too large. In those cases it may be more convenient to implant a tissue engineered construct in which the regeneration process has already started. Another advantage is the potential to produce large quantities of tissue on demand for specific applications, eliminating the problems of tissue shortages as a relatively small number of cells would need to be harvested from the patient and then expanded *in vitro*. The use of autologous cells may also prevent undesired potential risks such as immune rejection and disease transmission. Additionally, tissue engineering may allow for a high level of control of cell culture conditions, a situation which is not possible after implantation in the body. For example, it is possible to apply mechanical stimuli to cell-scaffold constructs during culture in order to encourage the formation of extracellular matrix, or control the supply of

nutrients and oxygens using techniques specifically developed for this purpose, such as dynamic cell cultures using fluid perfusion. This control becomes more difficult as the culture process progresses, as the extracellular matrix produced by the cells in the scaffolds may reduce the passage of nutrients and oxygen, reducing their availability to the cells residing in the core of the scaffold and resulting in their necrosis. The absence of a vascular network is a major drawback for tissue engineered constructs, especially if their dimensions are large (Ikada, 2006). Finally, the success of the tissue engineered construct will be strongly influenced by the age, health status, systemic conditions and genetic background of the donor.

In situ tissue regeneration seems, in principle, simpler than tissue engineering as the cell seeding and culture steps are eliminated. The biological conditions required for the development of the new tissues are directly provided by the body, as it occurs for natural regeneration processes. However, the implanted biomaterial should be designed in such a way as to provide the surrounding tissues with a suitable environment for the regeneration process to successfully occur. For example, it may be possible to induce the formation of a vascular network supporting the growth of the new tissue if angiogenic factors are included and slowly released by the implant (Ikada, 2006). Additional advantages of *in situ* tissue regeneration is that there are fewer immunorejection and ethical concerns compared with tissue engineering, and it may be easier to fabricate devices which would be easily used in the surgical theatre. Despite these attractive characteristics of *in situ* tissue regeneration, the possibility of dealing with larger defects and the potential of greater control on the culture conditions make tissue engineering a discipline which has attracted great attention for the treatment of many defects.

2.2.1 Design of scaffolds for tissue engineering

Most cells reside in an environment called the extracellular matrix, which is essential for the healthy development of tissues in the body. The various functions of extracellular matrix are: the provision of support for cells to attach, proliferate, migrate and respond to signals; the contribution of

mechanical properties to the tissue; the provision of biological cues that regulate cellular activity; the formation of a reservoir of growth factors and other biological cues; and the provision of a dynamic environment that may change in response to tissue processes such as morphogenesis, homeostasis and wound healing (Chan and Leong, 2008).

The native extracellular matrix is usually considered as the best possible scaffold for any particular tissue engineering application in terms of structure and function. All scaffolds should then attempt to mimic it as close as possible. The fundamental design criteria for any scaffold for tissue engineering should then take in account the following factors (Chan and Leong, 2008):

1) Architecture: the scaffold should provide space for vascularisation, tissue growth and remodelling. The structure should be porous for the efficient transport of nutrients and other substances without compromising the mechanical stability of the scaffold. The scaffold should ideally be degradable after implantation, with a rate matching the rate of new matrix production.
2) Cyto- and tissue compatibility: the scaffold should provide support for cells to attach, proliferate and differentiate both *in vitro* and *in vivo*. The biomaterials selected should be compatible with the cellular components in the tissue engineered construct and in the host.
3) Bioactivity: the scaffold may interact with the cellular components of the tissue engineered construct, facilitating and regulating their activity. The biomaterials may include biological of physical cues to enhance attachment (i.e. cell-adhesive ligands) or to influence morphology and alignment (i.e. topography). The structure may also work as a delivery system of biochemical signals that may enhance tissue regeneration (i.e. growth factors).
4) Mechanical properties: the scaffold should provide mechanical and shape stability to support the regeneration of the tissue in the defect site. If possible, the mechanical properties of the biomaterials used to fabricate the scaffold or their post-processing properties should match that of the host tissue.

Two main approaches have been investigated to fabricate porous scaffolds. The first approach involves the processing of synthetic (e.g. ceramics, polymers) or natural (e.g. chitosan, cellulose) materials in order to fabricate pre-made of artificial porous scaffolds. The second approach involves the removal of cellular elements from tissues and organs in order to produce collagenous porous scaffolds that retain the shape of the native tissues. These two approaches are schematically represented in Figure 2.5.

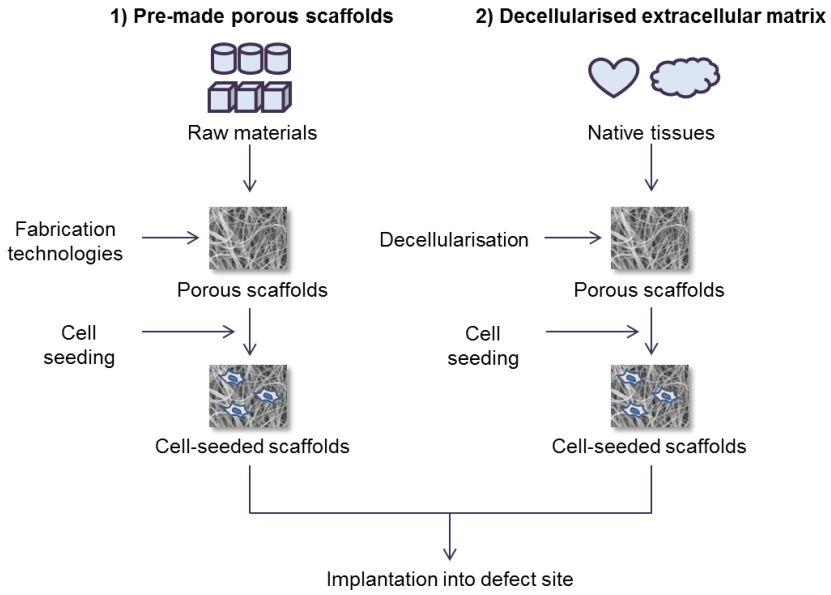

Figure 2.5. Schematic diagram of two approaches for the production of porous scaffolds for tissue engineering applications. Adapted from Chan and Leong (2008).

The fabrication of pre-made scaffolds using natural or synthetic materials presents various advantages over the use of decellularised tissues and organs: firstly, there is a wide range of biomaterials and manufacturing methods that may be used; and secondly, the properties of the scaffold may be more easily engineered in order to mimic the characteristics of the native extracellular matrix. This way, the resulting structures may be more easily sourced and more reproducible. The main disadvantage is the potentially inefficient seeding of the structure due to the limited penetration of cells into the scaffold. Various methods have been investigated to enhance penetrability, such as agitation or perfusion, but these are not free of problems and may increase the cost and complexity of the tissue engineering process. The manufacturing techniques used may be classified

within the following categories: processes using porogens in the biomaterials, solid free-form or additive manufacturing technologies, and techniques generating woven or non-woven fibres. Decellularised tissues and organs usually exhibit good levels of biocompatibility, mainly due to very closely mimicking the native structure of extracellular matrix. Specialized techniques are used to remove cellular components, usually through a combination of physical, chemical and enzymatic methods (Chan and Leong, 2008). However, the structures may require a crosslinking treatment with glutaraldehyde (Tedder *et al*., 2009; Zhao *et al*., 2011) or other chemicals (Lu *et al*., 2010) to reinforce their mechanical properties and stabilise their shape (Chan and Leong, 2008). Additionally, cell seeding may also result in inhomogeneous cellular distributions while incomplete removal of cellular components may elicit immune reactions upon implantation. Examples of this approach include veins (Schaner *et al*., 2004), liver (Lin *et al*., 2004; Shirakigawa *et al*., 2012), or trachea (Baiguera *et al*., 2010; Remlinger *et al*., 2010).

The criterion used to select a biomaterial for the fabrication of artificial structures is also very important. As mentioned above, it should be biocompatible and, ideally, should degrade through a mechanism that does not generate toxic by-products. Any by-product should also be easily removed from the implantation site through metabolic routes in order to prevent a negative effect on the implant and the surrounding tissues. The degradation process should ideally occur at a rate matching the regeneration rate of the tissues to maximise the healing process.

The mechanical properties of the scaffold and of the biomaterials selected to fabricate it will influence its application and the techniques used for its processing. Scaffolds with small pores exhibit greater strengths but the small size will greatly limit the penetration of cells and nutrients, and the vascularisation of the new tissues, while larger pores will reduce the overall strength of the structure. Additionally, the mechanical properties of the biomaterial will have an important influence on the seeded cells. Many mature cell types, such as epithelial cells, fibroblasts, muscle cells and neurons, are able to sense the stiffness of the substrate and may show

dissimilar morphology and adhesive characteristics as a result (Discher *et al.*, 2005). Stem cells may also be influenced by this, as it was shown that MSCs may differentiate into different cell lineages in response to the elasticity of the matrix they attach to, depending on how similar it was to the elasticity of the native tissues (Engler *et al.*, 2006). Natural materials, as mentioned above, may require treatments to improve their stability and mechanical properties. Synthetic materials may offer better controlled physical and mechanical properties, and may be used to tailor for both soft and hard tissues (Chan and Leong, 2008).

The capacity of any particular biomaterial to withstand sterilisation is another crucial issue in the development of scaffolds as they will be implanted in the body and the risk of potential infection needs to be fundamentally reduced to zero. The sterilisation of biomaterials has usually been performed using various techniques such as dry heat sterilisation, autoclaving, ultraviolet light, radiation and treatment with various chemical agents. In the particular case of polymers, sterilisation is a complex issue because their thermal and chemical stability are lower than in other materials. Only some polymers (e.g. polytetrafluoroethylene, silicon rubber) can be safely dry-sterilised at temperatures between 160˚C and 190˚C, which are above the melting temperature of bioresorbable poly(α-hydroxy esters), such as poly(lactic-co-glycolic acid). In general, poly(α-hydroxy esters) will also be affected if sterilised through autoclaving due to the presence of water in the process, as they degrade by hydrolysis. Radiation treatments at high dosages may result in the dissociation or cross-linkage of the polymer chains, altering the properties of the material. Chemical agents such as ethylene oxide gas and hypochloride solutions can be used to sterilise polymers at low temperatures if the exposure time is relatively short, although they may still suffer some damage if residual molecules are present (Khang, 2012).

Besides the choice of material, the architecture given to the scaffold will play an essential role in the regeneration process. The structure should be porous without significantly compromising its mechanical stability (Chan and Leong, 2008). Additionally, a large surface area will favour cell attachment and proliferation, while a large pore volume will be able to accommodate a mass

of cells large enough for tissue regeneration. In general, a high porosity and a good level of interconnectivity between the pores are desirable for the easy transport of materials and for the migration of cells into the structure, as well as to provide sufficient space for the synthesis of extracellular matrix and its vascularisation, which will be required for the long term viability of the construct (Yang *et al.*, 2001).

2.2.2 Bone tissue engineering

The aim of bone tissue engineering is to create a healing response in a precise anatomic area of the skeleton so that the new tissue is structurally integrated with the surrounding tissues and has the appropriate biomechanical characteristics in order to be durable and effective (Kakar and Einhorn, 2005).

This may be achieved by promoting, aiding and/or regulating the filling of the defect through new bone tissue formation by implanting cell-seeded scaffolds, or through the ingrowth of bone into the defect by implanting cell-free scaffolds (Bueno and Glowacki, 2011). Cell-seeded scaffolds may be used when the implantation of bone cells or tissue in the defect site is desired. The *in vitro* cultivation of these scaffolds may also allow for the addition of physical or chemical cues in the structure that will guide cell proliferation and differentiation. Cell-free scaffolds may be used to fill the void created by a defect and to encourage the formation of new bone tissue as it grows from the implant-tissue interface (Bueno and Glowacki, 2011).

Bone tissue engineering requires many of the same properties as other tissue engineering areas for scaffolds and the biomaterials used in their fabrication. This includes biocompatibility, biodegradability and high porosity. Ideally, the scaffold should degrade at a rate similar to the rate of bone growth but this will depend on the choice of biomaterials used and the architecture. For example, surgeons usually prefer to see regeneration of large bone defects over a period of approximately 12 months (Jones, 2013). With respect to the porosity, it has been suggested that the ideal pore size for bone tissue engineering is 200-500 µm, with smaller pores generally not being able to support the vascularisation of the new tissue (Gauthier *et al*.,

1998; Yang, 2001; Bueno and Glowacki, 2011). Additionally, specific desirable characteristics of scaffolds for bone tissue engineering include: acting as substrate for osteoid deposition, supporting and promoting osteogenic differentiation, promoting osseointegration, prevention of soft tissue growth at bone-implant interface, being malleable and adaptable to irregular wound sites, being sterilisable without losing its properties and being available to surgeons on short notice (Katsanevakis *et al.*, 2012).

Materials frequently used in the fabrication of scaffolds for bone tissue engineering have been demineralised bone matrix, synthetic and natural polymers, ceramics and bioactive glasses. However, as no single material is able to fulfil all the requirements for bone tissue engineering applications, composite biomaterials that attempt to mimic the composite nature of bone tissue have generally been investigated. Several ceramics, glass-ceramics and bioactive glasses have been studied for this purpose, as reviewed in different publications (Hench, 1998; Barone *et al.*, 2010; Holzwarth and Ma, 2011).

Ideally, the scaffolds used for bone tissue engineering should exhibit a strength and stiffness similar to that of the native bone tissue that is trying to regenerate. Bone strength can range from 20 MPa (trabecular) to 200 MPa (cortical). One advantage of synthetic polymers is the ability to tailor the mechanical properties to match the desired function, although there is a trade-off between strength and the ability to degrade. Generally, strong polymers degrade slowly while highly degradable polymers are weak. Also, polymers become stronger, stiffer, tougher and more resistant to wear with an increase in molecular weight and crystallinity. Crosslinking can also increase the strength and rigidity of polymers by reducing the ability of polymer chains to slide relative to each other (Wang *et al.*, 2010). Ceramics like HA may be manufactured as dense structures, which show considerable compressive strength but are brittle and not suitable for load-bearing applications; and as porous structures, which possess poor mechanical properties. Bioactive glasses are considered to be weaker than most other bioactive materials, restricting their use to non-load bearing sites as well. However, bioactive glass-ceramics possess enhanced mechanical properties

while exhibiting moderate bioactivity (Barone *et al.*, 2010). Table 2.8 presents the mechanical properties of various biomaterials compared with those of cancellous and cortical bone.

Table 2.8. Mechanical properties of various bioceramics compared with cancellous and cortical bone. Adapted from Middleton and Tipton (2000), Rezwan *et al.* (2006) and Barone *et al.* (2010). PGA=Poly(glycolic acid); P(L)LA=Poly(L-lactic acid); P(DL)LA=Poly(DL-lactic acid); PCL=Poly(caprolactone); PLGA=Poly(lactic-co-glycolic acid); HA=Hydroxyapatite; A/W=Apatite/Wollastonite glass-ceramic.

Biomaterial	Strength (MPa)		Young's modulus (GPa)	Fracture toughness ($MPa \cdot m^{1/2}$)
	Compressive	Bending		
Polymers				
PGA	Fibre: 340–920	-	7.0	-
P(L)LA	Pellet: 40–120 Film or disk: 28–50 Fibre: 870–2300	-	2.7	-
P(DL)LA	Pellet: 35–150 Film or disk: 29–35	-	1.9	-
PCL	-	-	0.4	-
PLGA	41.4–55.2	-	2.0	
Bioceramics				
45S5 bioglass	-	42	35	-
HA	500-1000	115-200	80-110	1.0
A/W	1080	220	118	2.0
Human bone				
Cancellous	2-12	-	0.05-0.5	-
Cortical	100-230	50-150	7-30	2-12

The approaches used in the fabrication of porous scaffolds for bone tissue engineering applications are various and include the use of wide range of techniques. Conventional methods to fabricate scaffolds, such as the production of fibre meshes through standard textile technologies, gas foaming, phase separation, freeze drying and particulate leaching, do not generally allow for a fine control over pore connectivity and the structures tend to lack structural stability (Moroni *et al*., 2008; Bueno and Glowacki, 2011). Alternative approaches, such as additive manufacturing, electrospinning and surface-based technologies, allow for more precise

control over the structural characteristics of the scaffolds. Additive manufacturing employs a CAD/CAM approach to design and fabricate precise three-dimensional scaffolds layer by layer (Seitz *et al*., 2005; Wilson *et al*., 2011; Seol *et al*., 2013). Electrospinning, which will be explained with detail in section of this Literature Review, applies a high voltage electric current to a polymer solution to generate fibres with dimensions potentially similar to fibrils present in bone extracellular matrix (Jang *et al*., 2009; Holzwarth and Ma, 2011). Surface-based technologies include a range of lithographic tools used to fabricate bi-dimensional structures with specific surface topologies, which can then be stacked to form three-dimensional scaffolds (Moroni *et al.*, 2008; Papenburg *et al*., 2007; Sellgren and Ma, 2012).

The cells most frequently used in bone tissue engineering have been sourced from the bone marrow. Mesenchymal stromal cells (MSCs) are a population of bone marrow cells which exhibit adherence to culture substrates *in vitro* and are able to differentiate into osteoblasts and form bone *in vivo*. With the appropriate stimulation they are able to differentiate into other cellular lineages including chondrocyte, adipocyte and fibroblast (Pittenger *et al*, 1999). The main issue with MSCs is that the number of cells found in bone marrow tends to be low, with estimations of one cell per fifty thousand nucleated cells in young individuals and even lower numbers in the elderly (Kakar and Einhorn, 2005). Therefore, alternative sources of MSCs with osteogenic potential have been investigated and isolated from adipose tissue, peripheral blood, the placenta and the umbilical cord (Hass, 2011). It has been suggested that allogeneic adult MSCs may be implanted without eliciting immune rejections in the host, especially when it was observed that the cells did not express cell-surface HLA-Class II antigens after expansion *in vitro* (Le Blanc *et al*., 2003) and that the expanded cells did not persist for long after implantation (Bueno and Glowacki, 2011).

Finally, bone tissue engineering approaches often attempt to mimic the natural environment surrounding bone formation through the addition of bioactive components that may stimulate cell proliferation, migration, differentiation, osteogenesis and/or vascularisation. These may be

incorporated into the scaffold to be released after cultivation or implantation, and their effect will depend on dosage and release kinetics, which in turn are dependent on pore size and degradation rate. High doses may be necessary to obtain the desired effect due to the generally short half-lives of many of those components, potentially leading to undesirable bone formation outside the defect area (Bueno and Glowacki, 2011). Some of the bioactive components used are bone-morphogenetic proteins (e.g. BMP2), angiogenic factors (e.g. vascular endothelial growth factor), factors promoting cell adhesion (e.g. peptides containing Arg-Gly-Asp), protein mixtures (e.g. cocktail of enamel matrix proteins) and synthetic compounds (e.g. simvastatin).

2.3 Electrospinning

Electrospinning is a versatile method used to generate fibres with diameters from a few micrometres to tens of nanometres through the application of electrostatic forces to polymeric solutions or melts (Doshi and Reneker, 1995; Huang *et al*., 2003; Martins *et al*., 2008).

The history of electrospinning began in the late 16th century, when William Gilbert recorded the first observations of the electrostatic attraction of a liquid and the existence of what later would be known as the Taylor cone. Research on the science behind this phenomenon continued during the following centuries but it did not gain wide popularity until the beginning of the 20th century, when it began to be used in the fabrication of textiles and filters and when J. F. Cooley filed the first patent for the electrospinning method. Its introduction in the field of biomaterials occurred during the 1990's, when Doshi and Reneker (1995) successfully demonstrated that fibres with small diameters could be spun from solutions of different polymers and then suggested several potential applications for them. Since then, the number of publications about electrospinning has generally increased every year at an exponential rate (Tucker *et al*., 2012).

The versatility of this method is due to the ability to tailor several properties of the electrospun fibres and membranes, such as diameter, morphology,

porosity and chemistry, by controlling the parameters and conditions of the process and by selecting appropriate starting materials. Electrospinning has been used for a broad range of purposes, including: biomedical applications, such as tissue engineering, drug delivery and wound dressing (Goh *et al*., 2013); the development of electronic components and devices (Miao *et al*., 2010); the creation of oil sorbents for environmental protection (Lin *et al*., 2012); and the development of materials for energy-related applications, such as fuel cells or supercapacitors (Dong *et al*., 2011).

2.3.1 The electrospinning process

There are three basic elements that form an electrospinning system: a high voltage power supply, a capillary tube, and a grounded metal collecting plate (Figure 2.6). The system is usually placed inside a chemical hood to allow for the elimination of vapours originating from the organic solvents used to create the polymer solutions. Additionally, a closed environment with regulated temperature and humidity may be installed to prevent the interference of environmental factors in the process, such as air turbulence or the sudden variations of temperature (Martins *et al.*, 2008).

The electrospinning process involves the application of a high voltage electrical current to a capillary filled with a polymer solution, inducing a charge on the surface of the liquid. This results in the creation of mutual charge repulsions that generate forces directly opposite to the surface tension. As the intensity of the electric field increases, the hemispherical surface of the fluid at the tip of the capillary tube elongates to form a conical shape known as the ‘Taylor cone’. When the electric field reaches a critical value, at which the repulsive electric force overcomes the surface tension force, a charged jet is ejected from the tip of the Taylor cone and travels in the air towards the collecting plate. As long as the molecular cohesion in the liquid is sufficiently high, the jet will not break down.

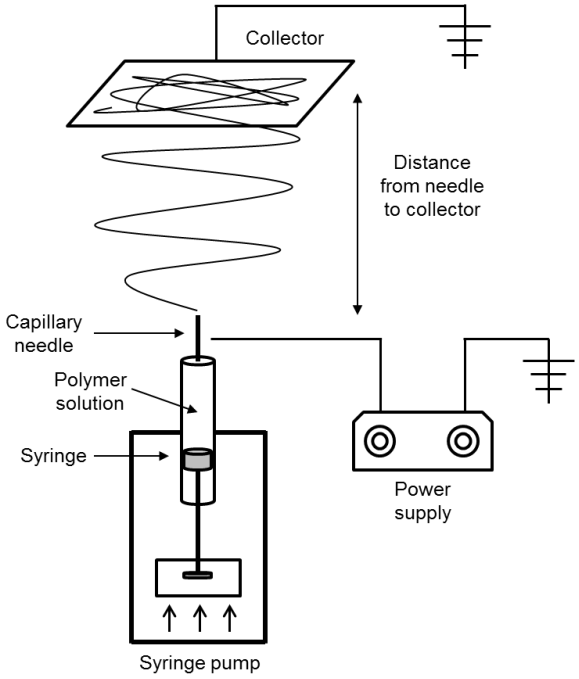

Figure 2.6. Schematic diagram of an electrospinning system, identifying the main components that form it. Adapted from Martins *et al.* (2008).

According to Reneker and Yarin (2008), the typical path of the jet is initially a stable and straight segment followed by a coil of increasing diameter. The coil is created by electrically driven bending instabilities generated by the repulsive interactions between the charges in the polymer solution. As it travels toward the collecting plate, the jet continues to coil and stretch while the solvent evaporates. When the jet finally reaches the plate it deposits, forming a non-woven mat of randomly distributed fibres. Since the generation of the fibre may occur uninterruptedly, it is theoretically possible to fabricate mats formed by very long fibres and exhibiting high levels of porosity (Doshi and Reneker, 1995; Huang *et al*., 2003; Martins *et al*., 2008).

Several variations can be made to the basic system to allow for a more precise control on the results. For example, the capillary and the collecting plate can be arranged both vertically and horizontally. If arranged in a vertical orientation, with the collector placed directly above the capillary, then it will be possible to prevent drops of polymer solution from falling from the needle on the mat. A syringe pump may also be used to accurately control the flow rate of the polymer solution, which will play a significant role determining fibre diameter. Specially designed collector systems, such as rotating drum

collectors and static parallel electrodes, may be used to produce mats made of aligned fibres. Finally, it is known that the nature of the collector can have an influence in the density of the fibres per unit area and in arrangement of the fibres. Conductive collectors (i.e. aluminium foil) help dissipate the charges in the fibres upon deposition and reduce repulsion between them, resulting in the production of smooth and densely packed fibres. Conversely, non-conducting materials (i.e. paper) will not dissipate the charges, increasing repulsion between the fibres and will result in more loosely packed mats (Baji *et al*., 2010).

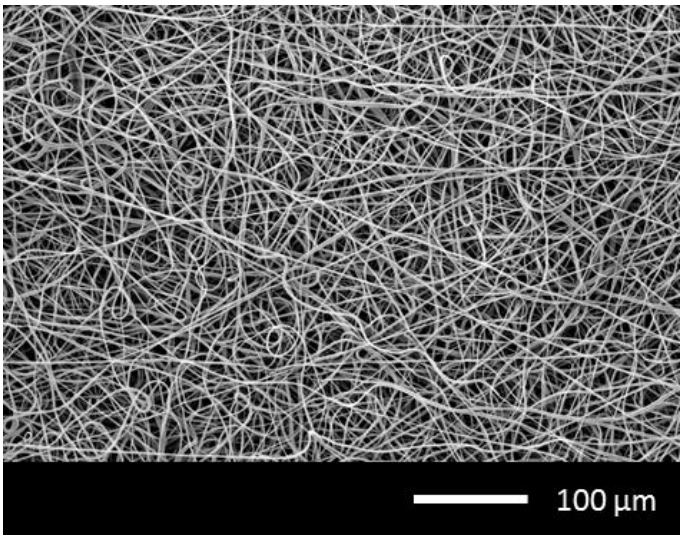

Figure 2.7. Scanning electron microscopy micrograph of electrospun poly(caprolactone) showing the random distribution of fibres in the mat.

The processing parameters governing the electrospinning method are multiple. In order of relative importance, from higher to lower impact in the results, these are: applied voltage, polymer flow rate, and distance from the capillary tip to the collecting plate. Additionally, a number of solution parameters play an important role in fibre formation and structure. In order of relative importance, from higher to lower impact, these are: polymer concentration, solvent volatility, and solvent conductivity (Sill and von Recum, 2008). The effects these have on the electrospinning process are presented in Table 2.9.

Table 2.9. Effects of the variation of processing and solution parameters on electrospun fibre diameter and morphology. Adapted from Sill and von Recum (2008).

Parameter	Effect on fibre diameter and morphology
Increase of applied voltage	Fibre diameter will initially decrease, but it will then increase after reaching a certain voltage value.
Increase of flow rate	Fibre diameter will generally increase. A beaded morphology may appear if the flow rate is too high.
Increase of distance from capillary to collector	Fibre diameter will generally decrease. A beaded morphology may appear if the distance is too short.
Increase of polymer solution concentration	Fibre diameter will generally increase if concentration is within an optimal range.
Increase of solvent conductivity	Fibre diameter will generally decrease. Fibres may present a broad diameter distribution.
Increase of solvent volatility	Fibres will generally exhibit pores on their surface, increasing surface area.

Environmental parameters such as temperature and relative humidity also have an important effect on the electrospinning process (Tripatanasuwan *et al*., 2007; De Vrieze *et al*., 2009) and, as previously mentioned, it may be necessary to take special measures in order to produce fibres with regular diameters and morphologies. De Vrieze *et al.* (2009) reported that there were two main and opposing effects of the temperature on electrospun poly(vinylpyrrolidone) (PVP) and cellulose acetate (CA). The first effect was the evaporation rate of the solvent, which decreased at lower temperatures and, thus, it took longer for the jet to solidify. The second effect was the rigidity of the polymer chains, which had more freedom to move at higher temperatures and resulted in lower solution viscosity. At lower temperatures (i.e. 283 K) the first effect was dominant, while at higher temperatures (i.e. 303 K) the second effect was dominant. Both resulted in decreased fibre diameters, but intermediate temperatures (i.e. 293 K) resulted in larger fibre diameters. With respect to humidity (i.e. concentration of water in the atmosphere), De Vrieze *et al*. (2009) reported that PVP fibre diameters generally decreased at higher humidity levels although this effect stopped at certain levels, when the fibres began to fuse upon deposition. Additionally, their observations suggested that these effects may vary depending on the polymer used. Although the effect of the temperature on CA was similar to what happened to PVP, CA fibres presented larger average diameters at high humidity levels.

2.3.2 Electrospinning for bone tissue engineering

Electrospinning is a technique which has received considerable attention for the production of scaffolds for bone tissue engineering due to the wide range of polymers which can be processed and to the potential of producing fibrous materials which may mimic native bone matrix in terms of scale and structure (Goh *et al*., 2013). The diameter of electrospun fibres usually range from a few micrometers down to tens of nanometers, similar to the thickness of collagen fibres in bone tissue (i.e. 50 – 500 nm) (Holzwarth and Ma, 2011). Additionally, the materials produced can exhibit large surface area to volume ratio, high porosity and may be degradable if fabricated with appropriate biomaterials. Table 2.10 and Table 2.11 present a summarised list of electrospun systems fabricated and investigated for potential bone regeneration applications.

Table 2.10. Summary of electrospun systems produced for potential bone regeneration applications. PLA=poly(lactic acid); PGA=poly(glycolic acid); PLGA=poly(lactic-co-glycolic acid); PCL=poly(caprolactone); PLCL=poly(lactic acid-co-caprolactone); PEO=poly(ethylene oxide); HA=hydroxyapatite; TCP=tricalcium phosphate.

Material	Composition	Reference
Inorganic materials	Bioactive glass	Kim *et al*., 2008 Lu *et al*., 2009
	Silicates	Sakai *et al*., 2006 Yamaguchi *et al*., 2010
Natural polymers	Collagen	Matthews *et al*., 2002 Shih *et al*., 2006
	Chitosan	Shin *et al*., 2005
	Silk fibroin	Park *et al*., 2010
	Cellulose	Li, K.N. *et al*., 2012
	Fibrin	Sreerekha *et al*., 2013
	Gelatin	Zhang *et al*., 2005
	Composite Gelatin and bioactive glass	Gao *et al*., 2013
Synthetic polymers	PLA	Li *et al*., 2006 Schofer *et al*., 2008 Prabhakaran *et al*., 2009
	PGA	Li *et al*., 2006
	PLGA	Li *et al*., 2006 Xin *et al*., 2008
	PCL	Yoshimoto *et al*., 2003 Li *et al*., 2006 Wutticharoenmongkol *et al*., 2006
	PLCL	Kwon *et al*., 2005 Bottino *et al*., 2011
	Composite PLA and HA	Ngiam *et al*., 2009 Prabhakaran *et al*., 2009

Table 2.11. (Continuation) Summary of electrospun systems produced for potential bone regeneration applications. PLA=poly(lactic acid); PGA=poly(glycolic acid); PLGA=poly(lactic-co-glycolic acid); PCL=poly(caprolactone); PLCL=poly(lactic acid-co-caprolactone); PEO=poly(ethylene oxide); HA=hydroxyapatite; TCP=tricalcium phosphate.

Material	Composition	Reference
Synthetic polymers	Composite PLA and HA	Ngiam *et al*., 2009 Prabhakaran *et al*., 2009
	Composite PLGA and amorphous TCP	Schneider *et al*., 2008
	Composite PLA and HA	Ngiam *et al*., 2009 Prabhakaran *et al*., 2009
	Composite PLGA and amorphous TCP	Schneider *et al*., 2008
	Composite PLGA and SiO_2-CaO gel	Kim *et al*., 2010
	Composite PCL and HA	Wutticharoenmongkol *et al*., 2006 Yang *et al*., 2009
	Composite PCL and HA/TCP	Patlolla *et al*., 2010
	Composite PCL and $CaCO_3$	Fujihara *et al*., 2005 Wutticharoenmongkol *et al*., 2006
	Composite PEO and silica	Toskas *et al*., 2011
Polymer blends	PLGA/Collagen	Liao *et al*., 2008
	PCL/Gelatin	Zhang *et al*., 2005
	PCL/Collagen	Chakrapani *et al*., 2012
	Collagen/Gelatin	Jha *et al*., 2011
	Chitosan/PEO	Desai *et al*., 2008
	Composite PLA/Collagen and HA	Ngiam *et al*., 2009 Prabhakaran *et al*., 2009

The main issue with the application of electrospun materials for bone tissue engineering is associated with the difficulty in creating pores large enough to allow cellular migration and tissue perfusion, which may be particularly challenging for the treatment of large defects (Shin *et al*., 2012). Zhang *et al.* (2005) reported the enhanced infiltration of bone marrow MSCs into an mesh made of electrospun PCL and gelatin (i.e. 114 μm) compared with PCL on its own (i.e. 48 μm), suggesting that it may be possible to improve the situation by using natural polymers. However, achieving an adequate penetration of cells still remains a difficulty to be overcome. Another significant issue of the technique is limited reproducibility due to potential differences between electrospinning systems used by various research groups and laboratories. Many of those systems are custom built and may lack accurate humidity and temperature control, which would allow reducing variability introduced by environmental changes.

Among polymeric materials, bioresorbable poly(α-hydroxy esters) such as PGA, PLA, PCL and their copolymers have been the most extensively investigated for electrospinning. These polymers and their characteristics will be described with detail in section 2.4 of this review. Additionally, the fabrication of composite electrospun materials using bioresorbable polymers and bioceramics has received considerable attention due to the possibility of combining the properties of bioresorbable polymers with bioceramics in one single structure. This way, the inorganic phase may improve the biological properties of the polymeric fibres (i.e. enhancement of biocompatibility and osteogenetic potential of the biomaterial) while the polymeric phase may introduce some degree of flexibility that bioceramics lack. Also, as there is no need of thermal treatment because of the binding polymer phase, electrospun composite fibres may also be used in drug delivery applications. Finally, the addition of bioceramics in particulate form to electrospun fibres is considered a promising approach for bone tissue regeneration as it may make it possible to develop structures that mimic the composite nature of bone extracellular matrix (Jang *et al*., 2009).

Potential problems of composite electrospun materials are similar to those that affect all composites. The main concern usually is the mechanical integrity of the material, especially if there is no interfacial bonding between the polymer and the bioceramic particles. This issue is particularly challenging when using poly(α-hydroxy esters), since the bioceramic phase tends to be highly hydrophilic and the polymers are hydrophobic. This may be solved by increasing the bonding at the interface using surfactants chemisorbed to the surface of the particles, but this may potentially affect the biocompatibility and degradation properties of the composite (Rezwan *et al.*, 2006). Additionally, both phases should ideally degrade at similar rates to maintain the mechanical properties of the structure and to match the rate of tissue regeneration. However, current polymer-bioceramic composites present different rates of degradation for each phase. The hydrolytic degradation of the ester bonds in bioresorbable polymers creates carboxylic groups, reducing the local pH and autocatalysing and accelerating its degradation. Natural polymers, which tend to degrade through enzymatic

activity, exhibit more linear degradation rates and may be adequate alternatives. However, it is usually more difficult to obtain reproducible sources than in the case of synthetic polymers (Jones, 2013). The production of composites with bioceramic nanoparticles also present a challenge as the particles tend to agglomerate and will not disperse homogeneously throughout the composite, which will result in the formation of beads in the electrospun fibres. Surfactants may be added to facilitate this step, by stabilising the interface of the nanoparticles and the polymer solution (Jang *et al.*, 2009). However, this may present similar issues as those mentioned above for the increase of the interfacial bonding.

2.4 Bioresorbable polymers

Certain clinical circumstances may require the use of implants that will serve a temporary purpose rather than a permanent one. In those situations, degradable materials are of interest because the implants fabricated with these materials will not need to be surgically removed after they have fulfilled their purpose. The removal process can create new wounds, increasing the risk of surgical complications and infections, and, therefore, that is usually avoided if possible. Additionally, the use of degradable implants can prevent problems associated with the long-term safety of permanent implants, such as immune rejection, chronic inflammation at the implant-tissue interface, and final failure of the device. However, degradable implants are not exempt of safety concerns, such as the potential toxicity of degradation by-products, and the possible premature failure of the implant as the degradation process occurs. Therefore, the design of degradable implants will require the careful selection and testing of all the biomaterials used (Treiser *et al*., 2013).

All biomaterials undergo some degree of degradation and, as a consequence, the strict differentiation between ‘degradable’ and ‘non-degradable’ materials is often difficult. Gopferich (1996) suggested that this distinction may be based on the relation between the time-scale of the degradation and the time-scale of the desired application. Therefore, the term ‘degradable’ may be attributed to materials which degrade during their application or immediately after it, and ‘non-degradable’ may be attributed to

those materials that require a period of time to degrade substantially longer than the duration of the application. Several terms have generally been used in the literature to indicate that a material will eventually disappear after implantation into a living organism: biodegradation, bioerosion, bioabsorption and bioresorption (Treiser *et al*., 2013). 'Biodegradation' refers to the chemical breakdown of the material through a biologically-mediated process (i.e. enzymatic or cellular activity). If the breakdown occurs through non-biological processes, such as hydrolysis, then the process is known as 'degradation'. 'Bioerosion' refers to the degradation process of a water-insoluble material that is converted into a water-soluble material through physical and chemical mechanisms under physiological conditions. Finally, the terms 'bioabsorption' and 'bioresorption' are often used interchangeably and refer to the elimination of the material and its degradation by-products through cellular activity (i.e. phagocytosis).

For the sake of consistency, the term 'bioresorbable material' will be used in this review for all those materials which are degradable and are bioresorbed by the body, leading to the total elimination of the implant and its degradation by-products with no residual side-effects. This process finally results in the replacement of the implant by the surrounding tissues, preventing additional surgical interventions to remove it and, thus, eliminating associated risks to the patient (Vert *et al*., 1992; Middleton and Tipton, 2000).

2.4.1 Bioresorbable polymers

Bioresorbable polymers may be of natural or synthetic origins. Natural polymers, such as collagen, polysaccharides (e.g. chitin, cellulose) and microbial polyesters (e.g. poly(hydroxybutyrate), poly(hydroxyvalerate)), have been investigated to be used as implantable materials (Pulapura and Kohn, 1992). However, synthetic polymers have generally been preferred because they offer several advantages over natural polymers as they can be produced under controlled conditions and can be tailored to provide a wider range of properties, offering less variability than natural materials. Also, they are a more reliable source of raw materials and are generally free of concerns of immunogenicity (Pulapura and Kohn, 1992; Middleton and

Tipton, 2000). A summary of several degradable polymers and their applications under investigation are presented in Table 2.12.

Table 2.12. Summary of degradable polymers and their applications under investigation. Adapted from Treiser *et al.* (2013).

Polymers	Applications
Synthetic degradable polymer	
Poly(glycolic acid), poly(lactic acid) and copolymers	Barrier membranes, drug and hormone delivery, guided tissue regeneration, orthopaedic applications, vascular/urological stents, staples, sutures, injectable fillers, dura mater substitutes, skin replacement materials, tissue engineering
Poly(caprolactone)	Drug delivery, orthopaedic applications, staples, stents, tissue engineering
Poly(dioxanone)	Fracture fixation in non-load bearing bones, sutures, wound clips
Other synthetic degradable polymers	
Poly(anhydrides)	Drug delivery
Poly(cyanoacrylates)	Adhesives, drug delivery
Poly(amino acids) and 'pseudo' poly(amino acids)	Drug delivery, tissue engineering, orthopaedic applications, stents, anti-adhesion barriers
Poly(ortho esters)	Drug delivery, stents
Poly(phosphazenes)	Blood containing devices, drug delivery, skeletal reconstruction, vaccine adjuvants
Poly(propylene fumarate)	Orthopaedic applications
Poly(trimethylene carbonate)	Sutures, orthopaedic applications
Natural resorbable polymers	
Poly(hydroxybutyrate) and poly(hydroxyvalerate)	Drug delivery, orthopaedic applications, stents, artificial skin, surgical patching materials for congenital heart defects, sutures
Collagen	Drug delivery, gene delivery, artificial skin, coatings to improve cellular adhesion, guided tissue regeneration, spinal dural repair, orthopaedic applications, soft tissue augmentation, tissue engineering, scaffold for blood vessel reconstruction, wound closure, haemostatic agents
Fibrinogen and fibrin	Tissue sealant, cell delivery
Elastin-like peptides	Drug delivery, coating of vascular grafts
Natural resorbable polymers	
Gelatin	Capsule coating for oral drug delivery, haemorrhage arrester
Hyaluronic acid	Wound dressing applications, drug delivery, tissue engineering, synthetic bone grafts, synovial fluid substitutes
Cellulose	Adhesion barrier, haemostat
Various polysaccharides (e.g. chitosan, alginate)	Drug/vaccine delivery, encapsulation of cells, sutures, wound dressings/healing
Starch and amylose	Oral drug delivery

The most frequently used bioresorbable polymers for the production of scaffolds for bone tissue engineering are those in the group of poly(α-

hydroxy esters), such as poly(glycolic acid) (PGA), poly(lactic acid) (PLA), poly(lactic-co-glycolic acid) (PLGA) and poly(caprolactone) (PCL). These polymers may be either semicrystalline (e.g. PGA, PCL) or amorphous (e.g. PLGA). Semicrystalline polymers have regular repeating units that allow the chains to fold into dense regions called crystallites, which act as crosslinks and give the polymer higher tensile strengths and higher modulus (i.e. stiffness) than the amorphous forms. However, as no polymer can completely organise into a crystalline material, many amorphous regions remain between the crystallites in semicrystalline polymers. When a semicrystalline polymer is heated to a temperature above its melting point it may be shaped into moulded parts. Amorphous polymers and the amorphous regions in semicrystalline polymers also exhibit a glass transition temperature. If they are heated above that temperature, the polymers will behave rubber-like, while below that point they will behave more like a glass. These properties will affect their mechanical and degradation characteristics (Middleton and Tipton, 2000).

PGA is a highly crystalline, hydrophilic, linear aliphatic poly(ester) with a high melting point and relatively low solubility in most common organic solvents. PLA is also a linear poly(ester) which is usually easily dissolved in common organic solvents such as chloroform, methylene chloride, methanol, ethanol, benzene, acetone, dioxane, dimethylformamide and tetrahydrofuran. The presence of an extra methyl group in the molecule results in a more hydrophobic and amorphous character than PGA. That methyl group also creates a chiral centre, forming two enantiomeric forms of the polymer, P(D)LA and P(L)LA. The most frequently used form is P(L)LA. Through the co-polymerisation of PGA and PLA it is possible to control the physical and mechanical properties of the polymers formed, with most co-polymers exhibiting an amorphous character and degradation rates that depend on the relative amount of each co-monomer. Those with high or low PGA:PLA ratios are less sensitive to hydrolysis than those with more equal ratios, mainly due to their greater crystallinity. Finally, PCL is a linear, hydrophobic, semi-crystalline polymer which is capable of forming blends and co-polymers with a wide range of molecules (Suggs *et al.*, 2007). A detailed description of PCL

will be presented in section 2.4.2 of this review. Table 2.13 presents the thermal, mechanical and degradation characteristics of PGA, PLA, and PCL, as well as various enantiomers and co-polymers. Bone was included as a reference material.

Table 2.13. Physical, mechanical and degradation properties of selected bioresorbable polymers from the poly(α-hydroxy ester) group and copolymers. PGA=Poly(glycolic acid); P(L)LA=Poly(L-lactic acid); P(DL)LA=Poly(DL-lactic acid); PCL=Poly(caprolactone); PLGA=Poly(lactic-co-glycolic acid). Adapted from Middleton and Tipton (2000) and Wang *et al*. (2010).

Polymer	Melting Point (°C)	Glass transition temperature (°C)	Tensile modulus (GPa)	Elongation (%)	Degradation time (months)
PGA	225-230	35-40	7.0	15-20	6 to 12
P(L)LA	173-178	60-65	2.7	5-10	> 24
P(DL)LA	Amorphous	55-60	1.9	3-10	12 to 16
PCL	58-63	(-65)-(-60)	0.4	300-500	> 24
85/15 PLGA	Amorphous	50-55	2.0	3-10	5 to 6
75/25 PLGA	Amorphous	50-55	2.0	3-10	4 to 5
65/35 PLGA	Amorphous	45-50	2.0	3-10	3 to 4
85/15 PLGA	Amorphous	45-50	2.0	3-10	1 to 2

2.4.2 Poly(Caprolactone)

PCL is an aliphatic, hydrophobic, semi-crystalline polymer which is soluble in chloroform, dichloromethane, carbon tetrachloride, benzene, toluene, cyclohexanone and 2-nitropropane at room temperature. It has a low solubility in acetone, 2-butanone, ethyl acetate, dimethylformamide and acetonitrile and is insoluble in alcohol, petroleum ether and diethyl ether (Woodruff *et al.*, 2010). It may also be mixed with various other polymers, such as poly(vinyl chloride), poly(styrene–acrylonitrile) and nitrocellulose; and is mechanically compatible with others, such as poly(ethylene), poly(propylene) and natural rubber (Labet and Thielemans, 2009).

PCL degrades within several months to several years depending on the molecular weight, the degree of crystallinity and the conditions of degradation. The amorphous phase is degraded first, resulting in an increase in the degree of crystallinity while the molecular weight remains constant.

This is followed by the cleavage of ester bonds, resulting in mass loss. The degradation process is autocatalysed by the carboxylic acids liberated during hydrolysis and by enzymes, resulting in faster decomposition (Labet and Thielemans, 2009).

The low glass transition temperature of PCL (i.e. -65°C - -60°C) means that it always exists in a rubbery state at room temperature, making it a highly permeable polymer (Suggs *et al.*, 2007). This, along with its biocompatibility and controlled degradability, makes it a very useful polymer for biomedical applications such as scaffolds for tissue engineering, sutures, drug-delivery systems, wound dressings, contraceptive devices, internal fixation devices for bone fractures and dental treatments. Other applications where PCL has been frequently used include microelectronics, adhesives and packaging (Labet and Thielemans, 2009; Woodruff *et al*., 2010).

The main method used to synthesise PCL is the ring opening polymerisation of ε-caprolactone (Figure 2.8). This can be achieved through four mechanisms which depend on the catalyst employed: anionic, cationic, monomer-activated and coordination-insertion ring opening polymerisation (Labet and Thielemans, 2009). Each mechanism affects the resulting molecular weight, molecular weight distribution, end group composition and chemical structure of the co-polymers (Woodruff *et al*., 2010) The alternative method to synthesise PCL is the polycondensation of 6-hydroxycaproic (6-hydroxyhexanoic) acid. However, the ring opening polymerisation of ε-caprolactone is usually the preferred route as it gives polymers with higher molecular weight and lower polydispersity (Labet and Thielemans, 2009).

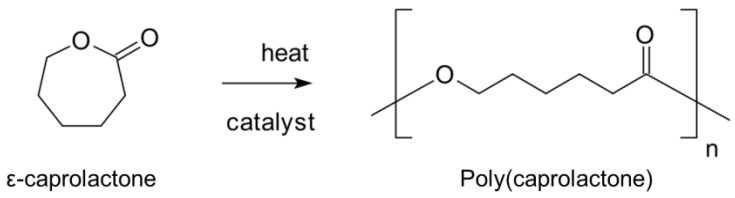

Figure 2.8. Schematic diagram of the synthesis of poly(caprolactone) from the ring form of ε-caprolactone to the polymerised form.

PCL may be processed using a wide range of techniques, including electrospinning (Woodruff *et al.*, 2010). The vast majority of the research work involving the electrospinning of PCL has been done using polymers with average molecular weight ranging from 65000 Da to above 80000 Da, providing the viscosity necessary for the electrospun jet to be formed. Solvents regularly used are DMF, DCM, chloroform, methanol, hexafluoroisopropanol and tetrahydrofuran (Cipitria *et al.*, 2011).

2.4.3 Mechanisms of degradation and resorption

There are two main mechanisms through which polymer bonds can be broken: passively, by hydrolysis; and actively, by enzymatic reaction (Gopferich, 1996). The main mode of degradation for most synthetic polymers is through hydrolysis, while the enzymatic reaction is generally only available for naturally occurring polymers such as poly(saccharides) and proteins.

The factors determining the rate of the hydrolytic reaction are the type of bond within the polymer backbone, pH of the environment, copolymer composition, and water uptake (Gopferich, 1996). Anhydrides and ortho-ester bonds are the most reactive, followed by esters and amides. Environmental pH can promote degradation through acid or base catalysis, resulting in the fastest degradation rates at low and high pH values. The introduction of other type of monomer into the polymer chain can influence material properties such as crystallinity and glass transition temperature, causing indirect effects on the degradation rates which depend on the prevailing type of bond. Finally, with respect to water uptake, hydrophilic polymers can take up larger amounts of water than hydrophobic polymers and, thus, their degradation rates may increase. As hydrolysis is a bimolecular reaction, the reaction velocity will be determined by the ‘concentration’ of the reagents and a larger content of water will result in a faster reaction.

In semicrystalline bioresorbable polymers the hydrolytic process occurs in two phases (Middleton and Tipton, 2000). In the first phase water penetrates the bulk of the material, preferentially attacking the chemical bonds in the

amorphous regions. This results in the conversion of long polymer chains into shorter, water-soluble fragments, as represented in Figure 2.9. Because this occurs in the amorphous regions, the molecular weight of the polymer will be reduced without incurring into significant losses of physical properties since the matrix is held together by the crystalline regions. However, the physical properties of the structure will eventually be negatively affected as water begins to fragment the crystalline regions as well.

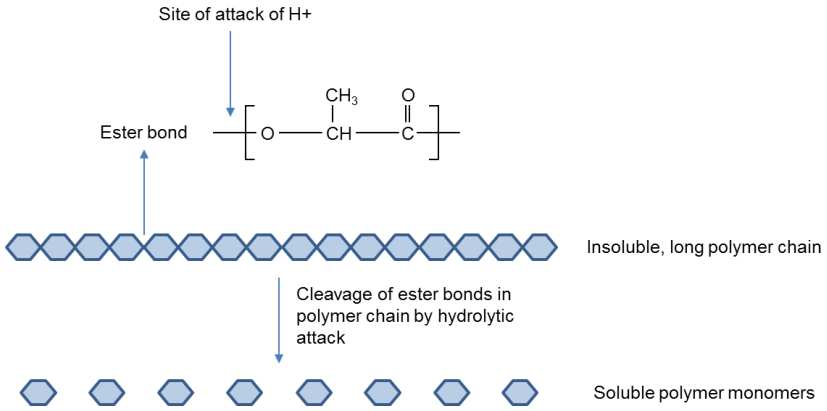

Figure 2.9. Schematic diagram of hydrolytic degradation of poly(α-hydroxy ester) polymers from insoluble, long polymer chains to soluble polymer monomers.

In the second phase, the metabolising of the smaller fragments results in a rapid loss of polymer mass. The degradation by-products of bioresorbable polymers such as poly(glycolic acid), poly(lactic acid) and poly(caprolactone) are metabolised through the citric acid cycle (Figure 2.10).

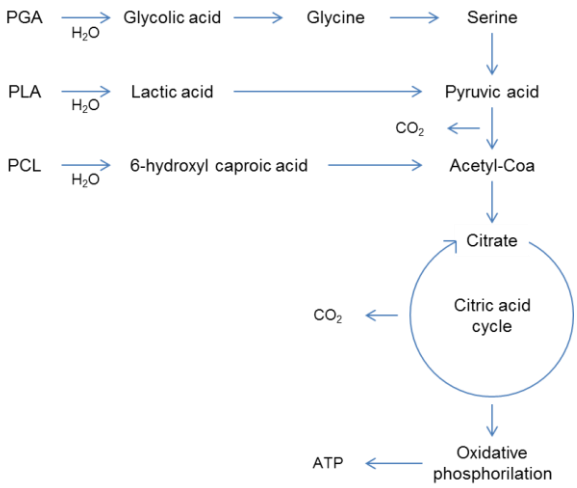

Figure 2.10. Routes of degradation and excretion of some poly(α-hydroxy ester) polymers: poly(glycolic acid) (PGA), poly(lactic acid) (PLA) and poly(caprolactone) (PCL). Adapted from Santos Jr (2010) and Woodruff and Hutmacher (2010).

Therin *et al*. (1992) reported that the degradation process at the surface of poly(lactic-co-glycolic acid) implants initially occurs more rapidly due to a greater availability of water. The degradation by-products at the surface are then dissolved in the surrounding fluid. In the interior of the material, however, the inability of degradation by-products to diffuse away results in the development of a local acidic environment that further catalyses polymer degradation and accelerates hydrolysis.

The location of the device plays an important role in the degradation rate of implants as well, as large devices implanted in areas with poor vascularization may degrade and overwhelm the body's ability to eliminate degradation by-products. This may lead to a build-up of acidic by-products and the development of an acidic environment that will catalyse the further degradation and cause further reduction in pH. The local reduction in pH may also be responsible for adverse tissue reactions. The metabolical routes through which the degradation products of some poly(α-hydroxy esters) are eliminated are shown in Figure 2.10.

All bioresorbable polymers suffer erosion when degrading. Depending on the way this process occurs, it may be possible to differentiate between surface (heterogeneous) and bulk (homogeneous) eroding polymers (Gopferich, 1996). Surface eroding polymers will gradually lose material from their surface, decreasing in size while maintaining the original shape of the device and its structural integrity. In the case of bulk eroding polymers, the process will occur throughout the whole structure and, as a result, the size of the device will be maintained while its structural integrity is diminished. Figure 2.11 shows a schematic representation of how these two processes affect a polymeric device.

The distinction between a surface eroding and a bulk eroding polymer will depend on several factors (Treiser *et al*., 2013). The chemistry of the polymer will determine the rate at which water is transported into the device. In bulk eroding polymers water penetrates the device at a faster rate than the rate at which the material is degraded into water-soluble fragments, resulting in the formation of cracks throughout the whole structure and in its final

disintegration into small fragments. In surface eroding polymers the material severely limits the rapid penetration of water and the rate at which the material is degraded into water-soluble fragments is fast, limiting the erosion process to the surface of the device. The architecture will also play a significant role, as sizes above certain critical thickness, specific for each polymer, will result in surface erosion, while sizes below that will result in bulk erosion (Von Burkersroda *et al*., 2002). The main advantage of surface erosion is that, knowing the characteristics of the polymer used, it may be possible to predict the outcomes of the erosion process, which may be interesting for applications such as drug delivery.

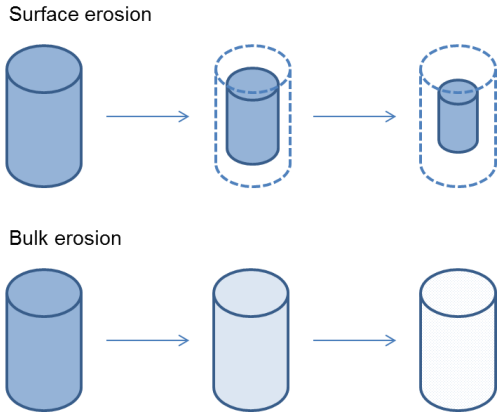

Figure 2.11. Schematic diagram of surface erosion and bulk erosion processes on a polymeric device. Adapted from Gopferich (1996).

Finally, it is known that the degradation process of synthetic polymers may also be influenced by biological activity (Williams and Zhong, 1995; Azevedo and Reis, 2004). Inflammation is usually observed in the region where a biomaterial has been implanted, especially at the implant-tissue interface, resulting in the release of elevated concentrations of hydrolytic enzymes which may potentially accelerate the degradation of the implant. For example, cholesterol esterase presents a high level of activity towards polyurethanes, proteinase K is able to accelerate the degradation of poly(L-lactic acid) and lipase is able to catalyse the hydrolysis of poly(caprolactone). Additionally, chemical and enzymatic oxidation may play an important role in the degradation of various polymers. Leukocytes and macrophages are able to produce highly reactive oxygen species during inflammation, such as superoxide (O_2^-) and hydrogen peroxide (H_2O_2), which may induce polymer

chain cleavage and thus contribute to the degradation of the implant. Many oxidative enzymes use dioxygen (O_2) as a substrate, incorporating it into other substrates during the reaction (i.e. oxygenase) or using it as an acceptor of electrons (i.e. oxidase), and may play an important role in the degradation of implanted polymeric devices (Williams and Zhong, 1995). For example, Beranova *et al*. (1990) discovered that a multi-enzyme monoxygenase system with cytochrome P450 in the microsomal fraction of mouse and rat livers had a significant effect on the degradation of poly(ethylene). Santerre *et al.* (1994) and Labow (1999) investigated the effect of horseradish peroxidase, catalase and xanthine oxidase on poly(urethanes) but these oxidative systems were not able to induce the polymer degradation (Azevedo and Reis, 2004).

2.4.4 Cell-polymer interactions

Cell adhesion to a substrate is necessary for good implant-cell interaction. Several factors associated with the characteristics of the polymer surface will play an essential role in the ability of cells to attach, proliferate and differentiate (Santos JR, 2010). Additionally, any material implanted in the body will become quickly coated with proteins from the surrounding fluids. Many of the subsequent implant-cell interactions will depend on, or derive from, the composition of that layer of proteins (Saltzman and Kyriakides, 2007).

Factors such as the presence of polar groups on the surface of the polymer and its wettability have an effect on the adsorption of proteins and cell adhesion. Cell adhesion appears to be maximised on surfaces with intermediate wettability. For most surfaces, adhesion requires the presence of tissue culture serum, which indicates that this is probably associated with the ability of proteins in the serum to adsorb to the surface. In the absence of serum, cell adhesion is enhanced on positively charged surfaces (Saltzman and Kyriakides, 2007).

It is also possible to generate polymer surfaces more suitable for cell adhesion and proliferation by surface modification. For example, polystyrene substrates used in tissue culture applications are usually treated by glow

discharge or exposure to chemicals to increase the number of charged groups, improving cell attachment and growth. Again, the effect of these modifications seems to be also associated with the ability of proteins to adsorb on the surface, providing points of cell attachment. However, certain chemical groups at the polymer surface, such as hydroxyl (-OH) or surface C-O functionalities, may play important roles in modulating the fate of attached cells and it may influence cell interactions *in vivo*. For example, the ability of macrophages to form multinucleated cells on the surface varies depending on the chemical groups present (Saltzman and Kyriakides, 2007).

The use of bioresorbable polymers increases the complexity of these issues *in vivo*, as the presence of degradation by-products may cause additional and prolonged consequences on attached cells and surrounding tissues. The effects will mainly depend on the chemical properties of the polymer and are not difficult to determine, especially in the case of those by-products released through hydrolysis or enzymatic digestion. However, the effects of by-products released due to cellular activity are more difficult to predict because all the chemical and biological mechanisms have not been clearly described (Saltzman and Kyriakides, 2007).

2.5 Bioactive glasses

A bioactive material can be defined as a biomaterial ‘that elicits a specific response at the interface of the material, which results in the formation of a bond between the tissues and the implant’ (Hench, 1998)

Bioactive materials include ceramics, glasses and glass-ceramics. Once a bioactive material is implanted in the body, a series of biophysical and biochemical reactions occur at the implant-tissue interface, resulting in the formation of a bond via the formation of a biologically active layer of hydroxy-carbonate apatite. This layer provides the interfacial bonding and is chemically and structurally equivalent to the mineral phase of bone (Barone *et al*., 2010).

2.5.1 Bioactive glasses

Bioactive glasses were introduced in the late 1960s by Larry Hench (2006), when he developed a degradable glass with a composition close to a ternary eutectic in the Na_2O-CaO-SiO_2 diagram which provided a large amount of CaO with some P_2O_5 in a Na_2O-SiO_2 matrix. The first bioactive glass which was able to form a mechanically strong bond to bone *in vivo*, called 45S5 bioglass, was also developed by Hench and had the composition 46.1 mol% SiO_2, 24.4 mol% Na_2O, 26.9 mol% CaO and 2.6 mol% P_2O_5. The name 45S5 refers to both the SiO_2 content (45 wt%) and the Ca/P molar ratio. The adhesion strengths observed were equivalent to, or even greater, than the cohesive force of the implanted material or the tissue bonded to the implant (Hench and Wilson, 1984). There are three features that distinguish bioactive glasses from other glass compositions: <60 mol% SiO_2, high Na_2O and CaO content and high Ca/P ratios (Hench, 1998).

Figure 2.12 shows a ternary diagram representing the compositional dependence, in wt%, of Na_2O-CaO-P_2O_5-SiO_2 glasses to bond to bone and soft tissues. All the glass compositions represented have a constant 6 wt% of P_2O_5, while the proportion of the other three components will vary depending on the distance to each of the three vertices. The lines inside the triangle represent lines of iso-bioactivity.

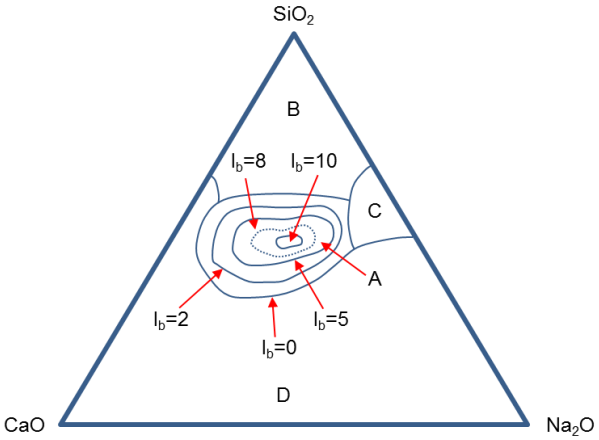

Figure 2.12. Ternary diagram showing the compositional dependence (in wt%) of bone and soft tissue bonding for Na_2O-CaO-P_2O_5-SiO_2 glasses. All compositions contain a constant 6 wt% of P_2O_5. I_b=Index of bioactivity. Adapted from Hench (1998).

Many of the glass compositions developed by Hench were characterised in terms of the index of bioactivity (I_b), which is a measure of the level of bioactivity of bioactive materials. I_b is defined as the inverse of the time required for more than 50% of the interface of the glass to bond to bone (Equation 2.1)

$$I_b = {}^{100}/_{t_{0.5}} \text{ (days}^{-1}\text{)} \qquad \textbf{Equation 2.1}$$

Glasses with compositions inside region A (I_b=5) are able to form a strong bond with bone. Those compositions in the region enclosed by the dashed line (Ib=8) are also able to bind to soft tissues. Compositions in region B are inert and will stimulate the formation of a fibrous tissue capsule surrounding the implant. Those in region C are resorbed within a period of 10 to 30 days, and those in region D cannot be produced (Hench, 1998; De Aza *et al*., 2007).

Bioactive glasses may be made using two routes: the melt-quenching route and the sol-gel route. The melt-quench route consists in melting together a series of oxides at high temperatures in platinum crucibles and then quenching the melt in graphite moulds, to produce rods or blocks; or quenching in water, to produce a frit. In the sol-gel route a solution containing the precursors of the bioactive glass undergoes a series of chemical reactions to form a gel, which is an inorganic network of covalently bonded silica. This can then be dried and heated to form a glass (Jones, 2013). Glasses produced through the sol-gel route tend to be more porous than those produced through the melt-quench route (Sepulveda *et al*, 2001), potentially increasing their solubility and bioactivity.

The fabrication of porous scaffolds made of bioactive glass has been investigated employing three main approaches: using melt-derived bioactive glass, using sol-gel derived bioactive glass and using additive manufacturing techniques (Jones, 2013). Porous scaffolds using melt-derived bioactive glasses are usually made with techniques involving the sintering of glass particles around a template. Alternatively, the sintering may be performed after a foaming process or after the advanced manufacturing of a desired

structure. The main issue of this approach is that bioactive glasses based on the composition of 45S5 bioglass tend to crystallise when heated at temperatures above their glass transition temperature, potentially affecting several properties including their bioactivity (Jones, 2013). Introducing different oxides in the glass composition, such as SrO or ZnO, may help by increasing the window of temperature at which the sintering may be performed (O'Donnell *et al.*, 2010; Oudadesse *et al.*, 2011). Scaffolds made with sol-gel derived bioactive glasses do not present this problem as they do not need to be heated at such high temperatures. Porous structures have been developed by adding a foaming step to the sol-gel process (Sepulveda *et al.*, 2002), creating hierarchical pore structures with interconnected macropores (Jones and Hench, 2004). Finally, the pore morphology can be controlled more efficiently using additive manufacturing techniques, by building the structure layer by layer (Jones, 2013). For example, porous structures have been fabricated using lithography-based additive manufacturing technologies (Tesavibul *et al.*, 2012).

2.5.2 Atomic structure of bioactive glasses

The properties of bioactive glasses with respect to its dissolution rate and the rate of formation of the HCA layer are directly related with its atomic structure.

Zachariasen (1932) developed a theory to explain the atomic arrangement in glass which derived from the observation that, over large ranges of temperature, the mechanical properties of glasses and crystals are comparable and, thus, the forces that link the atoms in both materials must essentially be the same. Therefore the atoms in glass must form extended three-dimensional networks, similar to those in crystals. However, these networks are neither periodic nor symmetrical and no two atoms are structurally equivalent. Figure 2.13 shows a two-dimensional schematic representation of the atomic network in crystalline oxides and vitreous oxides.

In oxide glasses the oxygen atoms form polyhedra around a central atom, creating the geometric unit of the glass network. The connection between

every geometric unit is achieved by the sharing of corners between different polyhedra. Those cations which can form a glass structure such as this are called network formers and usually exhibit small ionic radii and large valences. In the specific case of vitreous silica (i.e. pure SiO_2) the glass structure consists of a three-dimensional network of SiO_4 tetrahedra. Each tetrahedron is formed by four oxygen atoms surrounding a central silicon atom and is linked to four other tetrahedra through an oxygen atom common to both units.

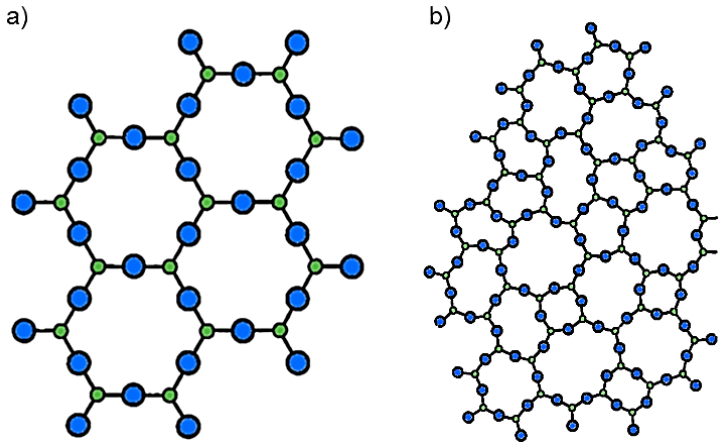

Figure 2.13. Two-dimensional schematic representation of the atomic network in: a) a crystalline oxide and b) a vitrous oxide. The large blue circles represent oxygen atoms and the smaller green circles represent network-forming cations. Adapted from Zachariasen (1932).

Ray (1974) proposed that silicate glasses may also be considered as polymers of oxygen with a cross-linked network structure that can have different packing densities and varying degrees of cross-linking. The network may be formed by alternating oxygen atoms with intermediate atoms such as boron, silicon and phosphorus. It may also contain other cations which can terminate the chains and reduce the connectivity of the network, altering the density of packing of the oxygen atoms. These factors may have an important effect on the properties of the glass.

When the silicate glass contains other ionic components than silica, as in bioactive glasses, the network structure is modified. These cations, usually known as network modifiers, have large ionic radii and low valences, and will occupy the empty spaces in the network. When this happens some of the oxygen atoms will no longer be bonded to two silicon atoms and are said to

be non-bridging oxygens (NBOs), created to compensate the charge brought by the addition of the modifier cations. The distribution of NBOs over the tetrahedron unit is characterised in terms of a quantity known as Q^n, where n refers to the number of bridging oxygens on the tetrahedron: Q^3 units are tetrahedra with one NBO, Q^2 units have 2 NBOs, and so on. This can also be characterised in terms of the network connectivity (NC), which measures the average number of bridging oxygens on each tetrahedron. For example, vitreous silica has a NC value of four, while a structure comprised of strings of tetrahedra would have a NC value of two. NC has been found to be useful to predict different properties of bioactive glasses, particularly their bioactivity (Hill, 1996; Hill and Brauer, 2011).

Melt-derived bioactive glasses contain considerable amounts of network modifiers. In the particular case of 45S5 bioglass silicon is the network former, generating Si-O-Si bonds, and sodium and calcium are the network modifiers, disrupting the glass network and forming NBOs. Phosphorus, according to nuclear magnetic resonance analysis (Elgayar *et al.*, 2005; Pedone *et al*., 2010), is present in an orthophosphate environment (i.e. Q^0 unit) with charges balanced by sodium and/or calcium and not forming P-O-Si bonds. This means that phosphorus is isolated from the silica network and prevents sodium and calcium from working as network modifiers. P-O-Si bonds can actually be observed in glasses with more than 50 mol% of phosphorus (Li *et al*., 2011), becoming phosphate glasses.

The connectivity of the silica network in bioactive glass depends on the composition. For example, a high content of silica will generate a highly connected network with a large proportion of bridging oxygen (BO) bonds (i.e. high NC values), resulting in low dissolution and low bioactivity. The NC of the glass can then be lowered by adding network modifiers, such as calcium or strontium. However, it can be increased by adding a larger proportion of phosphorus, resulting in the repolymerisation of the silicate network due to the extraction of network modifiers in order to counter-balance the charges introduced by phosphorus (Mercier *et al*., 2011). In melt-derived glasses the composition in mol% can be used to calculate the NC value. Assuming that phosphorus is in the form of orthophosphate and

not part of the silica network (i.e. no formation of P-O-Si bonds) the NC value for 45S5 bioglass has been reported to be 2.12 (Jones, 2013). Edén (2011) suggested a range of NC values between 2.0 and 2.7 for optimal glass bioactivity, with greater values indicating that the glass will likely be not bioactive due to resistance to dissolution. A previous model of NC (Hill, 1996), which assumed that phosphorus entered the silica network forming P-O-Si bonds, reported NC values of 1.90 for 45S5 bioglass. However, as phosphorus was shown not to enter the silica network in bioactive glasses (Elgayar *et al.*, 2005; Pedone *et al.*, 2010), this earlier model was superseded replaced by the later model (Hill and Brauer, 2004).

In conclusion, the composition of a bioactive glass should be designed in such a way that its bioactivity is optimised for any particular application. Since bioactivity tends to be enhanced by relatively low silicate network polymerisation or by large amounts of orthophosphate groups, these two factors should be taken in account when designing bioactive glasses (Mathew *et al.*, 2013): first, the network connectivity should present values corresponding to open structures mainly built by Q^3 and Q^2 units (i.e. <2.7), which will readily degrade when exposed to an aqueous environment; and second, the negative charges of the phosphorus content, present as orthophosphate anions dispersed across the glass matrix, should be balanced by the positive charges of the network modifier cations in order to increase solubility and bioactivity. The composition 45S5 bioglass is often considered as the one that presents the best biological properties of all bioactive glasses. Therefore, it is not surprising that it has been thoroughly investigated and frequently used as the basis for the development of other compositions (Jones, 2013)

2.5.3 Mechanism of activity of bioactive glasses

The mechanism of bonding to bone has been attributed to the formation of a layer of hydroxy-carbonate apatite (HCA) on the glass surface, which is able to interact with collagen fibrils in bone tissue to form a strong bond (Hench, 1998). This HCA layer is formed through a time-dependent modification of

the glass surface, which occurs in five stages in physiological fluids or in simulated body fluids (SBF) *in vitro*:

1) Rapid exchange of Na^+ and/or Ca^{2+} with H^+ from solution, creating silanol bonds (Si-OH) on the glass surface. This results in an increase of the pH and the creation of a region rich in silica near the surface.
2) The high pH results in an attack of the silica glass network by OH^-, breaking Si-O-Si bonds. More Si-OH bonds are formed on the surface.
3) Condensation of the Si-OH groups on the surface, forming a silica-gel layer.
4) Migration of Ca^{2+} and PO_4^{3-} groups to the surface from the solution, forming a film rich in $CaO\text{-}P_2O_5$ on the silica-gel layer.
5) Incorporation of hydroxyls and carbonate from solution and crystallisation of the $CaO\text{-}P_2O_5$ film into HCA.

Glass composition has a great effect on the rate of HCA formation and bone bonding. For example, a lower content in silica will result in a less connected glass network and higher dissolution rates, accelerating the stages listed above. As bioactivity has been related to the connectivity of the glass network, it will depend on silica content and the presence of other cations in the glass composition.

According to Hench and Best (2013), the interfacial reactions that lead to the formation of a strong bond of bioactive glass with bone tissue are:

1) Adsorption of biological components on the HCA layer.
2) Action of macrophages.
3) Bonding of osteoprogenitor stem cells.
4) Differentiation of osteoprogenitor stem cells.
5) Production of extracellular matrix.
6) Mineralisation of the extracellular matrix.

However, the stages after the HCA layer is formed are not well defined and are still under extensive investigation. It is known that the adsorption of proteins from serum attracts macrophages, mesenchymal stromal cells and

osteoprogenitor cells. For example, fibronectin, a major glycoprotein in serum, is known to increase the attachment of osteoblasts to the calcium phosphate layer (El-Ghannam *et al*., 1999). Additionally, the adsorption of proteins may affect the surface reactions forming the HCA layer, interfering in the maturation of the amorphous calcium-phosphate layer to crystalline hydroxyapatite (Ducheyne and Qiu, 1999). The attachment of osteoprogenitor stem cells, and their proliferation and differentiation towards the osteoblastic phenotype, is suggested to occur within 24 to 48 hours, beginning the production of various growth factors which further stimulate cell proliferation and the production of extracellular matrix. The mineralisation process will begin shortly after, with mature osteocytes being the final result by 6 to 12 days both *in vitro* and *in vivo* (Hench and Best, 2013).

Additionally, bioactive glasses are able to induce the formation of bone on the glass apart from the implant-bone interface (Jones, 2013). Xynos *et al*. (2000a, 2001) showed that the release of critical concentrations of calcium and silicon ions from the composition 45S5 bioglass had an important effect in the control of human osteoblast cell cycle. Seven families of genes involved in processes associated with osteoblast metabolism and bone homeostasis were activated. Xynos *et al.* (2000b) also reported a significant increase in the production by human osteoblasts of insulin-like growth factor II (IGF-II), a potent growth factor that induces cellular proliferation, suggesting that the stimulatory effect of bioactive glass dissolution products may have been mediated by IGF-II. Various studies have been performed investigating this topic, as reviewed by Hench (2009), in cells from various sources.

Regarding the study of the osteogenic effect on MSCs, Radin *et al*. (2005) reported that the presence of 45S5 bioglass resulted in increased levels of alkaline phosphatase activity cultured both in contact with the samples and apart from them, suggesting that the glasses had a stimulatory effect on the osteoblastic differentiation of the cells. Yao *et al.* (2005) reported an increased expression of alkaline phosphatase, osteocalcin and bone sialoprotein in RNA extracted from rat MSCs exposed to the dissolution products released from PLGA microspheres containing 45S5 bioglass

particles. Bosetti and Cannas (2005) also showed that the dissolution of calcium ions and silica from the glass stimulated cell proliferation and the production of growth factors and extracellular matrix on rat bone marrow cells. However, Reilly *et al.* (2007) reported that human MSCs generally produced significantly lower levels of alkaline phosphatase activity than rat MSCs when exposed to bioactive glasses. No significant differences were observed in human MSCs cultured in 45S5 bioglass and cell culture plastic and no consistent effects were observed in response to bioactive glass dissolution, suggesting that the beneficial effects of bioactive glass on bone regeneration may not be mediated by an accelerated differentiation of MSCs. Karpov *et al.* (2008) observed the differentiation of human MSCs into osteoblasts and osteoclasts when the cells were cultured on bioactive glass produced through the sol–gel route with low silica content. However, when the glass used had high silica content the cells differentiated only into osteoblasts.

2.5.4 Strontium substitution in bioactive glasses

Strontium is a chemical element which is mainly present in bones, although it can also be found in muscles and physiological fluids. It also has a role in the endocrine system, acting in a similar way to calcium. Most of the administered strontium is deposited on bone tissue, substituting calcium in hydroxyapatite, and is preferentially incorporated into new bones and in trabecular bone. In overall, the total content of strontium in bone is significantly lower than the amount of calcium (Nielsen, 2004).

Currently, strontium is used as a treatment for osteoporosis, a disease characterised by low bone mass and susceptibility to fracture, in the form of strontium ranelate (Marie, 2005). This drug has proved to be an effective treatment, acting through a mechanism combining the inhibition of bone resorption and the stimulation of new bone tissue formation (Marie *et al*, 2001). A study by Sila-Asna *et al*. (2007) showed that strontium was able to stimulate the differentiation of human mesenchymal stromal cells into osteoblasts, enhancing the expression of certain osteogenic genetic markers, as well as increasing the levels of alkaline phosphatase activity.

Pharmacological analyses from preclinical studies have shown that strontium is able to modulate bone cell recruitment and activity through modulation of the calcium sensing receptor (CaSR), extracellular-signal-regulated kinase 1/2-mitogen-activated protein kinase (ERK1/2-MAPK), nuclear factors of activated T-cells (NFATc) and Wnt signalling pathways. This results in decreased bone resorption and increased, or at least maintained, bone formation in models with lower bone mineral density (Saidak and Marie, 2012).

The inclusion of strontium in bioactive glasses has received the attention of different researchers. This can be done by substituting calcium in their composition and it may be an effective way of delivering a source of strontium ions into defect sites. Several studies have been dedicated to understanding the effect of the strontium substitution on glass formation, its properties and its mechanism of bioactivity using experimental (Fredholm *et al*., 2010, 2011; O'Donnell *et al*., 2010) and molecular dynamic simulation approaches (Xiang and Du, 2011; Du and Xiang, 2012). The potentially enhanced osteogenic effect of these glasses on osteoprogenitor cells has also been investigated (Gentleman *et al*., 2010; Isaac *et al*., 2011; Li *et al*., 2012b). In general, it has been reported that increasing the proportion of strontium substitution results in an increase of glass density (Fredholm *et al.*, 2010) and a decrease of glass transition temperature (Fredholm *et al*., 2010; O'Donnell *et al*., 2010). Molecular dynamic simulations (Xiang and Du., 2011; Du and Xiang, 2012) and solid-state NMR data (Fredholm *et al*., 2010, 2011) have agreed that network connectivity does not change with the substitution. *In vitro* studies on osteoblasts and osteoclasts (Gentleman *et al*., 2010) showed that strontium-substituted bioactive glasses were able to increase osteoblast metabolic activity, proliferation and alkaline phosphatase activity, while osteoclast differentiation and bone resorption was inhibited. Isaac *et al*. (2011) studied a strontium-substituted bioactive glass manufactured through the sol-gel process on foetal mouse calvarial cells, observing greater alkaline phosphatase activity and the up-regulation of several genetic markers, including alkaline phosphatase, type I collagen and osteocalcin. *In vivo* studies have also been performed (Gorustovich *et al*., 2010) to study the

osteoconductivity of these glasses. Although a good bone-bonding ability was observed, it is important to note that the substitution of calcium by strontium was made on a weight basis rather than on a molar basis. As strontium is heavier than calcium, replacing an equivalent weight of strontium will result in a smaller amount of strontium atoms in the glass than there were calcium atoms. It was suggested by O'Donnell and Hill (2010) that this will result in an increase of the network connectivity and a potential reduction of glass bioactivity, making it difficult to compare between different glass compositions.

2.6 Summary

The regenerative capacity of bone tissue means that it can repair itself in response to injury. However, surgical intervention may be necessary when the defects are large and the conditions required for the tissue regeneration process to occur are missing, especially in older patients.

The clinical procedure that presents the best clinical outcomes is the transplantation of autogenous bone grafts. However, there are significant issues that can complicate the treatment, such as the limited amount of bone which can be obtained from the patient. Allografts and xenografts may also be used for this purpose, but the risk of disease transmission and immune rejection make other alternatives be preferred over these.

The pressing clinical needs created by these issues have led to the use of materials of diverse composition as bone substitutes and to the development of novel approaches to tissue regeneration, such as tissue engineering. Bone tissue engineering will require the creation of scaffolds with appropriate characteristics to support the formation of new bone tissue: the scaffolds should be made of biocompatible and bioresorbable materials; they should be sterilised without compromising its characteristics; and the composition and architecture of the scaffolds should facilitate cell attachment, proliferation, differentiation and the formation of new blood vessels that will guarantee its viability.

Electrospinning is a versatile method which may be used to generate fine fibres through the application of electrostatic forces to polymeric solutions or melts. This technique has received significant attention for the fabrication of scaffolds for tissue engineering because the membranes produced are highly porous and exhibit large-specific surface areas. Bioresorbable polymers, such as poly(α-hydroxy esters), are generally favoured to fabricate electrospun scaffolds as they degrade through time without generating toxic by-products and may be resorbed by the body after implantation without inducing serious side-effects. Their bioresorption also means that a second surgery to remove the implant is eliminated, being eventually replaced by the new bone tissue as the regeneration process occurs.

Composite materials with potentially improved biological characteristics may also be fabricated using electrospinning by combining bioresorbable polymers and particles of different bioceramics or bioactive glasses, resulting in structures which may display the chemical and mechanical properties of both materials simultaneously. Bioactive glasses are of particular interest for this purpose, as their dissolution in an aqueous environment and subsequent surface changes may encourage the formation of new bone tissue. Additionally, their composition may be modified to include the presence of additional chemical elements which may enhance the osteogenic effect of the material, such as strontium.

The strontium cation has been reported to encourage the formation of new bone tissue by stimulating osteoblasts and inhibiting osteoclasts when used as part of the osteoporotic drug strontium ranelate. The substitution of calcium by strontium in bioactive glasses and its effect on different material and biological properties has been investigated by several researchers, reporting that it may indeed present a similar osteogenic effect and may potentially encourage the formation of new bone tissue as well.

3 Aim and objectives

Electrospun membranes have significant potential to be used as scaffolds for bone tissue engineering as they exhibit high porosity and large specific surface areas. Additionally, electrospun composite materials may be produced by incorporating ceramic or glass particles within the fibres, potentially enhancing its biological properties.

Recently, strontium-substituted bioactive glasses have received the attention of several researchers as a potential material to be used in bone regeneration applications (Lao *et al.*, 2009; Gentleman *et al.*, 2010; Gorustovich *et al.*, 2010; O'Donnell *et al.*, 2010; Isaac *et al.*, 2011). It has been reported that these glasses have the ability to encourage the formation of new bone tissue through the release of the strontium cation in dissolution and its subsequent action on bone cells. Hence, these glasses may form the basis of promising new materials for bone tissue regeneration. However, relatively little work has been directed towards the use of strontium-substituted bioactive glasses in systems aimed to be used as scaffolds for bone tissue engineering.

Thus, the aim of this project was to design and fabricate an electrospun composite material made of PCL, a bioresorbable polymer, and particles of strontium-substituted bioactive glass, and to evaluate its potential use as a scaffold for bone tissue engineering.

To achieve this, the following objectives were identified:

1) To fabricate a series of strontium-substituted bioactive glasses in which calcium is substituted by strontium in an increasing proportion based on the composition 45S5 bioglass.
2) To assess and discuss the effect of the strontium substitution on the physical properties of the glasses using a range of characterisation techniques; and on the mechanism of bioactive glass bioactivity based on the data obtained from the different experiments.
3) To optimise the electrospinning process to produce regular fibres in the experimental conditions available in the laboratory.

4) To fabricate and characterise a series of electrospun materials using PCL and particles of the strontium-substituted bioactive glasses.
5) To develop suitable methods to place additional bioactive glass particles on the surface of the electrospun fibres.
6) To study the *in vitro* biocompatibility of all the electrospun materials produced by assessing their cytotoxicity on cultures of a particular cell line.
7) To investigate the effect of the dissolution products of strontium-substituted bioactive glass on the viability of osteoprogenitor cells by assessing its cytotoxicity.
8) To study the potential osteogenic effect of the dissolution products of strontium-substituted bioactive glass on osteoprogenitor cells by measuring the expression of genes involved in the process of osteoblastic differentiation.

PCL was selected for this study because it is a biocompatible and bioresorbable polymer that may be processed using various techniques, including electrospinning. Additionally, PCL is a highly permeable polymer, making it suitable for the potential release of bioactive glass dissolution products from within the polymeric fibres. Finally, PCL was selected as it was not expected that the electrospun material would suffer structural shrinkage during incubation as it occurs with other bioresorbable polymers, such as PLGA (Li *et al*., 2006).

Electrospinning was selected because it is a versatile technique capable of generating fibres with diameters ranging from a few micrometers down to tens of nanometers, fabricating materials potentially capable of physically mimicking the extracellular matrix of bone tissue in terms of scale and structure. Additionally, it was considered a suitable technique to fabricate composite fibres combining PCL and particles of strontium-substituted bioactive glass. The resulting materials were considered to be a promising system to be used as a scaffold for bone tissue engineering. Alternative applications may be working as a filler of bone voids in non-load bearing sites of the skeleton or as a bioresorbable component in barrier membranes

for guided bone regeneration applications, where it may encourage bone growth in structures affected by periodontal disease.

On completion of this work, a novel electrospun composite biomaterial will be produced. A good understanding of the manufacturing process and of several physical and biological properties of the material will be gained, providing clear indications of its potential to be used as a scaffold in bone tissue engineering applications. Finally, a better understanding of the mechanism of bioactivity of these glasses may also be gained.

4 Materials and methods

4.1 Bioactive glass production and characterisation

4.1.1 Bioactive glass batch preparation and melting

Three bioactive glasses were produced (i.e. Sr0, Sr50 and Sr100) based on compositions published by O'Donnell *et al.* (2010), where Sr0 was based on the composition of the original 45S5 bioactive glass, initially reported by Hench (1998). Sr50 and Sr100 were compositions where CaO was substituted by SrO in proportions of 50 mol% and 100 mol% respectively. The substitutions were performed on a molar basis to maintain atomic proportionality in the glass structure. Table 4.1 presents the mol% and wt% compositions of each bioactive glass, as well as the raw materials used and the amounts required to produce 300 g of glass.

Analytical grade silicon dioxide, calcium carbonate, sodium carbonate, sodium phosphate (Fisher Scientific, UK) and strontium carbonate (Sigma Aldrich, UK) were thoroughly mixed and slowly loaded into a platinum crucible. Each batch was then melted in an electric furnace preheated to 1350 °C. After an initial hour of melting, the mixture was homogenised by continuous stirring using a rotating platinum paddle at a speed of 60 rpm for 2 hours.

Table 4.1. Molar percentage (Mol%), weight percentage (Wt%), raw materials and amounts required to obtain 300 g of Sr0, Sr50 and Sr100 bioactive glasses.

Bioactive glass	Oxide	Mol%	Wt%	Raw material	For 300 g glass
Sr0	SiO_2	46.13	45.00	SiO_2	135.0 g
	Na_2O	24.35	24.50	Na_2CO_3	85.4 g
	CaO	26.91	24.50	$CaCO_3$	131.2 g
	P_2O_5	2.60	6.00	Na_3PO_4	41.6 g
Sr50	SiO_2	46.13	40.77	SiO_2	122.3 g
	Na_2O	24.35	22.19	Na_2CO_3	77.3 g
	CaO	13.46	11.10	$CaCO_3$	59.4 g
	SrO	13.46	20.51	$SrCO_3$	87.7 g
	P_2O_5	2.60	5.44	Na_3PO_4	37.7 g
Sr100	SiO_2	46.13	37.26	SiO_2	111.8 g
	Na_2O	24.35	20.29	Na_2CO_3	71.0 g
	SrO	26.91	37.49	$SrCO_3$	160.2 g
	P_2O_5	2.60	4.97	Na_3PO_4	34.4 g

4.1.2 Processing of bioactive glass melts

A volume of each melt was poured into graphite moulds to produce blocks of bioactive glass of dimensions 60 x 20 x 15 mm. The blocks were annealed in an electric furnace for 1 hour at 518 °C for Sr0, 486 °C for Sr50 and 456 °C for Sr100. The annealing temperatures were based on the glass transition temperatures reported by O'Donnell *et al*. (2010) for each glass composition. Finally, all the glasses were cooled down to room temperature at a rate of 1 °C/minute.

The remaining melt from each composition was quenched in distilled water to form a frit and then left to dry overnight at room temperature. The frit was processed to reduce the particle size using a pellet crusher and then it was ball milled for a minimum time of 15 hours using cylindrical zirconia milling media (10 mm diameter). The resulting materials were sieved on stainless steel laboratory test sieves with aperture sizes of 150 μm and 45 μm (Fisher Scientific, UK) to obtain powders with particle size <45 μm.

4.1.3 XRD analysis of bioactive glasses

X-ray diffraction (XRD) analyses were performed on the bioactive glasses to confirm their amorphous nature. Samples of Sr0, Sr50 and Sr100 bioactive glasses and of PerioGlas® (Novabone Products LLC, USA), a commercial product made of 45S5 bioglass and used in periodontal bone regeneration, were grounded to a fine powder using a mortar and pestle and then sieved to obtain particles with sizes <45 μm. Each sample was loaded on sample trays and analysed in a Philips PW1825/00 diffractometer using Cu radiation, with angles ranging from 10° 2θ to 70° 2θ, step sizes of 0.02° 2θ, and a scanning speed of 2° per minute. XRD spectra were then processed using WinXPow software and Traces software.

4.1.4 DTA of bioactive glasses

The glass transition temperature (T_g), the onset of crystallisation temperature (T_c) and the peak crystallisation temperature (T_p) of Sr0, Sr50 and Sr100 bioactive glasses and of PerioGlas® were determined using differential thermal analysis (DTA). Samples from all the materials were grounded to a

fine powder using a mortar and pestle and then sieved to obtain particles with sizes <45 μm. The powders were then loaded into platinum crucibles and heated to a temperature of 1200 °C at a rate of 10 °C/minute in a Perkin-Elmer Diamond DTA/TG. The DTA patterns obtained were processed using the Pyris software (Perkin Elmer, UK) and mjograph 4.4.1 software (Ochiai Lab, Yokohama National University, Japan). T_g and T_c were determined from the point of intersection of curve tangents, and T_p was determined from the exothermic plot, as shown in Figure 4.1.

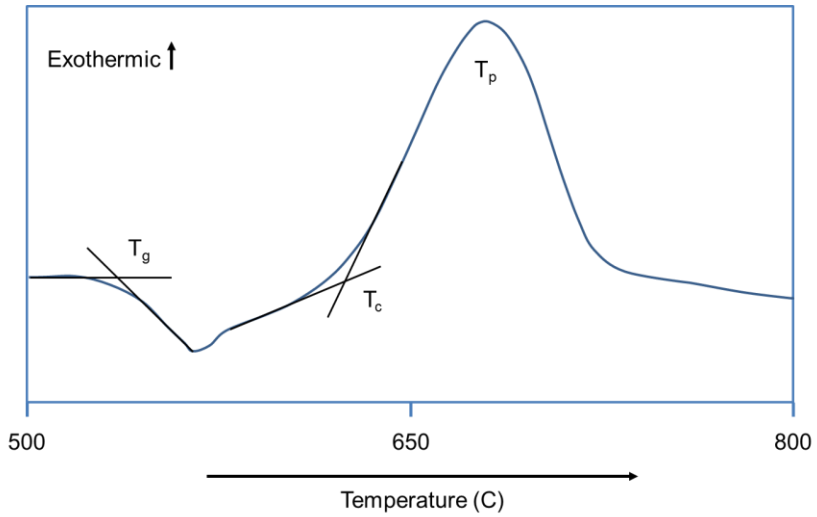

Figure 4.1. Determination of glass transition temperature (T_g), onset of crystallisation temperature (T_c) and peak crystallisation temperature (T_p) on a schematic representation of a differential thermal analysis pattern. Adapted from Clupper and Hench (2003).

4.1.5 Experimental measurement of the density of bioactive glasses

The density of Sr0, Sr50 and Sr100 bioactive glasses was determined using the Archimedean principle, which states that when a solid body is completely immersed in a fluid, then the volume of the body is equal to the volume of the displaced fluid. This makes it possible to derive a relationship (Equation 4.1) between the density and the mass of the fluid and the solid:

$$\rho_s = \rho_{fl} \cdot \frac{m_s}{m_{fl}} \qquad \textbf{Equation 4.1}$$

where ρ_s is the density of the body, ρ_{fl} is the density of the fluid, m_s is the mass of the body, and m_{fl} is the mass of the displaced fluid.

In this method, also known as the Archimedes method, the mass of the displaced fluid was measured by placing a beaker containing distilled water on a balance while the solid body was suspended from a thread and immersed in the beaker. Because the weight of the body ($W_s=m_s \cdot g$) was carried by the thread and the balance was not loaded, the balance readout indicated the mass of the displaced liquid, m_{fl}, assuming that the weight of the beaker was zeroed beforehand.

Three samples of each bioactive glass were produced from the glass blocks and were weighed on a precision weighing balance (0.1 mg in resolution). A beaker filled with distilled water was placed on the balance dish and the balance was zeroed. Meanwhile, the temperature of the distilled water was measured to determine its density. Each sample was then hung from a thread above the beaker, in such a way that the sample was completely immersed in the liquid without touching either the walls or the bottom of the beaker.

4.1.6 Theoretical glass density according to Doweidar's model

Doweidar's model of glass density (1996, 1999) may be used to estimate the density of a particular glass from the volume, mass and the molar composition of its Q^n structural units.

Each Q^n unit is structured as follows (Fredholm *et al.*, 2010):

1) One Si^{4+}
2) n/2 bridging oxygen (BO)
3) (4-n) non-bridging oxygen (NBO)
4) (4-n) alkali metal ions or (4n-2)/2 alkaline earth cations, to equilibrate the electronic charge if NBOs are present.

The addition of a modifier oxide R_2O/RO to the glass, where R is an alkali or an alkaline earth metal, creates NBOs in the SiO_2 network, modifying the number of NBOs in a way that depends on the concentration of the modifier oxide. For example, a Q^2 unit would contain one Si^{4+} atom, 1 BO, 2 NBOs, and 2 alkali metal ions or 3 alkaline earth cations.

According to Doweidar (1996, 1999), all Q^4 units are transformed into Q^3 before Q^2 units are formed, and all Q^3 units are transformed into Q^2 before Q^1 units are formed. Table 4.2 shows the compositional regions and type of unit conversion which occurs within each compositional range of modifier oxide R_2O/RO.

Table 4.2. Q^n units within the different compositional regions in alkali silicate glasses. Adapted from Doweidar (1996) and Fredholm *et al.* (2010).

Compositional region	Q^n unit formation
Up to 33.3 mol% R_2O/RO	Q^4 conversion to Q^3
33.3 mol% < R_2O/RO < 50 mol%	Q^3 conversion to Q^2
50 mol% < R_2O/RO < 60 mol%	Q^2 conversion to Q^1
60 mol% < R_2O/RO < 66.7 mol%	Q^1 conversion to Q^0

In this case the Sr0, Sr50 and Sr100 bioactive glass compositions were normalised to exclude the phosphate content. As a result, the total R_2O/RO concentration fell within the 33.3 mol% < R_2O/RO < 50 mol% region, and consequently the Q^n unit formation model was Q^3 to Q^2. The density was then calculated using the following equation:

$$\rho = \frac{(2-4x_t)(\sum_i \frac{x_i}{x_t} M_i^3) + (3x_t - 1)\left(\sum_i \frac{x_i}{x_t} M_i^2\right)}{(2-4x_t)(\sum_i \frac{x_i}{x_t} V_i^3) + (3x_t - 1)\left(\sum_i \frac{x_i}{x_t} V_i^2\right)} \qquad \text{Equation 4.2}$$

for i = a, b, c.

where x_a, x_b and x_c are the molar fractions; $x_t = x_a + x_b + x_c$; M_a^n, M_b^n and M_c^n are the masses; and V_a^n, V_b^n and V_c^n are the volumes of Na_2O, SrO and CaO Q^n units respectively. Table 4.3 presents the unit volumes of Q^3 and Q^2 units containing sodium, calcium and strontium.

Table 4.3. Volume of the Q3 and Q2 units containing sodium, calcium and strontium. Adapted from Doweidar (1999).

Ions	V^3 (10^{-23} cm^3)	V^2 (10^{-23} cm^3)
Na^+	6.05	7.90
Ca^{2+}	5.45	6.64
Sr^{2+}	5.69	7.48

4.1.7 Oxygen density of bioactive glasses

The oxygen density of a glass may be used to estimate the compactness of the glass network. It is calculated by dividing the mass of oxygen atoms

present in one mole of glass by the molar volume of the glass. The molar volume of a glass is the mass of one mole of glass divided by the experimental density (Fredholm *et al.*, 2010)

In the case of Sr0, Sr50 and Sr100 bioactive glasses, the oxygen density was calculated using the following equation:

$$\rho_O = \frac{M_O \times (2x_{SiO_2} + 5x_{P_2O_5} + x_{Na_2O} + x_{CaO} + x_{SrO})}{[x_{SiO_2}M_{SiO_2} + x_{P_2O_5}M_{P_2O_5} + x_{Na_2O}M_{Na_2O} + x_{CaO}M_{CaO} + x_{SrO}M_{SrO}] \times \rho_{exp}} \quad \textbf{Equation 4.3}$$

where x_{SiO_2}, $x_{P_2O_5}$, x_{Na_2O}, x_{CaO} and x_{SrO} are the molar fractions of SiO_2, P_2O_5, Na_2O, CaO and SrO respectively; $M_O$is the atomic mass of oxygen; M_{SiO_2}, $M_{P_2O_5}$, M_{Na_2O}, M_{CaO} and M_{SrO} are the masses of SiO_2, P_2O_5, Na_2O, CaO and SrO respectively; and ρ_{exp} is the experimentally measured density of the glass.

4.1.8 Solubility study of bioactive glasses

Solubility studies of Sr0, Sr50 and Sr100 bioactive glasses were performed using a method based on the International Standard ISO6872 'Dentistry – Ceramic Materials' (2008). Ten discs of 12 ± 0.2 mm in diameter and 1.6 ± 0.1 mm in thickness were produced from each block of bioactive glass using a core driller and a Buehler precision diamond saw. The discs were washed in distilled water and dried in an electric furnace at 150°C for 4 hours. After weighing and determining the total surface area of each individual disc, the samples were placed in 100 ml of a 4% v/v acetic acid solution maintained at a temperature of 80°C for a total time of 16 hours. Finally, the samples were washed in distilled water, dried in an electric furnace at 150°C and weighed again to determine the total mass loss.

4.1.9 Network connectivity of bioactive glasses

The theoretical network connectivity of a bioactive glass is a measure of the degree of cross-linking and connectivity of SiO_2 in the glass network, and may be used to predict the bioactivity of the material (Hill, 1996).

The network connectivity may be calculated using the following general equation (O'Donnell and Hill, 2010):

$$NC = 2 + \frac{BO - NBO}{G} \qquad \textbf{Equation 4.4}$$

where BO is the total number of bridging oxygens per network-forming ion, NBO the number of non-bridging oxygens per network-modifying ion and G is the total number of glass forming units.

The equations used to calculate the network connectivity for Sr0, Sr50 and Sr100 bioactive glasses, assuming that phosphorus enters the glass network forming of P-O-Si bonds, are shown in Table 4.4.

Table 4.4. Network connectivity equations for Sr0, Sr50 and Sr100 bioactive glasses.

Glass	Equation	
Sr0	$NC'' = 2 + \frac{[(2 \times SiO_2) + (2 \times P_2O_5)] - [(2 \times Na_2O) + (2 \times CaO)]}{[SiO_2 + (2 \times P_2O_5)]}$	**Equation 4.5**
Sr50	$NC'' = 2 + \frac{[(2 \times SiO_2) + (2 \times P_2O_5)] - [(2 \times Na_2O) + (2 \times SrO) + (2 \times CaO)]}{[SiO_2 + (2 \times P_2O_5)]}$	**Equation 4.6**
Sr100	$NC'' = 2 + \frac{[(2 \times SiO_2) + (2 \times P_2O_5)] - [(2 \times Na_2O) + (2 \times SrO)]}{[SiO_2 + (2 \times P_2O_5)]}$	**Equation 4.7**

However, in melt-derived bioactive glass systems, phosphate typically forms orthophosphate units (PO_4^{3-}) rather than becoming part of the silicate network, requiring modifier ions to balance the charge (O'Donnell and Hill, 2010). The modified equations considering this issue are shown in Table 4.5.

Table 4.5. Modified equations for network connectivity of Sr0, Sr50 and Sr100 bioactive glasses.

Glass	Equation	
Sr0	$NC' = 2 + \frac{(2 \times SiO_2) - [(2 \times Na_2O) + (2 \times CaO) + (6 \times P_2O_5)]}{SiO_2}$	**Equation 4.8**
Sr50	$NC' = 2 + \frac{(2 \times SiO_2) - [(2 \times Na_2O) + (2 \times CaO) + (2 \times SrO) + (6 \times P_2O_5)]}{SiO_2}$	**Equation 4.9**
Sr100	$NC' = 2 + \frac{(2 \times SiO_2) - [(2 \times Na_2O) + (2 \times SrO) + (6 \times P_2O_5)]}{SiO_2}$	**Equation 4.10**

4.1.10 SEM analysis of bioactive glasses

The surface of Sr0, Sr50 and Sr100 bioactive glass discs was examined using scanning electron microscopy (SEM) before and after the solubility tests were performed. All the samples were placed on cylindrical aluminium

stubs using double-sided adhesive conductive carbon discs and then were gold coated by sputtering (3 minutes total sputtering time). SEM micrographs were taken on a Jeol JSM6400 scanning electron microscope at various magnifications using an emission current of 20 kV.

4.1.11 EDS analysis of bioactive glasses

Qualitative energy dispersive X-ray spectroscopy (EDS) was used to study the elemental chemical composition of Sr0, Sr50 and Sr100 bioactive glasses, before and after the solubility tests. All the samples were placed on cylindrical aluminium stubs using double-sided adhesive conductive carbon discs and then were carbon coated by sputtering (10 to 15 seconds total sputtering time). The EDS analyses were performed on a Jeol JSM6400 scanning electron microscope equipped with an Oxford Instruments INCAx-sight energy dispersive X-ray spectrometer at various magnifications, using an emission current of 20 kV. EDS patterns were then processed using the IncaEnergy software (Oxford Instruments, UK).

The peaks corresponding to the different chemical elements were identified using those characteristic X-ray lines with energy values lower than 5 KeV highlighted in Table 4.6 in bold type. In the particular case of strontium, the X-ray lines with energy values higher than 5 KeV were not used because the peaks observed were generally too small for accurate identification.

Table 4.6. Characteristic X-ray line energies (KeV) of the chemical elements present in Sr0, Sr50 and Sr100 bioactive glasses. The values used to identify the peaks are highlighted in bold type.

Atomic number and element	Characteristic X-ray line energies (KeV)									
	$K\beta_2$	**$K\beta_1$**	**$K\beta_3$**	**$K\alpha_1$**	**$K\alpha_2$**	**$L\beta_3$**	**$L\beta_4$**	**$L\beta_1$**	**$L\alpha_1$**	**$L\alpha_2$**
6 C				**0.28**						
8 O				**0.53**						
11 Na		1.07		**1.04**						
14 Si		1.08		**1.74**	**1.74**					
15 P		1.84		**2.01**	**2.01**					
20 Ca		**4.01**		**3.69**	**3.69**					
38 Sr	16.09	15.84	15.83	14.17	14.10	**1.95**	**1.94**	**1.87**	**1.81**	**1.80**

4.1.12 Particle size analysis of milled bioactive glasses

Particle size analysis of Sr0, Sr50 and Sr100 bioactive glass powders was performed using the static light scattering technique on a Beckman LS-130 Coulter device. A laser with a wavelength of 750 nm was used as a light source. This method is able to obtain information about the size of particles by measuring the intensity characteristics of light scattered by a suspension at various angles. When the laser beam interacts with particles, diffraction, refraction, reflection and absorption events result in the formation of scattering patterns characteristic for the particle size. If the particle is bigger than the wavelength of the light, patterns preferentially caused by diffraction will be generated and the size information will be derived from the forward direction for small diffraction angles. If the particle is similar in size or smaller than the wavelength then the light is gradually more scattered with large angles to the side and backwards. The smaller the particles are, the greater the contribution of refraction and absorption to the light scattering pattern will be. Therefore, the scattering patterns should be detected over the entire range of angles to perform appropriate measurements of particle size distribution. Each sample was slowly loaded into a volume of 1.7 L of water with no added deflocculant. The ultrasonic mode was activated to facilitate the dispersion of the particles in the suspension fluid. The suspension was then pumped through the system until a PIDS (Polarisation intensity differential scattering) obscuration value between 45% and 55% was reported by the computer. Individual measurements were taken over a period of 90 seconds in triplicate. All the samples were analysed using the ‘Fraunhofer’ optical model of light scattering.

4.1.13 SEM analysis of bioactive glass powders

Sr0, Sr50 and Sr100 bioactive glass powders were examined using scanning electron microscopy (SEM). Small samples of each glass were placed on cylindrical aluminium stubs using double-sided adhesive conductive carbon discs and then were gold coated by sputtering (3 minutes total sputtering time). SEM micrographs were taken on a Jeol JSM6400 scanning electron microscope at various magnifications using an emission current of 20 kV.

4.2 Design, fabrication and characterisation of electrospun composite materials

4.2.1 Electrospinning system

The fabrication of the composite electrospun material was performed using a custom made electrospinning system arranged in a vertical configuration. The system was composed of a KdScientific pump, used to force a polymer solution from inside a 1 ml plastic syringe (Becton Dickinson, UK) into the capillary of a 20-gauge blunt metallic needle. The needle was connected to an external Alpha IV Brandenburg power source, supplying an electric current with voltages between 10 and 30 kV. The electrospun fibres deposited on a metallic collecting plate, forming a non-woven mat of randomly distributed fibres. The distance between the tip of the needle and the collector could be changed if necessary. All the components were enclosed inside a chemical fume hood and a switch was attached to the sash to prevent the system from being used while the fume hood was open, as shown in Figure 4.2.

Figure 4.2. Picture of the electrospinning system used in the project, within a chemical hood at the School of Clinical Dentistry of The University of Sheffield.

4.2.2 Optimisation study of electrospinning parameters

An optimisation study of various electrospinning parameters was performed to define the conditions that will result in the fabrication of membranes exhibiting a small amount of surface defects and consistent fibre diameters.

Effect of polymer concentration and solvent composition

In the first part of the study the effect of polymer concentration and solvent composition on the electrospinning process was investigated. A series of electrospinning solutions were prepared by dissolving poly(caprolactone) (PCL) (Average Mw, 80000 Da; Sigma Aldrich, UK) in a blend of dichloromethane (DCM) (Fisher Scientific, UK) and dimethylformamide (DMF) (Fisher Scientific, UK) at various ratios. This molecular weight was necessary to guarantee an appropriate viscosity in order to form the electrospun jet. Table 4.7 presents the physical properties of DCM and DMF.

Table 4.7. Physical properties of dichloromethane (DCM) and dimethylformamide (DMF).

Physical properties	Solvent	
	DCM	DMF
Formula	CH_2Cl_2	$(CH_3)_2NC(O)H$
Molecular weight	84.93	73.10
Boiling point	39.75°C	153.0°C
Density	1.326 g/mL at 20°C	0.9487 g/mL at 20°C
	1.317 g/mL at 25°C	0.9439 g/mL at 25°C
Dielectric constant	8.93 at 25°C	36.71 at 25°C
Polarity index (P')	3.1	6.4
Viscosity	0.44 cP at 20°C	0.92 cP at 20°C
Surface tension	28.12 dyn/cm at 20°C	36.76 dyn/cm at 20°C
Solubility in water	1.60% at 20°C	Miscible in all proportions

The solutions were thoroughly mixed with a magnetic stirrer for a minimum time of 2 hours and then were electrospun. The solutions and electrospinning conditions used are shown in Table 4.8.

Table 4.8. Solutions and conditions used in the study of the effect of polymer concentration and solvent composition on the electrospinning process.

Concentration (wt%)	DCM:DMF (vol:vol)	Voltage (kV)	Feed rate (ml/h)	Distance (cm)
8 – 14	100:0	17	2.5	21
8 – 14	95:5	17	2.5	21
8 – 14	90:10	17	2.5	21
8 – 14	85:15	17	2.5	21

All the materials were visually examined for physical defects and the compositions which produced materials with the lowest amount of defects due to sputtering were selected for the following part of the optimisation study. The materials were dried at room temperature overnight and stored in a desiccator for later use.

Effect of bioactive glass particle content

In the second part of the study the effect of the amount of bioactive glass particles added to the polymer solution on the electrospinning process was studied. A series of electrospinning solutions were prepared by dissolving PCL (Average Mw, 80000 Da; Sigma Aldrich, UK) in a blend of DCM (Sigma Aldrich, UK) and DMF (Sigma Aldrich, UK). Sr0, Sr50 and Sr100 bioactive glass powders were then added to the solution following PCL:glass weight ratios between 10:1 and 10:4. The solutions were thoroughly mixed with a magnetic stirrer for a minimum time of 2 hours and then were electrospun. Table 4.9 presents the solutions and electrospinning conditions used in the study.

Table 4.9. Solutions and conditions used in the study of the effect of bioactive glass particulate content on the electrospinning process.

Concentration (wt%)	DCM:DMF (vol:vol)	PCL:Glass weight ratio	Voltage (kV)	Feed rate (ml/h)	Distance (cm)
10	90:10	10:1 – 10:4	17	2.5	21
10	85:15	10:1 – 10:4	17	2.5	21

All the materials were visually examined for physical defects and the composition which produced materials with the lowest amount of defects was selected to fabricate the electrospun materials that were used in the following experiments of the project. The materials were dried at room temperature overnight and stored in a desiccator for later use.

4.2.3 SEM analysis of electrospun materials

The surface of the electrospun materials was characterised using scanning electron microscopy (SEM). Samples (13 mm diameter) were cut from each mat using a cork borer and were set on cylindrical aluminium stubs using double-sided adhesive conductive carbon discs. The samples were then gold

coated by sputtering (3 minutes total sputtering time). SEM micrographs were taken on a Jeol JSM6400 scanning electron microscope at various magnifications, using emission currents between 9 and 20 kV. Average fibre diameters were calculated using the ImageJ software (US NIH, USA) by measuring the thickness of the most superficial fibres. A total of 60 measurements were performed for each material.

4.2.4 EDS analysis of electrospun materials

Energy dispersive X-Ray spectroscopy (EDS) was used to determine the presence of bioactive glass particles within the fibres of the electrospun composite materials.

Samples (13 mm diameter) were cut from each mat using a cork borer and were set on cylindrical aluminium stubs using double-sided adhesive conductive carbon discs. The samples were then carbon coated by sputtering (10 to 15 seconds total sputtering time) and analysed on a Jeol JSM6400 scanning electron microscope equipped with an Oxford Instruments INCAx-sight energy dispersive X-ray spectrometer at various magnifications, using an emission current of 20 kV. EDS patterns were then processed using the IncaEnergy software (Oxford Instruments, UK). The peaks corresponding to the different chemical elements were identified as previously described in section 4.1.11.

4.2.5 Solubility study of electrospun materials

The dissolution of bioactive glass particles from within the electrospun fibres was studied by immersion of the materials in deionised water and by the measurement of the variation of environmental pH through time.

Samples (10 mm diameter) were produced from each electrospun mat using a cork borer. A total mass of 10 mg of electrospun samples was placed in 20 ml of deionised water in sterile plastic vials in triplicate and then maintained at a constant temperature of 37°C in a water bath for 14 days. Additionally, vials with 1 mg from Sr0, Sr50 and Sr100 bioactive glass powders (particle size <45 μm) were placed in similar conditions in order to compare the results. The pH readings were performed with a Hanna Instruments pH 211

Microprocessor pH meter at 0, 12, 24, 48, 72, 120, 168, 192, 264 and 336 hours.

4.2.6 Addition of particles to the surface of electrospun fibres

The addition of extra bioactive glass particles to the surface of the electrospun fibres was investigated in order to create new configurations of the materials and to study if this had a significant effect on their cytotoxicity and potential to work as a scaffold. For this, two methods were developed: the ‘loading method’ and the ‘filtering method’.

Loading method

The ‘loading method’, based on work published by Dinarvand *et al*. (2011), consisted in placing a sample of the electrospun material in a suspension of bioactive glass particles in tissue culture media and then allowing enough time for the particles to deposit on its surface due to the gravity force.

Samples (13 mm diameter) were produced from each electrospun mat using a cork borer and then were placed on 24-well plates, where they were sterilised by immersion in 200 µl of isopropyl alcohol (Fisher Scientific, UK) for a minimum time of 20 minutes. This step increased the hydrophilicity of PCL as well, facilitating the handling of the electrospun samples and the absorption of the medium. After the isopropyl alcohol was removed, the samples were washed twice in 200 µl of sterile phosphate buffered saline (PBS; Sigma Aldrich, UK) and were transferred to a new 24-well plate.

Suspensions of Sr0, Sr50 and Sr100 bioactive glass powders were prepared in Dulbecco’s modified Eagle’s medium (DMEM; Sigma Aldrich, UK) or in minimum essential medium Eagle’s medium - alpha modification (αMEM; Sigma Aldrich, UK) and were placed in an ultrasonic bath for 20 minutes to facilitate the dispersion of the particles. A total volume of 1 ml from the suspension was added to each sample and the plates were then placed overnight in a cell culture incubator at a temperature of 37°C in a 5% CO_2 atmosphere. The following day the suspensions were removed and the samples were transferred to a new 24-well plate, where they were washed

twice in 200 µl of deionised water. Finally, the samples were left to dry overnight at room temperature.

Filtering method

The 'filtering method' consisted in using the electrospun material as a filter through which a suspension of bioactive glass particles was forced, causing the particles to be trapped within the fibrous mesh of the sample.

Samples were produced and sterilised as previously described. After being washed twice in 200 µl of sterile PBS (Sigma Aldrich, UK), the samples were placed inside a sterile syringe filter holder (13 mm diameter) (Whatman, UK). Suspensions of Sr0, Sr50 and Sr100 bioactive glass powders were prepared as previously described and a sterile plastic syringe (Becton Dickinson, UK) was used to force a total volume of 1 ml of each suspension through the filter holder. After this, the samples were placed in a new 24-well plate and 1 ml of DMEM or α-MEM was added to each well. All the plates were then placed overnight in a cell culture incubator at a temperature of 37°C in a 5% CO_2 atmosphere. The following day the media were removed and the samples were washed twice in 200 µl of deionised water. Finally, the samples were left to dry overnight at room temperature.

Comparison of 'loading' and 'filtering' methods – Different compositions

The 'loading' and 'filtering' methods were compared using suspensions of Sr0, Sr50 and Sr100 bioactive glass powders at a concentration of 1% w/v in DMEM cell culture medium as previously described. The electrospun samples were initially weighed using a precision balance (0.1 mg resolution) and then processed as previously described to add the particles. After the samples were dried overnight, they were reweighed to measure mass variation using the following formula:

$$Mass\ variation = Mass\ before - Mass\ after \qquad \textbf{Equation 4.11}$$

The different combinations of materials tested, as well as the names given to each one, are presented in Table 4.10. A total of 6 replicates were used in

the study. Statistical analysis was performed in Microsoft Excel 2010 software using two-tailed Student's t-test to determine the significance levels.

Table 4.10. Combinations of materials and methods tested to add bioactive glass particles to the surface of electrospun fibres.

Type of electrospun samples	No glass	Bioactive glass compositions		
		Sr0	Sr50	Sr100
Filled samples	PCL	PCL/Sr0	PCL/Sr50	PCL/Sr100
Loaded samples	PCL	PCL + $Sr0^{L}$	PCL + $Sr50^{L}$	PCL + $Sr100^{L}$
Filtered samples	PCL	PCL + $Sr0^{F}$	PCL + $Sr50^{F}$	PCL + $Sr100^{F}$
Filled + loaded samples	PCL	PCL/Sr0 + $Sr0^{L}$	PCL/Sr50 + $Sr50^{L}$	PCL/Sr100 + $Sr100^{L}$
Filled + filtered samples	PCL	PCL/Sr0 + $Sr0^{F}$	PCL/Sr50 + $Sr50^{F}$	PCL/Sr100 + $Sr100^{F}$

'Filled samples' are those with bioactive glass particles within the polymeric fibres, as a result of the electrospinning process, 'loaded samples' are those with bioactive glass particles added using the 'loading method' and 'filtered samples' are those with bioactive glass particles added using the 'filtering method'.

Comparison of 'loading' and 'filtering' methods – Series of suspension

The 'loading' and 'filtering' methods were also compared using a series of suspensions of bioactive glass particles of increasing concentration. Suspensions of Sr0 bioactive glass powder with concentrations 0.05, 0.1, 0.25, 0.5 and 1 % w/v were prepared in αMEM cell culture medium as previously described. The electrospun samples were then weighed using a precision balance (0.1 mg resolution) and processed as previously described to add the particles. After the samples were dried overnight, they were reweighed to measure mass variation using Equation 4.11.

A total of 12 replicates were used in each test. Statistical analysis was performed in Microsoft Excel 2010 software using two-tailed Student's t-test to determine the significance levels.

4.3 Cytotoxicity of electrospun composite materials

4.3.1 Expansion of a rat osteosarcoma cell line

A rat osteosarcoma (ROS) cell line was cultured in order to obtain the required number of cells to perform the cytotoxicity assessments.

Vials containing ROS cells, which were stored in liquid nitrogen, were thawed at room temperature and then resuspended in 1 ml of fully supplemented cell culture medium, which was composed of DMEM (Sigma Aldrich, UK) supplemented with 10 units/ml penicillin (Sigma Aldrich, UK), 0.1 mg/ml streptomycin (Sigma Aldrich, UK), 20 mM L-alanyl glutamine and 10% v/v foetal calf serum (Biosera, UK).

After resuspension, the cells were transferred to a sterile 20 ml vial containing 10 ml of fully supplemented cell culture medium and then centrifuged at a speed of 1000 rpm for 5 minutes to form a pellet. The supernatant was removed and the pellet was resuspended in 10 ml of fully supplemented cell culture medium. Finally, the number of cells per ml of resuspension was determined using a haemocytometer. The cells were then seeded in T-75 tissue culture flasks (Greiner Bio-One, UK) at a density of 10^6 cells/flask and fresh fully supplemented cell culture medium was added to complete a total volume of 15 ml.

For passaging, the medium was removed from the flask and the monolayer of ROS cells was washed twice with 5 ml of sterile PBS (Sigma Aldrich, UK) before being covered with 5 ml of a solution 0.05% trypsin/0.02% EDTA (Sigma Aldrich, UK) and then being incubated at 37°C in a 5% CO_2 atmosphere for a total time of 5 minutes to induce their detachment from the plastic surface. The effect of the trypsin/EDTA solution was then stopped by adding 0.5 ml of FCS (Biosera, UK) to the flask, creating a suspension of cells which was transferred to a sterile plastic vial and was then centrifuged at 1000 rpm for 5 minutes to form a pellet. The supernatant was removed and the cells were resuspended in fully supplemented cell culture medium. Finally, the number of cells per ml of resuspension was determined using a haemocytometer. For further expansion, the ROS cells were seeded at a

density of 10^6 cells in new T-75 flasks and were incubated until the following passage.

4.3.2 Cytotoxicity assessment of electrospun composite materials

The cytotoxicity of the electrospun materials was assessed by culturing ROS cells directly on the electrospun samples and then applying a resazurin dye-based assay.

This non-destructive assay is able to measure respiratory activity via a redox reaction, which can be quantified by monitoring a colorimetric change associated with the reduction of the dye. In the presence of respiration products, such as NADH, the dye is reduced to resorufin, as shown in Figure 4.3. The concentration of resorufin is therefore dependent on the metabolic activity of the cells and it can be measured by detecting the fluorescence emission from the cell culture medium using a spectrophotometer.

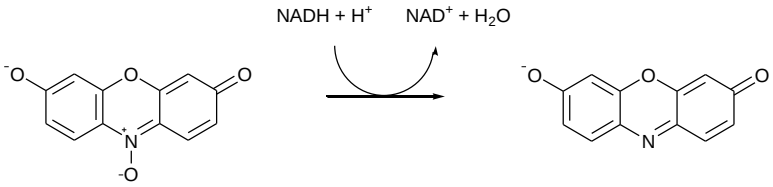

Figure 4.3. Reduction of the resazurin molecule to resorufin by NADH.

Samples (13 mm diameter) were produced from each electrospun material using a cork borer and were placed in 24-well plates to be sterilised by immersion in 200 µl of isopropyl alcohol (Fisher Scientific, UK), for a minimum time of 20 minutes. Afterwards, the samples were washed twice in 200 µl of sterile PBS (Sigma Aldrich, UK) and then were transferred to a new 24-well plate, where they were re-washed in 200 µl of sterile PBS. The potential cytotoxic effect of the addition of bioactive glass particles to the surface of the electrospun fibres using the 'filtering method' was also studied. Suspensions of 0.05, 0.25 and 1 % w/v of Sr0, Sr50 and Sr100 bioactive glass particles in DMEM (Sigma Aldrich, UK) were prepared and the samples were processed as previously described.

All the samples were seeded by adding a volume of the cell suspension containing 2.5 x 10^4 ROS cells and fresh fully supplemented cell culture

medium was added to each well to complete a total volume of 1 ml. The same amount of cells was directly seeded on wells without any electrospun material, to act as untreated controls. Cell-free controls from each material were also prepared in order to discard interferences arising from interactions between the resazurin dye and the material. The plates were then incubated at a temperature of 37°C in a 5% CO_2 atmosphere for 72 hours. After this time, the cell culture medium was removed and the plates were examined with an optical microscope to observe cell attachment and proliferation in the bottom of the wells. The electrospun samples were then transferred to a sterile 24-well plate, generating two sets of plates: a) plates containing ROS cells on the plastic, and b) plates containing the electrospun samples.

A solution of 10% v/v resazurin in fully supplemented cell culture medium was prepared and 2 ml were added to each well on all plates. The plates were then incubated at a temperature of 37°C in a 5% CO_2 atmosphere and the medium surrounding the materials was sampled at 20, 40 and 60 minutes by transferring two aliquots of 200 µl each per sample to a 96-well plate for spectrophotometric analysis. Distilled water and cell culture medium were used as internal standards. A volume of 200 µl of the 10% v/v solution of resazurin was also included to provide a baseline reading.

The metabolic activity was finally assessed by measuring the fluorescence emission intensity at a wavelength of 590 nm following excitation at a wavelength of 560 nm. Equation 4.12 was used to calculate the final fluorescence value.

$$Fluorescence = (F_S + F_C - F_{CF}) \qquad \textbf{Equation 4.12}$$

where F_S is the value of the fluorescence emission obtained from the cells attached and proliferating on the bottom of the well, F_C is the value of the fluorescence emission obtained from the wells containing the electrospun samples and F_{CF} is the value of the fluorescence emission obtained from the wells containing cell-free controls.

A total of 4 replicates were prepared for each test. Statistical analyses were performed in Microsoft Excel 2010 software using one-way ANOVA and two-tailed Student's t-test to determine the significance levels.

4.4 Isolation, expansion and characterisation of mesenchymal stromal cells

4.4.1 Isolation of mesenchymal stromal cells

Mesenchymal stromal cells (MSCs) were obtained from the bone marrow of 4-5 weeks old male Wistar rats following the method described by Maniatopoulos *et al.* (1988). A total number of 4 animals were used.

The femora were dissected from the animals in aseptic conditions using sterile instrumentation, cleaned of soft tissues, and were immediately immersed in 10 ml of DMEM (Sigma Aldrich, UK) supplemented with 100 units/ml of penicillin (Sigma Aldrich, UK) and 1 mg/ml of streptomycin (Sigma Aldrich, UK). The ends of the femora were then removed and the bone marrow was flushed into a sterile plastic vial with 5 ml of fully supplemented cell culture medium ejected from a sterile syringe with a 20 gauge needle. The fully supplemented culture medium was composed of DMEM (Sigma Aldrich, UK) supplemented with 10 units/ml penicillin (Sigma Aldrich, UK), 0.1 mg/ml streptomycin (Sigma Aldrich, UK), 20 mM L-alanyl glutamine (Sigma Aldrich, UK), and 10% v/v MSCs qualified foetal calf serum (qFCS; Biosera, UK). The media containing each bone marrow were then transferred to sterile T-75 flasks and 10 ml of fresh fully supplemented cell culture medium were added, making up a total volume of 15 ml.

All the flasks were incubated at a temperature of 37°C in a 5% CO_2 atmosphere for 24 hours, after which the MSCs attached to the bottom of the flask. Non-adherent cells and tissue debris in suspension was then removed from each flask by replacing the medium with fresh fully supplemented cell culture medium. The cells were daily inspected and the medium was changed every 48 to 72 hours until near confluence was achieved. At that point the cells were passaged to a new flask or stored for later use.

4.4.2 Expansion and storage of mesenchymal stromal cells

For passaging, the medium was removed from the flask and the monolayer of MSCs was washed twice with 5 ml of sterile PBS (Sigma Aldrich, UK) before being covered with 5 ml of a solution 0.05% trypsin/0.02% EDTA (Sigma Aldrich, UK) and then being incubated at 37°C in a 5% CO_2 atmosphere for a total time between 3 and 5 minutes, to induce their detachment from the plastic surface. The effect of the trypsin/EDTA solution was then stopped by adding 0.5 ml of FCS (Biosera, UK) to the flask, creating a suspension of cells which was transferred to a sterile plastic vial and was then centrifuged at 1000 rpm for 5 minutes to form a pellet. The supernatant was removed and the cells were resuspended in fully supplemented cell culture medium. For further expansion, the MSCs were seeded at a density of 1 x 10^6 cells in T-75 flasks or in petri dishes (Greiner Bio-One, UK) and were incubated until the following passage. The storage of MSCs was done by transferring a volume of resuspended cells containing a total of 2 x 10^6 cells to a sterile vial. Fully supplemented cell culture medium was then added to make up a total volume of 10 ml. The vial was centrifuged at 1000 rpm for 5 minutes to form a pellet and the supernatant was removed. The cells were then resuspended in 1 ml of a 10% v/v solution of dimethylsulfoxide (DMSO; Sigma Aldrich, UK) in FCS and then transferred to a 2 ml vial which was stored overnight at -80°C. The following day the vials were transferred to a liquid nitrogen dewar for indefinite storage.

4.4.3 Characterisation of cell population

Fluorescence-activated cell sorting (FACS) analysis was performed in order to characterise the population of MSCs by detecting the presence of specific surface molecular markers on the cells. All the antibodies, their isotypes and the conjugated fluorochromes (Biolegend, UK) are shown in Table 4.11.

Table 4.11. Surface marker antibodies, isotypes and conjugated fluorochromes used in the characterisation of the population of MSCs by FACS analysis.

Surface marker antibody	Isotype	Fluorochrome
Anti-rat CD44	Anti-mouse IgG2a, κ Isotype	Alexa Fluor 647 (AF)
Anti-rat CD90	Anti-mouse IgG1, κ Isotype	Pacific Blue (PB)
Anti-rat CD45	Anti-mouse IgG1, κ Isotype	Phycoerythrin (PE)

Solutions of the antibodies and their isotypes (20 µg/ml concentration; 50 µl per test) were prepared in FACS buffer (5% v/v foetal calf serum and 0.1% v/v sodium azide in PBS) with the compositions shown in Table 4.12.

Table 4.12. Composition of the different tubes for FACS analysis of rat MSCs.

Tube	Description	CD45 Ab	CD44 Ab	CD90 Ab	CD45 Iso	CD44 Iso	CD90 Iso	FACS buffer
1	Unstained cells	-	-	-	-	-	-	50 µl
2	Only isotypes	-	-	-	5 µl	10 µl	2 µl	33 µl
3	CD45 Ab + Isotypes	5 µl	-	-	-	10 µl	2 µl	33 µl
4	CD44 Ab + Isotypes	-	2 µl	-	5 µl	-	2 µl	41 µl
5	CD90 Ab + Isotypes	-	-	2 µl	5 µl	10 µl	-	33 µl
6	Only antibodies	5 µl	2 µl	2 µl	-	-	-	41 µl

Passage 3 MSCs were removed from the T-75 flasks as previously explained and then were resuspended in fully supplemented cell culture medium composed of DMEM (Sigma Aldrich, UK) supplemented with 10 units/ml penicillin (Sigma Aldrich, UK), 0.1 mg/ml streptomycin (Sigma Aldrich, UK), 20 mM L-alanyl glutamine (Sigma Aldrich, UK), and 10% v/v qFCS (Biosera, UK).

Volumes containing 5 x 10^5 cells were aliquoted in sterile Eppendorf tubes, were centrifuged at 5000 rpm for 2 minutes and then all the pellets were resuspended in 500 µl of FACS buffer. This step was performed twice to wash the cells from any remains of cell culture medium. Afterwards, the MSCs were resuspended in 50 µl of the antibody solutions as required and were incubated for 30 minutes in ice (4°C) in dark conditions. Afterwards, the cells were centrifuged at 5000 rpm for 2 minutes and washed twice with 500 µl of FACS buffer. Finally, the cells were fixed in 300 µl of 4% paraformaldehyde in PBS at room temperature for a total time of 15 minutes in dark conditions before the FACS analysis was performed.

All the analyses were performed on a Beckton Dickinson LSRII flow cytometer and the data generated was processed using FACS Diva software v. 6.1.2, provided by the manufacturer.

4.5 Osteogenic effect of strontium-substituted bioactive glasses

The expression of six genes associated with the process of osteoblastic differentiation of MSCs was investigated to study the potential osteogenic effect of Sr0, Sr50 and Sr100 bioactive glasses. The cells were cultured in monolayer as previously described and then were exposed to the dissolution products of bioactive glass powders. The minimum amount of bioactive glass powders which induced a significant reduction in cell viability was initially determined by assessing their cytotoxicity. Finally, the cells were exposed to that amount of glass powders and total RNA extraction and reverse transcription quantitative polymerase chain reaction (RT-qPCR) analyses of those genes were performed.

4.5.1 Effect of bioactive glass dissolution on cell viability

The effect of the dissolution products of Sr0, Sr50 and Sr100 bioactive glass powders on the viability of MSCs was studied by assessing the cytotoxicity of the glasses using a resazurin dye-based assay, in a similar way to what was previously described in the study of the cytotoxicity of the electrospun materials in section 4.3.2 of this report.

Passage 3 MSCs were cultured in monolayer in sterile 6-well plates. A total of 1.5 x 10^5 cells were seeded per well and 2 ml of fully supplemented cell culture medium was added, which was composed of DMEM (Sigma Aldrich, UK) supplemented with 10 units/ml penicillin (Sigma Aldrich, UK), 0.1 mg/ml streptomycin (Sigma Aldrich, UK), 20 mM L-alanyl glutamine (Sigma Aldrich, UK) and 10% v/v FCS (Biosera, UK). The plates were then incubated for 24 hours at a temperature of 37°C in a 5% CO_2 atmosphere to ensure cell attachment.

Sr0, Sr50 and Sr100 bioactive glass powders were heat sterilised in a dry oven for 2 hours at 160°C, and samples containing 5, 10, 20, 40, 80, 160 and 320 mg from each glass were then prepared by weighing them in sterile Eppendorf tubes on a precision weighing balance (0.1 mg resolution). All the samples were placed in sterile cell culture inserts of 0.4 μm pore size

(Greiner Bio-one, UK) in such a way that MSCs would be exposed to the dissolution products but would not be in direct contact with the bioactive glass particles. Additionally, wells containing MSCs not exposed to any bioactive glass were used as untreated controls. Cell-free controls for each glass sample were also prepared in order to discard interferences arising from interactions between the resazurin dye and the glass dissolution products.

After 24 hours of incubation the cell culture medium was removed from the 6-well plates and the inserts were placed in. Fresh fully supplemented cell culture medium (3 ml) was added to each sample (2 ml in each well and 1 ml in each insert) and all the plates were incubated for 72 hours at a temperature of 37°C in a 5% CO_2 atmosphere. A solution of 10% v/v resazurin in fully supplemented cell culture medium was prepared and 2 ml of this solution were added to each well. The plates were then incubated and the medium was sampled at 15, 45, 100 and 130 minutes. Two aliquots of 200 µl each were taken per sample and transferred to a 96-well plate for spectrophotometric analysis. Distilled water and fully supplemented cell culture medium were used as internal standards and the solution of 10% v/v resazurin was also included to provide a baseline reading.

A total of 3 replicates were used in each test. Statistical analysis was performed in Microsoft Excel 2010 software using one-way ANOVA and two-tailed Student's t-test to calculate the significance levels.

4.5.2 Total RNA isolation from rat MSCs

Passage 3 MSCs were cultured in monolayer in sterile 6-well plates. A total of 1.5 x 10^5 cells were seeded per well and 2 ml of fully supplemented cell culture medium was added, which was composed of α-MEM (Sigma Aldrich, UK) supplemented with 10 units/ml penicillin (Sigma Aldrich, UK), 0.1 mg/ml streptomycin (Sigma Aldrich, UK), 10 mM L-alanyl glutamine and 10% v/v FCS (Biosera, UK). The plates were then incubated for 24 hours at a temperature of 37°C in a 5% CO_2 atmosphere to ensure cell attachment.

Sr0, Sr50 and Sr100 bioactive glasses powders were heat sterilised in a dry oven for 2 hours at 160°C, and samples containing 20 mg from each glass were then prepared by weighing them in sterile Eppendorf tubes on a precision weighing balance (0.1 mg resolution). All the samples were placed in sterile cell culture inserts of 0.4 μm pore size (Greiner Bio-one, UK) in such a way that MSCs would be exposed to the dissolution products but would not be in direct contact with the bioactive glass particles.

After 24 hours of incubation the cell culture medium was removed from the 6-well plates, the cell culture inserts were placed in and a volume (3 ml; 2 ml in each well and 1 ml in each insert) of standard and osteogenic cell culture media were added to the wells. The compositions of both cell culture media are shown in Table 4.13. All the plates were then incubated at a temperature of 37°C in a 5% CO_2 atmosphere for 14 days, with the cell culture media changed every 72 hours.

Table 4.13. Standard and Osteogenic cell culture media compositions.

Component	Standard medium	Osteogenic medium
Cell culture medium	α-MEM (Sigma Aldrich, UK)	α-MEM (Sigma Aldrich, UK)
Penicillin (P)	10 units/ml (Sigma Aldrich, UK)	10 units/ml (Sigma Aldrich, UK)
Streptomycin (S)	0.1 mg/ml (Sigma Aldrich, UK)	0.1 mg/ml (Sigma Aldrich, UK)
L-Alanyl Glutamine (L-Glu)	10 mM (Sigma Aldrich, UK)	10 mM (Sigma Aldrich, UK)
Foetal calf serum (FCS)	10% v/v (Biosera, UK)	10% v/v (Biosera, UK)
Ascorbic Acid (AA)	-	50 μg/ml (Sigma Aldrich, UK)
β-Glycerophosphate (β-GP)	-	10 mM (Fluka Biochemika, UK)
Dexamethasone (Dex)	-	10^{-8} M (Sigma Aldrich, UK)

On days 1, 3, 6 and 14 of the experiment, certain plates were terminated and, following the manufacturer's instructions, total RNA extraction from the cells was performed using the RNeasy® Mini Kit (Qiagen, UK). For this purpose, the cell culture medium was removed from each well and the cells were washed three times in 300 μl of sterile PBS (Sigma Aldrich, UK). Then 350 μl of buffer RLT with 10% v/v β-mercaptoethanol (Sigma Aldrich, UK)

were added to the wells and the lysate was collected using a sterile cell scraper and pipetted into a QIAshredder® spin column (Qiagen, UK). The columns were centrifuged for 2 minutes at full speed and then 350 µl of 70% solution of ethanol in nuclease-free water were added to the homogenised lysate. Up to 700 µl of each lysate was then transferred to an RNeasy spin column and were centrifuged for 15 seconds at ≥8000 g. The flow-through was discarded and 700 µl of buffer RW1 were added to the column and were centrifuged for 15 seconds at ≥8000 g. After discarding the flow-through, the columns were washed by adding 500 µl of buffer RPE and were centrifuging for 15 seconds at ≥8000 g. Another 500 µl of buffer RPE were later added, followed by centrifugation again for 2 minutes at ≥8000 g. Finally, the spin columns were placed in new 1.5 ml tubes and 30 to 50 µl of RNase-free water were added and were centrifuged for 1 minute at ≥8000 g to elute the RNA.

The final concentration of isolated RNA in ng/µl was then determined using the Nanodrop 1000 spectrophotometer (Thermo Scientific, UK). Light absorbance measurements were performed at wavelengths of 260 nm and 180 nm to assess the purity of the RNA by calculating the ratio between both absorbance values. The RNA samples were then stored at -80°C until used. All the work was performed using nuclease-free Fisherbrand SureOne® pipet tips (Fisher Scientific, UK).

4.5.3 Reverse transcription of total isolated RNA to cDNA

Reverse transcription of total RNA to single-stranded cDNA was performed on all the RNA samples using the High Capacity cDNA RT Kit (Applied Biosystems, UK), following the manufacturer's instructions.

Initially, a 2X reverse transcription master mix was prepared with the composition shown in Table 4.14. A volume of 10 µl of total RNA was pipetted and mixed with an equal volume of master mix in a 0.5 ml Eppendorf tube to create a 1X solution with a total volume per reverse transcription reaction of 20 µl. The tubes were vortexed to thoroughly mix the solution and then briefly centrifuged (30 seconds at 3000 g). Reverse

transcription was finally performed on a thermal cycler using the conditions shown in Table 4.15.

Table 4.14. Amounts required to produce a volume of 10 µl of Master Mix per reaction using the High-Capacity cDNA RT Kit.

High-Capacity cDNA RT Kit components	Volumen (µl)
10X RT Buffer	2.0
25X dNTP Mix (100 mM)	0.8
10X RT Random Primers	2.0
MultiScribe™ Reverse Transcriptase	1.0
Nuclease-free water	3.2
Total volume per reaction	10

Table 4.15. Thermal cycle conditions recommended by the manufacturer of the High Capacity cDNA RT kit.

	Step 1	Step 2	Step 3	Step 4
Temperature (°C)	25	37	85	4
Time (min)	10	120	5	∞

A number of additional reactions were included in the preparation of the reverse transcription Master Mix to provide excess volume for the loss that may occur during pipetting. All the samples were prepared using nuclease-free Fisherbrand SureOne® pipet tips (Fisher Scientific, UK) and were kept in ice (4°C) while they were not in use. Finally, all the cDNA samples were stored at -80°C.

4.5.4 RT-qPCR analyses of cDNA

Reverse transcription quantitative polymerase chain reaction (RT-qPCR) was performed on a 7900HT Fast Real-Time PCR System (Applied Biosystems, UK) using TaqMan® Gene Expression Assays (Applied Biosystems, UK), following the manufacturers' instructions. The genetic markers of osteogenic differentiation to be investigated and the endogenous control used, as well as their function, the probe dye and the TaqMan assay ID, are shown in Table 4.16.

Table 4.16. Name, symbol, function and TaqMan assay ID of the genes selected for the experiment.

Gene	Gene symbol	Function	Probe dye	TaqMan Assay ID
Runt-related transcription factor 2	*Runx2*	Encodes nuclear protein essential for osteoblastic differentiation and skeletal morphogenesis.	FAM	Rn01512298_m1
Alkaline phosphatase, liver/bone/kidney	*Alpl*	Encodes a membrane bound enzyme that may play a role in bone mineralisation.	FAM	Rn01516028_m1
Collagen type I, Alpha I	*Col1a1*	Encodes the pro-alpha1 chains of type I collagen, abundant in bone and other connective tissues.	FAM	Rn01463848_m1
Bone gamma-carboxyglutamate (gla) protein	*Bglap*	Encodes a protein composing 1-2% of the total bone protein and which binds strongly to apatite and calcium.	FAM	Rn00566386_g1
Bone morphogenetic protein 2	*Bmp2*	Encodes a protein which induces bone and cartilage formation.	FAM	Rn00567818_m1
Secreted phosphoprotein 1	*Spp1*	Encodes a protein which forms an integral part of the mineralised matrix. May play an important role in cell attachment.	FAM	Rn01449972_m1
Glyceraldehyde-3-phosphate dehydrogenase	*Gapdh*	Encodes a protein involved in glycolysis and nuclear functions. Used as endogenous control.	VIC	Rn01775763_g1

All the TaqMan assays and cDNA samples were thawed in ice and briefly centrifuged to bring the liquid to the bottom of the tubes. A PCR reaction mix was prepared with the composition per RT-qPCR reaction shown in Table 4.17. The total volume of PCR reaction mix required was calculated by determining the number of RT-qPCR reactions to be performed. Extra reactions were included to compensate for the potential loss of volume that may occur when pipetting.

A volume of 9.5 µl of PCR reaction mix was then transferred into the wells of Fast 96-well reaction plates (Applied Biosystems, UK). A volume of 0.5 µl of cDNA was then added to each well and was thoroughly mixed by pipetting. Controls were also included to determine the presence of contaminating DNA in the plate, by replacing the cDNA with the original RNA and with water. The plates were then loaded into the system and the process was

configured following the manufacturer's instructions. Each reaction was run in triplicate.

Table 4.17. Composition of PCR reaction mix per single 10 µl RT-qPCR reaction

Component	Volume (For 10 µl reaction)
2X TaqMan Gene Expression Master Mix	5 µl
20X TaqMan Gene Expression Assay Primer and Probe	0.5 µl
20X TaqMan Gapdh Endogenous Control	0.5 µl
RNase-free water	3.5 µl
Total volume	9.5 µl

4.5.5 Analysis of RT-qPCR data

The data obtained from all the RT-qPCR analyses was collected by a computer running the Sequence Detection Systems (SDS) software v. 2.4 (Applied Biosystems, UK) and was then analysed using the comparative Ct method (i.e. ΔΔCt method). All the calculations were performed in Microsoft Excel 2010.

First, the mean Ct values and the standard deviation for all the RT-qPCR reactions were calculated using the data provided by the SDS software. Then the ΔCt value was calculated with Equation 4.13.

$$\Delta C_t = C_t\ (Gene) - C_t\ (Gapdh) \qquad \textbf{Equation 4.13}$$

The standard deviation (sd) of the ΔCt value was calculated from the standard deviations of the gene and the Gapdh value, as shown in Equation 4.14.

$$sd = (sd_{Gene}^2 + sd_{Gapdh}^2)^{1/2} \qquad \textbf{Equation 4.14}$$

Then the ΔΔCt was calculated by subtracting the ΔCt value of the untreated control from the sample being studied.

$$\Delta\Delta C_t = \Delta C_t\ (Sample) - \Delta C_t\ (Untreated\ control) \qquad \textbf{Equation 4.15}$$

The standard deviation of ΔΔCt was the same as the standard deviation of the ΔCt value.

The fold difference in gene expression was calculated by $2^{-\Delta\Delta Ct}$. This difference may also be expressed as a range by incorporating the standard deviation of the ΔΔCt value into the fold difference calculation by replacing ΔΔCt with (ΔΔCt + sd) and (ΔΔCt – sd), where sd was the standard deviation of the ΔΔCt value.

Statistical analysis was performed on the ΔCt values in Microsoft Excel 2010 software using the Wilcoxon two group test, as recommended by Yuan *et al.* (2006).

5 Results

5.1 Bioactive glass characterisation

5.1.1 XRD analyses of bioactive glasses

X-ray diffraction (XRD) spectra of Sr0, Sr50 and Sr100 bioactive glasses are presented in Figure 5.1. The presence of one broad peak in every spectrum confirmed the absence of any significant crystalline phase and, therefore, showed that all the materials were amorphous. It was observed that the peaks progressively moved toward smaller values of angle 2θ with the increase of calcium substitution by strontium in the glass compositions. Finally, the spectra were comparable to the spectrum produced by PerioGlas®, a commercial bone graft material made of 45S5 bioglass.

5.1.2 DTA of bioactive glasses

Differential thermal analysis (DTA) patterns of Sr0, Sr50 and Sr100 bioactive glasses and of PerioGlas® are presented in Figure 5.2. The estimated values for glass transition temperature (T_g), onset of crystallisation temperature (T_c) and peak crystallisation temperature (T_p) are presented in Table 5.1. It was observed that the T_g of the glasses decreased as the substitution of calcium by strontium in the composition increased. Both T_c and T_p presented a minimum value in Sr50 bioactive glass. The working range, which is calculated by subtracting T_g from T_c, generally increased with the strontium substitution in the in-house bioactive glasses.

Table 5.1. Estimated glass transition temperature (T_g), onset of crystallisation temperature (T_c), peak crystallisation temperature (T_p) and working range for Sr0, Sr50 and Sr100 bioactive glasses and PerioGlas®.

	Bioactive glasses			
	PerioGlas®	**Sr0**	**Sr50**	**Sr100**
Glass transition temperature (T_g)	523	525	492	479
Onset of crystallisation temperature (T_c)	630	613	583	610
Peak crystallisation temperature (T_p)	690	682	671	691
Working range (T_c - T_g)	107	88	91	131

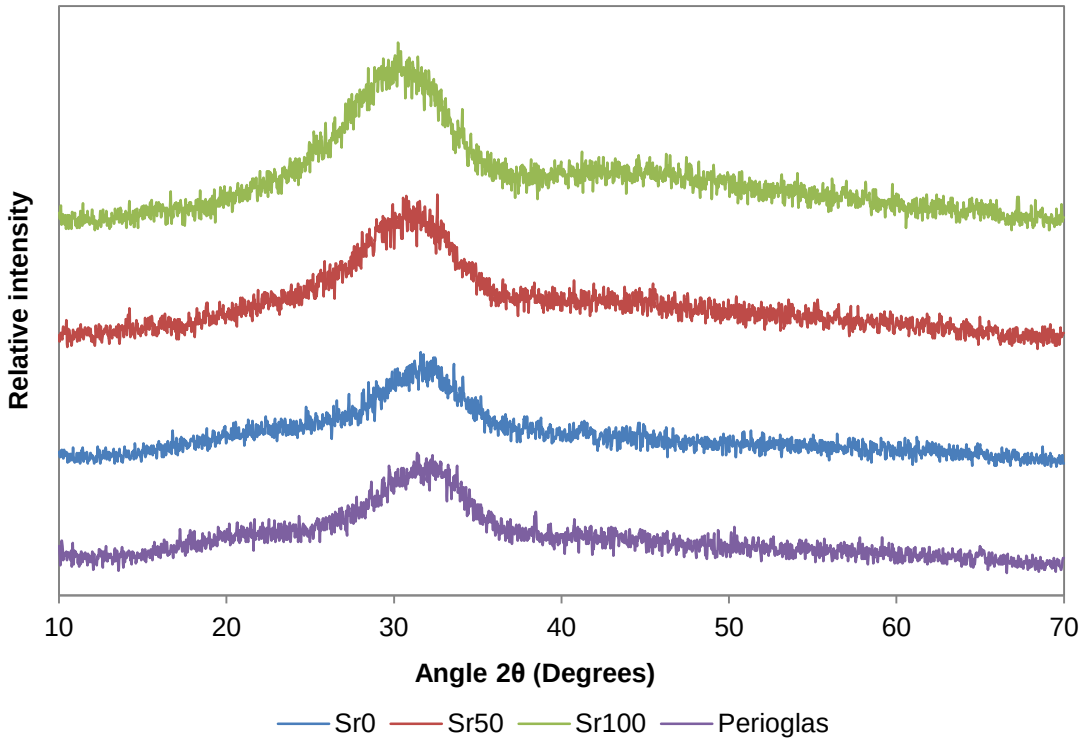

Figure 5.1. X-ray diffraction spectra of Sr0, Sr50 and Sr100 bioactive glasses, and of PerioGlas®.

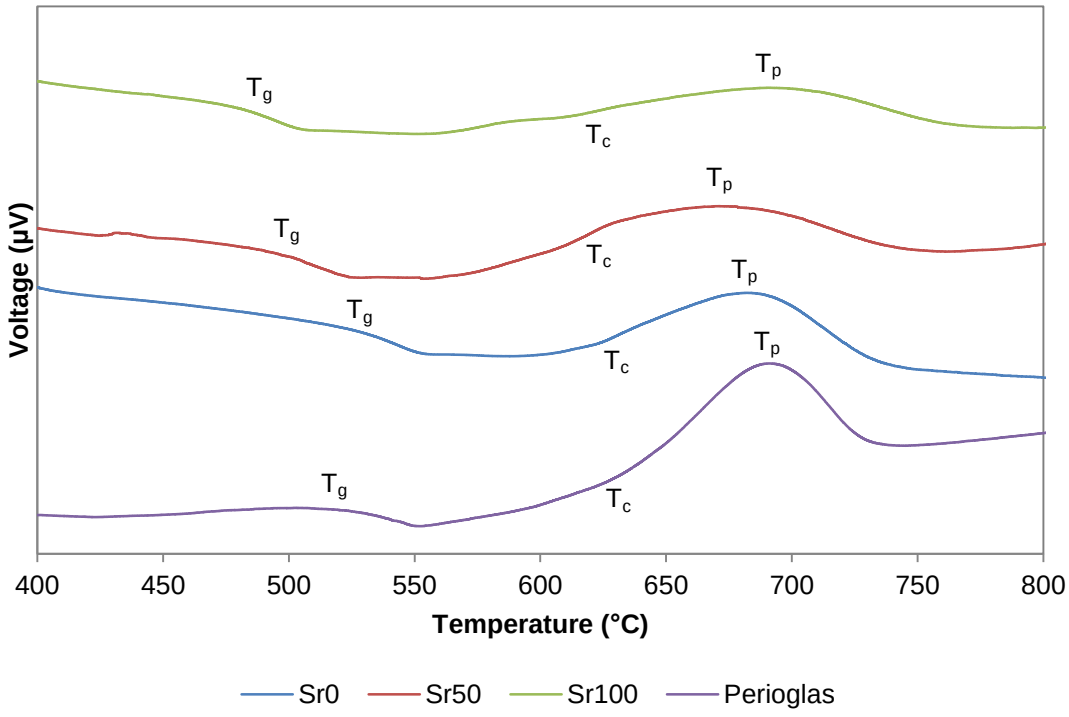

Figure 5.2. Differential thermal analysis patterns of Sr0, Sr50 and Sr100 bioactive glasses, and of PerioGlas®. The regions where the glass transition temperature, the onset of crystallisation temperature and the peak crystallisation temperature were estimated are identified with T_g, T_c and T_p, respectively.

5.1.3 Experimental and theoretical density of bioactive glasses

The experimentally measured densities of Sr0, Sr50 and Sr100 bioactive glasses and the theoretical densities, calculated using Doweidar's model of glass density, are shown in Table 5.5 and are graphically represented in Figure 5.3. It was observed that glass density increased linearly in proportion to the substitution of calcium by strontium in the glass composition. The theoretical densities of the three glass compositions showed a similar linear increase with increasing strontium substitution.

Table 5.2. Values of experimentally measured and theoretically calculated densities of Sr0, Sr50 and Sr100 bioactive glasses.

	Bioactive glasses		
	Sr0	**Sr50**	**Sr100**
Experimental density ($g \cdot cm^{-3}$)	2.73 ± 0.02	2.95 ± 0.02	3.14 ± 0.01
Theoretical density ($g \cdot cm^{-3}$)	2.73	2.93	3.11

5.1.4 Oxygen density of bioactive glasses

The estimated oxygen densities of Sr0, Sr50 and Sr100 bioactive glasses are shown in Table 5.3 and are graphically presented in Figure 5.4. It was observed that the oxygen density of the bioactive glasses decreased linearly as the proportion of calcium substitution by strontium in the glass composition increased.

Table 5.3. Estimated oxygen density for Sr0, Sr50 and Sr100 bioactive glasses.

	Bioactive glass		
	Sr0	**Sr50**	**Sr100**
Oxygen density ($g \cdot cm^{-3}$)	1.11	1.09	1.06

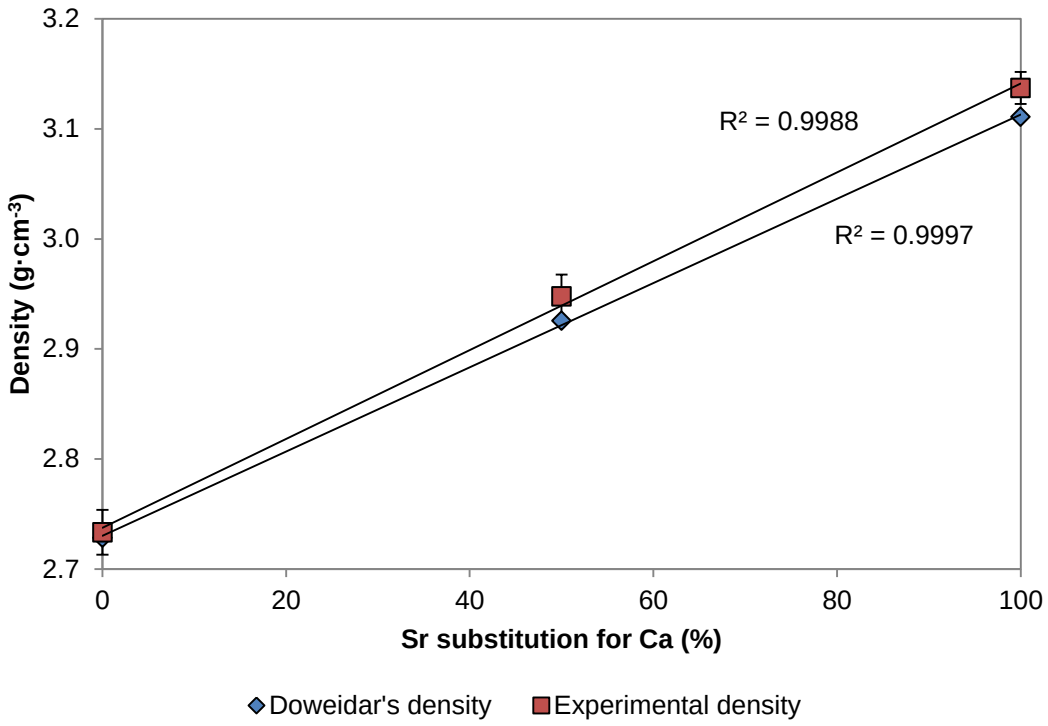

Figure 5.3. Graphical representation of the experimentally measured densities and the theoretically calculated densities (Doweidar's density) of Sr0, Sr50 and Sr100 bioactive glasses.

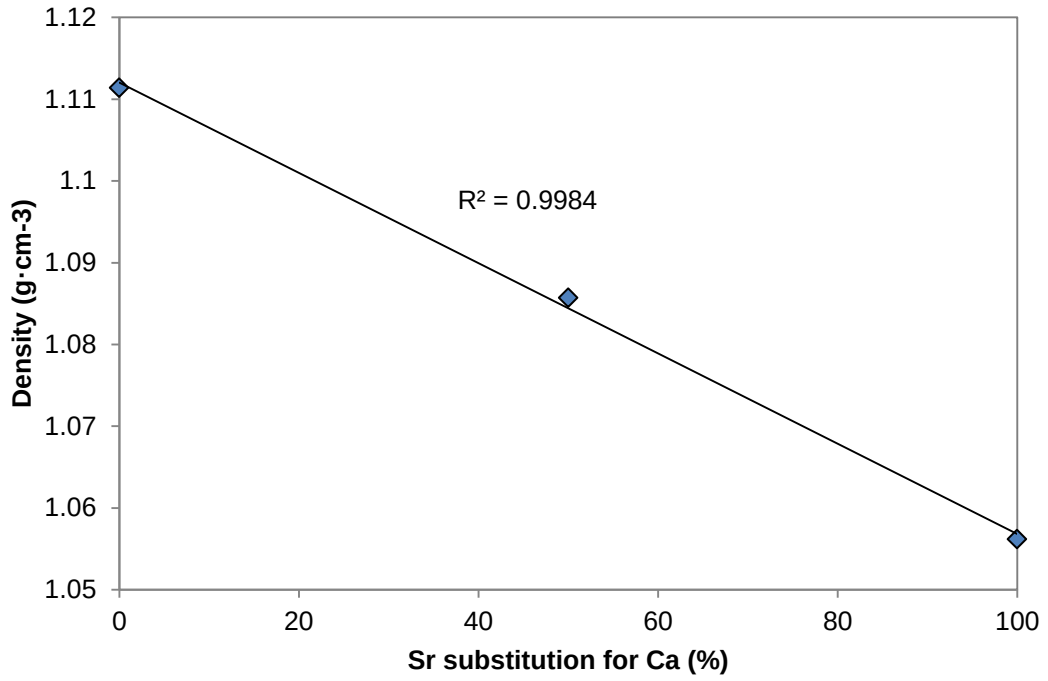

Figure 5.4. Estimated oxygen densities of Sr0, Sr50 and Sr100 bioactive glasses.

5.1.5 Solubility study of bioactive glasses

The values of the solubility of Sr0, Sr50 and Sr100 bioactive glasses, measured using a method based on the International Standard ISO 6872 'Dentistry –Ceramic Materials' (2008), are graphically represented in Figure 5.5. It was observed that the solubility of the glasses increased linearly in proportion to the substitution of calcium by strontium in the glass composition, from 2.78 x 10^4 µg·cm^{-2} for Sr0 to 3.88 µg·cm^{-2} for Sr100.

Each bioactive glass composition was also observed to react differently to the treatment of immersion in acetic acid. The surface of the discs was modified after the solubility tests were performed, changing in colour and became more brittle. The most external layer of material could then be removed from the discs by mechanical action, exposing an unmodified surface of bioactive glass. However, it was more difficult to remove the modified surface layer as the proportion of substitution of calcium by strontium in the glass composition increased.

5.1.6 Network connectivity of bioactive glasses

The calculated values of network connectivity for Sr0, Sr50 and Sr100 bioactive glasses are presented in Table 5.4. The results of the calculations assuming that phosphorus entered the glass network forming P-O-Si bonds (NC'') were consistently lower than the values calculated assuming that phosphorus formed orthophosphate units instead of becoming part of the silicate network (NC'). The NC values were the same for the three compositions in both cases.

Table 5.4. Network connectivity values of Sr0, Sr50 and Sr100 bioactive glasses.

	Bioactive glass		
	Sr0	**Sr50**	**Sr100**
NC'	2.12	2.12	2.12
NC''	1.90	1.90	1.90

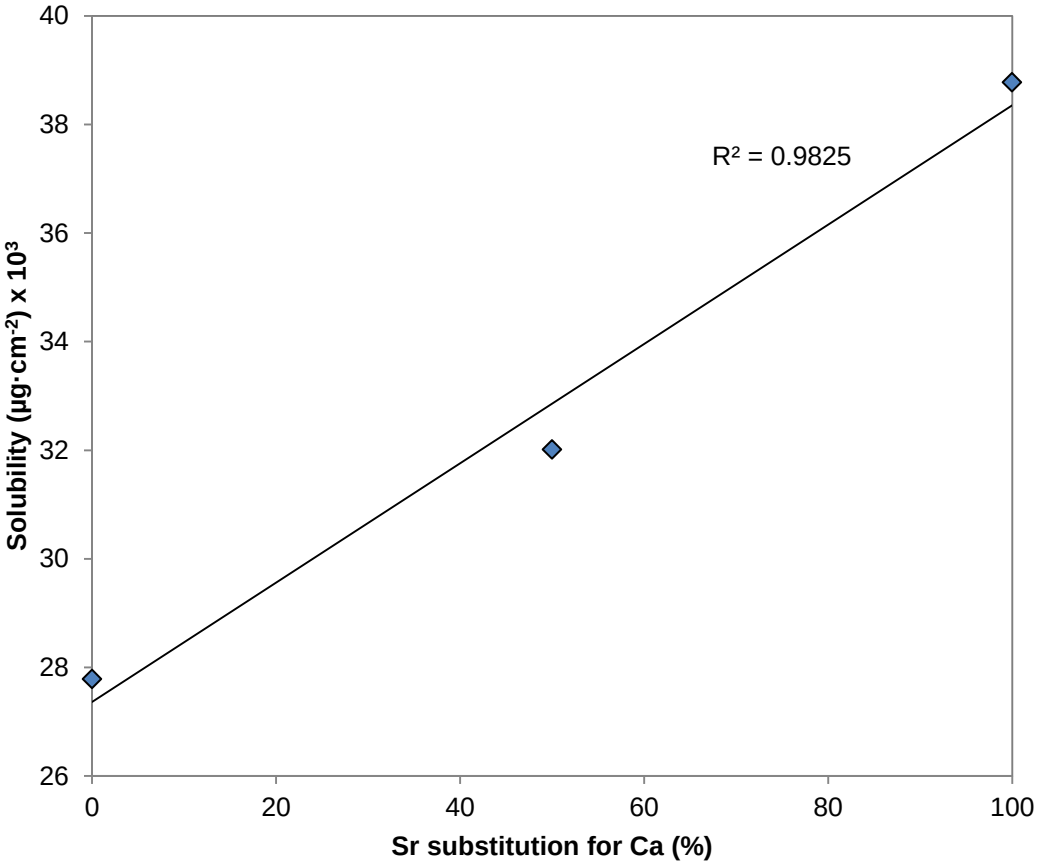

Figure 5.5. Solubility of Sr0, Sr50 and Sr100 bioactive glasses, determined using a method based on the International Standard ISO6872 'Dentistry –Ceramic Materials' (2008).

5.1.7 SEM analysis of bioactive glasses

Scanning electron microscopy (SEM) micrographs of Sr0, Sr50 and Sr100 bioactive glass discs are presented in Figure 5.6, Figure 5.7 and Figure 5.8 respectively. The micrographs showed materials exhibiting a generally coarse surface which changed after the solubility tests were performed, adopting a smoother texture. It was observed that the surface of samples made of bioactive glasses containing a larger proportion of strontium in their composition (i.e. Sr50 and Sr100) usually exhibited a coarser surface than those samples made of Sr0 bioactive glass after the solubility tests were performed and the modified surface layer was removed, mainly because a fraction of the modified surface remained attached to those samples.

5.1.8 EDS analysis of bioactive glasses

Plots of the energy dispersive X-ray spectroscopy (EDS) analysis of Sr0, Sr50 and Sr100 bioactive glasses are shown in Figure 5.6, Figure 5.7 and Figure 5.8 respectively. EDS confirmed the presence of all the chemical elements which form each bioactive glass compositions (i.e. oxygen, sodium, silicon, phosphorus, calcium and strontium), demonstrating that the technique was appropriate to differentiate between the three glasses. The data also confirmed that a compositional change occurred on the surface of the bioactive glass discs during the solubility test. The main chemical elements detected in the detached surface material were silicon and oxygen, suggesting that the material may be mainly composed by an oxidised form of silicon which remained after the dissolution of the other chemical elements present in the glass composition.

<table>
<tr><th colspan="2">Sr0 bioactive glass</th></tr>
<tr><td colspan="2">Bioactive glass disc surface before solubility test</td></tr>
<tr><td>SEM</td><td>EDS</td></tr>
<tr><td> 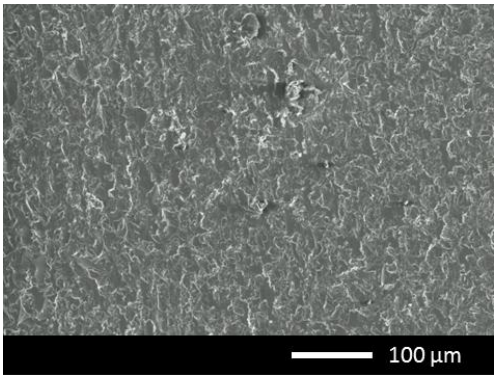
</td><td> 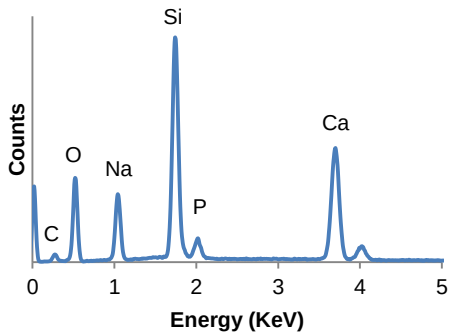
</td></tr>
<tr><td colspan="2">Bioactive glass disc surface after solubility test
and removal of surface material</td></tr>
<tr><td>SEM</td><td>EDS</td></tr>
<tr><td> 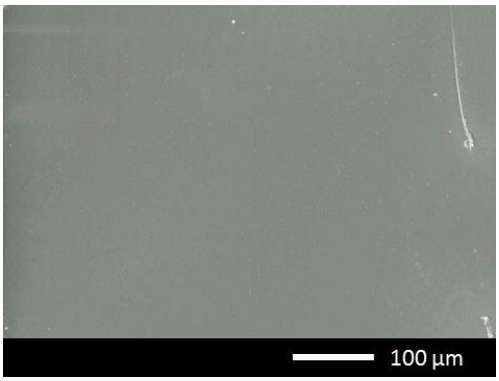
</td><td> 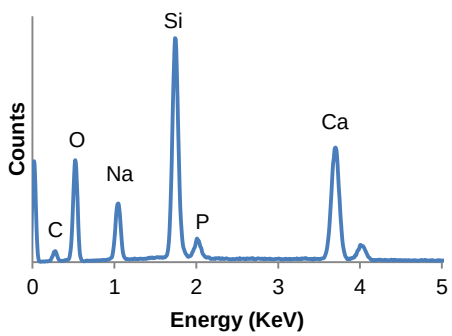
</td></tr>
<tr><td colspan="2">Fragment of detached surface material after solubility test</td></tr>
<tr><td>SEM</td><td>EDS</td></tr>
<tr><td> 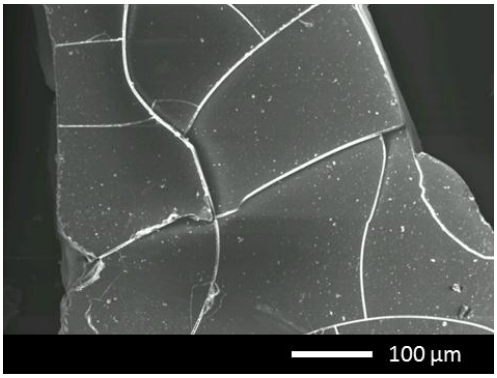
</td><td> 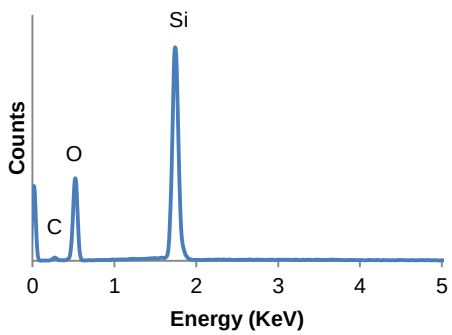
</td></tr>
</table>

Figure 5.6. Scanning electron microscopy (SEM) micrographs and energy dispersive X-ray spectroscopy (EDS) spectra of Sr0 bioactive glass discs before and after the solubility tests, and of the surface material which became detached after the solubility tests.

<table>
<tr><th colspan="2">Sr50 bioactive glass</th></tr>
<tr><td colspan="2">Bioactive glass disc surface before solubility test</td></tr>
<tr><td>SEM</td><td>EDS</td></tr>
<tr><td> 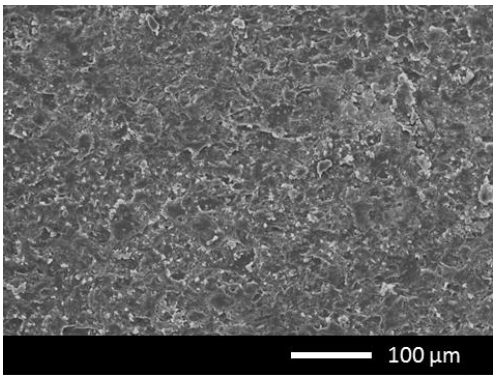
</td><td> 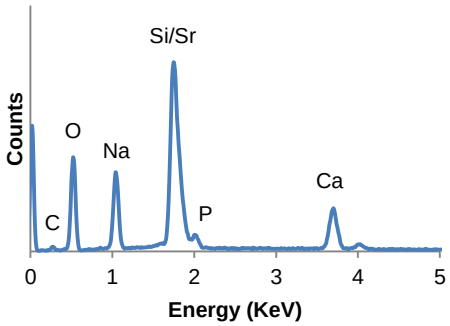
</td></tr>
<tr><td colspan="2">Bioactive glass disc surface after solubility test
and removal of surface material</td></tr>
<tr><td>SEM</td><td>EDS</td></tr>
<tr><td> 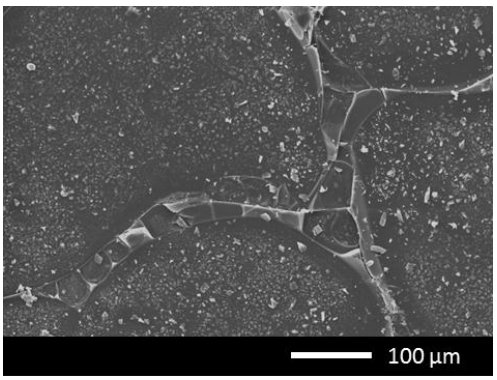
</td><td> 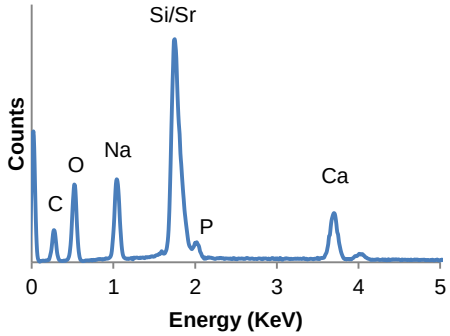
</td></tr>
<tr><td colspan="2">Fragment of detached surface material after solubility test</td></tr>
<tr><td>SEM</td><td>EDS</td></tr>
<tr><td> 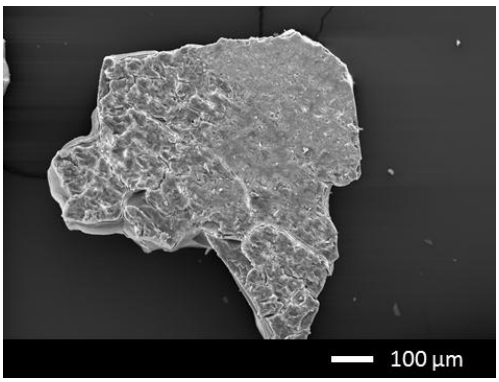
</td><td> 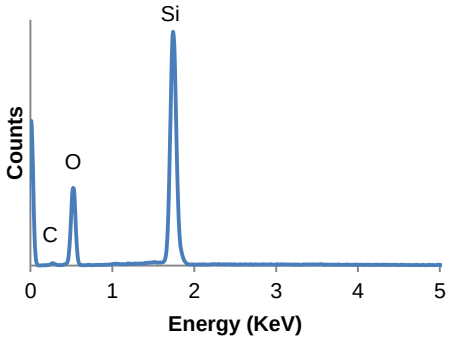
</td></tr>
</table>

Figure 5.7. Scanning electron microscopy (SEM) micrographs and energy dispersive X-ray spectroscopy (EDS) spectra of Sr50 bioactive glass discs before and after the solubility tests, and of the surface material which became detached after the solubility tests.

<table>
<tr><th colspan="2">Sr100 bioactive glass</th></tr>
<tr><td colspan="2">Bioactive glass disc surface before solubility test</td></tr>
<tr><td>SEM</td><td>EDS</td></tr>
<tr><td> 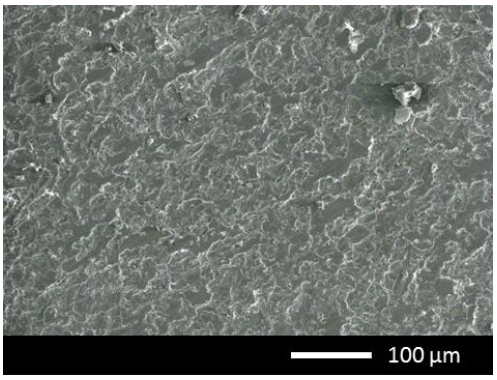
</td><td> 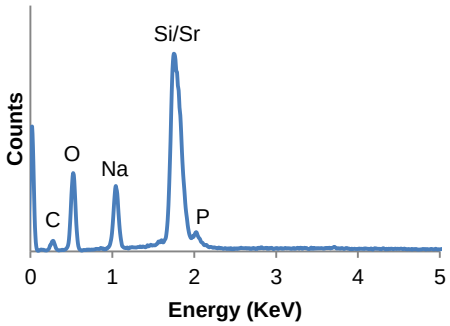
</td></tr>
<tr><td colspan="2">Bioactive glass disc surface after solubility test
and removal of surface material</td></tr>
<tr><td>SEM</td><td>EDS</td></tr>
<tr><td> 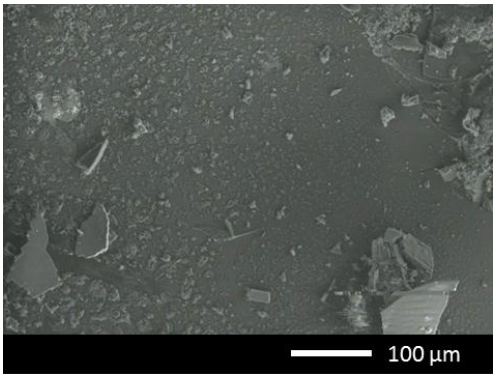
</td><td> 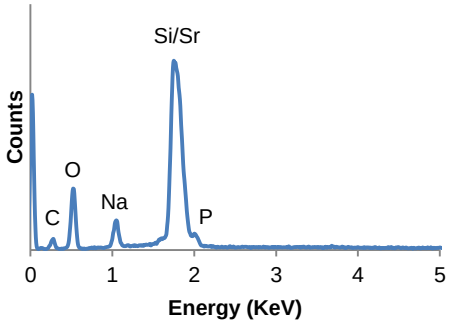
</td></tr>
<tr><td colspan="2">Fragment of detached surface material after solubility test</td></tr>
<tr><td>SEM</td><td>EDS</td></tr>
<tr><td> 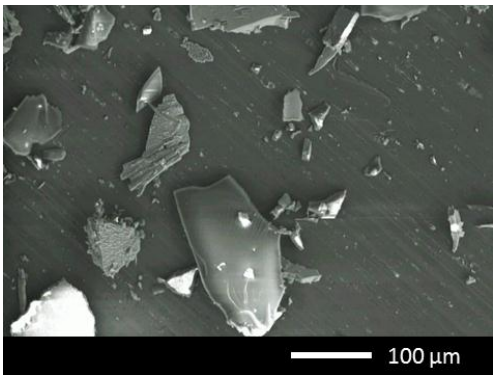
</td><td> 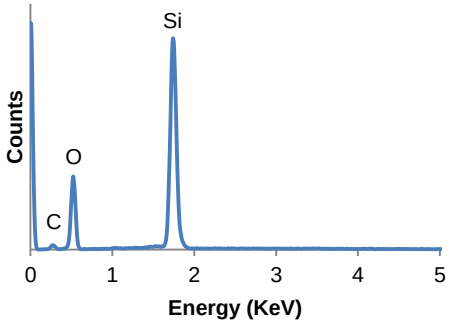
</td></tr>
</table>

Figure 5.8. Scanning electron microscopy (SEM) micrographs and energy dispersive X-ray spectroscopy (EDS) spectra of Sr100 bioactive glass discs before and after the solubility tests, and of the surface material which became detached after the solubility tests.

5.1.9 Particle size analysis of milled bioactive glasses

Particle size analyses of the bioactive glass powders were performed using static light scattering particle size analysis. The distributions of the differential volume and the differential number of particles of Sr0, Sr50 and Sr100 bioactive glass powders produced through milling and sieving are shown in Figure 5.9 and Figure 5.10, respectively. Table 5.5 also presents the largest detected particle size, the mean particle size and the median particle size of each sample, as well as the standard deviation values.

The differential volume plots (Figure 5.9) show the volume occupied by each particle size, revealing that the greatest proportion of the volume in the three samples was occupied by particles with sizes around 10 μm and that a significant volume was occupied by particles with sizes below 1 μm. The differential number plots (Figure 5.10) show the number of particles detected for each particle size, revealing that particles with sizes below 1 μm were the most abundant in the three samples.

It was also observed that the particle size appeared to increase as the substitution of calcium by strontium in the glass composition increased (Table 5.5). SEM micrographs of the bioactive glass powders (Figure 5.11) showed that the samples exhibited a large variety of particle sizes and morphologies. The micrographs also confirmed the presence of a significant amount of particles smaller than 10 μm, which tended to agglomerate together or on the surface of larger particles.

Table 5.5. Largest detected particle size, mean particle size, median particle size and standard deviations of the distributions of Sr0, Sr50 and Sr100 bioactive glass powders.

Bioactive glass	Largest detected particle size (μm)	Mean particle size (μm)	Median particle size (μm)	Standard deviation (μm)
Sr0	44.6	9.9	7.9	8.2
Sr50	48.9	11.2	8.6	9.5
Sr100	58.6	12.2	9.7	10.0

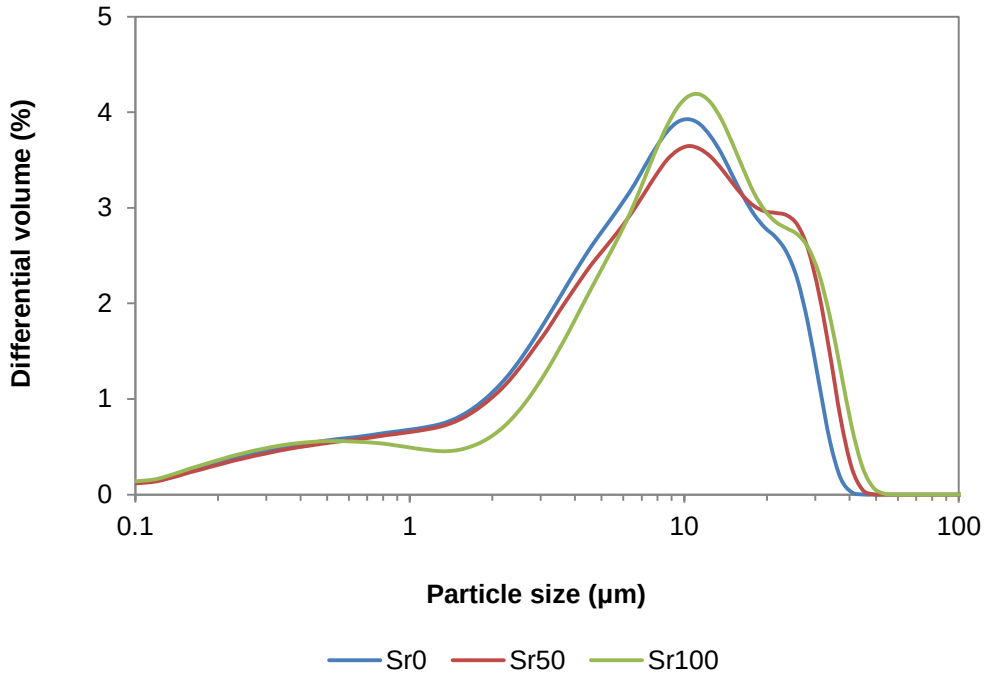

Figure 5.9. Graphical representation of the differential volume distribution of Sr0, Sr50 and Sr100 bioactive glass powders. This showed that particles with sizes around 10 µm occupied the greatest proportion of the volume in the three samples and that a significant volume was occupied with particles with sizes below 1 µm.

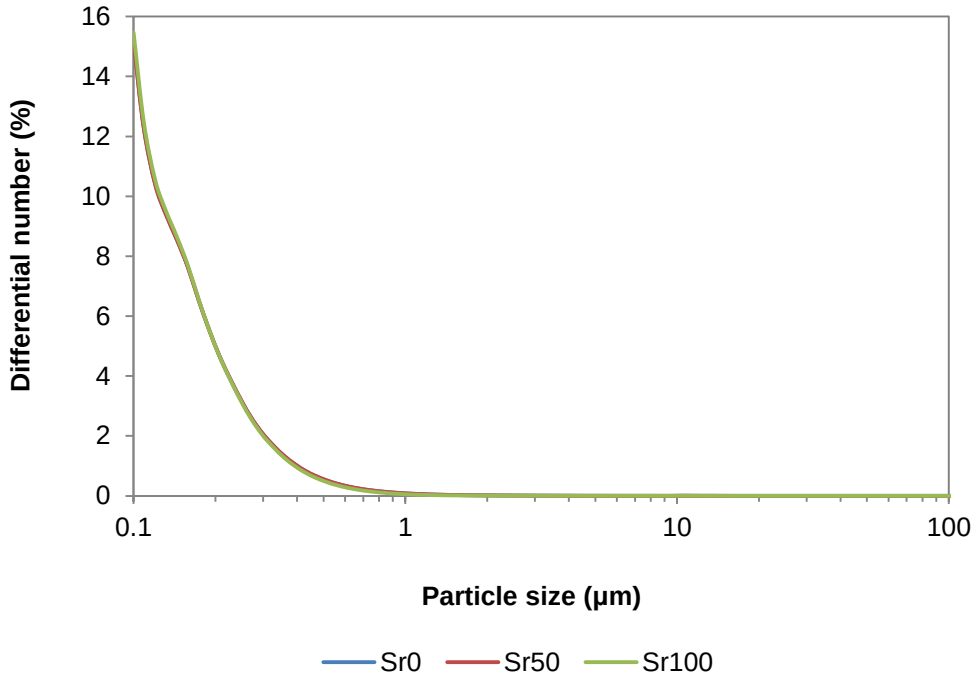

Figure 5.10. Graphical representation of the differential number distribution of Sr0, Sr50 and Sr100 bioactive glass powders. This showed that particles with sizes <1 µm were the most abundant in the samples of the three bioactive glasses.

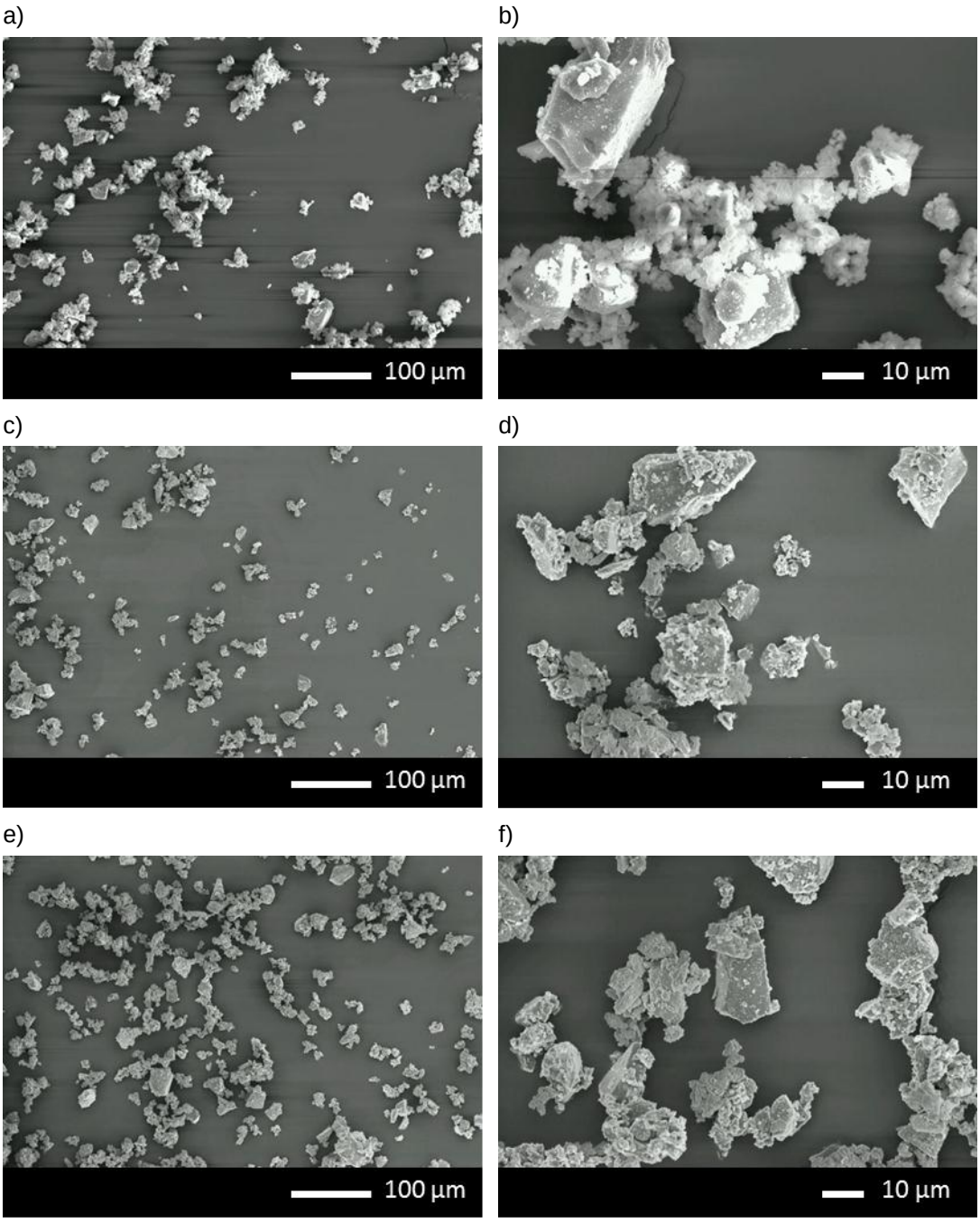

Figure 5.11. Scanning electron microscopy micrographs of Sr0 (a and b), Sr50 (c and d) and Sr100 (e and f) bioactive glass powders at various magnifications.

5.2 Electrospinning of composite materials

5.2.1 Optimisation study of electrospinning parameters

Effect of polymer concentration and solvent composition

The first part of this study investigated the effect of poly(caprolactone) (PCL) concentration and solvent composition on the electrospinning process.

Visual examination of the electrospun materials showed that the surface of the membranes displayed the lowest levels of defects caused by sputtering when concentrations between 10 and 12 wt% of PCL dissolved in blends of DCM and DMF with ratios 90:10 v/v and 85:15 v/v were used. Other concentrations of PCL and ratios of DCM:DMF generally produced rougher surfaces. In addition, solutions using only DCM generated materials which were too fragile and broke easily, in particular those made with a concentration of 8 wt% PCL.

Scanning electron microscopy (SEM) micrographs of the materials, presented in Figure 5.12 and Figure 5.13, showed that the samples produced with the solvent blend DCM:DMF 100:0 v/v exhibited an irregular distribution of fibre diameters. Increasing the proportion of DMF in the solvent blend resulted in the production of fibres with less variability in fibre diameter and, potentially, a more homogeneous distribution of fibre sizes.

Regarding the effect of polymer concentration, the samples produced with solutions of 8 wt% PCL exhibited fibres with beads. Increasing the concentration of PCL appeared to generate a more regular distribution of fibre sizes and to reduce the amount of beads. At 10 wt% a small amount of beading could still be observed in the samples fabricated using DCM:DMF 95:5 v/v, but this effect was eliminated in those samples fabricated using DCM:DMF 90:10 v/v and 85:15 v/v. However, the higher concentrations also resulted in an apparent increase in fibre diameter. SEM micrographs of the materials generated with solutions of 10 wt% PCL, presented in Figure 5.12 and Figure 5.13, appeared to exhibit an apparently more homogeneous distribution of fibre sizes and smaller diameters.

In conclusion, the solution compositions of 10 wt% PCL in DCM:DMF 90:10 v/v and in DCM:DMF 85:15 v/v were selected to be used in the following part of the optimisation study as these appeared to produce the most regular fibre diameters and morphologies of electrospun fibres.

Effect of bioactive glass particle content

The second part of the study investigated the effect of bioactive glass particle content in the electrospinning process.

Visual examination of the materials showed that the surface of the membranes exhibited a larger amount of defects caused by sputtering as the amount of glass particles added to the PCL solution increased. The smallest amount of surface defects were observed in those materials fabricated using solutions of PCL with bioactive glass particles added following a 10:1 PCL:glass weight ratio. In addition, it was observed that the solvent blend DCM:DMF 90:10 v/v generally produced smoother surfaces than DCM:DMF 85:15 v/v. Finally, the increase in glass particle content also resulted in the generation of more fragile materials.

SEM micrographs of the composite materials, shown in Figure 5.14, also exhibited an apparent increase in fibre diameter after the bioactive glass particles were added to the solutions.

In conclusion, the solution composition of 10 wt% PCL in DCM:DMF 90:10 v/v was selected to fabricate the electrospun composite materials to be used in the rest of the project. This composition was considered appropriate due to generally producing electrospun materials which could be handled without breaking; they presented the smallest observed amounts of surface and fibre defects; and generated relatively regular distributions of fibre sizes compared with other compositions.

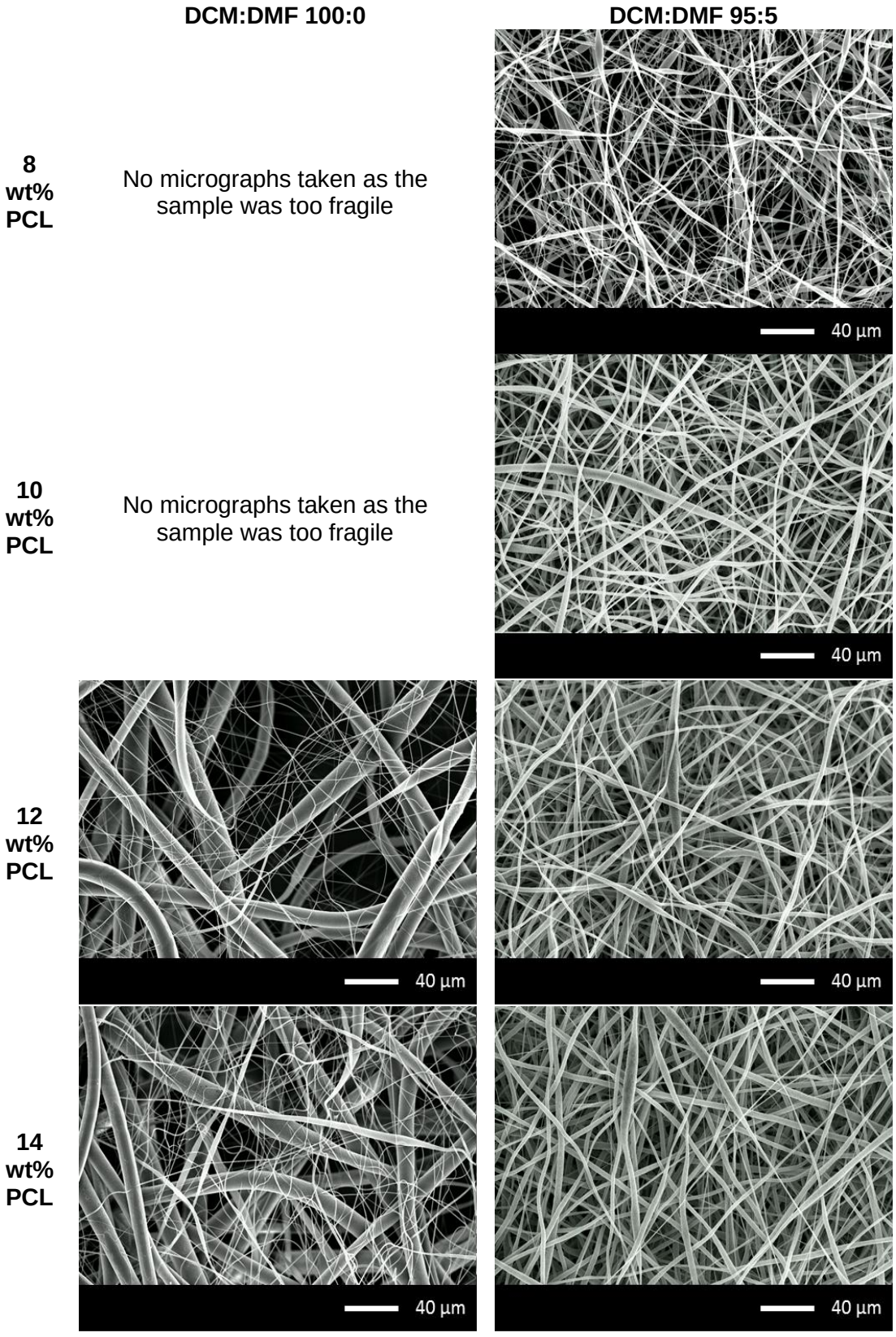

Figure 5.12. Scanning electron microscopy micrographs of non-composite electrospun materials produced for the first part of the optimisation study. The composition of the polymer solutions used were 8 wt%, 10 wt%, 12 wt% and 14 wt% of poly(caprolactone) (PCL) in blends of dichloromethane (DCM) and dimethylformamide (DMF) with ratios of 100:0 v/v and 95:5 v/v.

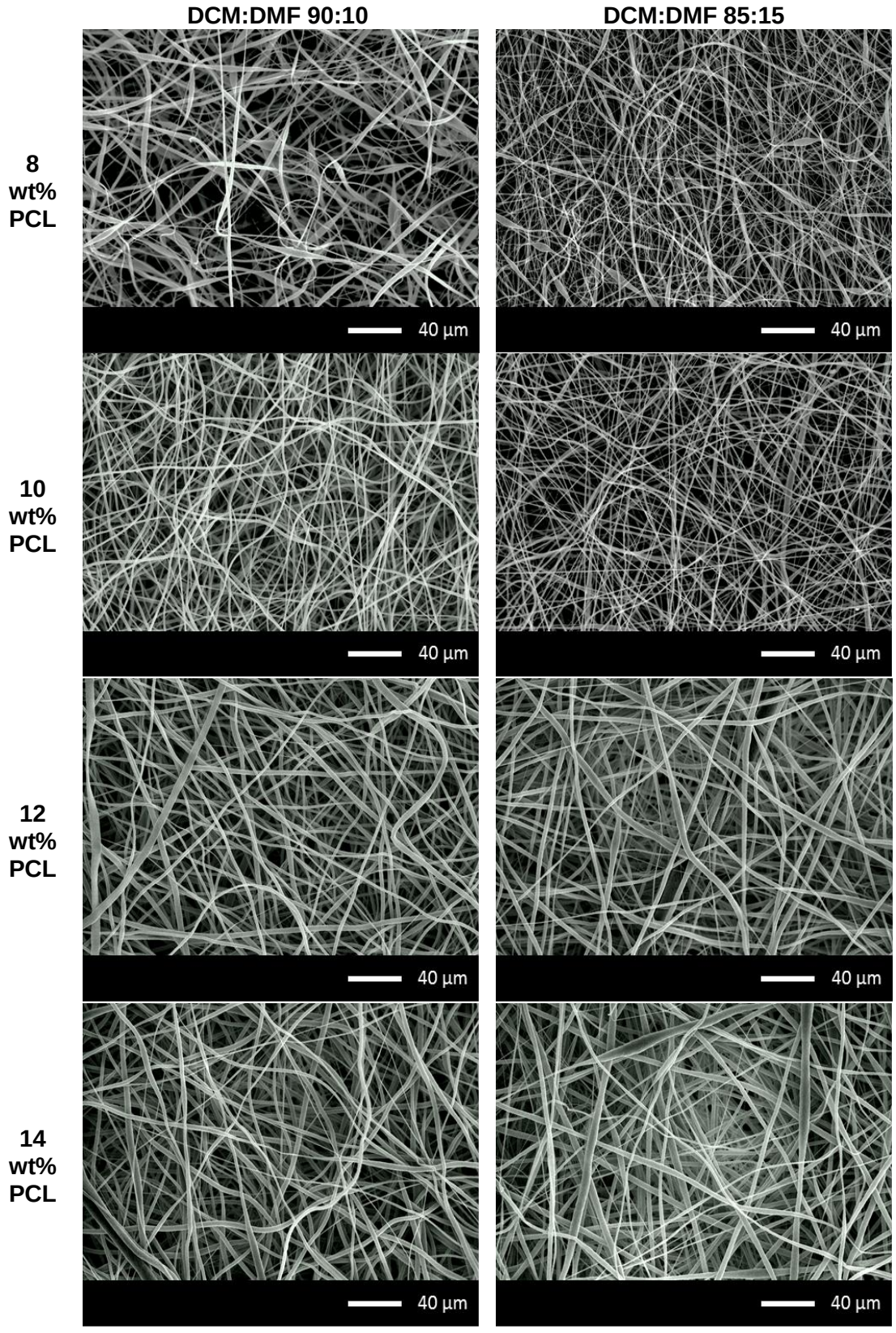

Figure 5.13. Scanning electron microscopy micrographs of non-composite electrospun materials produced for the first part of the optimisation study. The composition of the polymer solutions used were 8 wt%, 10 wt%, 12 wt% and 14 wt% of poly(caprolactone) (PCL) in blends of dichloromethane (DCM) and dimethylformamide (DMF) with ratios of 90:10 v/v and 85:15 v/v.

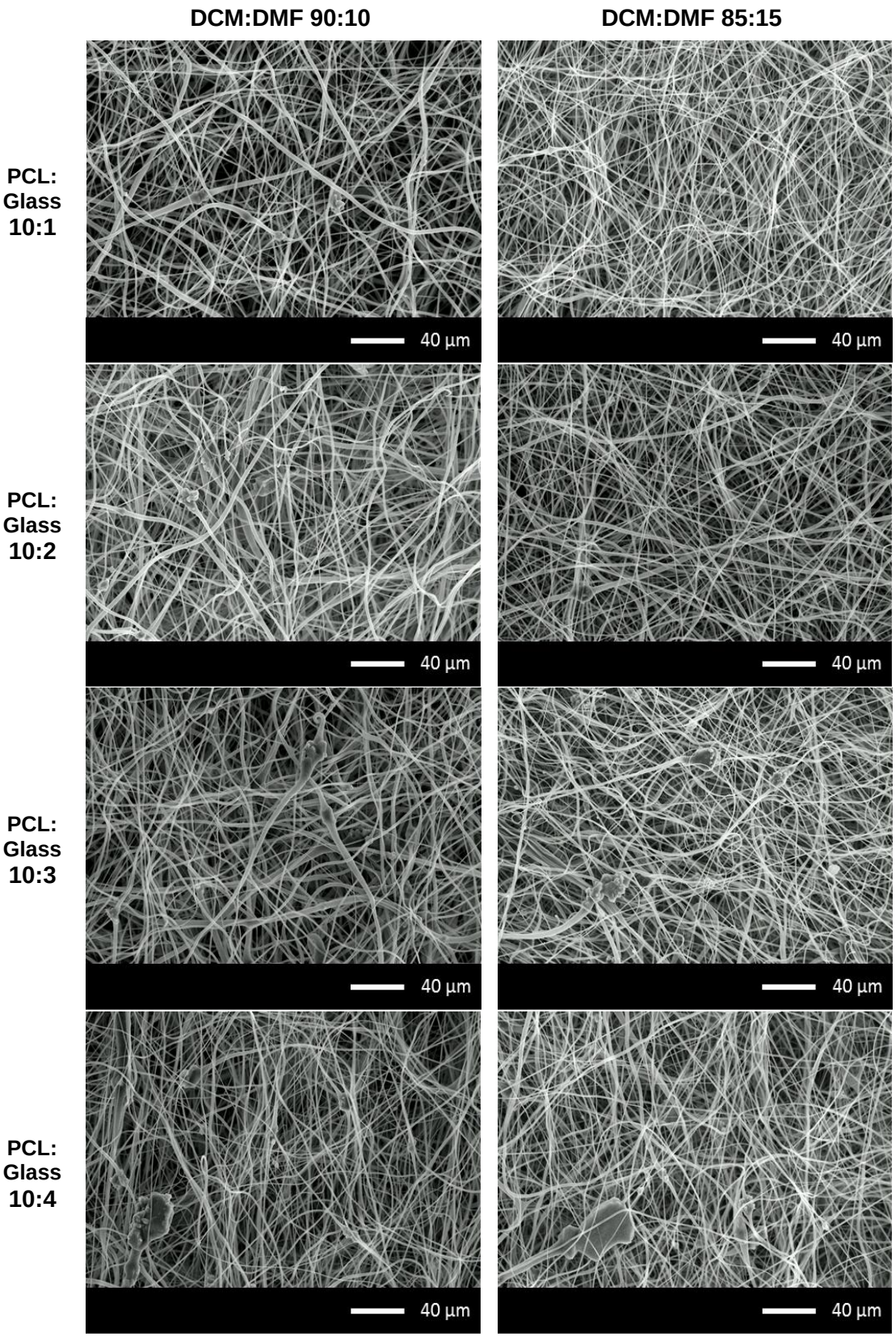

Figure 5.14. Scanning electron microscopy micrographs of the composite electrospun materials fabricated for the second part of the optimisation study. Sr0, Sr50 and Sr100 bioactive glass particles were added to the poly(caprolactone) (PCL) solution following PCL:glass weight ratios 10:1, 10:2, 10:3 and 10:4.

5.2.2 SEM analysis of electrospun materials

SEM micrographs of the electrospun materials fabricated using the composition selected in the optimisation study showed that the non-composite materials made of only PCL (Figure 5.15, a and b) were composed of fibres with relatively regular diameters and no apparent defects on their surface. Larger magnification micrographs of the materials (Figure 5.15, c and d) showed that the surface of the fibres was generally porous.

In the case of the composite electrospun materials made of PCL and particles of Sr0 (Figure 5.16), Sr50 (Figure 5.17) and Sr100 (Figure 5.18) bioactive glasses, it was observed that many of the fibres presented regions with increased diameters and irregular morphologies where the glass particles may be contained. The distribution of such regions in the material appeared to be random and no areas were identified on the mats where those regions may have been preferentially formed.

The micrographs also showed an apparent increase in the variability of fibre diameter compared to the non-composite materials, as previously mentioned in the optimisation study. No significant differences were observed between samples containing particles of different bioactive glass compositions. The surface of the fibres in the composite materials was also observed to be porous, with the irregular regions potentially showing a higher degree of porosity (Figure 5.16, d; and Figure 5.18, d).

The non-composite fibres, showing no apparent variations in their morphology, were labelled ‘unfilled fibres’. The irregular regions, observed in the composite fibres, were labelled ‘filled regions’. The average diameters of both ‘unfilled fibres’ and ‘filled regions’ were calculated using SEM micrographs of the electrospun materials and the results are shown in Table 5.6.

Table 5.6. Average diameters and standard deviation for the 'unfilled’ fibres and the 'filled’ regions on the composite electrospun materials.

	Unfilled fibres	**Filled regions**
Diameter ± SD (μm)	1.99 ± 0.36	14.02 ± 7.67

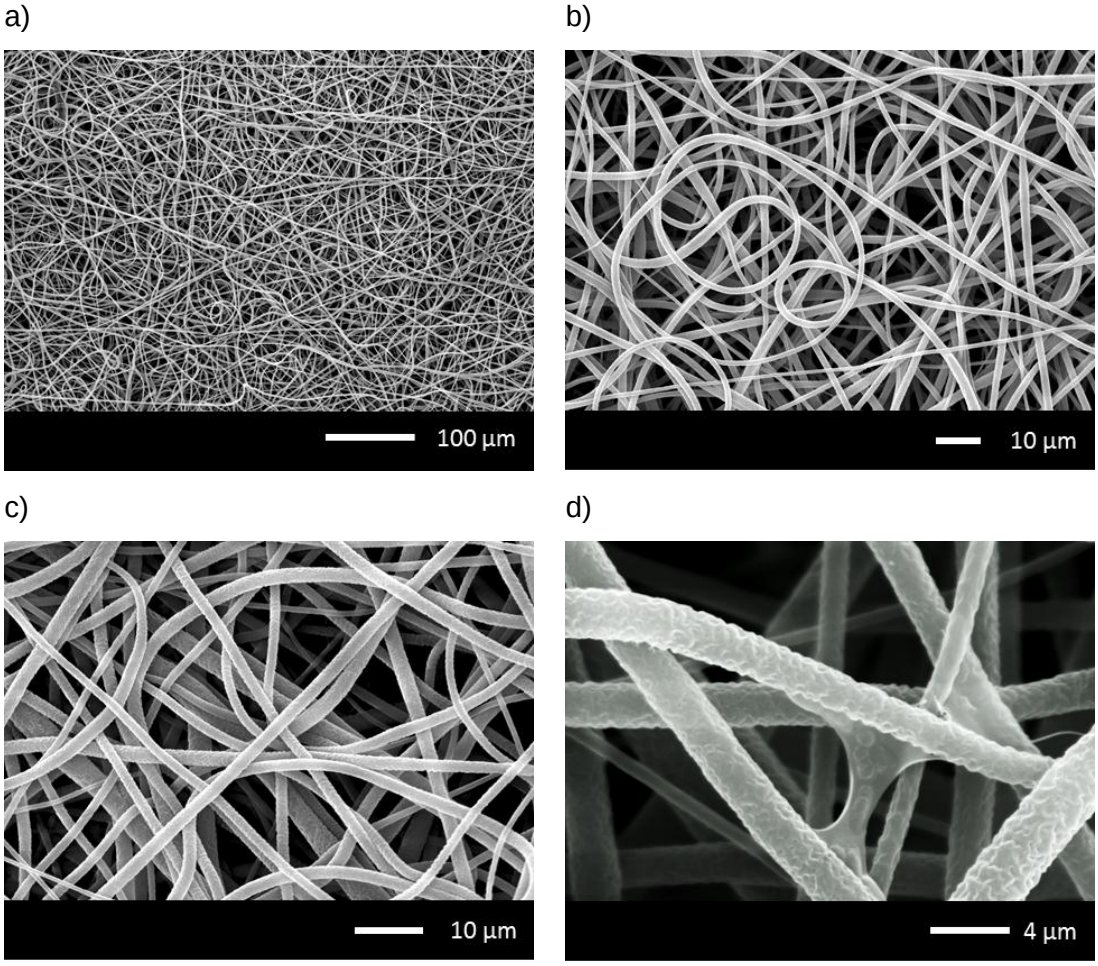

Figure 5.15. Scanning electron microscopy micrographs of non-composite electrospun PCL at various magnifications.

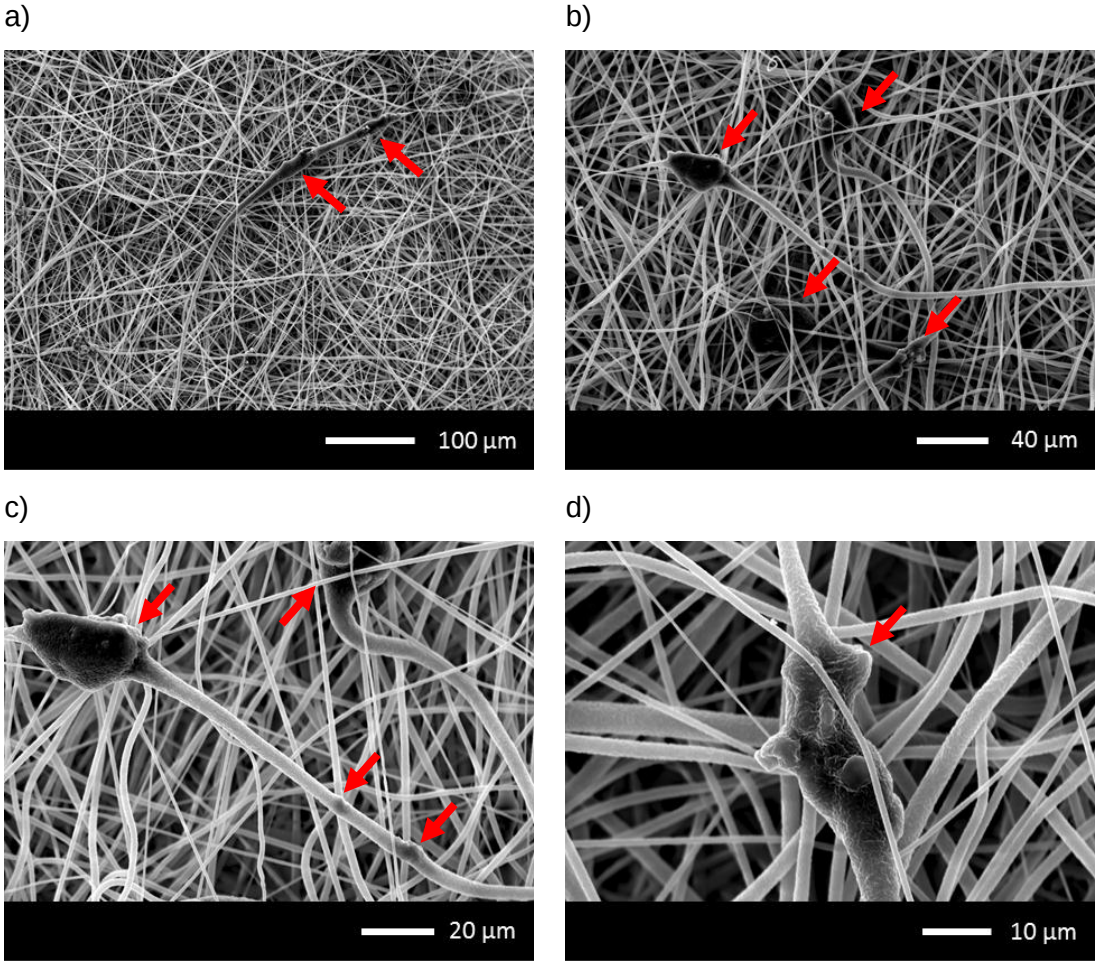

Figure 5.16. Scanning electron microscopy micrographs of composite electrospun materials made of PCL and Sr0 bioactive glass particles at various magnifications. The red arrows indicate regions in the fibres with increased diameters and irregular morphologies where the particles may be contained.

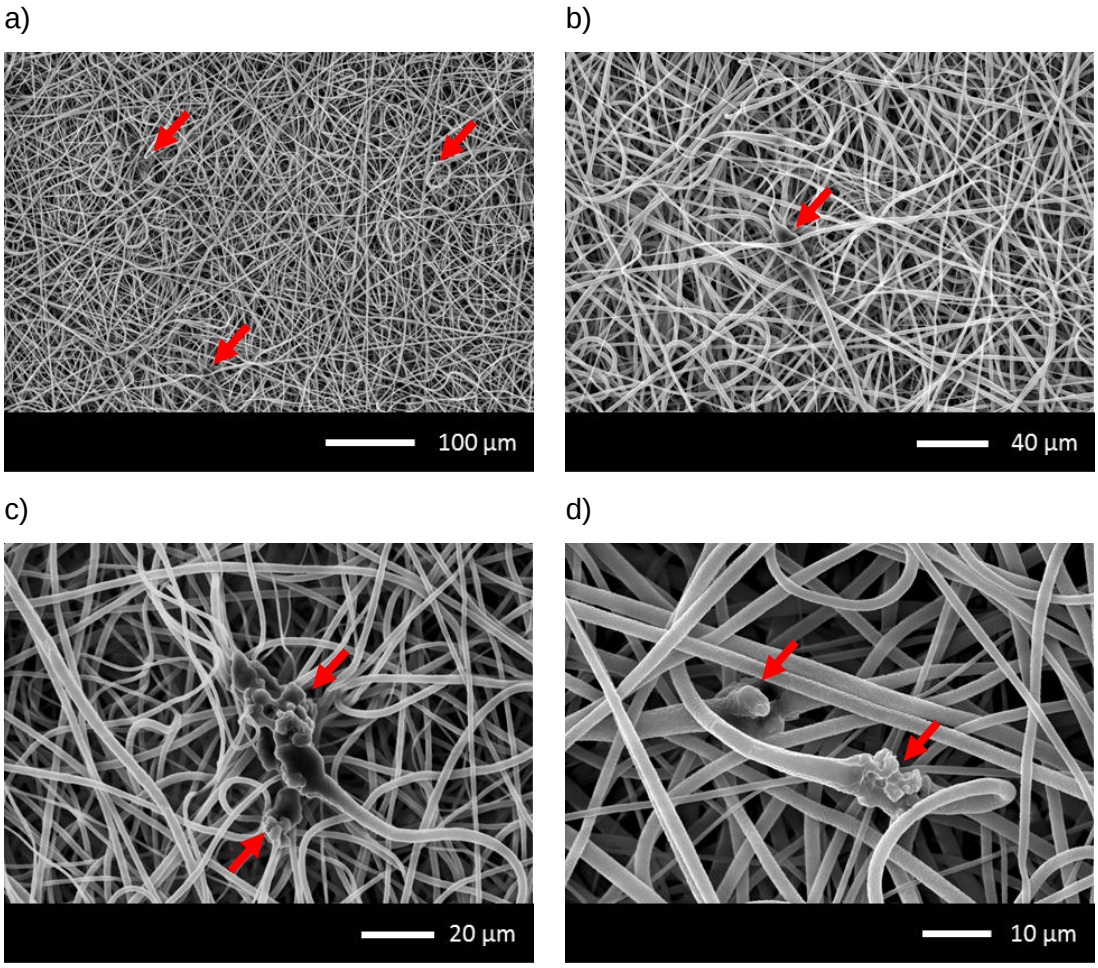

Figure 5.17. Scanning electron microscopy micrographs of composite electrospun materials made of PCL and Sr50 bioactive glass particles at various magnifications. The red arrows indicate regions in the fibres with increased diameters and irregular morphologies where the particles may be contained.

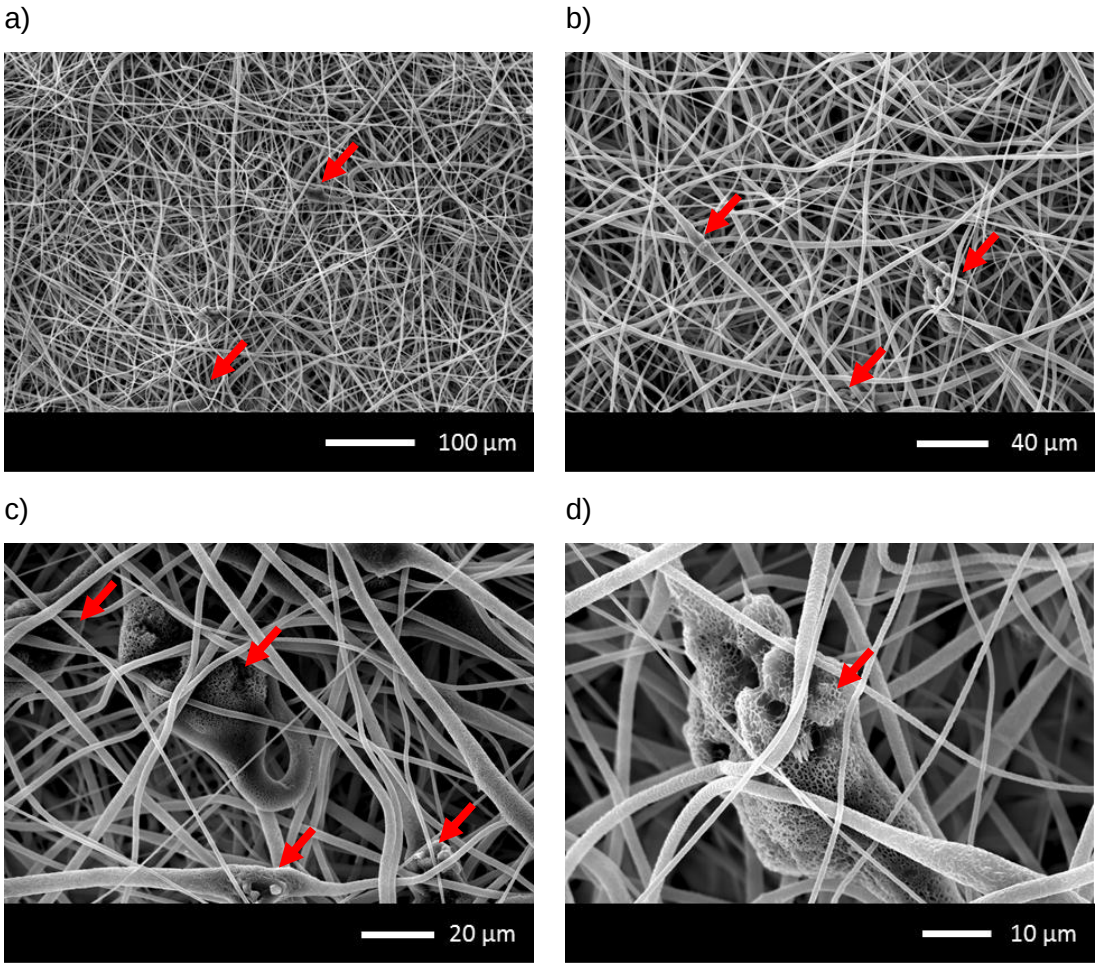

Figure 5.18. Scanning electron microscopy micrographs of composite electrospun materials made of PCL and Sr100 bioactive glass particles at various magnifications. The red arrows indicate regions in the fibres with increased diameters and irregular morphologies where the particles may be contained.

5.2.3 EDS analysis of electrospun materials

Energy dispersive X-ray spectroscopy (EDS) plots of the electrospun materials are presented in Figure 5.19. In the case of the 'unfilled fibres' in the non-composite material EDS detected the presence of only carbon and oxygen. However, in the case of the 'filled regions' in the composite materials, made of PCL and particles of Sr0, Sr50 and Sr100 bioactive glass, the analyses also detected the presence of the chemical elements which constitute each bioactive glass composition (i.e. oxygen, sodium, silicon, phosphorus, calcium and strontium), being able to differentiate between the three glasses.

5.2.4 Solubility study of electrospun materials

The pH variation plots of the solubility study of the electrospun materials are presented in Figure 5.20. In the case of the bioactive glass powders (Figure 5.20, a), it was observed that there was an initial rapid increase of the pH towards alkaline values. It peaked at values around 10 by the end of the first 24 hours and then slowly decreased to values around 8 by the end of the experiment. The pH of the control samples, composed of deionised water only, remained approximately constant throughout the whole study. In the case of the composite electrospun materials (Figure 5.20, b), a similar initial increase of the pH was observed, with peak values around 10 after 24 hours as well. However, the subsequent reduction of pH occurred significantly faster, reaching values between 8 and 9 after 168 hours and then stabilising at values around 7 by the end of the study. The pH of the control samples also remained approximately constant throughout the whole experiment.

Statistically significant differences (Two-tailed Student's t-test) between the pH values of the electrospun materials PCL/Sr0 and PCL/Sr100 were observed in the period of time between 48 hours and 192 hours; and were also observed between the pH values of the electrospun materials PCL/Sr50 and PCL/Sr100 in the period comprised between 72 hours and 168 hours. PCL/Sr0 and PCL/Sr50 presented statistically significant differences only at 24 hours. The relevant statistical information is shown in Table 5.7.

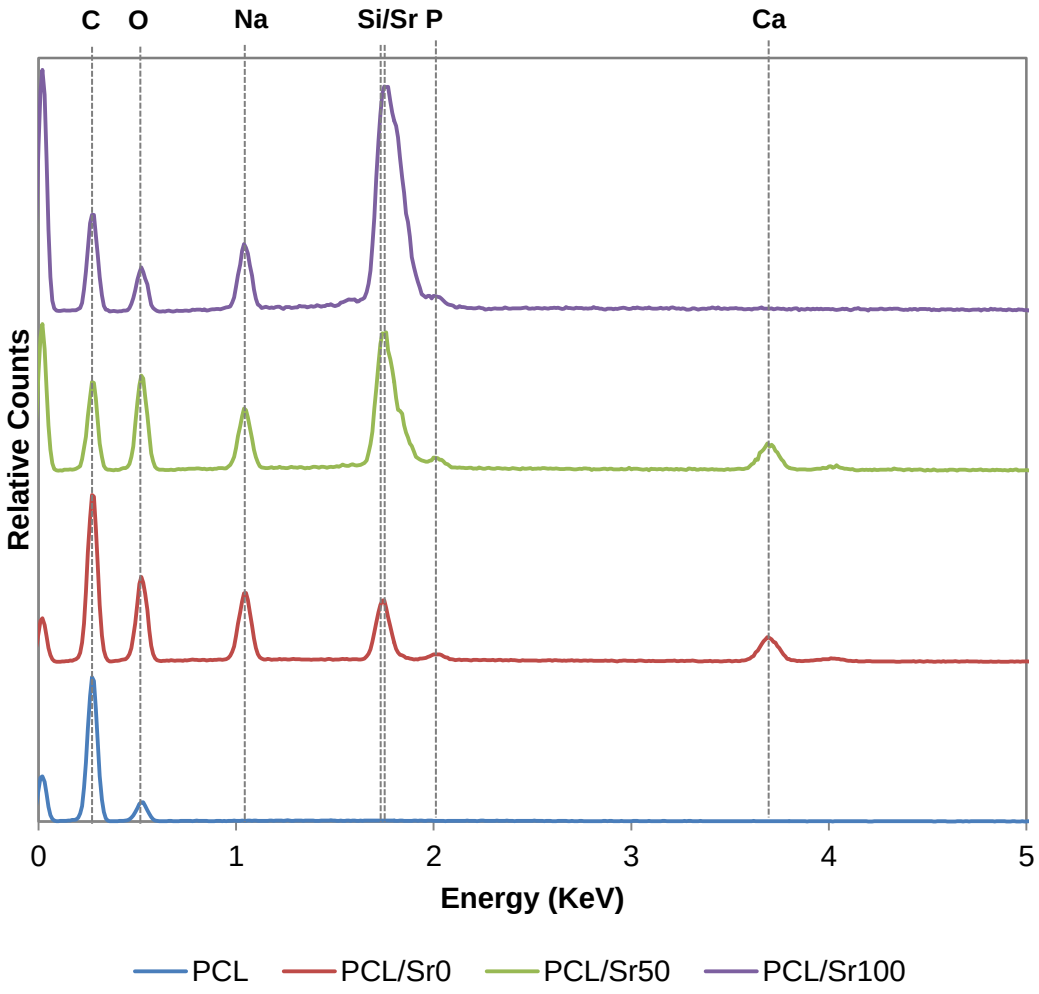

Figure 5.19. Energy dispersive X-ray spectroscopy plots of non-composite 'unfilled fibres' made of electrospun poly(caprolactone) (PCL) and of composite 'filled regions' made of PCL containing Sr0 (PCL/Sr0), Sr50 (PCL/Sr50) and Sr100 (PCL/Sr100) bioactive glass particles. The peaks belonging to the detected chemical elements are identified using their corresponding symbols (i.e. Si, Na, Ca, Sr, O, C).

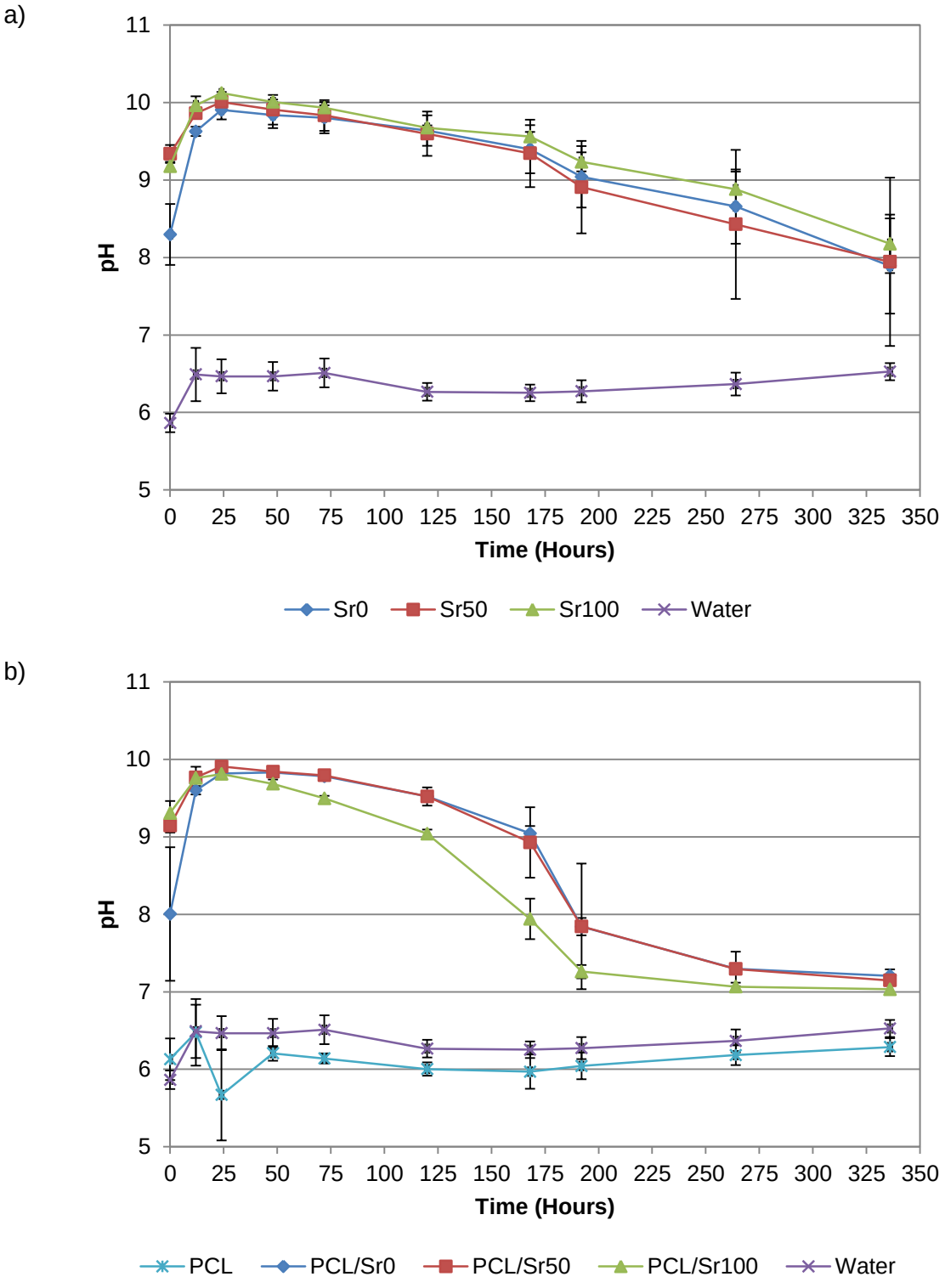

Figure 5.20. pH variation plots of the solubility study of electrospun materials: a) 1 mg of Sr0, Sr50 and Sr100 bioactive glass powders in 20 ml of deionised water; b) 10 mg of non-composite electrospun poly(caprolactone) in 20 ml of deionised water (PCL) and 10 mg of composite electrospun PCL containing particles of Sr0 (PCL/Sr0), Sr50 (PCL/Sr50) and Sr100 (PCL/Sr100) bioactive glass. The control samples were vials containing only 20 ml of deionised water.

Table 5.7. Statistical information from two-tail Student's t-test analyses of the pH values in the time period between 24 hours and 264 hours for: a) PCL/Sr0 vs. PCL/Sr50; b) PCL/Sr0 vs. PCL/Sr100; and c) PCL/Sr50 vs. PCL/Sr100 (n = 3; α = 0.05).

a)

PCL/Sr0 vs PCL/Sr50					
Time	Sample	Mean	SD	*t* - value	*p* - value
24 h	PCL/Sr0	9.82	0.07	-5.20	0.035
	PCL/Sr50	9.91	0.05		
48 h	PCL/Sr0	9.83	0.02	-0.58	0.622
	PCL/Sr50	9.84	0.03		
72 h	PCL/Sr0	9.78	0.03	-0.33	0.774
	PCL/Sr50	9.79	0.04		
120 h	PCL/Sr0	9.52	0.02	<-0.01	1.000
	PCL/Sr50	9.52	0.05		
168 h	PCL/Sr0	9.04	0.10	0.41	0.720
	PCL/Sr50	8.93	0.45		
192 h	PCL/Sr0	7.84	0.11	<-0.01	0.995
	PCL/Sr50	7.84	0.81		
264 h	PCL/Sr0	7.30	0.05	0.03	0.977
	PCL/Sr50	7.29	0.22		

b)

PCL/Sr0 vs PCL/Sr100					
Time	Sample	Mean	SD	*t* - value	*p* - value
24 h	PCL/Sr0	9.82	0.07	0.16	0.888
	PCL/Sr100	9.81	0.01		
48 h	PCL/Sr0	9.83	0.02	4.61	0.044
	PCL/Sr100	9.68	0.06		
72 h	PCL/Sr0	9.78	0.03	42.50	<0.001
	PCL/Sr100	9.50	0.03		
120 h	PCL/Sr0	9.52	0.02	24.00	0.002
	PCL/Sr100	9.04	0.05		
168 h	PCL/Sr0	9.04	0.10	6.69	0.022
	PCL/Sr100	7.94	0.26		
192 h	PCL/Sr0	7.84	0.11	16.09	0.004
	PCL/Sr100	7.26	0.09		
264 h	PCL/Sr0	7.30	0.05	4.13	0.054
	PCL/Sr100	7.07	0.05		

c)

PCL/Sr50 vs PCL/Sr100					
Time	Sample	Mean	SD	*t* - value	*p* - value
24 h	PCL/Sr50	9.91	0.05	3.33	0.080
	PCL/Sr100	9.81	0.01		
48 h	PCL/Sr50	9.84	0.03	3.33	0.080
	PCL/Sr100	9.68	0.06		
72 h	PCL/Sr50	9.79	0.04	7.32	0.018
	PCL/Sr100	9.50	0.03		
120 h	PCL/Sr50	9.52	0.12	5.20	0.035
	PCL/Sr100	9.04	0.05		
168 h	PCL/Sr50	8.93	0.45	8.32	0.014
	PCL/Sr100	7.94	0.26		
192 h	PCL/Sr50	7.84	0.81	1.25	0.340
	PCL/Sr100	7.26	0.09		
264 h	PCL/Sr50	7.29	0.22	1.45	0.285
	PCL/Sr100	7.07	0.05		

5.2.5 Addition of particles to the surface of electrospun fibres

The ‘loading method’ and the ‘filtering method’ were developed to add bioactive glass particles on the surface of the electrospun fibres.

Figure 5.21a presents the average mass variation in electrospun samples processed using both methods and suspensions of bioactive glass powders in DMEM cell culture medium at a concentration of 1% w/v. The control samples, processed using DMEM without any glass content (i.e. PCL, PCL/Sr0, PCL/Sr50 and PCL/Sr100), showed small negative mass variations. However, all the samples processed using the bioactive glass powder suspensions exhibited some degree of mass increase, which was significantly greater in the case of the ‘filtering method’. Figure 5.21b presents the average mass variation of electrospun samples processed using both methods and a series of suspensions of Sr0 bioactive glass powder in αMEM cell culture medium at various concentrations (i.e. 0% w/v, 0.05% w/v, 0.10% w/v, 0.25% w/v, 0.50% w/v and 1.00% w/v). The ‘filtering method’ showed significant increases of mass starting at a concentration of 0.05% w/v, while the ‘loading method’ showed it starting at a concentration of 0.50% w/v. In general, the ‘filtering method’ consistently presented greater mass variations. Statistical analyses (Two-tailed Student’s t-test, Table 5.8 and Table 5.9) reported significant differences in the mass variation between both methods in both tests.

Figure 5.22 and Figure 5.23 show SEM micrographs of electrospun samples processed using the ‘loading method’ and the ‘filtering method’ respectively. The micrographs showed particles of varying size and shape on the surface of the material. It was observed that the amount of particles was significantly greater in samples processed using the ‘filtering method’, forming larger masses of particles with more homogeneous distributions. In any case, the distribution of particles appeared to be random in both methods. Large amounts of deposited particles also appeared to block the pores of the electrospun mesh.

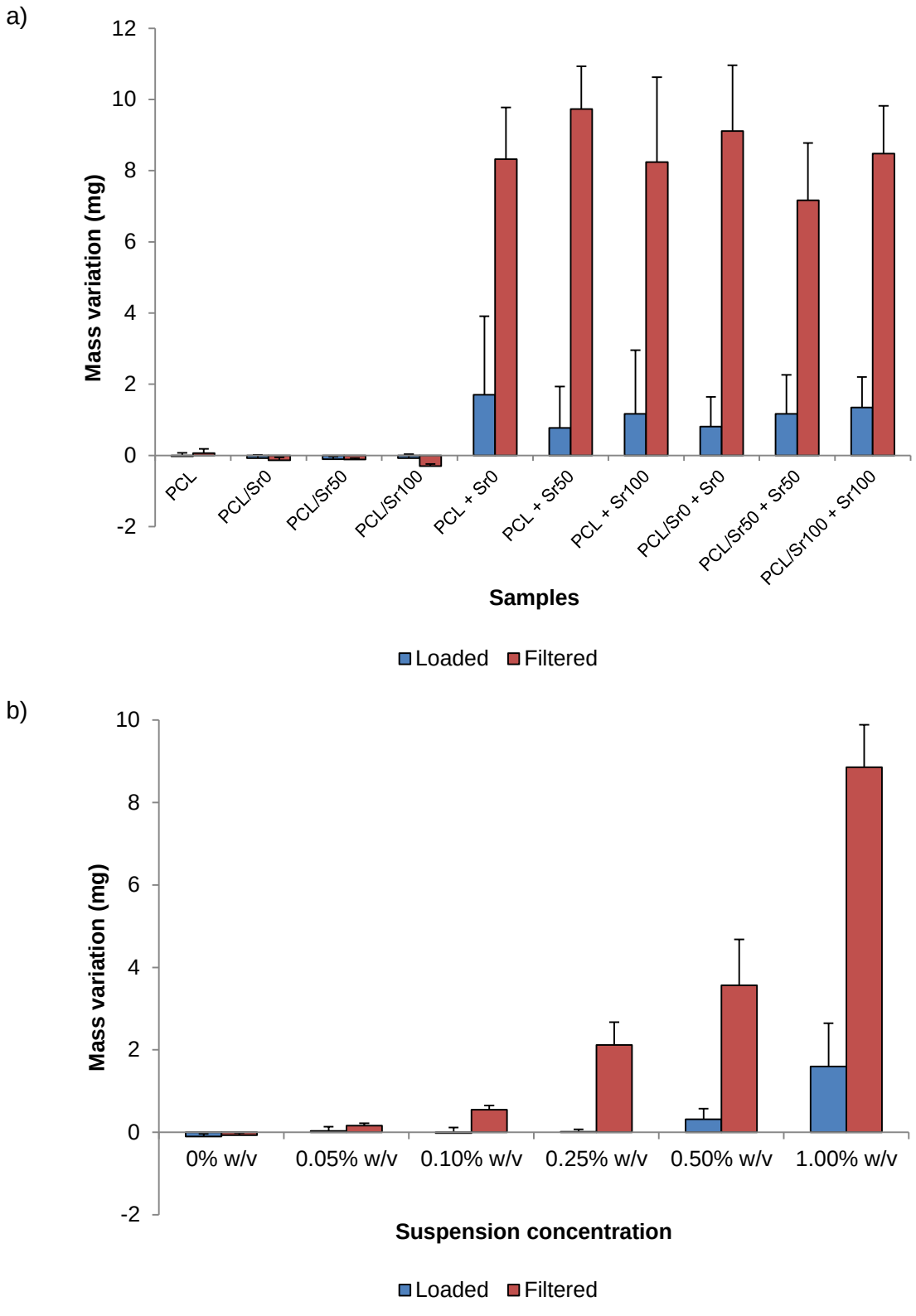

Figure 5.21. Average mass variation of non-composite electrospun PCL samples processed using the 'loading' and 'filtering' methods to add further bioactive glass particles on the surface of the materials: a) Samples processed using a 1% w/v suspension of Sr0, Sr50 and Sr100 bioactive glass powders in DMEM cell culture medium. b) Samples processed using a series of suspensions of increasing concentration of Sr0 bioactive glass powder in αMEM cell culture medium.

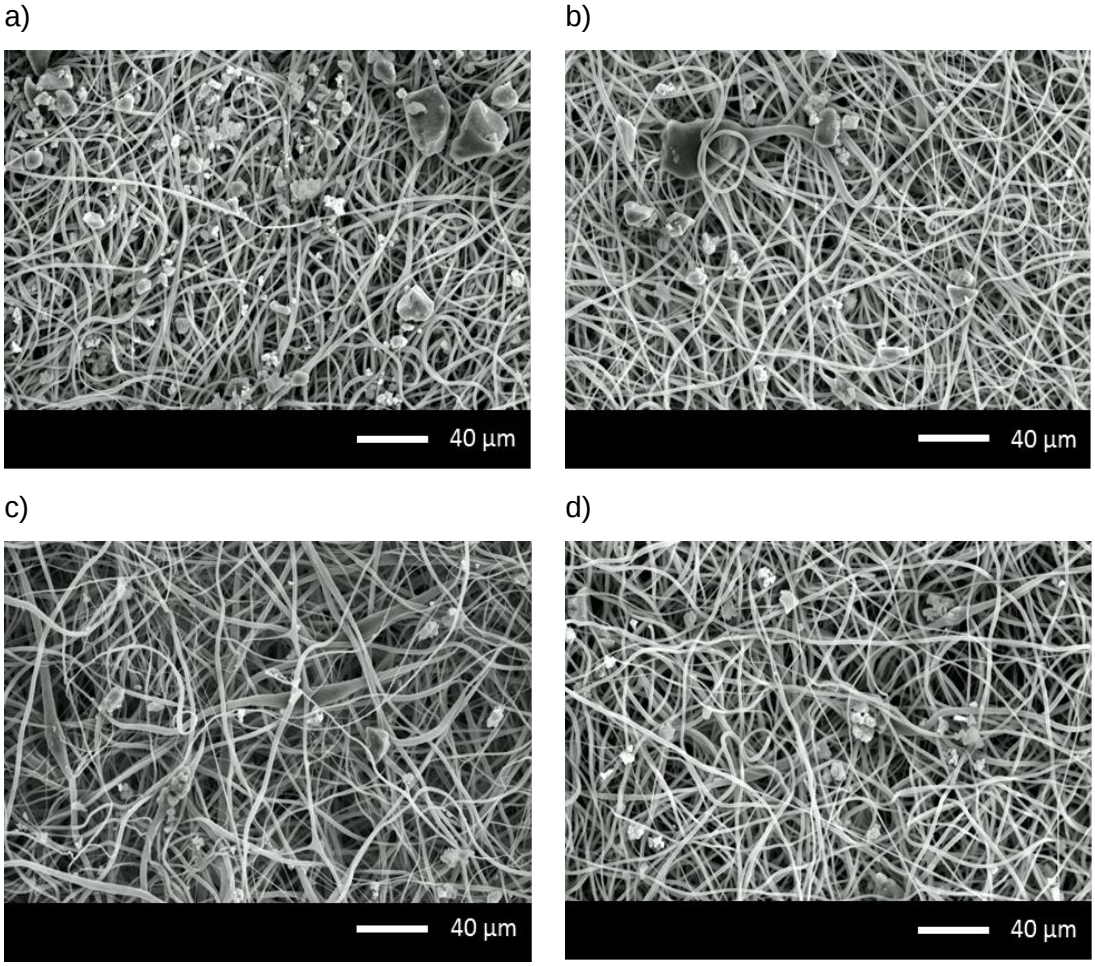

Figure 5.22. Scanning electron microscopy micrographs of electrospun materials processed using the 'loading method' and a 1% w/v suspension of bioactive glass powders. a) PCL + $Sr0^{L}$; b) PCL/Sr0 + $Sr0^{L}$; c) PCL/Sr50 + $Sr50^{L}$; d) PCL/Sr100 + $Sr100^{L}$.

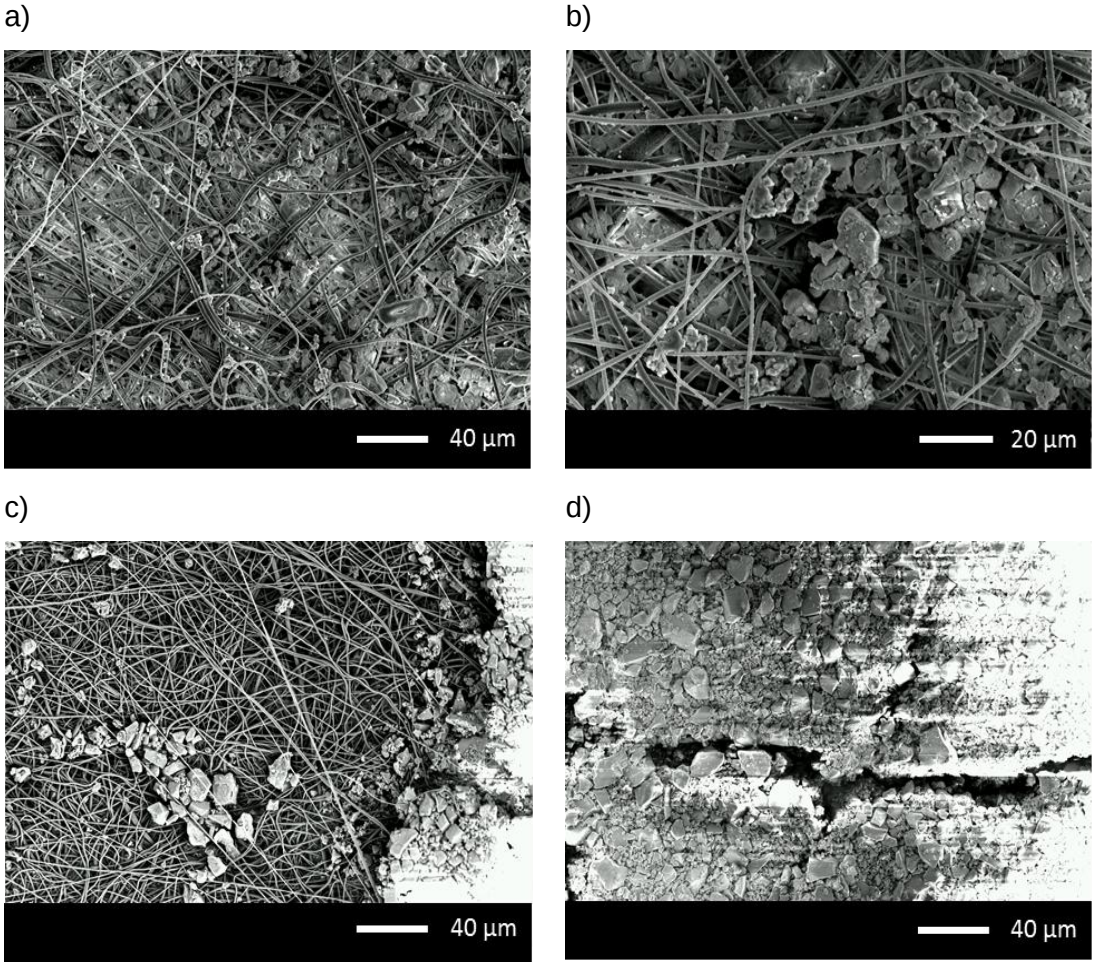

Figure 5.23. Scanning electron microscopy micrographs of electrospun materials processed using the 'filtering method' and two suspensions of bioactive glass powders of different concentration. a) and b) PCL + $Sr0^F$ with 0.05% w/v suspension; c) and d) PCL + $Sr0^F$ with 0.25% w/v suspension.

Table 5.8. Statistical information from two-tailed Student's t-tests of the mass variation of electrospun samples processed using the 'loading' and 'filtering' methods to add further bioactive glass particles to the surface of the materials (n = 12; α = 0.05).

Analysis	Material	Mean mass variation (mg)	SD	*t*-value	*p*-value
1	PCL^F	0.07	0.12	1.78	0.102
	PCL^L	-0.03	0.10		
2	$PCL/Sr0^F$	-0.13	0.08	-1.47	0.171
	$PCL/Sr0^L$	-0.08	0.09		
3	$PCL/Sr50^F$	-0.12	0.04	-0.36	0.723
	$PCL/Sr50^L$	-0.11	0.08		
4	$PCL/Sr100^F$	-0.3	0.06	-5.48	<0.001
	$PCL/Sr100^L$	-0.08	0.11		
5	$PCL + Sr0^F$	9.12	1.76	8.38	<0.001
	$PCL + Sr0^L$	1.71	2.21		
6	$PCL + Sr50^F$	9.73	1.03	17.28	<0.001
	$PCL + Sr50^L$	0.76	1.17		
7	$PCL + Sr100^F$	8.15	2.05	9.17	<0.001
	$PCL + Sr100^L$	1.17	1.79		
8	$PCL/Sr0 + Sr0^F$	9.12	1.76	12.87	<0.001
	$PCL/Sr0 + Sr0^L$	0.81	0.84		
9	$PCL/Sr50 + Sr50^F$	7.17	1.54	10.02	<0.001
	$PCL/Sr50 + Sr50^L$	1.17	1.10		
10	$PCL/Sr100 + Sr100^F$	8.48	1.28	16.44	<0.001
	$PCL/Sr100 + Sr100^L$	1.35	0.85		

Table 5.9. Statistical information from two-tailed Student's t-tests of the mass variation of electrospun samples processed using the 'loading' and 'filtering' methods to add further bioactive glass particles on the surface of the materials (n = 6; α = 0.05).

Analysis	Material	Mean weight variation (mg)	SD	*t*-value	*p*-value
1	$PCL + Sr0^F$ 0% w/v	-0.10	0.06	-1	0.363
	$PCL + Sr0^L$ 0% w/v	-0.07	0.05		
2	$PCL + Sr0^F$ 0.05% w/v	0.17	0.05	4	0.010
	$PCL + Sr0^L$ 0.05% w/v	0.03	0.10		
3	$PCL + Sr0^F$ 0.10% w/v	0.55	0.11	9.22	<0.001
	$PCL + Sr0^L$ 0.10% w/v	-0.02	0.13		
4	$PCL + Sr0^F$ 0.25% w/v	2.12	0.56	9.84	<0.001
	$PCL + Sr0^L$ 0.25% w/v	-0.05	0.06		
5	$PCL + Sr0^F$ 0.50% w/v	3.57	1.11	6.10	0.002
	$PCL + Sr0^L$ 0.50% w/v	0.32	0.26		
6	$PCL + Sr0^F$ 1.00% w/v	8.85	1.03	10.61	<0.001
	$PCL + Sr0^L$ 1.00% w/v	1.60	1.04		

5.2.6 Cytotoxicity assessment of electrospun materials

The cytotoxicity of the electrospun materials was assessed by culturing a rat osteosarcoma (ROS) cell line directly on the samples. Cellular respiratory activity was then measured using a resazurin dye-based assay and by determining fluorescence emission from the cell culture medium.

Figure 5.24a presents the fluorescence emission levels from the cell culture media used with electrospun materials PCL, PCL/Sr0, PCL/Sr50 and PCL/Sr100. Figure 5.24b and Figure 5.25 present the fluorescence emission levels from the cell culture media used with electrospun materials with added bioactive glass particles on their surface PCL/Sr0 + $Sr0^F$, PCL/Sr50 + $Sr50^F$ and PCL/Sr100 + $Sr100^F$. No statistically significant differences were reported between the means in the case of the electrospun materials PCL, PCL/Sr0, PCL/Sr50 and PCL/Sr100, and in the case of the samples processed with the 0.05% w/w suspension as determined by one-way ANOVA (Table 5.10). However, statistically significant differences between the means were reported in the case of the materials processed using the 0.25% w/v and 1.00 w/v suspensions as determined by one-way ANOVA (Table 5.10) and two-tailed Student's t-test (Table 5.11).

Figure 5.26 presents a comparison of the fluorescence emission levels in the cell culture media used on every electrospun material tested, represented as a percentage of the fluorescence emission values in the control samples. It was observed that the levels of fluorescence of the electrospun materials with no particles added on their surface and those processed using the 0.05% w/v suspensions presented comparable levels of fluorescence, but then the emission generally decreased as the amount of glass particles added to the materials increased.

a)

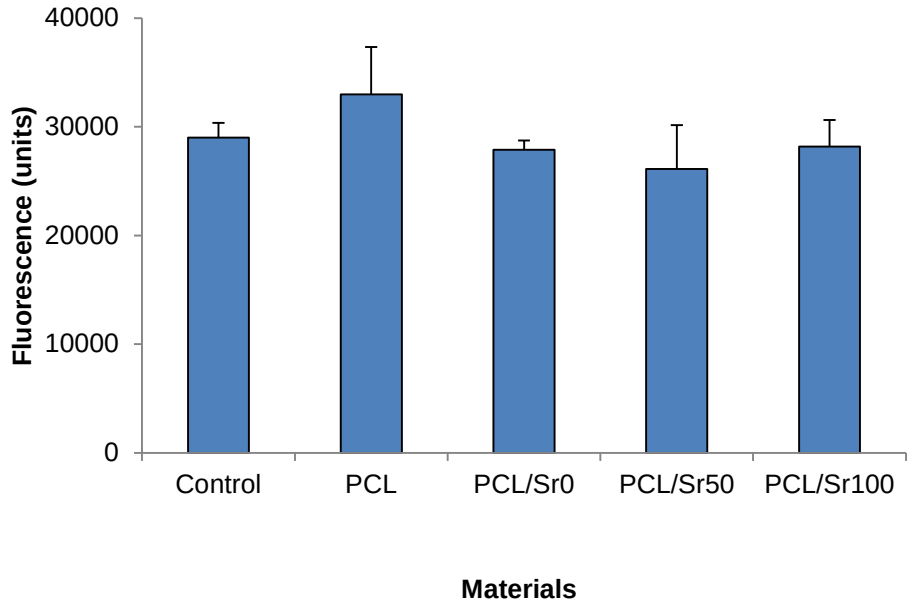

b)

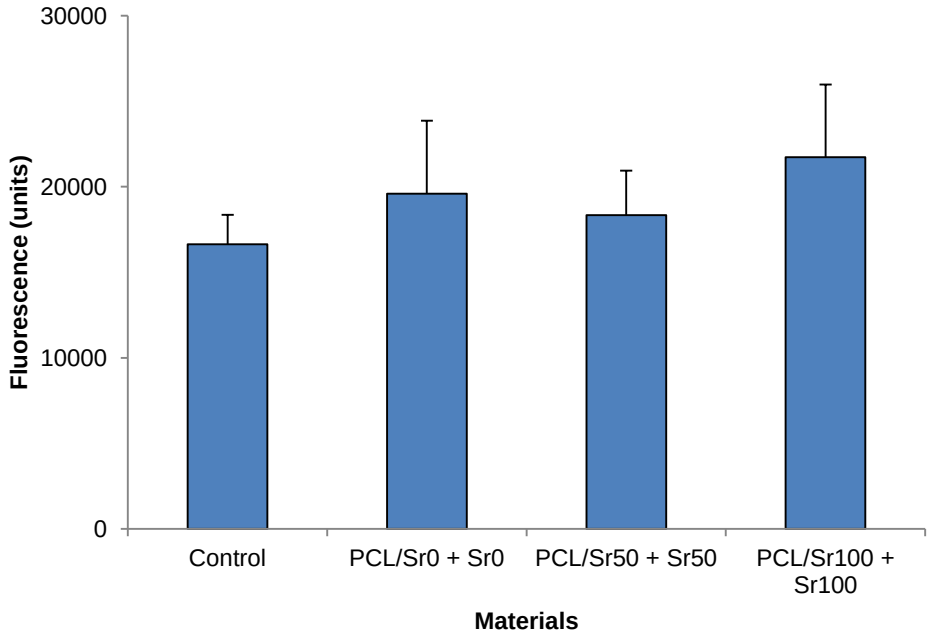

Figure 5.24. Fluorescence emission levels from cell culture media used in the study of the cytotoxic effect of the electrospun materials on a rat osteosarcoma (ROS) cell line. A) PCL, PCL/Sr0, PCL/Sr50 and PCL/Sr100; b) PCL/Sr0 + Sr0^{F}, PCL/Sr50 + Sr50^{F} and PCL/Sr100 + Sr100^{F} processed using the 'filtering' method and suspensions of bioactive glass powder of concentration 0.05% w/v. The control samples were ROS cells cultured directly on plastic.

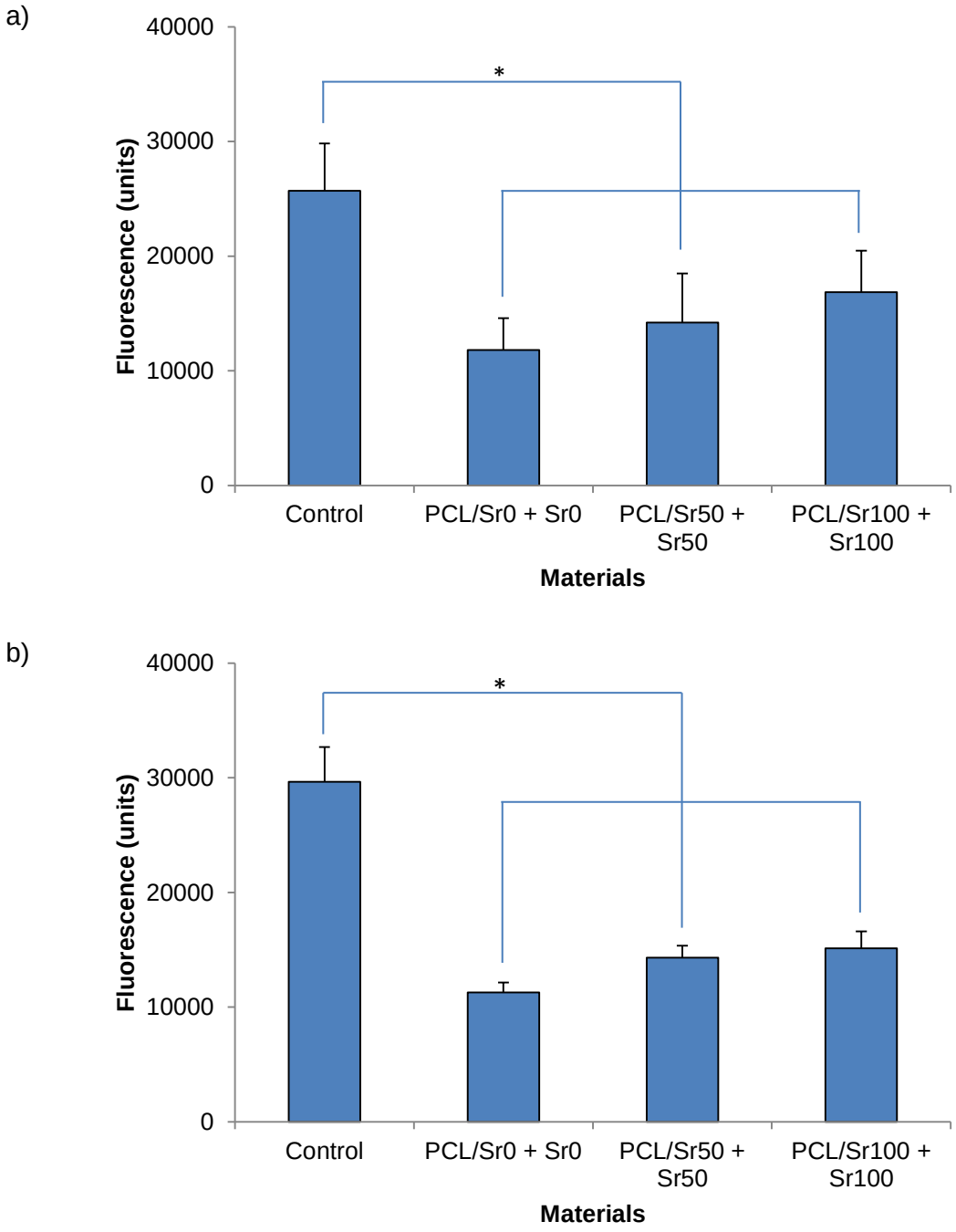

Figure 5.25. Fluorescence emission levels from cell culture media used in the study of the cytotoxic effect of the electrospun materials on a rat osteosarcoma (ROS) cell line. A) PCL/Sr0 + Sr0^{F}, PCL/Sr50 + Sr50^{F} and PCL/Sr100 + Sr100^{F} processed using suspensions of bioactive glass powder of concentration 0.25% w/v.; b) PCL/Sr0 + Sr0^{F}, PCL/Sr50 + Sr50^{F} and PCL/Sr100 + Sr100^{F} processed using the 'filtering' method and suspensions of bioactive glass powder of concentration 1.00% w/v. The control samples were ROS cells cultured directly on plastic. The lines indicate significant differences between the mean fluorescence of the control and the materials (* = $p < 0.05$).

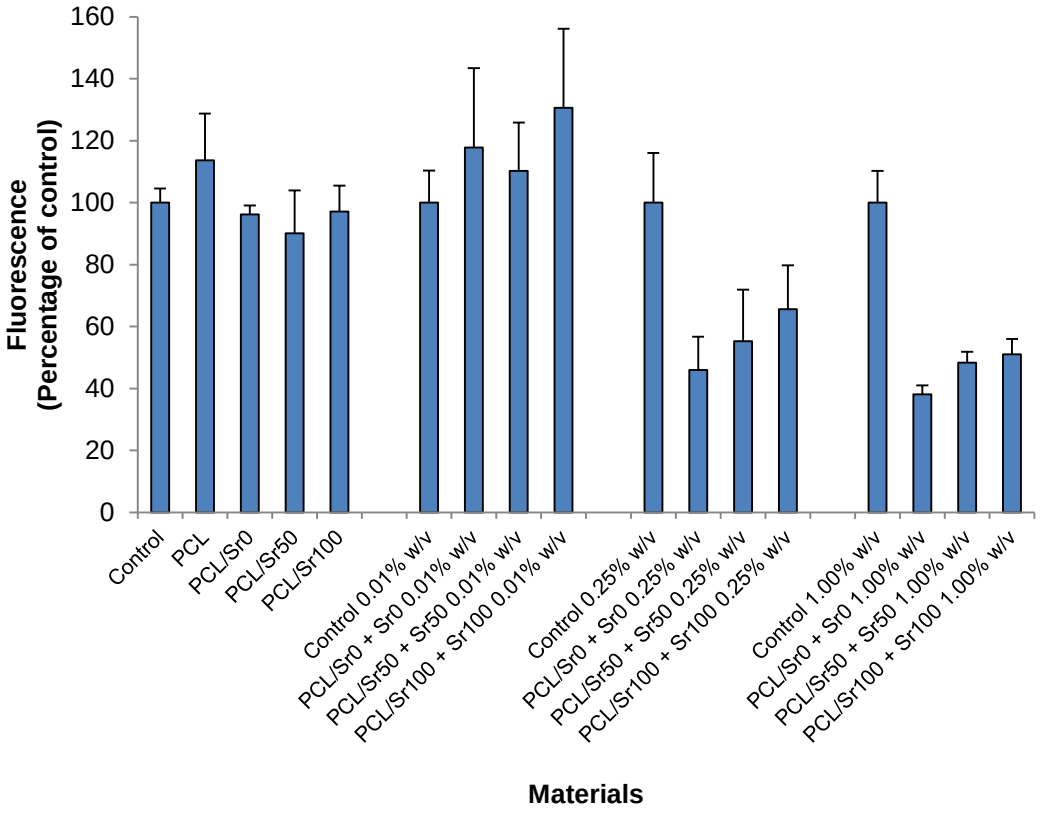

Figure 5.26. Comparison of the fluorescence emission levels from cell culture media used in the studies of the cytotoxic effect of the electrospun materials on a rat osteosarcoma cell line, presented as a percentage of the fluorescence emission levels in the control samples

Table 5.10. Statistical information from one-way ANOVA performed with the fluorescence emission levels of cell culture media used in the study of the cytotoxic effect of the electrospun materials (n = 4; α = 0.05).

Glass content	Material	Mean fluorescence	SD	DF Between groups	DF Within groups	*F*-value	*p*-value
0% w/v	Control	29007.38	1335.87	4	15	2.96	0.055
	PCL	32974.63	4366.77				
	PCL/Sr0	27889.88	850.60				
	PCL/Sr50	26125.63	4011.56				
	PCL/Sr100	28163.25	2448.78				
0.05% w/v	Control	16633.50	1723.55	3	12	1.60	0.240
	PCL/Sr0 + $Sr0^F$	19591.50	4272.99				
	PCL/Sr50 + $Sr50^F$	18331.63	2607.39				
	PCL/Sr100 + $Sr100^F$	21731.50	4242.64				
0.25% w/v	Control	25696.50	4119.31	3	12	10.45	0.001
	PCL/Sr0 + $Sr0^F$	11823.25	2760.72				
	PCL/Sr50 + $Sr50^F$	14198.38	4291.68				
	PCL/Sr100 + $Sr100^F$	16846.00	3639.23				
1.00% w/v	Control	29644.75	3046.40	3	12	80.95	<0.001
	PCL/Sr0 + $Sr0^F$	11283.50	864.98				
	PCL/Sr50 + $Sr50^F$	14315.88	1044.10				
	PCL/Sr100 + $Sr100^F$	15131.50	1476.59				

Table 5.11. Statistical information from two-tailed Student's t-test analysis performed with the fluorescence emission levels from cell culture media used in the study of the cytotoxic effect of the electrospun materials (n = 4; α = 0.05).

Glass content	Material	Mean fluorescence	SD	DF	*t* – value	*p* – value
0.25% w/v	Control	25696.50	4119.31	3	5.08	0.015
	PCL/Sr0 + $Sr0^F$	11823.25	2760.72	3		
	Control	25696.50	4119.31	3	6.09	0.009
	PCL/Sr50 + $Sr50^F$	14198.38	4291.68	3		
	Control	25696.50	4119.31	3	3.92	0.030
	PCL/Sr100 + $Sr100^F$	16846.00	3639.23	3		
1.00% w/v	Control	29644.75	3046.40	3	13.09	0.001
	PCL/Sr0 + $Sr0^F$	11283.50	864.98	3		
	Control	29644.75	3046.40	3	11.64	0.001
	PCL/Sr50 + $Sr50^F$	14315.88	1044.10	3		
	Control	29644.75	3046.40	3	17.58	<0.001
	PCL/Sr100 + $Sr100^F$	15131.50	1476.59	3		

5.3 Osteogenic effect of strontium-substituted bioactive glasses

5.3.1 Characterisation of cell population

Figure 5.27 presents the dot plots generated by FACS analysis for the 6 tubes of MSCs used: forward scatter channel vs. side scatter channel (FSC vs. SSC), CD45 Blue 575 channel vs. side scatter channel (CD45 vs. SSC), and CD90 Violet 450 channel vs. CD44 Red 660 channel (CD90 vs. CD44). The FSC vs. SSC plot identified a cellular subpopulation of 10000 elements which was then used in the analysis, differentiating between cellular and non-cellular elements (e.g. debris). The CD45 vs. SSC and the CD44 vs. CD90 plots were used to identify those cellular elements in the subpopulation which were positive for the presence of the antibodies, depending on the region of the plot where they appeared. Table 5.12 presents the numerical data for each dot plot and Table 5.13 presents the median fluorescence emission intensities detected in every tube by the CD45 Blue 575, CD90 Violet 450 and CD44 Red 660 channels.

In the case of Tube 1 (Unstained), all the cells appeared to be negative for CD45, CD44 and CD90 antibodies and no fluorescence emission from the cells was detected. Tube 2 (All isotypes) presented no positive results for CD44 and CD90 emissions, although a small group of CD45-isotype positive cells (0.4% of the parent population) was identified. A small subpopulation of CD45-antibody positive cells (1.3% of the parent population) was also detected in Tube 3 (CD45 Ab and other isotypes). Both Tube 4 (CD44 Ab and other isotypes) and Tube 5 (CD90 Ab and other isotypes) presented significant positive subpopulations for those antibodies. A sizable subpopulation of CD44-antibody positive cells (26% of parent population) was detected in Tube 4. The majority of cells in Tube 5 (99.9% of parent population) were CD90-antibody positive. Finally, Tube 6 (All antibodies) showed that 29.2% of the parent population was positive for both CD44 and CD90 antibodies, while 70.8% of the parent population was positive for only CD90 antibody.

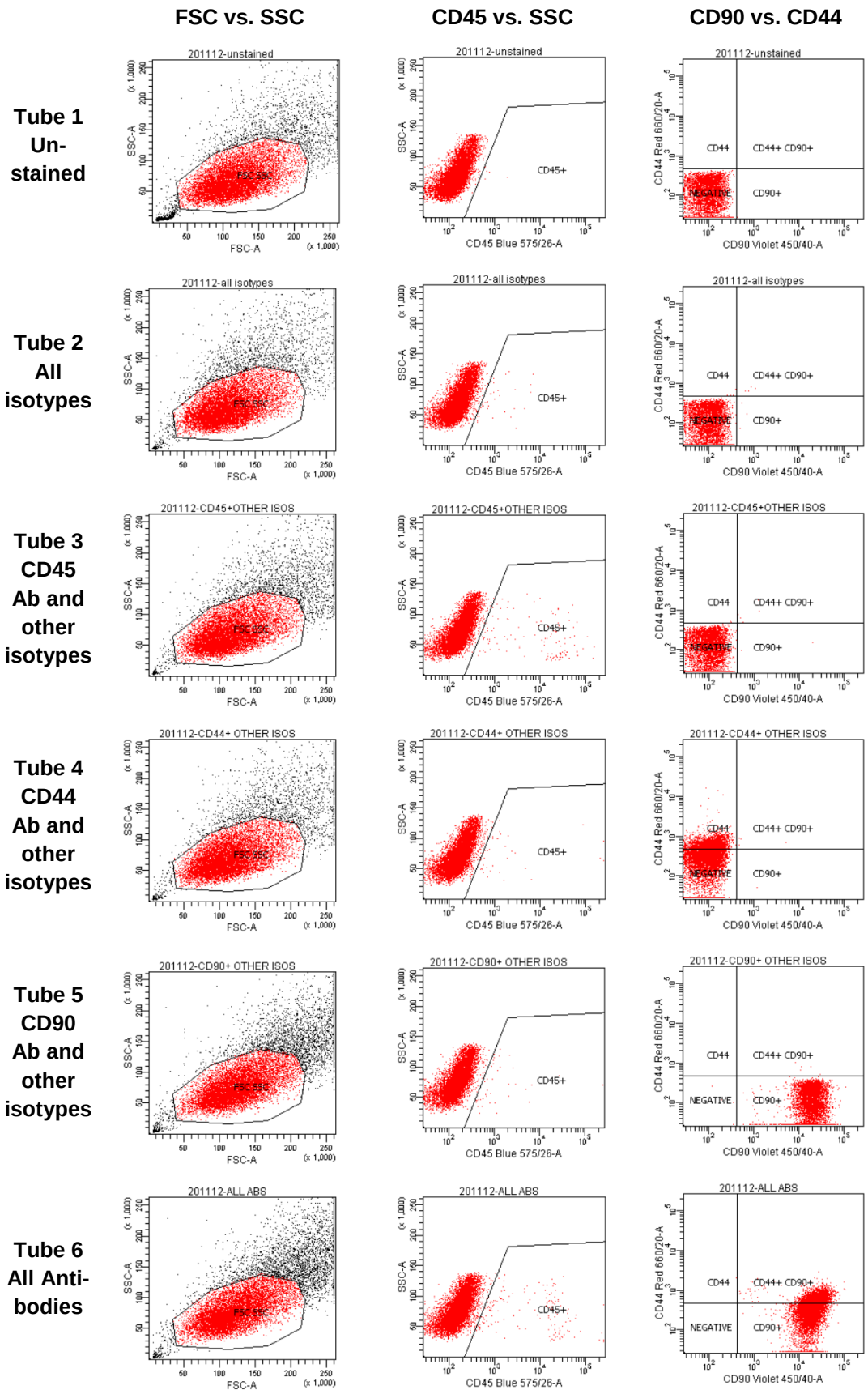

Figure 5.27. FSC vs. SSC, CD45 vs. SSC plots and CD90 vs. CD44 dot plots for the 6 tubes used in the characterisation of the population of rat mesenchymal stromal cells by FACS analysis.

Table 5.12. Numerical data of the dot plots for the 6 tubes used in the characterisation of the population of rat mesenchymal stromal cells by FACS analysis.

	Tube 1 - Unstained			Tube 2 - All isotypes		
	Events	**% Parent**	**% Total**	**Events**	**% Parent**	**% Total**
All events	12686	-	100.0	11921	-	100.0
FSC SSC	10000	78.8	78.8	10000	83.9	83.9
CD45+	8	0.1	0.1	44	0.4	0.4
CD44+	0	0.0	0.0	3	0.0	0.0
CD90+	1	0.0	0.0	3	0.0	0.0
CD44+ CD90+	0	0.0	0.0	5	0.0	0.0
Negative	9999	100.0	78.8	9989	99.9	83.8
	Tube 3 - CD45 Ab and other isotypes			**Tube 4 – CD44 Ab and other isotypes**		
	Events	**% Parent**	**% Total**	**Events**	**% Parent**	**% Total**
All events	12387	-	100.0	12025	-	100.0
FSC SSC	10000	80.7	80.7	10000	83.2	83.2
CD45+	134	1.3	1.1	45	0.4	0.4
CD44+	1	0.0	0.0	2603	26.0	21.6
CD90+	4	0.0	0.0	1	0.0	0.0
CD44+ CD90+	4	0.0	0.0	4	0.0	0.0
Negative	9991	99.9	80.7	7392	73.9	61.5
	Tube 5 – CD90 Ab and other isotypes			**Tube 6 – All antibodies**		
	Events	**% Parent**	**% Total**	**Events**	**% Parent**	**% Total**
All events	14307	-	100.0	15475	-	100.0
FSC SSC	10000	69.9	69.9	10000	64.6	64.6
CD45+	42	0.4	0.3	166	1.7	1.1
CD44+	0	0.0	0.0	1	0.0	0.0
CD90+	9990	99.9	69.8	7078	70.8	45.7
CD44+ CD90+	5	0.0	0.0	2921	29.2	18.9
Negative	5	0.0	0.0	0	0.0	0.0

Table 5.13. Median fluorescence emission intensities detected by the CD45 Blue 575, CD90 Violet 450 and CD44 Red 660 channels in the 6 tubes used in the characterisation of the population of rat mesenchymal stromal cells by FACS analysis.

Tube	Description	CD45 Blue 575	CD90 Violet 450	CD44 Red 660
1	Unstained	142	87	12
2	All isotypes	155	92	12
3	CD45 Ab and other isotypes	166	92	14
4	CD44 Ab and other isotypes	161	87	329
5	CD90 Ab and other isotypes	153	19480	13
6	All antibodies	158	19460	342

5.3.2 Effect of bioactive glass dissolution on cell viability

The effect of Sr0, Sr50 and Sr100 bioactive glass dissolution on the viability of MSCs was assessed by exposing a monolayer culture of the cells to a series of increasing amounts of bioactive glass powders. Cellular viability was assessed by measuring respiratory activity after exposition to the dissolution products using a resazurin dye-based assay and by determining fluorescence emission from cell culture medium.

Figure 5.28 presents the fluorescence emission levels of the samples exposed to 0, 5, 10, 20, 40, 80, 160 and 320 mg of bioactive glass powders. Figure 5.29 presents a comparison of the same results represented as a percentage of the fluorescence emission in the control samples. It was observed that the fluorescence emission generally decreased as the amount of bioactive glass powder used increased, indicating a reduction of cellular viability. The samples also exhibited different patterns of emission depending on the glass composition they were exposed to. In the case of samples treated with Sr0 and Sr100 bioactive glasses, fluorescence emission decreased from the beginning of the study. In contrast, samples treated with Sr50 bioactive glass exhibited an initial increase of emission at 5 mg and higher levels of emission than Sr0 and Sr100 up to 80 mg. The fastest rate of decrease of all samples was observed in those treated with Sr100, which generally presented lower levels of emission than both Sr0 and Sr50.

These results were compared with the fluorescence emission from the control samples, which were MSCs not exposed to bioactive glass powders, and if statistically significant reductions of fluorescence emission were reported then those materials would be considered as toxic. One-way ANOVA (Table 5.14) reported statistically significant differences between the means of the emission levels of samples treated with the three bioactive glass compositions. Two-tailed Student’s t-tests (Table 5.15) reported statistically significant differences between the control samples and the samples treated with amounts of bioactive glass powders greater than 20 mg for Sr0 and Sr50; and greater than 10 mg for Sr100.

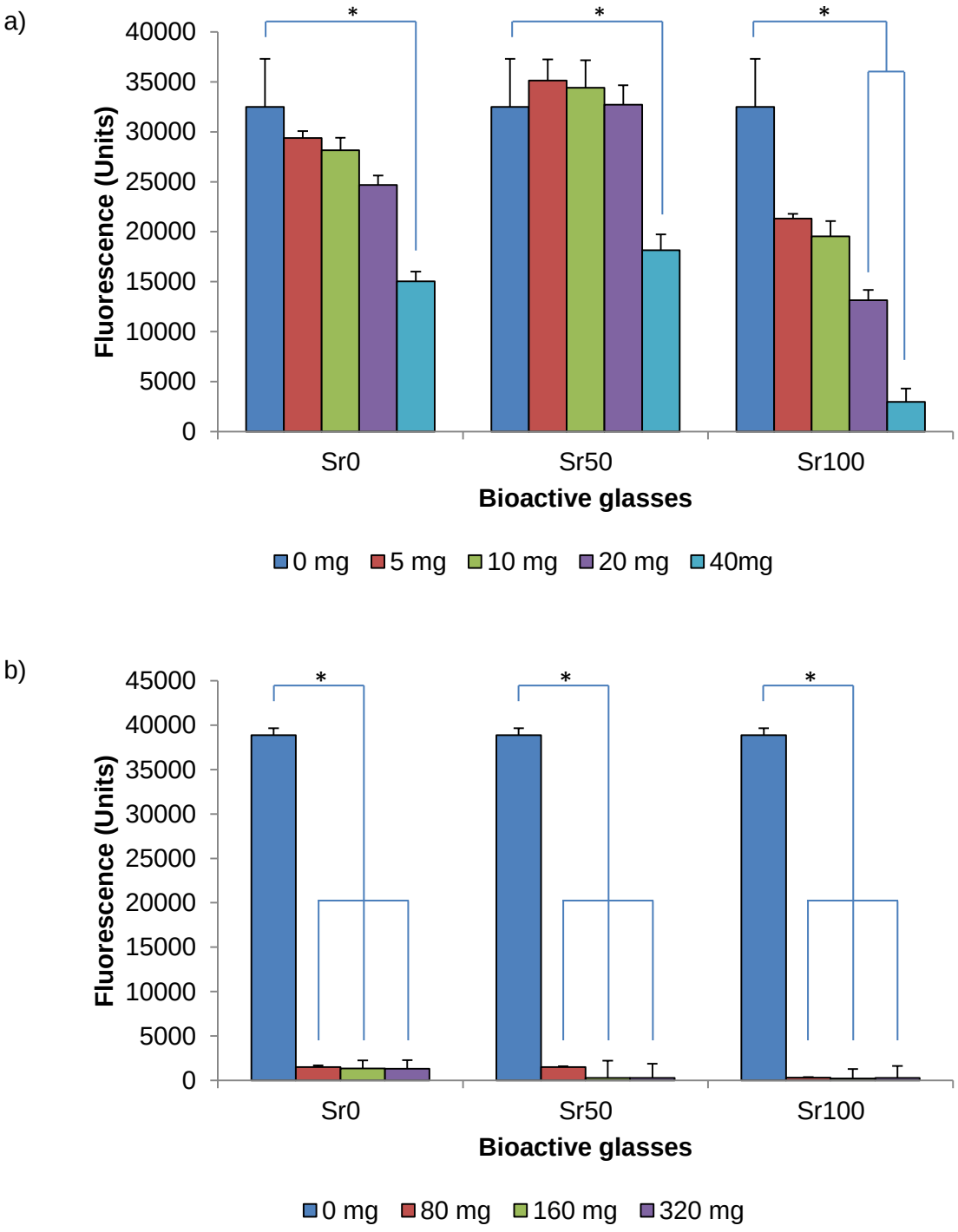

Figure 5.28. Fluorescence emission levels obtained from cell culture media used in the study of the effect of a series of increasing amounts of Sr0, Sr50 and Sr100 bioactive glass powders on the viability of rat mesenchymal stromal cells. The amounts tested were: a) 0, 5, 10, 20 and 40 mg of bioactive glass powders; b) 0, 80, 160 and 320 mg of bioactive glass powders. The lines indicate significant differences between the mean fluorescence emission levels of the control and the samples (n=3, * = $p < 0.05$).

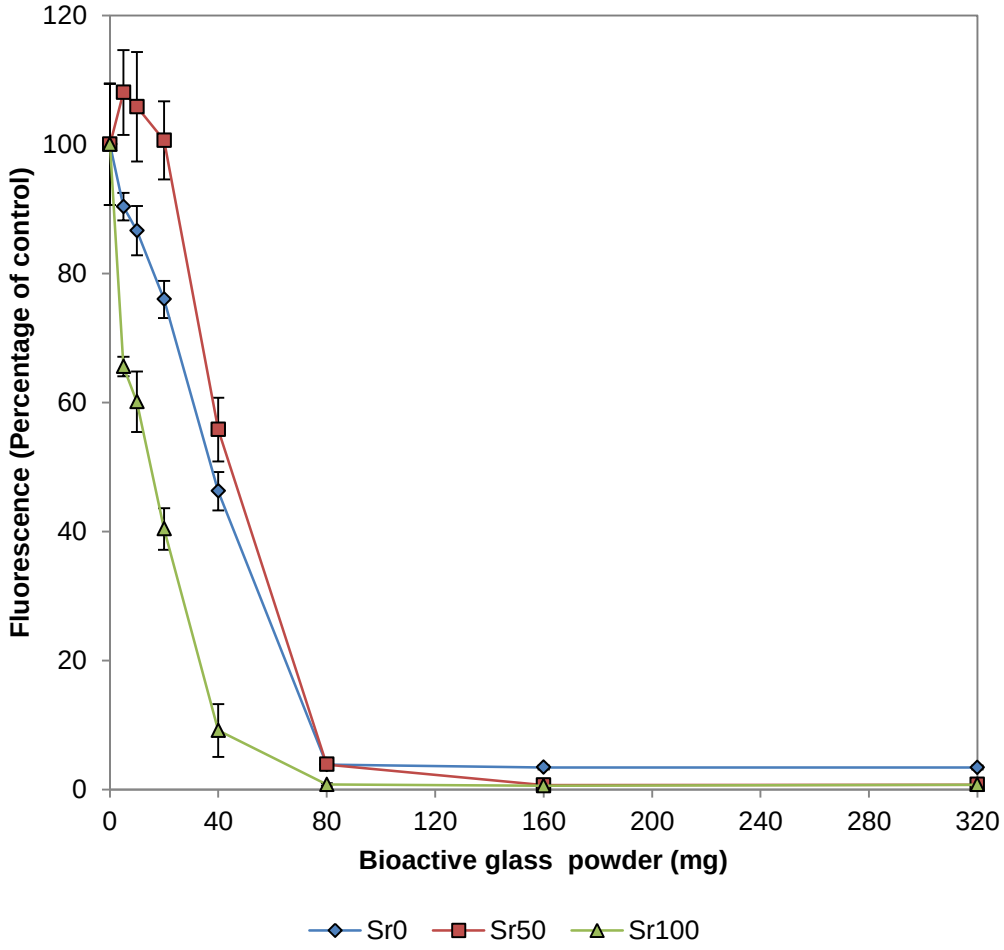

Figure 5.29. Comparison of the fluorescence emission levels obtained from cell culture media used in the study of the effect of a series of increasing amounts of Sr0, Sr50 and Sr100 bioactive glass powders on the viability of rat mesenchymal stromal cells, represented as percentage of the fluorescence emission levels in the control sample (n = 3).

Table 5.14. Statistical information from one-way ANOVA performed with the fluorescence emission levels obtained from the cell culture media used in the study of the effect of a series of increasing amounts of Sr0, Sr50 and Sr100 bioactive glass powders on the viability of rat mesenchymal stromal cells. (n = 3; α = 0.05).

Bioactive glass	Amount	Mean	SD	DF Between groups	DF Within groups	*F*-value	*p*-value
Sr0	0 mg	32502.23	4787.78	4	10	25.26	<0.001
	5 mg	29369.57	696.58				
	10 mg	28159.4	1243.73				
	20 mg	24695.73	932.45				
	40 mg	15036.40	962.81				
Sr0	0 mg	38863.83	789.79	3	8	6097.20	<0.001
	80 mg	1502.83	197.49				
	160 mg	1336.00	116.23				
	320 mg	1329.50	121.28				
Sr50	0 mg	32502.23	4787.78	4	10	17.89	<0.001
	5 mg	35120.73	2137.47				
	10 mg	34396.40	2758.86				
	20 mg	32707.73	1964.86				
	40 mg	18140.90	1605.63				
Sr50	0 mg	38863.83	789.79	3	8	6866.40	<0.001
	80 mg	1516.17	78.24				
	160 mg	271.50	33.62				
	320 mg	300.33	77.86				
Sr100	0 mg	32502.23	4787.78	4	10	62.49	<0.001
	5 mg	21313.73	485.36				
	10 mg	19539.40	1530.08				
	20 mg	13136.07	1046.70				
	40 mg	2982.07	1333.21				
Sr100	0 mg	38863.83	789.79	3	8	7063.10	<0.001
	80 mg	311.33	75.55				
	160 mg	227.00	46.49				
	320 mg	296.33	27.43				

Table 5.15. Statistical information from two-tailed Student's t-test performed with the fluorescence emission levels obtained from the cell culture media used in the study of the effect of a series of increasing amounts of Sr0, Sr50 and Sr100 bioactive glass powders on the viability of rat mesenchymal stromal cells. (n = 3; α = 0.05).

Bioactive glass	Amount	Mean fluorescence	SD	*t*-value	*p*-value
Sr0	0 mg	32502.23	4787.78	1.33	0.316
	5 mg	29369.57	696.58		
	0 mg	32502.23	4787.78	1.45	0.285
	10 mg	28159.40	1243.73		
	0 mg	32502.23	4787.78	3.06	0.093
	20 mg	24695.73	932.45		
	0 mg	32502.23	4787.78	7.67	0.017
	40 mg	15036.40	962.81		
	0 mg	38863.83	789.79	104.77	<0.001
	80 mg	1502.83	197.49		
	0 mg	38863.83	789.79	94.66	<0.001
	160 mg	1336.00	116.23		
	0 mg	38863.83	789.79	95.01	<0.001
	320 mg	1329.50	121.28		
Sr50	0 mg	32502.23	4787.78	-1.07	0.398
	5 mg	35120.73	2137.47		
	0 mg	32502.23	4787.78	-0.98	0.430
	10 mg	34396.40	2758.86		
	0 mg	32502.23	4787.78	-0.06	0.960
	20 mg	32707.73	1964.86		
	0 mg	32502.23	4787.78	4.57	0.045
	40 mg	18140.90	1605.63		
	0 mg	38863.83	789.79	90.44	<0.001
	80 mg	1516.17	78.24		
	0 mg	38863.83	789.79	87.37	<0.001
	160 mg	271.50	33.62		
	0 mg	38863.83	789.79	93.57	<0.001
	320 mg	300.33	77.86		
Sr100	0 mg	32502.23	4787.78	3.85	0.061
	5 mg	21313.73	485.36		
	0 mg	32502.23	4787.78	3.55	0.071
	10 mg	19539.40	1530.08		
	0 mg	32502.23	4787.78	6.07	0.026
	20 mg	13136.07	1046.70		
	0 mg	32502.23	4787.78	12.61	0.006
	40 mg	2982.10	1333.21		
	0 mg	38863.83	789.79	91.96	<0.001
	80 mg	311.33	75.55		
	0 mg	38863.83	789.79	89.88	<0.001
	160 mg	227.00	46.49		
	0 mg	38863.83	789.79	87.33	<0.001
	320 mg	296.33	27.43		

5.3.3 Total RNA isolation

Total RNA was isolated from MSCs cultured in monolayer and exposed to 20 mg of Sr0, Sr50 and Sr100 bioactive glass powders placed on tissue culture inserts. The concentration of the elution of isolated RNA and the A260/A280 and A260/A230 ratios, determined by spectrophotometry, for days 1, 3, 6 and 14 are shown in Table 5.16 and Table 5.17. The mean amount of isolated RNA for each experimental condition is presented in Figure 5.30.

It was observed that the total amount of isolated RNA generally increased with the passage of time. However, it was also observed that the isolated amounts were smaller in the case of the samples treated with bioactive glass powders compared to the untreated controls. A similar reduction was also observed in the case of the samples cultured in osteogenic cell culture medium compared to the samples cultured in standard cell culture medium. The samples cultured in osteogenic cell culture medium at day 14 had decreased significantly in cell number and the amount of total RNA isolated from them was too small to perform quantitative real-time PCR analyses. Therefore, those samples were excluded from the study.

The A260/A280 and A260/A230 ratios measured by spectrophotometry provided an estimate of the purity of the isolated RNA. A sample of RNA would usually be considered as ‘pure’ if the A260/A280 ratio is around 2.0 or higher, and if the A260/A230 ratio is around 2.0 or higher. Lower ratios may indicate contamination with elements which absorb at those wavelengths, such as proteins at 280 nm and phenol at 230 nm. All the samples of total RNA presented A260/A280 ratios higher than 2.0, except those isolated from MSCs cultured with osteogenic cell culture medium at day 14. A larger variability was observed in the values of the A260/A230 ratio, with several samples presenting values lower than 2.0.

Table 5.16. Concentration, A260/A280 ratio and A260/A230 ratio of the total RNA isolated from rat mesenchymal stromal cells at days 1 and 3 for the study of the osteogenic effect of Sr0, Sr50 and Sr100 bioactive glass powders.

Day	Sample	Standard cell culture medium			Osteogenic cell culture medium		
		RNA (ng/µl)	A260/A280 ratio	A260/A230 ratio	RNA (ng/µl)	A260/A280 ratio	A260/A230 ratio
1	Control – 1	162.57	2.08	2.03	237.33	2.09	2.15
	Control – 2	166.47	2.09	1.77	255.80	2.07	2.15
	Control – 3	144.66	2.10	1.09	224.40	2.07	2.03
	Sr0 – 1	168.38	2.09	2.05	118.26	2.08	2.13
	Sr0 – 2	171.63	2.08	2.08	143.10	2.08	2.01
	Sr0 – 3	171.92	2.10	0.78	119.79	2.09	2.03
	Sr50 - 1	163.70	2.10	1.92	112.28	2.07	2.00
	Sr50 – 2	176.97	2.08	2.07	119.83	2.09	2.07
	Sr50 – 3	160.37	2.13	0.42	117.16	2.08	2.04
	Sr100 – 1	153.95	2.09	2.00	85.06	2.09	0.75
	Sr100 – 2	149.42	2.09	1.36	130.75	2.07	2.07
	Sr100 – 3	161.98	2.10	1.51	131.70	2.10	1.27
3	Control – 1	246.34	2.08	2.32	276.72	2.08	2.07
	Control – 2	323.51	2.07	2.17	287.86	2.08	2.11
	Control – 3	297.43	2.09	2.13	358.81	2.06	1.96
	Sr0 – 1	243.95	2.07	2.05	180.90	2.09	2.03
	Sr0 – 2	286.01	2.10	1.25	223.22	2.09	2.11
	Sr0 – 3	210.61	2.04	2.04	184.50	2.09	1.82
	Sr50 - 1	226.76	2.09	2.13	130.20	2.09	1.85
	Sr50 – 2	241.74	2.08	2.09	148.63	2.09	2.13
	Sr50 – 3	230.10	2.10	1.67	163.60	2.09	1.98
	Sr100 – 1	200.57	2.09	2.15	132.08	2.07	1.92
	Sr100 – 2	182.52	2.10	0.88	146.63	2.10	2.08
	Sr100 – 3	201.76	2.11	1.25	123.84	2.10	0.86

Table 5.17. Concentration, A260/A280 ratio and A260/A230 ratio of the total RNA isolated from rat mesenchymal stromal cells at days 6 and 14 for the study of the osteogenic effect of Sr0, Sr50 and Sr100 bioactive glass powders.

Day	Sample	Standard cell culture medium			Osteogenic cell culture medium		
		RNA (ng/µl)	A260/A280 ratio	A260/A230 ratio	RNA (ng/µl)	A260/A280 ratio	A260/A230 ratio
6	Control – 1	330.08	2.07	2.11	333.38	2.07	1.85
	Control – 2	286.22	2.08	1.64	413.34	2.06	2.15
	Control – 3	379.74	2.07	2.14	426.64	2.05	1.85
	Sr0 – 1	241.76	2.1	2.16	241.24	2.09	1.9
	Sr0 – 2	244.38	2.1	2.16	227.61	2.13	0.57
	Sr0 – 3	234.42	2.09	2.17	216.79	2.1	2.08
	Sr50 - 1	235.74	2.1	2.17	230.18	2.1	1.34
	Sr50 – 2	214.09	2.11	1.81	206.11	2.07	1.89
	Sr50 – 3	256.55	2.08	2.16	166.71	2.1	1.26
	Sr100 – 1	230.2	2.09	2.11	152.83	2.09	2.06
	Sr100 – 2	208.55	2.1	1.81	183.8	2.06	2.16
	Sr100 – 3	226.45	2.13	0.51	193.68	2.1	2.15
14	Control – 1	446.52	2.05	1.98	278.35	2.09	1.76
	Control – 2	428.45	2.05	2.12	292.46	2.08	2.09
	Control – 3	556.63	2.12	2.15	208.61	2.07	1.89
	Sr0 – 1	274.6	2.08	1.89	1.22	1.25	0.07
	Sr0 – 2	278.22	2.09	2.1	1.12	1.86	0.17
	Sr0 – 3	347.16	2.07	2.11	0.89	1.87	0.12
	Sr50 - 1	310.62	2.08	2.15	264.01	2.09	2.08
	Sr50 – 2	323.88	2.07	1.76	251.24	2.08	2.13
	Sr50 – 3	361.41	2.05	2.19	179.75	2.1	0.96
	Sr100 – 1	331.55	2.06	2.16	170.27	2.1	1.99
	Sr100 – 2	345.88	2.05	2.16	170.01	2.09	2.02
	Sr100 – 3	443.88	2.05	2.1	126.5	2.11	2.05

a)

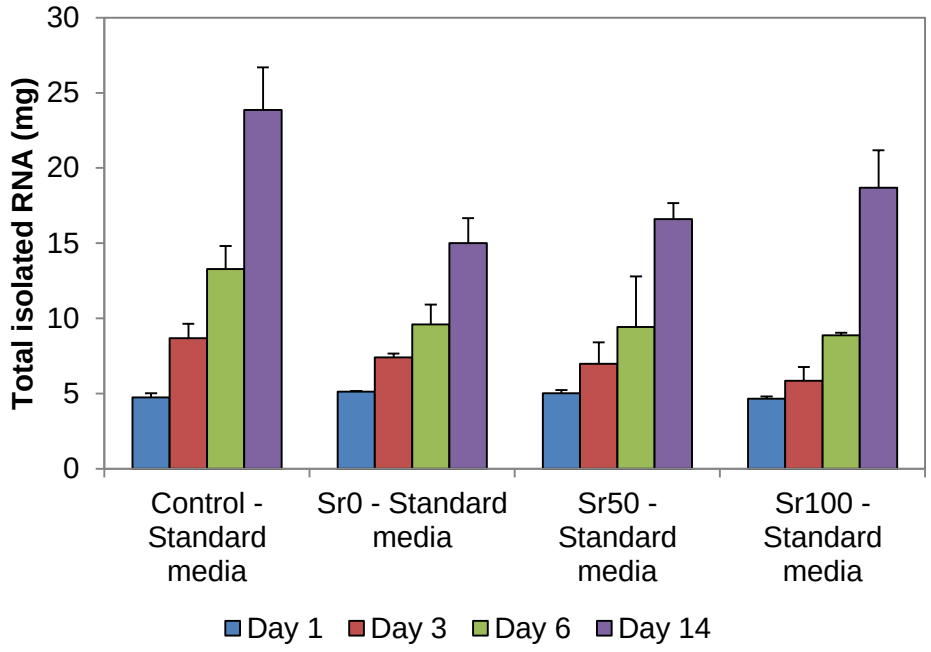

b)

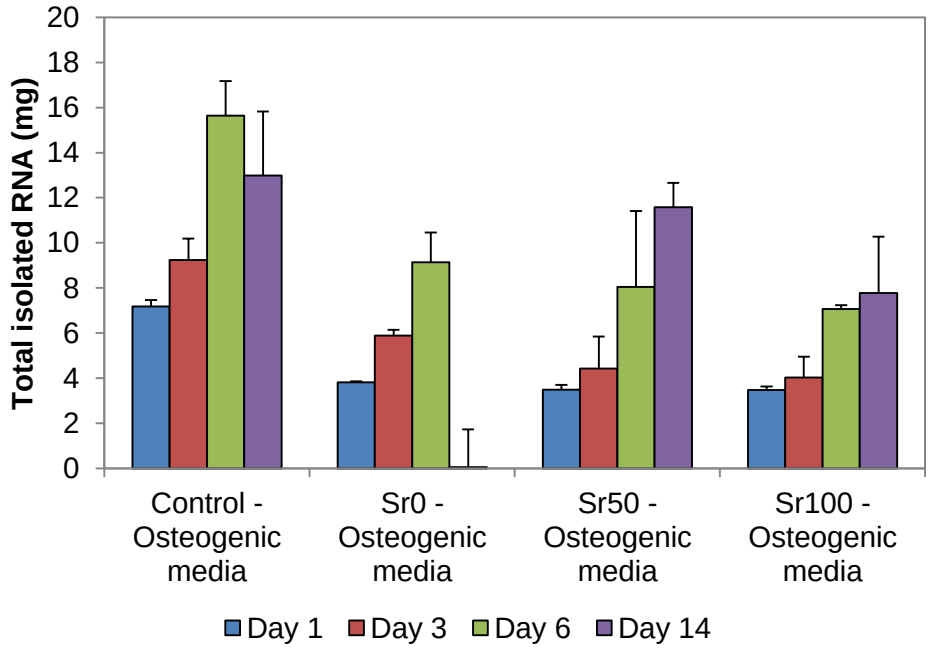

Figure 5.30. Mean amount of RNA isolated from rat mesenchymal stromal cells for the study of the osteogenic effect of Sr0, Sr50 and Sr100 bioactive glass powders. Cells were cultured in two different experimental conditions, using a) standard cell culture medium, and b) osteogenic cell culture medium (n = 3).

5.3.4 Analysis of RT-qPCR data

The levels of expression of the genes *Runx2*, *Alpl*, *Col1a1*, *Bglap*, *Bmp2* and *Spp1* in MSCs exposed to 20 mg of Sr0, Sr50 and Sr100 bioactive glass powders and cultured in both standard and osteogenic media are presented in a series of figures from Figure 5.31 to Figure 5.36. The fold changes in expression were calculated employing the ΔΔCt method, using the levels of expression of the same genes in MSCs not exposed to bioactive glasses as a standard. Statistically significant differences (Wilcoxon two-group test, Table 5.18 and Table 5.19) were reported between the samples treated with bioactive glass powder and the untreated controls, and also between samples treated with different bioactive glasses.

Runx2 presented significant differences between the control and the three bioactive glass compositions at days 3 and 6, in both standard and osteogenic media. An initial increase in the levels of expression in samples exposed to the glass was observed between days 1 and 6, with a peak at day 6 and a final decrease at day 14.

Alpl presented significant differences between the control and the three glass compositions at days 3, 6 and 14 in standard cell culture medium, exhibiting an initial increase that peaked at day 6 and a final decrease at day 14. The pattern of expression obtained when analysing cells exposed to osteogenic cell culture medium looked similar, although the increase occurred earlier in time. The significant differences were then observed at days 1, 3 and 6, peaking at day 3 and then decreasing from that point.

Col1a1 presented a pattern of expression similar to *Runx2*, with significant differences between the control and the three glass compositions at days 3 and 6 in both standard and osteogenic cell culture media. However, in the case of cells cultured standard cell culture medium the peak of expression was observed at day 6, while in osteogenic cell culture medium it occurred at day 3.

Bglap presented significant differences between the control and the three glass compositions only at day 6 in standard cell culture medium, while the

levels of expression at the other days were comparable to the untreated control. In osteogenic cell culture medium, however, significant differences were observed at days 3 and 6, peaking at day 3 and then exhibiting lower levels at day 6.

In the case of *Bmp2* no significant differences between the control and the three glass compositions in standard cell culture medium were observed simultaneously at any time point. However, there were significant differences in osteogenic cell culture medium at day 3.

Finally, *Spp1* presented simultaneous significant differences between the control and the three glass compositions at days 1 and 14 in standard cell culture medium. There was an initial decrease between days 1 and 6, and then a final increase by day 14. In osteogenic cell culture medium there were significant differences at days 1, 3 and 6, presenting a pattern of general decrease in the levels of expression as time progressed.

Significant differences between the control and only one or two of the bioactive glass compositions were also observed at some time points. In standard cell culture medium these were at: *Runx2*, in Sr0 at day 1 and in Sr50 at day 14; *Col1a1*, in Sr100 at day 1 and in Sr50 at day 14; *Bmp2*; in Sr0 at days 1 and 3, and in Sr50 at all days; and *Spp1*, in Sr100 at day 3 and in Sr50 at day 6. In osteogenic cell culture medium these were at: *Runx2*, in Sr0 and Sr50 at day 1; *Bmp2*, in Sr0 and Sr50 at day 1 and in Sr100 at day 14; and *Spp1*, in Sr50 at day 14.

The combined effect of the osteogenic cell culture medium and bioactive glass dissolution products was also studied by calculating the folding change in genetic expression of the six genes in MSCs cultured in osteogenic cell culture medium in relation to the levels of expression in the untreated controls in standard cell culture medium. Figure 5.37 shows the levels of expression for *Runx2* and *Alpl*, Figure 5.38 for *Col1a1* and *Bglap*, and Figure 5.39 for *Bmp2* and *Spp1*. Statistically significant differences (Wilcoxon two-group test, Table 5.20) were reported between the control in standard cell culture medium and most of the samples cultured in osteogenic cell culture medium.

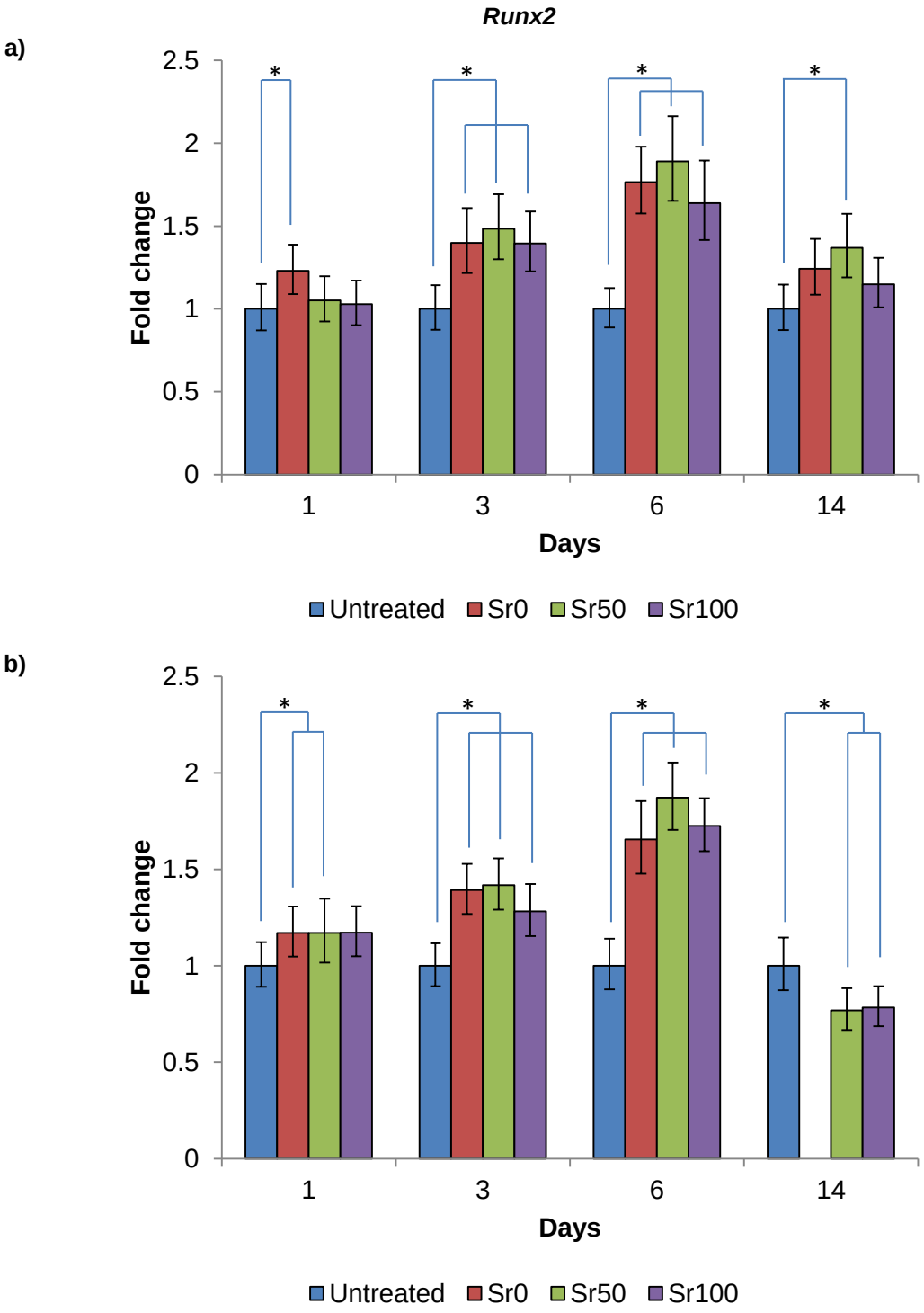

Figure 5.31. Variation in the expression of *Runx2* in rat mesenchymal stromal cells exposed to 20 mg of Sr0, Sr50 and Sr100 bioactive glass powders at various points in time. Studies were carried in two experimental conditions: a) cells cultured in standard cell culture medium and b) cells cultured in osteogenic medium. The lines indicate significant differences between the mean fluorescence of the control and the samples. (n = 9, * = $p < 0.05$).

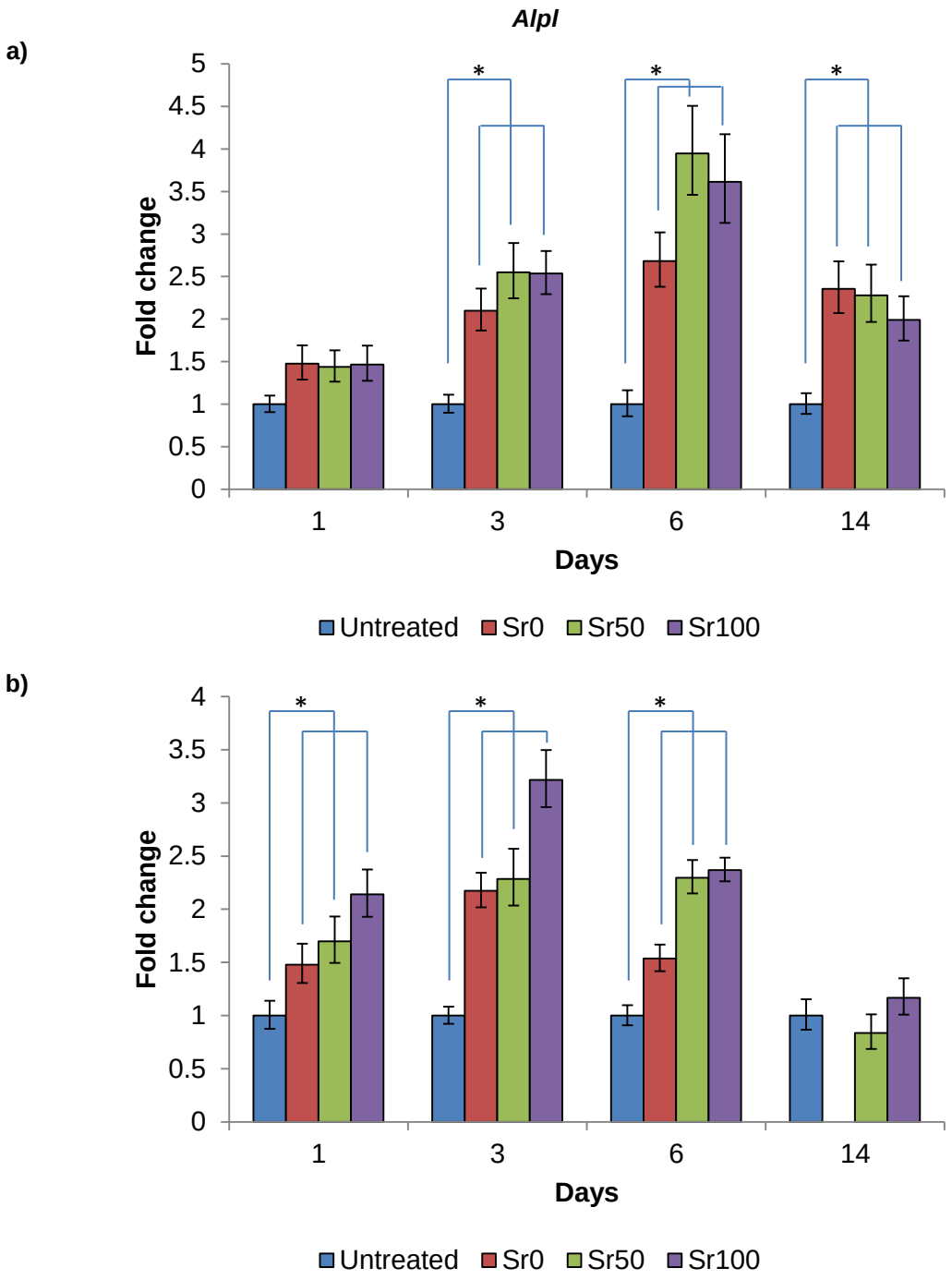

Figure 5.32. Variation in expression of *Alpl* in rat mesenchymal stromal cells exposed to 20 mg of Sr0, Sr50 and Sr100 bioactive glass powders at various points in time. Studies were carried in two experimental conditions: a) cells cultured in standard cell culture medium and b) cells cultured in osteogenic medium. The lines indicate significant differences between the mean fluorescence of the control and the samples. (n = 9, * = $p < 0.05$).

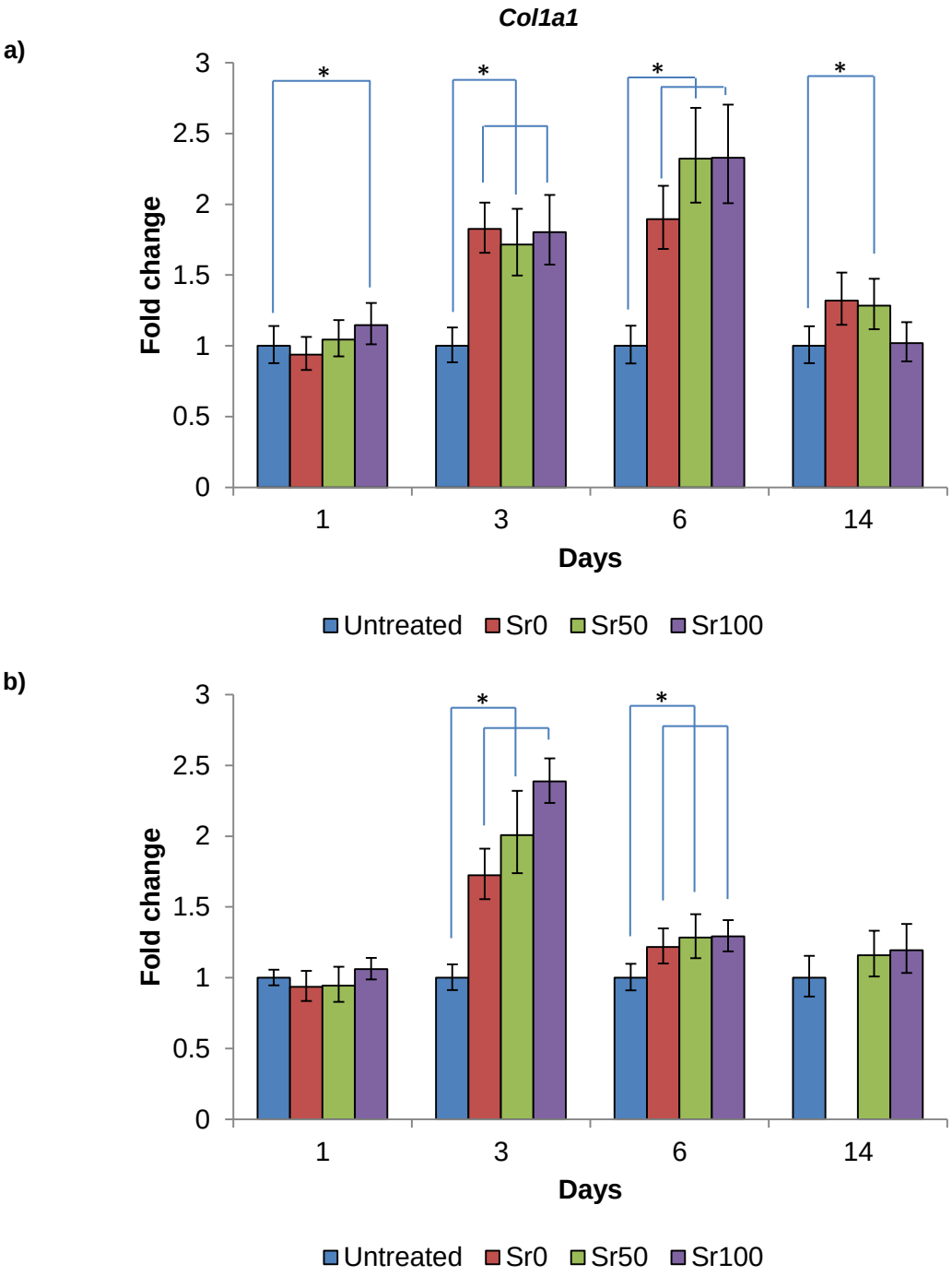

Figure 5.33. Variation in expression of *Col1a1* in rat mesenchymal stromal cells exposed to 20 mg of Sr0, Sr50 and Sr100 bioactive glass powders at various points in time. Studies were carried in two experimental conditions: a) cells cultured in standard cell culture medium and b) cells cultured in osteogenic medium. The lines indicate significant differences between the mean fluorescence of the control and the samples. (n = 9, * = $p < 0.05$).

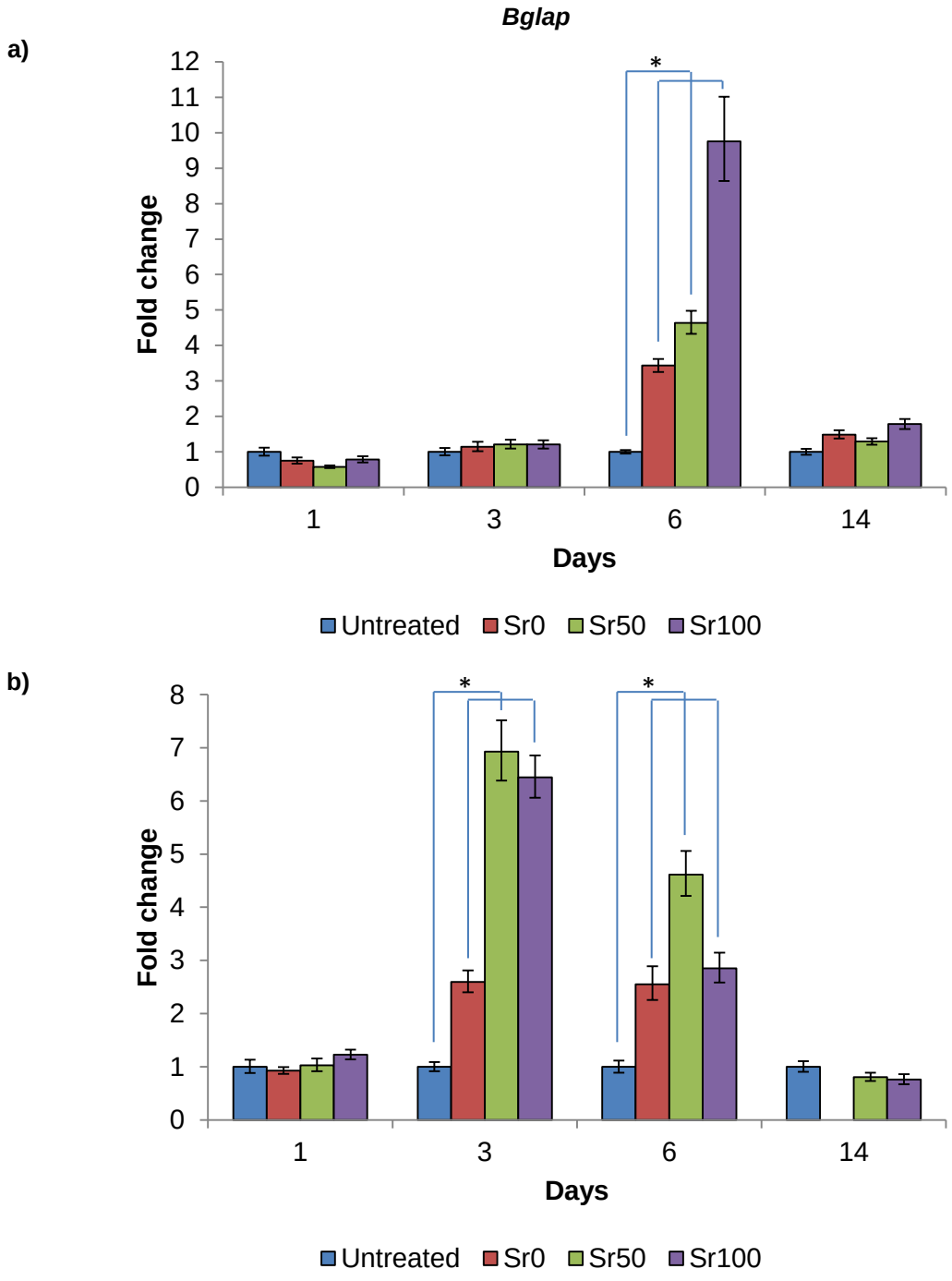

Figure 5.34. Variation in expression of *Bglap* in rat mesenchymal stromal cells exposed to 20 mg of Sr0, Sr50 and Sr100 bioactive glass powders at various points in time. Studies were carried in two experimental conditions: a) cells cultured in standard cell culture medium and b) cells cultured in osteogenic medium. The lines indicate significant differences between the mean fluorescence of the control and the samples. (n = 9, * = $p < 0.05$).

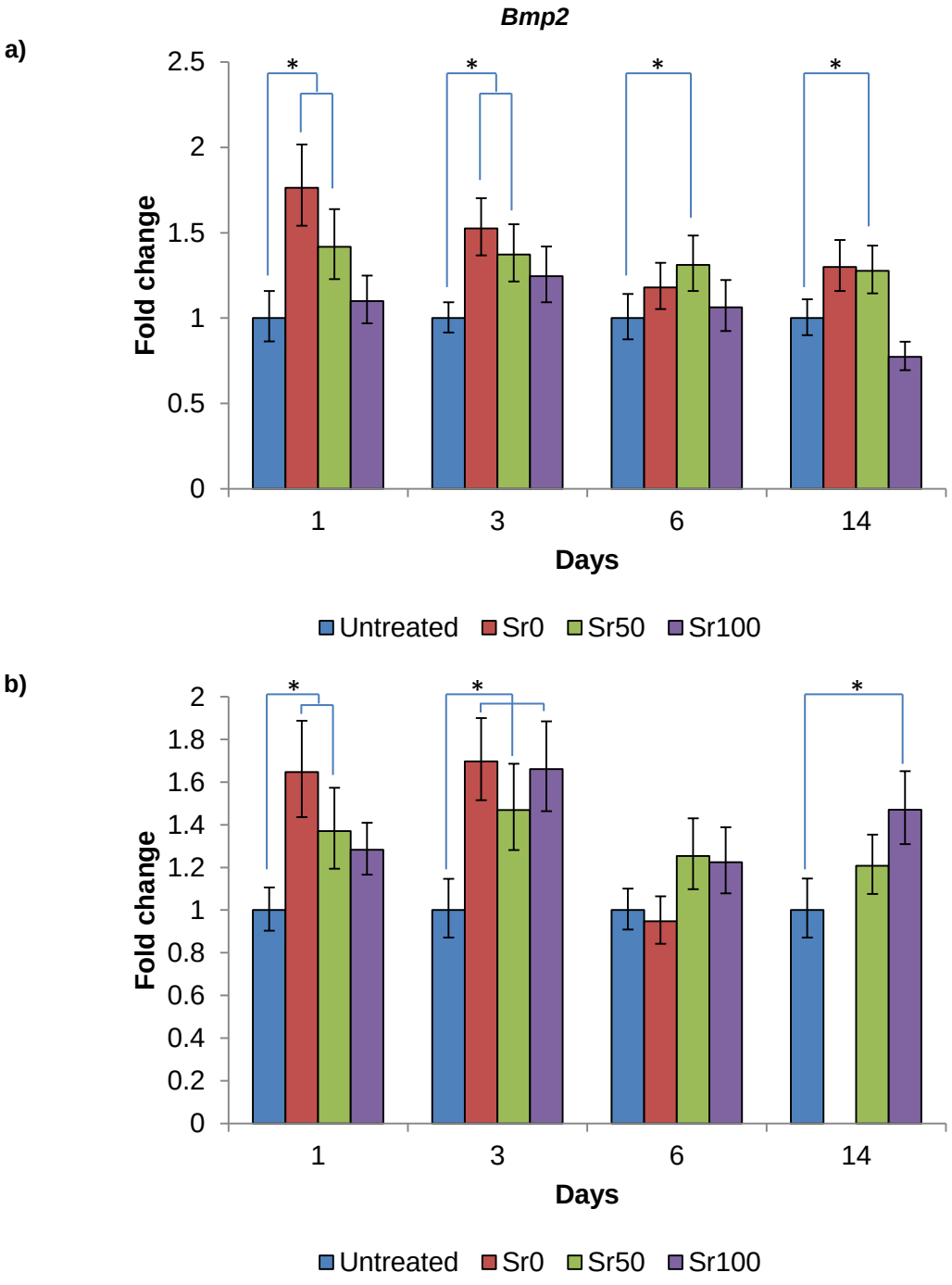

Figure 5.35. Variation in expression of *Bmp2* in rat mesenchymal stromal cells exposed to 20 mg of Sr0, Sr50 and Sr100 bioactive glass powders at various points in time. Studies were carried in two experimental conditions: a) cells cultured in standard cell culture medium and b) cells cultured in osteogenic medium. The lines indicate significant differences between the mean fluorescence of the control and the samples. (n = 9, * = $p < 0.05$).

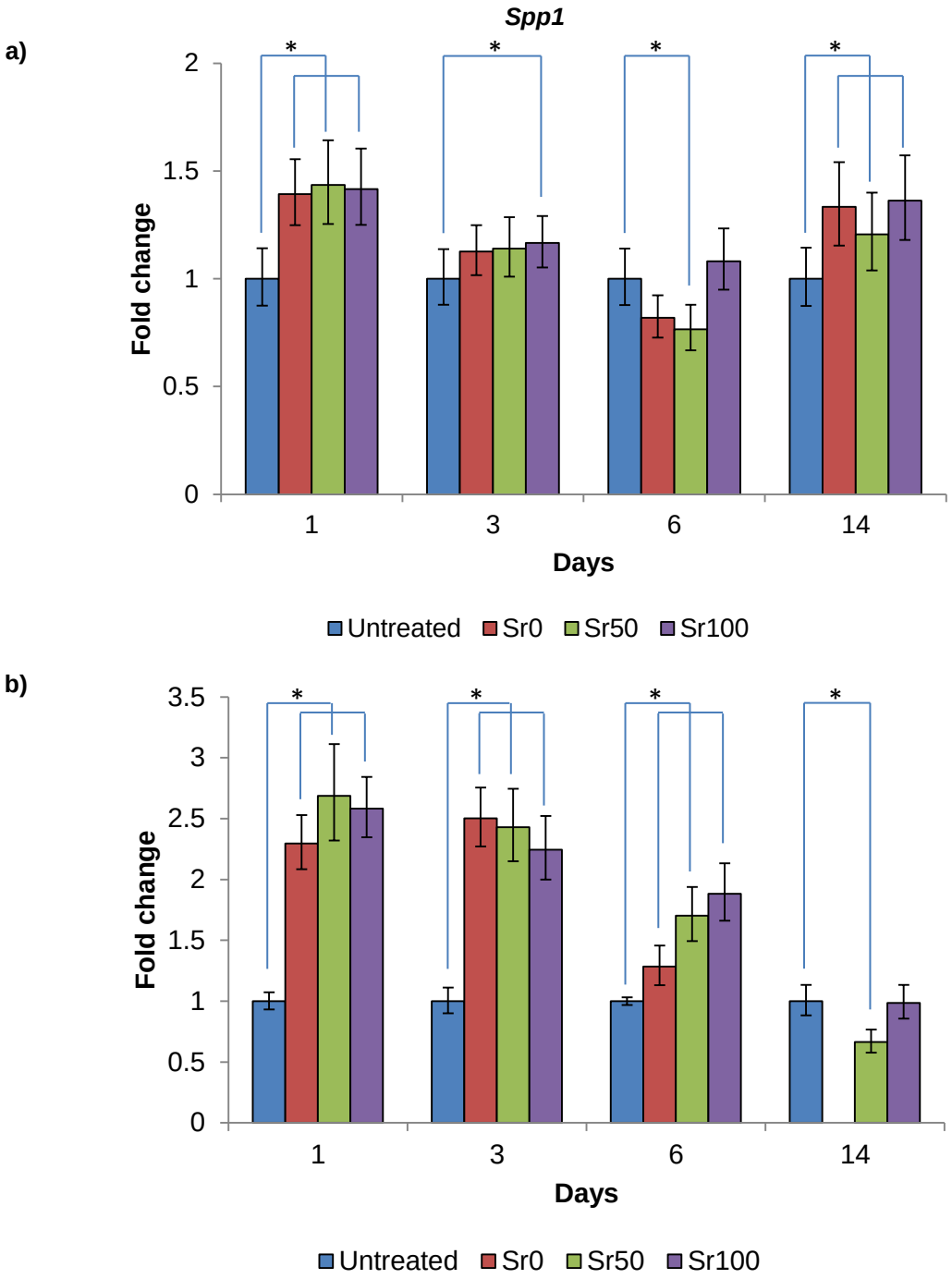

Figure 5.36. Variation in expression of *Spp1* in rat mesenchymal stromal cells exposed to 20 mg of Sr0, Sr50 and Sr100 bioactive glass powders at various points in time. Studies were carried in two experimental conditions: a) cells cultured in standard cell culture medium and B) cells cultured in osteogenic medium (Ost medium). The lines indicate significant differences between the mean fluorescence of the control and the samples. (n = 9, * = $p < 0.05$).

Table 5.18. P-values generated by Wilcoxon two-group test analysis performed between the ΔCt values obtained from RT-qPCR analyses of the genes *Runx2, Alpl, Col1a1, Bglap, Bmp2* and *Spp1* in rat mesenchymal stromal cells exposed to Sr0, Sr50 and Sr100 bioactive glass powders in standard cell culture medium. The background colour of each cell indicates if the analysis reported significant differences between both groups (i.e. Green) or not (i.e. Red). (n = 9; α = 0.05).

Standard cell culture medium							
Gene	**Day**	**Control vs. Sr0**	**Control vs. Sr50**	**Control vs. Sr100**	**Sr0 vs. Sr50**	**Sr0 vs. Sr100**	**Sr50 vs. Sr100**
Runx2	**1**	0.020	0.301	0.496	0.359	0.039	0.203
	3	0.004	0.004	0.004	0.250	0.910	0.359
	6	0.004	0.004	0.004	0.203	0.359	0.055
	14	0.055	0.020	0.301	0.129	0.203	0.055
Alpl	**1**	0.129	0.164	0.098	0.734	>0.999	>0.999
	3	0.004	0.004	0.004	0.012	0.098	>0.999
	6	0.004	0.004	0.004	0.004	0.004	0.301
	14	0.004	0.004	0.004	0.910	0.983	0.3594
Col1a1	**1**	0.734	0.496	0.020	0.359	0.203	0.250
	3	0.004	0.004	0.004	0.570	0.820	0.359
	6	0.004	0.004	0.004	0.020	0.004	>0.999
	14	0.098	0.039	0.496	0.426	0.004	0.008
Bglap	**1**	0.129	0.250	0.301	0.652	>0.999	0.496
	3	0.164	0.301	0.129	0.652	0.910	0.426
	6	0.039	0.012	0.004	0.301	0.004	0.027
	14	0.652	0.734	0.426	0.910	0.910	0.910
Bmp2	**1**	0.004	0.004	0.203	0.055	0.012	0.055
	3	0.004	0.004	0.055	0.129	0.012	0.359
	6	0.129	0.020	0.570	0.250	0.129	0.039
	14	0.129	0.039	0.496	0.734	0.039	0.074
Spp1	**1**	0.004	0.004	0.004	0.820	0.496	0.910
	3	0.129	0.129	0.020	0.910	0.426	>0.999
	6	0.055	0.008	0.570	0.359	0.008	0.004
	14	0.008	0.012	0.004	0.039	0.910	0.027

Table 5.19. P-values generated by Wilcoxon two-group test analysis performed between the ΔCt values obtained from the RT-q PCR analyses of the genes *Runx2*, *Alpl*, *Col1a1*, *Bglap*, *Bmp2* and *Spp1* in rat mesenchymal stromal cells exposed to Sr0, Sr50 and Sr100 bioactive glass powders in osteogenic cell culture medium. The background colour of each cell indicates if the analysis reported significant differences between both groups (i.e. Green) or not (i.e. Red). (n = 9; α = 0.05).

Osteogenic cell culture medium							
Gene	**Day**	**Control vs. Sr0**	**Control vs. Sr50**	**Control vs. Sr100**	**Sr0 vs. Sr50**	**Sr0 vs. Sr100**	**Sr50 vs. Sr100**
Runx2	**1**	0.020	0.020	0.129	0.910	>0.999	0.820
	3	0.004	0.004	0.004	0.570	0.426	0.203
	6	0.004	0.004	0.004	0.164	0.426	0.359
	14	-	0.004	0.004	-	-	>0.999
Alpl	**1**	0.004	0.008	0.008	0.250	0.020	0.098
	3	0.004	0.004	0.004	0.570	0.004	0.012
	6	0.004	0.004	0.004	0.004	0.004	0.734
	14	-	0.250	0.098	-	-	0.004
Col1a1	**1**	0.734	0.496	0.910	0.820	0.301	0.098
	3	0.020	0.004	0.008	0.250	0.359	0.496
	6	0.012	0.004	0.004	0.426	0.359	0.570
	14	-	0.129	0.129	-	-	>0.999
Bglap	**1**	0.910	0.734	0.129	0.570	0.098	0.496
	3	0.008	0.008	0.004	0.098	0.004	>0.999
	6	0.004	0.004	0.004	0.012	0.652	0.250
	14	-	0.652	0.055	-	-	0.734
Bmp2	**1**	0.004	0.012	0.074	0.020	0.039	0.570
	3	0.004	0.004	0.004	0.004	0.910	0.008
	6	0.652	0.055	0.164	0.012	0.004	0.820
	14	-	0.203	0.039	-	-	0.027
Spp1	**1**	0.004	0.004	0.004	0.098	0.426	0.570
	3	0.004	0.004	0.004	0.910	0.020	0.820
	6	0.004	0.004	0.004	0.004	0.004	0.098
	14	-	0.008	0.496	-	-	0.008

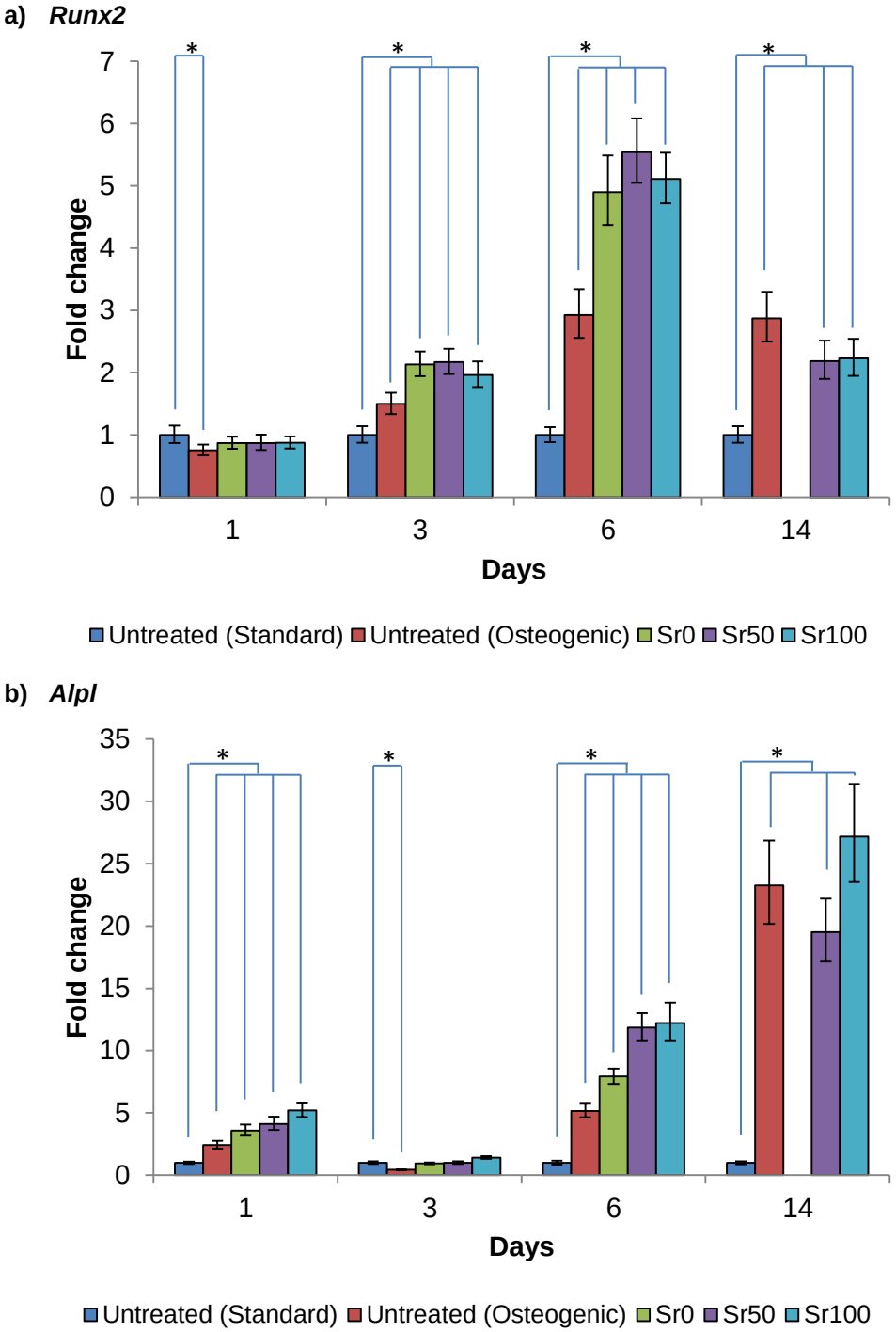

Figure 5.37. Variation in expression of a) *Runx2* and b) *Alpl* in rat mesenchymal stromal cells exposed to Sr0, Sr50 and Sr100 bioactive glass powders and cultured in osteogenic cell culture medium, in relation to the levels of expression in the untreated control in standard cell culture medium. The lines indicate significant differences between the mean fluorescence of the control and the samples. (n = 9, * = $p < 0.05$).

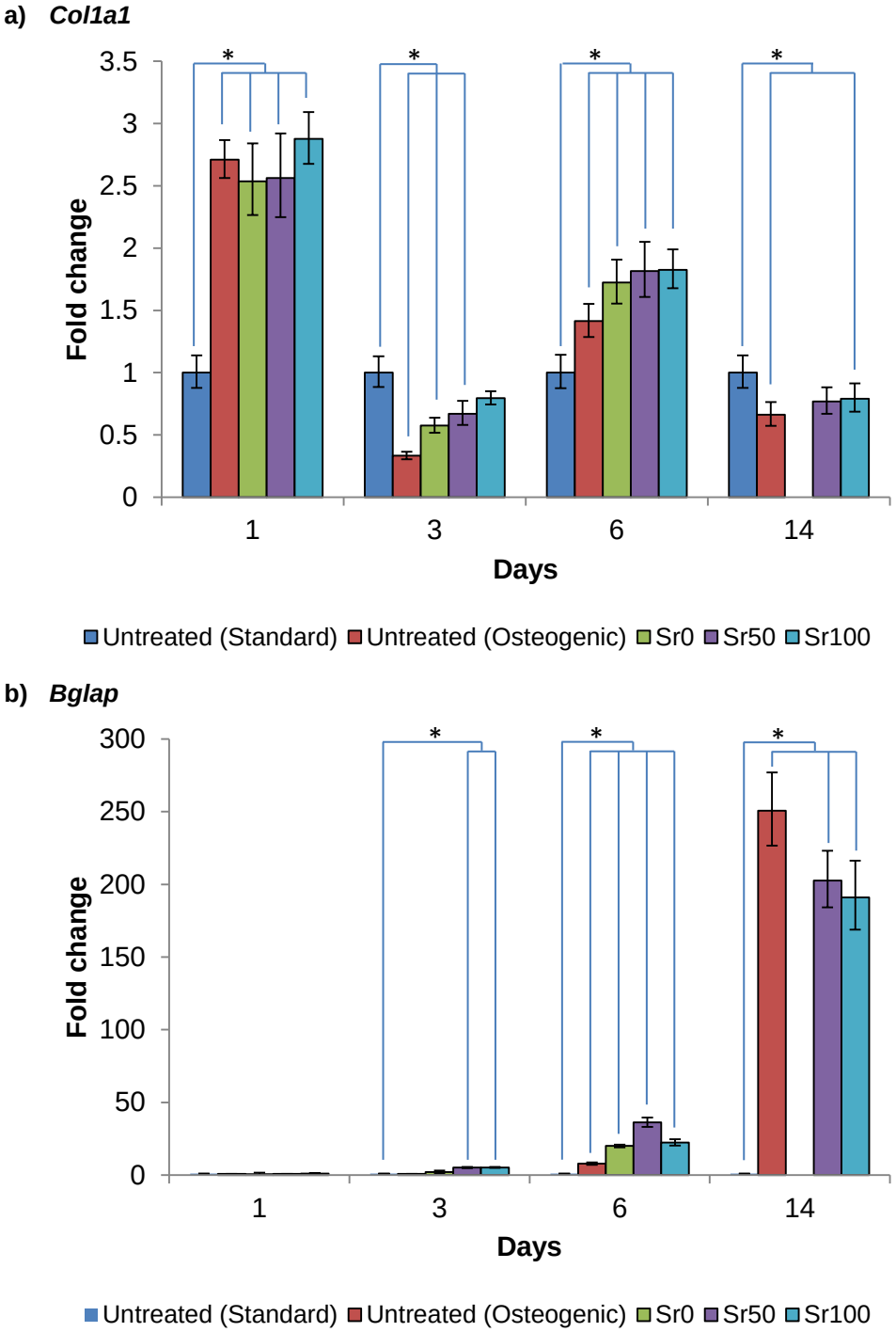

Figure 5.38. Variation in expression of a) *Col1a1* and b) *Bglap* in rat mesenchymal stromal cells exposed to Sr0, Sr50 and Sr100 bioactive glass powders cultured in osteogenic cell culture medium, in relation to the levels of expression in the untreated control in standard cell culture medium. The lines indicate significant differences between the mean fluorescence of the control and the samples. (n = 9, * = $p < 0.05$).

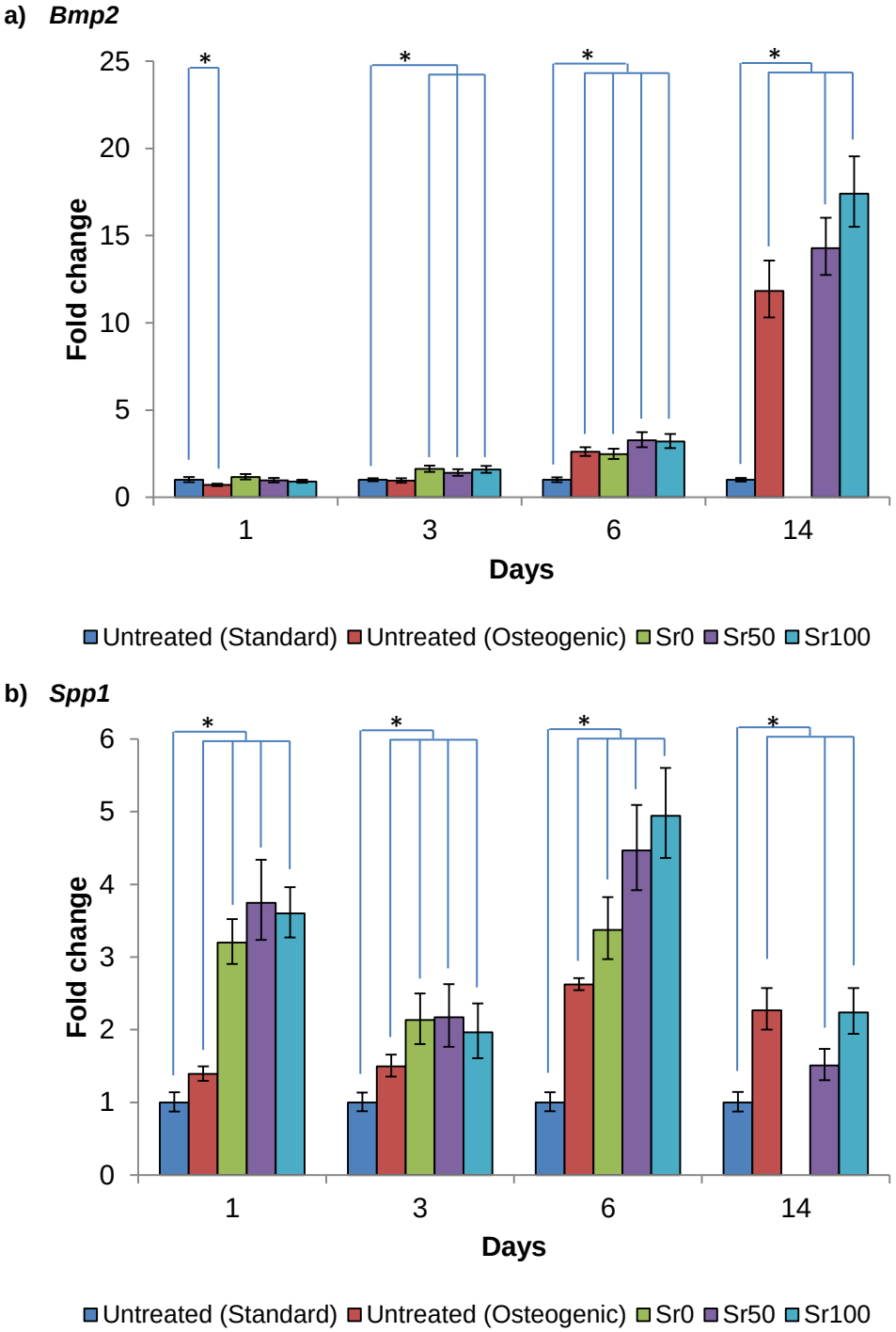

Figure 5.39. Variation in expression of a) *Bmp2* and b) *Spp1* in rat mesenchymal stromal cells exposed to Sr0, Sr50 and Sr100 bioactive glass powders cultured in osteogenic cell culture medium, in relation to the levels of expression in the untreated control in standard cell culture medium. The lines indicate significant differences between the mean fluorescence of the control and the samples. (n = 9, * = $p < 0.05$).

Table 5.20. P-values generated by Wilcoxon two-group test analysis performed between the ΔCt values obtained from RT-qPCR analyses of the genes *Runx2*, *Alpl*, *Col1a1*, *Bglap*, *Bmp2* and *Spp1* in rat mesenchymal stromal cells. The samples analysed were the control in standard cell culture medium (Std) versus all the samples in osteogenic cell culture medium (Ost). The background colour of each cell indicates if the analysis reported significant differences between both groups (i.e. Green) or not (i.e. Red). (n = 9; α = 0.05).

		Osteogenic cell culture medium			
Gene	**Day**	**Control Std vs. Control Ost**	**Control Std vs Sr0 Ost**	**Control Std vs Sr50 Ost**	**Control Std Sr100 Ost**
Runx2	**1**	0.039	0.301	0.164	0.203
	3	0.004	0.004	0.004	0.004
	6	0.004	0.004	0.004	0.004
	14	0.004	-	0.004	0.004
Alpl	**1**	0.004	0.004	0.004	0.004
	3	0.004	0.910	>0.999	0.055
	6	0.004	0.004	0.004	0.004
	14	0.004	-	0.004	0.004
Col1a1	**1**	0.004	0.004	0.004	0.004
	3	0.004	0.004	0.004	0.250
	6	0.004	0.004	0.004	0.004
	14	0.004	-	0.098	0.039
Bglap	**1**	0.250	>0.999	0.820	0.652
	3	0.734	0.055	0.004	0.008
	6	0.004	0.004	0.004	0.004
	14	0.004	-	0.004	0.004
Bmp2	**1**	0.012	0.129	0.734	0.426
	3	0.359	0.004	0.004	0.004
	6	0.004	0.004	0.004	0.004
	14	0.004	-	0.004	0.004
Spp1	**1**	0.004	0.004	0.004	0.004
	3	0.004	0.004	0.004	0.004
	6	0.004	0.004	0.004	0.004
	14	0.004	-	0.004	0.004

6 Discussion

The aim of this project was to produce a novel electrospun composite material combining poly(caprolactone) and particles of strontium-substituted bioactive glass, and to study its potential use as a scaffold for bone tissue engineering. The research work performed to fulfil this aim may be divided into three sections:

1) The production and characterisation of melt-derived strontium-substituted bioactive glass.
2) The fabrication, characterisation and cytotoxicity testing of electrospun composite materials made of poly(caprolactone) and particles of strontium-substituted bioactive glass.
3) The study of the osteogenic effect of strontium-substituted bioactive glass on osteoprogenitor cells.

6.1 Production and characterisation of strontium-substituted bioactive glass

Three melt-derived bioactive glasses were fabricated (Sr0, Sr50 and Sr100) in which calcium was substituted by strontium in molar proportions of 0, 50 and 100%, respectively. All the melts produced optically clear blocks of glass after pouring on moulds and annealing, and also optically clear glass frits after pouring on distilled water. These materials were then characterised using a range of methods.

6.1.1 XRD analysis of bioactive glasses

X-ray diffraction (XRD) analyses confirmed that Sr0, Sr50 and Sr100 bioactive glasses were amorphous in nature and were free of any significant crystalline phases. The diffraction maximum of the amorphous spectra (Figure 5.1) progressively moved toward smaller 2θ values with increasing strontium substitution, suggesting an expansion of the glass network in order to accommodate the larger strontium cation. This is in agreement with a previous study by Fredholm *et al*. (2010), which reported a similar movement of the diffraction maximum with increasing strontium substitution.

6.1.2 DTA of bioactive glasses

The decrease in glass transition temperature (T_g) observed with the increasing strontium substitution (Table 5.1) may have been caused by an expansion of the glass network in order to accommodate the larger strontium cation, weakening the silicate network and lowering the thermal energy barrier for the transition from glass to liquid state to occur. This is in general agreement with a study performed by O'Donnell *et al*. (2010), which reported that the T_g of bioactive glasses changed linearly in proportion to the strontium substitution.

The working range was observed to increase with strontium substitution, suggesting that it may be less difficult to process the strontium-substituted bioactive glasses than the unmodified parent compositions at temperatures higher than T_g. The working range is the difference between T_c and T_g, indicating the range of temperature in which the glasses can be shaped and sintered by a viscous flow process. The low silica content and high calcium content of 45S5 bioglass makes it prone to crystallisation during sintering (Huppa and Yli-Urpo, 2012; Jones, 2013), which is a problem if it is desired to process the glass in its more fluid form. However, it is known that increasing the oxide content in the glass composition may create a wider working range by increasing the difference between both characteristic temperatures (Huppa and Yli-Urpo, 2012). Although this increase in working range is not essential for this project because the glasses were used in a particulate form, melt-derived strontium-substituted bioactive glasses may also be of interest for applications which may require a larger working range. Examples of this are the production of glass coatings for metal implants or the generation of glass fibres.

Differences were observed in the estimated characteristic temperatures of PerioGlas® and Sr0 bioactive glass, both materials based on the composition of 45S5 bioglass. Although the T_g values are similar in both cases (523°C for PerioGlas® and 525°C for Sr0), the T_c and T_p values are consistently lower for Sr0 than for Perioglas® (T_c, 630°C vs. 613°C; T_p, 690°C vs. 682°C), resulting in a greater working range in Perioglas®. This

may be attributed to the manufacturing process, with Sr0 being produced in-house and PerioGlas® being produced under much stricter requirements in order to be commercialised as a medical device. This may require a study to determine if there were significant compositional variations with respect to the base composition of 45S5 bioglass, for example using X-ray fluorescence analysis.

6.1.3 Density and oxygen density of bioactive glasses

The experimentally measured density of the bioactive glasses increased linearly in proportion to strontium substitution (Table 5.2 and Figure 5.3), suggesting that the strontium cation increased the overall mass of the glasses. Additionally, a good agreement was observed between the experimentally measured densities and the theoretical densities calculated using Doweidar's model. Doweidar hypothesised that in alkali-silicate glasses the volume of the Q^n structural units depends only on the type of modifier ions present in the composition but not on their concentration. Therefore, the volume of the units can then be calculated as a function of the radius and charge of the modifier ion and the number of non-bridging oxygens (Doweidar, 1999; Fredholm *et al.*, 2010). The good agreement between the experimental and theoretical densities confirmed that the volume of the Q^n units with strontium was larger than the volume of the equivalent Q^n units with calcium because of the larger atomic radius of Sr^{2+}, as shown in Table 6.1. Although this increase in volume may seem contrary to an increase in density, the effect of strontium substitution on glass density may be explained by the higher atomic weight of strontium, which is proportionally greater than the increase in volume caused by the larger ionic radius.

Table 6.1 Ionic radius and atomic weight for sodium (Na^+), calcium (Ca^{2+}) and strontium (Sr^{2+}) cations. Adapted from Doweidar (1999).

Cation	Ionic radius (nm)	Atomic weight ($g \cdot mol^{-1}$)
Na^+	0.095 - 0.102	22.99
Ca^{2+}	0.094 - 0.106	40.078
Sr^{2+}	0.110 - 0.127	87.62

The linear decrease of oxygen density with strontium substitution (Table 5.3 and Figure 5.4) suggested an expanded and less rigidly bonded glass network. This was probably caused by the larger strontium cation and is consistent with the larger volumes of the Q^n units with strontium hypothesised by Doweidar. These results are in agreement with a previous study by Fredholm *et al*. (2010), which reported a linear increase of bioactive glass density from 2.71 g cm^{-3} to 3.10 g cm^{-3} and a linear decrease of oxygen density with strontium substitution.

6.1.4 Solubility study of bioactive glasses

The solubility of the bioactive glasses increased linearly in proportion to strontium substitution (Figure 5.5), suggesting an expansion of the glass network in order to accommodate the larger strontium cation which may allow the modifier ions (i.e. Na^+, Ca^{2+} and Sr^{2+}) to be more easily released to the local environment than in unmodified glasses.

This increase in solubility may have a potentially intensifying effect on the reactivity of the glasses and, consequently, on their bioactivity. O'Donnell *et al*. (2010) argued that this effect is possible because the substitution of calcium by strontium was done on a molar basis and not on a weight basis. If the substitution is done on a weight basis, as in the case of work reported by Lao *et al*. (2009) and Gorustovich *et al*. (2010), the contents of other components in the glass (e.g. silicon) will increase. If the silica content in a silicate glass is increased, the network becomes more polymerised (i.e. larger amount of Q^3 structural units at the expense of Q^2 units) and it results in reduced solubility, degradation rates and bioactivity. However, if the substitution is done on a molar basis the network structure is not significantly changed and the bioactivity may be retained. O'Donnell *et al*. also suggested that the bioactivity of strontium-substituted bioactive glasses may even be higher than in unmodified glasses due to the biological effect of strontium on bone-forming cells and, also, due to the increase in solubility caused by the expansion of the glass network produced by the larger strontium cation.

Results from qualitative energy dispersive x-ray spectroscopy (EDS) analyses performed before and after the solubility studies (Figure 5.6, Figure

5.7 and Figure 5.8) confirmed that the dissolution of the glasses began at the surface of the samples, as expected for bioactive glasses. The main chemical elements detected on fragments of the detached surface material after the solubility tests were performed were silicon and oxygen, suggesting that the modifier ions (i.e. Na^{+}, Ca^{2+} and Sr^{2+}) were released in dissolution and that the glass network composed of silicon and oxygen remained. The high temperature (80°C) and the acetic acid solution used in the study may have accelerated the ionic release due to a corrosive effect of the solution on the glass. This was also in general agreement with what is expected to occur during the first steps of bioactive glass dissolution, when the rapid exchange of the modifier ions with H^{+} from the solution creates Si-OH bonds on the surface of the glass (Hench, 1998).

6.1.5 Network connectivity of bioactive glasses

Although the results of the NC calculations may suggest that the substitution of calcium by strontium in the bioactive glass composition may not affect the bioactivity of the material, even if it results in an expanded glass network, it is certainly possible that two glasses with different dissolution rates may present identical network connectivity values if calculated with the models used in this report.

NC is a measure of the average number of bridging oxygens on each SiO_4 tetrahedron. It is calculated from the molar composition of the glass (Equation 4.4) and may be used to predict a number of properties, including its bioactivity. For example, the bioactivity of bioactive glasses generally increases as NC decreases (O'Donnell *et al*., 2010). To calculate NC, the number of non-bridging oxygens (NBOs) created by the network modifying oxides is subtracted from the number of bridging oxygens (BOs) formed by the network former oxide. This value is then divided by the number of glass forming units. Since a molecule of both CaO and SrO will form two NBOs each, it is expected that the substitution of calcium by strontium on a molar basis will not produce any changes in the theoretical values.

The NC' value (i.e. assuming that phosphorus is within the glass structure in the form of orthophosphate but does not enter the glass network) for Sr0,

Sr50 and Sr100 bioactive glass compositions were the same (i.e. 2.12) and were within the range suggested by Edén (2011) for optimal glass bioactivity (i.e. 2.0 ≤ NC' ≤ 2.6). This was also the same value calculated for 45S5 bioglass (Jones, 2013). The NC'' value (i.e. assuming that phosphorus enters the glass network forming P-O-Si bonds) for Sr0, Sr50 and Sr100 bioactive glass compositions was the same as the value reported for 45S5 bioglass (i.e. 1.90) (Hill, 1996). The composition of Sr0, Sr50 and Sr100 were based on the original composition of 45S5 bioglass, so it was expected to obtain the same values of NC.

NMR analyses of Sr0, Sr50 and Sr100 bioactive glasses should be performed to experimentally determine if the NC of the materials was actually altered in any significant way in response to the substitution. However, previous solid-state NMR studies by Fredholm *et al.* (2010) showed that the NC and the structure of the glass did not change significantly with the substitution of calcium by strontium in bioactive glasses. Therefore, these analyses of the glasses were not considered as necessary.

6.1.6 Particle size analysis of milled bioactive glasses

Particle size analyses of the bioactive glass powders produced by milling and sieving showed that the particle size distributions for Sr0, Sr50 and Sr100 bioactive glasses presented similar profiles (Figure 5.9 and Figure 5.10).

A general increase in particle size was observed (Table 5.5) as the proportion of strontium in the glass composition increased. This may be caused by a potential increase of material fragility as a consequence of the expansion of the glass network in order to accommodate the larger strontium cation. This may result in the production of greater amounts of smaller sized particles during milling, potentially forming aggregates which may be detected as larger particles during the particle size analysis. SEM micrographs of the glass powders (Figure 5.11) suggested that the smaller particles tended to aggregate together or to attach to the surface of larger particles. Therefore, it is possible that a powder sample containing a larger proportion of small sized particles may result in the formation of larger groups of particles.

6.1.7 Conclusions from the production and characterisation of strontium-substituted bioactive glass

Calcium was successfully substituted by strontium in the composition of bioactive glass, resulting in measureable changes to several material properties. The substitution affected the characteristic temperatures of the material, decreasing glass transition temperature due to the expansion of the glass network to accommodate the larger strontium cation. Additionally, the onset of crystallisation temperature and the peak crystallisation temperature presented a minimum value in Sr50 bioactive glass. The working range of temperature also increased with strontium substitution, a variation that may have potential benefits for the processing of these glasses for various applications.

The substitution also induced a linear increase of glass density, due to the presence of the heavier strontium cation; and a linear decrease of oxygen density, due to the expansion of the glass network. The solubility of the glasses also increased linearly in proportion to strontium substitution. This may potentially result in increased bioactivity levels due to higher reactivity. However, network connectivity calculations, a measurement used to estimate glass bioactivity, did not vary with strontium substitution. This may suggest that the substitution does not have an effect on glass bioactivity, but it has been hypothesised (O'Donnell and Hill, 2010) that the structural model used in these calculations does not take into account the field strength of the network modifier ions, so it is possible that two glasses with different dissolution rates may present identical network connectivity values

Finally, it is possible that strontium substitution may affect glass mechanical properties, increasing its fragility due to the expanded and less rigidly bonded glass network, as revealed by the decreased oxygen density. This may result in a larger proportion of smaller particles in powders produced by the milling of bioactive glasses with higher strontium content. The more abundant smaller particles may then aggregate to form clusters which may be identified as larger particles in the analyses of particle size.

6.2 Fabrication, characterisation and cytotoxicity testing of electrospun composite materials

6.2.1 Optimisation of electrospinning parameters

An optimisation study of several electrospinning parameters was performed in order to fabricate materials exhibiting a small amount of surface defects and consistent fibre diameters. The study was divided in two parts: first, the effect of polymer concentration and solvent composition was studied; and second, the effect of the addition of bioactive glass particles on the production of electrospun fibres was investigated.

Effect of polymer concentration and solvent composition

As previously mentioned in section 5.2.1 of this report, in the first stage of the optimisation study the solutions of 10 wt% PCL dissolved in blends of DCM:DMF 90:10 v/v and of DCM:DMF 85:15 v/v were selected because the electrospun mats produced presented the smallest amount of defects and the most regular fibres with respect to diameter and morphology.

The processing parameters governing the electrospinning process can be divided into three main categories: ‘system’ parameters, which are those related to the system used to produce the electrospun fibres (e.g. applied voltage); ‘solution’ parameters, which are those related to the polymer solution used to produce the electrospun fibres (e.g. polymer concentration); and ‘environmental’ parameters, which are those factors external to the electrospinning process (e.g. atmospheric humidity). The main ‘solution’ parameters affecting fibre diameter and morphology are the conductivity and volatility of the solvent used, and polymer concentration.

It is known that PCL dissolves well in DCM but poorly in DMF (Woodruff and Hutmacher, 2010). From the boiling point and dielectric constant values (Table 4.7) it is possible to derive that DCM is significantly more volatile and less conductive than DMF. Therefore, the addition of DMF to DCM had the overall effect of reducing the volatility and increasing the conductivity of the solvent mixture, resulting in the production of more regular electrospun fibres. Furthermore, the higher conductivity may have resulted in potentially

smaller fibre diameters by an associated increase in the tensile forces that the fibre jets are subjected to in the electric field (Supaphol *et al*., 2012). This effect may be observed in the micrographs of the materials produced with 10 wt% PCL dissolved in DCM:DMF 90:10 v/v and 85:15 v/v (Figure 5.13). This is in general agreement with work performed by Lee *et al*. (2003), in which a series of solutions of PCL dissolved in blends of DCM and DMF with ratios 100:0, 85:15, 75:25 and 40:60 v/v were electrospun and which showed that the diameter of the PCL fibres decreased as the content of DMF in the solution increased, probably due to increased conductivity and reduced surface tension and viscosity of the solution.

The beading observed in the electrospun samples produced using the 8 wt% PCL solution was probably caused by the low polymer concentration. Generally, the morphology of the fibres will gradually change from beaded to smooth as the polymer concentration increases. Within an optimal range it is possible to produce uniform fibres with diameters that increase with the concentration, but concentrations higher than optimal will usually result in a disruption of the flow due to an increase in solution viscosity (Supaphol *et al*., 2012). This effect was also observed in this study, as the samples produced using the 12 wt% and 14 wt% solutions presented a higher level of surface defects due to sputtering than those produced using the 10 wt% solution.

Effect of bioactive glass particle content

In the second stage of the optimisation study, the solution of 10 wt% PCL dissolved in DCM:DMF 90:10 v/v with bioactive glass particles added following a 10:1 PCL:glass weight ratio was selected to fabricate the electrospun materials used in the project. This composition produced materials which were generally strong enough to be handled without breaking and presented the smallest amount of surface defects due to sputtering. Additionally, it was considered that the composition using the lowest amount of DMF would be favoured due to the potential toxicity hazard posed by this solvent.

It was noted that increasing the amount of particles added to the polymer solution resulted in samples with more apparent defects on the surface of the

electrospun membrane due to sputtering. Additionally, the materials fabricated using the PCL:glass weight ratio 10:4 were more fragile than materials produced using other ratios. Finally, SEM micrographs (Figure 5.14) also suggested that the addition of glass particles may result in larger variations and less homogeneous distributions of fibre diameters compared to materials electrospun without glass particles.

The sputtering may be due to a disruption of the polymer jet caused by the addition of the particles to the polymer solution. SEM micrographs (Figure 5.16, Figure 5.17 and Figure 5.18) showed regions in the fibres with increased diameters and irregular morphologies which did not generally disrupt the fibre. However, if the glass particles were contained in those regions, it cannot be discarded that large particles or clusters of particles may result in broken fibres as the polymer jet is stretched on its way towards the collector. The variation in diameter due to the presence of glass particles may be caused by a non-homogeneous distribution of the polymer solution in the fibres containing the particles, potentially resulting in regions with increased polymer concentration and variable rates of solvent evaporation.

6.2.2 SEM and EDS analyses of electrospun materials

Electrospun materials were then fabricated using the solution composition selected in the optimisation study. The thickness of the mats were not experimentally determined, although they generally were <1 mm.

Low magnification SEM micrographs of non-composite electrospun materials (i.e. PCL with no added glass particles) showed regular fibres with no apparent defects on their surface (Figure 5.15, a, b and c). Higher magnification micrographs of the same samples suggested that the surface of the fibres was generally porous (Figure 5.15d). SEM micrographs of the composite electrospun materials (i.e. electrospun PCL with Sr0, Sr50 and Sr100 bioactive glass particles) showed that the fibres presented certain regions with increased diameters and irregular morphologies (Figure 5.16, Figure 5.17 and Figure 5.18). The presence of bioactive glass particles within those regions was confirmed by EDS analysis, through the detection of all the chemical elements that formed each glass composition (Figure 5.19).

These particular regions were consequently known as ‘filled regions’, while PCL fibres that did not contain glass particles were known as ‘unfilled fibres’. The micrographs of the ‘filled regions’ also showed that the particles were embedded within the fibres and were covered by a layer of PCL. The fibres were generally not broken by the presence of the glass particles, despite the particles being significantly larger in size than the average ‘unfilled fibres’. In some cases the glass particles were not completely covered by the polymer and some parts of them remained exposed to the local environment, potentially facilitating their dissolution and release of their ionic content. The surface of the polymer in the ‘filled regions’ was observed to be porous as well (Figure 5.16d and Figure 5.18d), suggesting that the process of pore formation may occur throughout the whole electrospun structure.

Porous electrospun fibres have been produced using diverse polymers, solvents, and process parameters (Megelski *et al*., 2002). Two main mechanisms have been found to be responsible for pore formation: breath figures process and phase separation. The breath figures process, first described by Srinivasarao *et al*. (2001), is able to generate ordered pore patterns on a polymer surface through the condensation of water droplets from atmospheric humidity. The rapid evaporation of the solvent reduces the temperature on the surface of the electrospinning jet as it travels from the Taylor cone to the collector and, depending on the properties of the solvent, this cooling may be sufficient to promote the condensation of water droplets. These droplets remain as individual entities and arrange themselves on the surface, partially sinking into the solution. The solution then surrounds the template created by the droplets and, as the droplets evaporate after the jet has completely dried, an imprint on the surface of the fibres appears in the form of pores. This process requires the presence of certain levels of atmospheric humidity and the use of a volatile solvent with low water solubility. The characteristics of the pores thus depend on the polymer (i.e. chemistry and molecular weight), the solvent (i.e. vapour pressure, surface tension) and the solution used (i.e. viscosity, hydrophilicity, thermal properties) (Megelski *et al*., 2002; Migliaresi *et al*., 2012).

Phase separation is a process which leads to the formation of two phases in a polymer solution. When a polymer solution is cast on a mould, evaporation occurs under convective conditions. As the solvent evaporates, the solution becomes thermodynamically unstable and separation occurs into polymer-rich and the polymer-poor phases. The polymer-rich phase solidifies shortly afterwards and forms a matrix, while the polymer-poor phase forms the pores. Megelski *et al*. (2002) suggested that these general aspects could be transferred to the formation of porous polymeric fibres. Bognitzki *et al*. (2001) described the formation of pores in electrospun fibres using several polymers and proposed that this occurred due to the rapid evaporation of the solvent caused by the increase in surface area in the electrospun material and subsequent rapid solidification.

The presence of pores on the surface suggests an increased surface area compared to a similar material made of non-porous fibres. As a consequence, the materials produced for this work may present a potentially larger capability to absorb water and release the ionic dissolution products contained in the bioactive glass particles to the local environment. Furthermore, fibre porosity has been proposed as of fundamental importance in the production of electrospun scaffolds for tissue engineering because cell behaviour may be influenced by the topographical features on the surface they attach to (Migliaresi *et al*., 2012). The characteristics of the polymer solution used to fabricate the electrospun materials here discussed support the breath figures process as a potential mechanism of pore formation. The main solvent used, DCM, is highly volatile and does not dissolve well in water. Additionally, PCL is highly hydrophobic, facilitating the conditions for the formation of water droplets on the fibre surface. However, the phase separation process has also been proposed by some researchers as the main cause of pore formation on electrospun PCL fibres (Hartman *et al*., 2010).

The average diameter of the ‘unfilled fibres’ was measured to be 1.99 ± 0.36 μm, while the average diameter of the ‘filled regions’ was 14.02 ± 7.67 μm. According to the plots of the particle size distribution (Figure 5.9), the greatest volume in the particle distribution was occupied by particles with

sizes around 10 μm. This range of sizes, combined with a layer of polymer covering the glass particles of potentially around 1 μm in thickness, may potentially yield diameters similar to the average diameter of the 'filled regions'. Particles with sizes <2 μm may not have produced apparent changes in fibre morphology and diameter because of their small dimensions.

6.2.3 Solubility study of electrospun materials

A solubility study of the electrospun materials was performed to investigate the dissolution of the bioactive glass particles from within the polymeric fibres and the subsequent release of the ionic dissolution products to the local environment.

When bioactive glasses are submerged in an aqueous environment a rapid exchange of sodium, calcium and/or strontium ions with H^+ from the solution occurs on the glass surface, resulting in an increase of the pH (Hench, 1998). It was previously described in this report that the substitution of calcium by strontium in the glass composition resulted in a linear increase in glass solubility. As a consequence of this increase, the electrospun materials containing Sr50 and Sr100 bioactive glass particles were probably able to induce higher increases of pH compared with those containing Sr0 bioactive glass particles (Figure 5.20). This agrees with a report by Fredholm *et al.* (2012), who observed a correlation between pH increases and the increasing content of strontium in bioactive glasses when particles of the material were immersed in simulated body fluids.

The high surface area of the glass powders and of the electrospun fibres may also have resulted in an increased dissolution rate due to the small particle size and the larger surface area of the electrospun fibres, allowing for a greater capacity to absorb water and release the ionic dissolution products to the environment.

The gradual decrease in pH observed after the initial 24 hours may have been caused by the dissolution of atmospheric CO_2, as the vials were not sealed from the atmosphere during the study and were regularly opened to

perform the pH measurements. In the case of the electrospun composite materials the decrease of pH values occurred at a faster rate than in the case of the samples only containing bioactive glass powders.

These results suggested two ideas: first, the glass particles may indeed dissolve from within the polymeric fibres, releasing their ionic content to the local environment and consequently increasing the pH. Second, an interaction may occur between the polymer and the bioactive glass particles in the composite materials, facilitating the faster decrease of pH. A potential mechanism for this effect may be as follows. It is known that the first stage of PCL degradation involves the random hydrolytic breakage of ester bonds in the polymeric chains of the amorphous regions of the polymer, reducing chain length (Middleton and Tipton, 2000; Woodruff and Hutmacher, 2010). Lam *et al*. (2008) performed a study of the *in vitro* degradation of porous, three-dimensional PCL scaffolds, including composite samples containing particulate tricalcium phosphate (TCP). NaOH was added to the media in order to accelerate polymer degradation through alkalinisation. They reported that the degradation process was regulated by polymer molecular weight, crystallinity, hydrophilicity and the design of the polymeric device, and observed that the scaffolds degraded via a surface degradation pathway in the alkalinised conditions instead of a bulk degradation pathway.

Surface degradation occurs when water penetrates the polymer at a slower rate than the hydrolytic cleavage of the polymer chains. The degradation by-products then diffuse rapidly into the media and no water molecules reach the centre of the matrix. Therefore, degradation mainly occurs at the surface and the device suffers a ‘thinning’ effect in which material is eliminated from the surface while the molecular weight of the polymer remains intact. As the degradation begins at the amorphous regions and occurs at a very fast rate, the remaining crystalline regions are held together by the amorphous segments until they are dislocated from the main polymer bulk. The erosion of the amorphous polymer regions induces the fragmentation and final erosion of the packed crystalline regions at the surface as well, thus contributing to a faster initial loss of mass. The process is schematically represented in Figure 6.1.

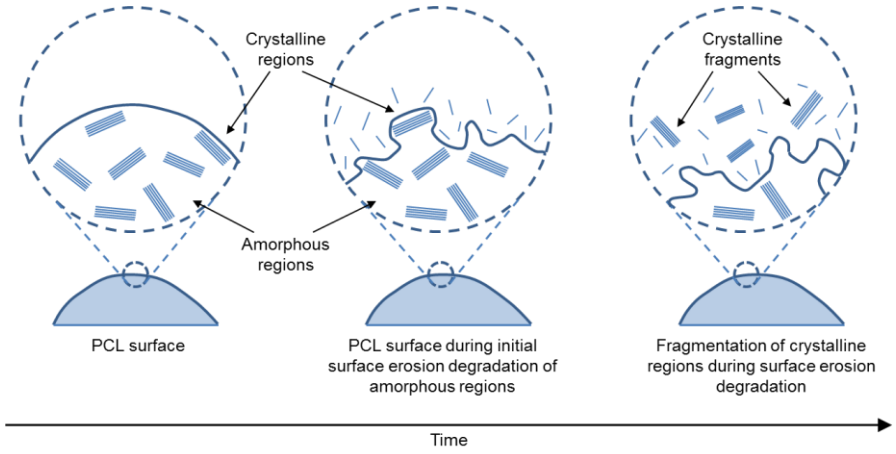

Figure 6.1. Schematic diagram of the potential mechanism of fragmentation of crystalline regions during the degradation of poly(caprolactone) (PCL). Adapted from Lam *et al*. (2008).

It has been suggested (Baji *et al*., 2010) that the rapid evaporation of the solvent from the electrospinning jet may lead to less developed structures in the fibres. This rapid evaporation may result in a reduction of the jet temperature and, consequently, polymer molecules that are aligned along the fibre axis have less time to realign themselves, leading to a less favourable packing and lower levels of crystallinity in semi-crystalline polymers due to non-optimal formation of crystalline lamellae. Lee *et al.* (2003) reported wide angle X-ray diffractions measurements that suggested a reduction in the crystallinity of electrospun PCL fibres compared to the crystallinity of PCL films. This reduction of the overall crystallinity in electrospun PCL fibres may potentially result in increased degradation rates by increasing the proportion of amorphous regions in the fibres, more susceptible to degradation than the crystalline regions.

Lam *et al*. (2008) also reported that PCL scaffolds containing TCP particles (60 μm particle size) degraded entirely after 54 hours in 5 M NaOH at 37˚C, while PCL only scaffolds degraded entirely within 6 weeks under the same conditions. They suggested that this substantial difference may be due to a reduction of the molecular weight of the scaffolds caused by the presence of the TCP particles, which affected the arrangement of the polymer chains surrounding them and exposed them more readily to hydrolytic cleavage of chain-end scissions. It is possible that the presence of the bioactive glass

particles in the electrospun materials, which were smaller in size than the particles used by Lam *et al*. (2008), may have resulted in a similar effect.

It is also possible that the rapid increase of environmental pH due to glass dissolution may accelerate the rate of PCL degradation, similar to the effect caused by the addition of NaOH in the study performed by Lam *et al*. (2008). Although the change of pH was global and affected the whole medium in each sample, the accelerating effect may have been particularly severe in the polymeric regions surrounding the glass particles. As the polymer degraded, acidic degradation products from PCL may have been released from the sample to the medium, decreasing the pH. The statistically significant differences observed in the experiments suggested that the increased solubility of the strontium-substituted bioactive glasses may result in a more pronounced accelerating effect.

It has been frequently proposed that the increase of pH induced by the dissolution of bioactive glasses may be used to neutralise the acidic effect caused by the degradation of bioresorbable polymers such as PCL. That way, it is argued, it may be possible to avoid potential inflammation responses post-implantation (Boccaccini and Maquet, 2003; Suggs *et al*., 2007; Jones, 2013). However, the degradation rate of the polymer and the dissolution rate of the glass should ideally match to optimise the buffering effect. The results here discussed suggested that bioactive glass dissolution occurs at a significantly faster rate than polymer degradation, which is usually counted in months rather than in days (Middleton and Tipton, 2000; Wang *et al*., 2010). Although some evidence of the buffering effect of bioactive glass on polymer degradation has been reported in the literature (Stamboulis *et al*., 2002), it may be argued that the large disparity between the two rates would not support the proposed buffered system. However, the results of this project suggested that the composite system may be used in the opposite way, with the accelerated polymer degradation buffering the rapid initial increase of pH induced by the glass dissolution.

No significant changes of pH were observed in those samples containing only electrospun PCL, suggesting that the polymer may not degrade at the

same rate without the presence of the bioactive glass particles. Similarly, no significant changes were observed in the samples containing only deionised water, suggesting that the medium used did not induce the pH changes observed in the previous cases.

6.2.4 Addition of glass particles to electrospun materials

Two methods used to place additional bioactive glass particles on the surface of the electrospun fibres were developed and investigated. The purpose of this study was to create new configurations of the materials and to study if the further addition of exposed bioactive glass particles had a significant effect on their cytotoxicity and potential to work as a scaffold.

Their efficiency was studied by performing two separate tests. The first test used suspensions of Sr0, Sr50 and Sr100 bioactive glass powders in cell culture medium at a constant concentration of 1% w/v, while the second test used a series of suspensions of increasing concentration of Sr0 bioactive glass powder in cell culture medium. Although the results of the tests showed that both methods were able to add bioactive glass particles on the electrospun samples, it was demonstrated that the ‘filtering method’ was consistently more efficient and was capable of adding most of the glass content present in the suspensions on the samples (Figure 5.21). The first test showed that the ‘loading method’ was able to add an average of 1.16 mg of glass particles on the samples, which is approximately 12% of the glass content present in 1 ml of the suspensions. The ‘filtering method’ was able to add an average of 8.51 mg of glass particles, which is approximately 85% of the glass content. The efficiency of the ‘filtering’ method was also shown to be higher in the second test, exhibiting values between 70% and 90% using suspensions with concentrations of 0.25% w/v and higher.

These differences in efficiency between both methods may be due to the way they work. The ‘loading method’ is based on the deposition of glass particles in suspension on the surface of the samples solely depending on gravitational force. As the path the particles take cannot be controlled, many will be deposited outside the sample. On the other hand, the ‘filtering method’ allows for a finer control as the whole suspension is pushed through

the electrospun material and, consequently, the majority of the content of glass particles present on the suspension will be deposited on the sample.

SEM micrographs showed that in the case of samples processed using the 'filtering method' (Figure 5.23, a and b) many particles were trapped in the mesh of electrospun fibres. However, as the amount of glass particles added increased, the new particles appeared to accumulate on top of the previously deposited particles, potentially block the pores of the mesh. This may be considered an undesirable outcome, especially for tissue engineering applications since the presence of open pores is an important requirement for scaffolds. However, it may be an interesting approach for other applications, such as the development of membranes for guided bone regeneration. It is suggested that suspensions of glass particles of low concentration (i.e. 0.05% w/v or lower) should be used if it is desired to minimise pore blockage.

It was also apparent from the SEM micrographs (Figure 5.23, c and d) that most of the last glass particles added were not in direct contact with the mesh. After drying, the glass particles were able to separate from the electrospun material with relative ease, suggesting that the glass did not firmly attach to the surface of the fibres. It is possible that the particles may attach to each other as the bioactive glass dissolves, inducing the formation of the HCA layer. According to Hench (1998), this process takes fewer than 20 hours from the moment in which the reactions begin. In this study the samples were incubated in cell culture medium for 24 hours after the particles were added, so the process of HCA formation may have already started. However, this may only be able to create a mechanic attachment of the glass particles to the electrospun fibres if the most external particles become attached through HCA formation to the particles trapped within the mesh. In general, the loss of particles appeared to increase as the amount of glass added to the electrospun samples increased.

Small reductions of mass were observed in the control composite samples (i.e. electrospun materials processed with cell culture medium without

bioactive glass particles), probably due to the dissolution of the glass particles and the potentially accelerated degradation of PCL.

The variability observed in the results of the 'filtering' method may be due to a series of reasons. The first source of variability may have been inaccuracies in the process of suspension preparation, including more or less amount of glass powder than required. Second, although the suspensions were stirred to homogenise the distribution of particles, it is possible that the sample of suspension did not contain the expected amount of glass particles. Third, it is also possible that some glass particles may have gone through the electrospun sample as the suspension was pushed through. Finally, it is possible that some of the glass particles deposited on the surface of the samples were lost in the final washing and drying steps or when handling the samples for weighing.

6.2.5 Cytotoxicity of electrospun composite materials

The cytotoxicity of all the electrospun materials produced was tested by culturing a rat osteosarcoma (ROS) cell line on the samples and then applying a resazurin-dye based assay, which assessed cellular metabolic activity by measuring fluorescence emission levels from the cell culture medium used.

Results from the study suggested that electrospun PCL and the inclusion of bioactive glass particles within the fibres did not induce an appreciable detrimental effect on cell viability *in vitro* (Figure 5.24a). Fabbri *et al*. (2010) reported similar results when testing the *in vitro* cytotoxicity of porous scaffolds made of PCL and particles of 45S5 bioglass fabricated using a solid-liquid phase separation method, observing no appreciable differences in cell proliferation as the content of added glass particles was varied between 25% and 50% by weight with respect to PCL. Although the cytotoxic effect of increasing the content of glass particles in the electrospun samples was not tested in this study, no significant differences were observed between the samples as the content of strontium in the glass was increased, which may intensify the cytotoxic effect due to higher dissolution rates and greater subsequent rises in pH. For example, an increase in cytotoxicity

associated with strontium content in the composition of bioactive glasses was reported by O'Donnell *et al*. (2010) after they observed that proliferation of human osteosarcoma cells cultured in media enriched with the dissolution products of a series of strontium-substituted bioactive glasses was reduced as the proportion of strontium substitution increased to 100%.

In the case of Fabbri *et al*. (2010), the amount of bioglass 45S5 particles in the scaffolds was increased, boosting the potential cytotoxicity of the material, while in this work the potential cytotoxicity of the materials was enlarged by increasing the amount of strontium present in the glass. In both situations no significant differences were observed between the controls (i.e. cell cultured on tissue culture plastic) and the samples containing glass particles.

Fabbri *et al*. (2010) also reported that cell proliferation on the samples was about 25% of the proliferation observed on tissue culture plastic and suggested that this may have been caused by the hydrophobicity and low wettability of PCL. It was also observed in this study that, before the sterilisation step by immersion in isopropyl alcohol, the electrospun PCL samples were highly hydrophobic. Results from the resazurin-dye based assays, which may also be used to measure cell proliferation, showed that there were no significant differences between the cells seeded on plastic and on the electrospun samples, suggesting that the increase in hydrophilicity due to immersion in isopropyl alcohol may have encouraged cell attachment.

Results from the study of the cytotoxic effect of the electrospun samples processed with the 'filtering' method suggested that the addition of 0.05 mg of glass particles on the surface of the electrospun fibres may not have a detrimental effect on cell viability (Figure 5.24b). Statistically significant differences were then observed (Figure 5.25) between the control (i.e. cells cultured directly on cell culture plastic without electrospun PCL and without bioactive glass particles) and the samples processed using suspensions of glass particles with concentrations of 0.25% w/v and 1.00% w/v, indicating that the addition of amounts over 0.05 mg of glass particles may have a detrimental effect on cellular viability. These results suggested that the

cytotoxic effect of the addition of bioactive glass particles on the surface of the electrospun fibres may be more influenced by the amount of glass added than by the content in strontium in the glass composition.

Isaac *et al*. (2011) tested the cytotoxic effect of strontium-substituted bioactive glass particles in direct contact with mouse osteoblastic cells at a concentration of 4 mg/ml, observing no significant differences in viability and metabolic activity after 72 hours between the samples and the control (i.e. cells cultured directly on cell culture plastic without bioactive glass particles) as the amount of strontium increased. The glass particles had been pre-incubated for 24 hours in cell culture medium prior to the experiments, a step similar to what was done to the electrospun materials after the glass particles were added to their surface. This may reduce the cytotoxic effect of the glasses as the initial dissolution and change in pH occurs during that period of time, before exposure to cells. Although this may be an interesting approach depending on the application for the material, reducing its potential detrimental effect, it is expected that a considerable proportion of the ionic content in the glass will be lost before their exposure to the cells and, consequently, the potential stimulatory effect may be diminished.

It is also possible that the potential cytotoxic effect of the bioactive glass dissolution may be dampened by the inclusion of the particles within the polymeric matrix. As the cells proliferate, they mainly attach to the surface of the fibres and, thus, may not be in direct contact with the glass particles. However, in the case of the samples with added bioactive glass particles on their surface, the cells will be in direct contact with the particles and may be more exposed to the effects of glass dissolution. This is expected to potentially induce a different cellular behaviour.

6.2.6 Conclusions from the fabrication, characterisation and cytotoxicity testing of electrospun composite material

The effect of polymer concentration, solvent composition and content of bioactive glass particles on the electrospinning process was studied in order to optimise the fabrication of electrospun materials with appropriate characteristics to fulfil the aim of this project. The solution of PCL which

generated electrospun materials presenting the lowest amount of observable defects and the most regular fibres was 10 wt% PCL dissolved in a blend of DCM and DMF mixed in a proportion 90:10 v/v. Bioactive glass particles with sizes <45 μm were then added to this solution following a 10:1 PCL:glass weight ratio prior to electrospinning, since this ratio produced materials with the smallest amount of observable defects.

The electrospun materials produced with this composition were composed of fibres (1.99 ± 0.36 μm mean diameter) exhibiting porous surfaces and regular morphologies. In the case of the composite materials, the bioactive glass particles were contained within certain regions of the fibres (i.e. 'filled regions') which presented an increased diameter (14.02 ± 7.67 μm mean diameter) and an irregular morphology. The polymeric surface on the 'filled regions' was also porous, increasing the surface area of the material and potentially facilitating water absorption, glass dissolution and the release of the ionic dissolution products to the environment.

Dissolution of bioactive glass particles from within the polymeric fibres and the release of the ionic dissolution products were confirmed by means of a study which showed a rapid initial increase of pH towards alkaline values, as expected to occur in bioactive glasses. In the case of the composite materials this initial increase was later reduced to values close to neutral levels faster than samples composed of bioactive glass powders only, suggesting a possible interaction between the polymer and the glass particles which may facilitate this effect. This reduction of pH may be associated to an accelerated degradation of PCL induced by the alkaline conditions created by the rapid glass dissolution, releasing acidic degradation products to the local environment and, thus, resulting in a reduction of pH. This effect may also be encouraged by a lower degree of crystallinity of the polymer caused by the electrospinning process and the presence of the glass particles within the matrix, potentially increasing its degradation rate. This may prove to be a useful approach to neutralise the possibly detrimental effect of glass dissolution on cells and tissues post-implantation.

Two methods to place bioactive glass particles on the surface of the electrospun fibres were also developed and studied. Although that both methods were successful, the 'filtering' method was demonstrated to be the most efficient, achieving efficiencies between 80% and 90% and allowing a finer control in the addition of glass particles than the 'loading' method. However, it was observed that the glass particles may not be firmly attached to the electrospun material and may detach with ease if they are not entrapped within the fibre mesh.

The electrospun materials generally presented good levels of *in vitro* biocompatibility. However, the addition of bioactive glass particles on the surface of the fibres generally increased the cytotoxic effect when amounts larger than 0.05 mg of glass particles were added. It is possible that the cytotoxic effect of these compositions may be more strongly influenced by the amount of glass particles used than by the level of strontium substitution.

6.3 Study of the osteogenic effect of strontium-substituted bioactive glass

6.3.1 Characterisation of rat MSCs by FACS analysis

Undifferentiated mesenchymal stromal cells (MSCs) were isolated from rat bone marrow and then pooled into one general population. The cells were cultured until passage 3 and then were characterised by evaluating the expression of several surface molecular markers using fluorescence-activated cell sorting (FACS) analysis. The results suggested that 29.2% of the parent population may be actual multipotent MSCs (Figure 5.27 and Table 5.12).

Rat MSCs express various molecular surface markers, including CD9, CD10, CD13, CD29, CD44, CD54, CD55, CD90, CD105, CD166, D7-FIB; and are negative for CD14, CD34, CD45 and CD133 (Pountos *et al*., 2007). However, only antibodies against three surface markers (i.e. CD90, CD44 and CD45) were initially selected to characterise the population due to cost concerns and because the aim of the study was to perform a general identification. CD90 is positively expressed in bone marrow MSCs of several

species and is one of the main surface molecular markers used in the identification of human MSCs as determined by the International Society of Cell Therapy (Boxall and Jones, 2012).

CD44 is also positively expressed in MSCs, although there is evidence that it may display irregular expression patterns depending on rat strain and passage (Barzilay *et al*., 2009). The levels of CD44 expression in rat bone marrow MSCs isolated from Wistar rats reported by Barzilay *et al*. were significantly lower (9.76%) than those measured in this study (26%). Kim *et al*. (2010) characterised passage 2 bone marrow MSCs isolated from Sprague Dawley rats, observing that CD44 was expressed at higher levels (74.24%) than those reported in this study and by Barzilay *et al*. Yue *et al*. (2008) characterised passage 3 MSCs obtained from Wistar rats and reported even higher levels of CD44 expression (98.2%). The high variability of CD44 in rat MSCs, as evidenced by all these studies, suggests that this may not be the most appropriate surface molecular marker for the identification of rat bone marrow MSCs. Boxall *et al*. (2012) also suggested that, as CD44 is expressed in different types of cells simultaneously in various tissues, its lack of specificity may limit its usefulness as a marker for MSCs. Both CD90 and CD44 surface molecular markers are expressed in MSCs and haematopoietic stem cells, but CD44 is also expressed in cells from the lymphoid, myeloid, megakaryotic, erythroid and endothelial lineages.

CD45 is a surface molecular marker which is expressed in haematopoietic stem cells and is absent on MSCs of multiple species, although it is known that in some cases rat bone marrow MSCs may express CD45 at levels below 5% (Barzilay *et al*., 2009; Boxall *et al*., 2012). The generally low levels of positive detection of CD45 observed in this study appear to agree with this and suggested that few haematopoietic stem cells were isolated together with the MSCs.

Based on the results of this study and the evidence found in the literature, it is concluded that alternative surface molecular markers to CD44 may provide more consistent results. For example, it is reported that CD105 is usually

expressed in rat MSCs, as well as in the myeloid and endothelial lineages, at levels between 50% and 100% (Boxall *et al*., 2012).

6.3.2 Effect of bioactive glass dissolution on cell viability

The observed reduction in MSCs viability (Figure 5.28) suggested that, in general, increasing the amount of bioactive glass powder used and the level of strontium substitution may result in significant increases of material cytotoxicity. This effect was particularly clear when the cells were exposed to the dissolution products of amounts of glass powders greater than 20 mg.

As previously discussed, this effect may be a consequence of the increase in glass solubility induced by the strontium substitution and its associated increase of environmental pH (O'Donnell *et al*., 2010). The study of the cytotoxicity of the electrospun materials suggested that the increased cytotoxic effect may have been mainly caused by the amount of glass particles placed on the surface of the fibres rather than by the increased solubility induced by the strontium content. However, the amounts of glass powders used in that study were considerably smaller than the amounts used here (i.e. 0.05 mg vs. 5 mg, smallest amounts used in each study). It is expected that larger amounts of glass powders will have a more severe effect on environmental pH, which may consequently make the differences caused by the various glass composition more evident. Additionally, although the bioactive glass compositions used in both studies were the same, it cannot be discarded that the presence of the polymer in the electrospun materials may have resulted in more favourable conditions for the cells. ROS cells were also cultured in direct contact with the particles, while in this case the MSCs were only exposed to the glass dissolution products. The process to add the particles on the surface of the electrospun fibres also required a step in cell culture medium for 24 hours, which resulted in the pre-incubation of the particles and a reduction of their potential impact, while in this study the glass particles were not pre-incubated. Finally, it is also possible that MSCs may react differently to the dissolution products of bioactive glass dissolution than ROS cells.

The apparently lower cytotoxicity of Sr50 bioactive glass (Figure 5.29) may be due to a stimulatory effect of that specific composition on MSCs. Isaac *et al*. (2011) reported a similar result when they assessed the viability of mouse osteoblastic cells exposed to strontium-substituted bioactive glasses. They observed that cell viability after 24 hours of direct exposition to particles of a glass with a 5 wt% strontium substitution was higher than in the control (i.e. cells cultured without bioactive glass), and than in cells exposed to other glass composition (i.e. 0 wt% and 1 wt% strontium). That amount of strontium in the glass was equivalent to 2.9 mol%, which is considerably lower than the 13.46 mol% used on Sr50 bioactive glass. However, it should be noted that the glasses used by Isaac *et al*. (2011) were pre-incubated, losing part of its content in strontium and diminishing their potential enhancing effect. It may be expected that a non-pre-incubated glass may take longer time to release their complete ionic content and may have a more prolonged effect, which is what was observed in Sr50 as the results here discussed were observed after 72 hours of exposition. Similarly, O'Donnell *et al*. (2010) reported higher levels of proliferation of human osteosarcoma cells in exposition to the dissolution products from a bioactive glass with a similar composition to Sr50, than in exposition to the dissolution products of an unmodified glass or a glass with a similar composition to Sr100. However, the composition that, according to O'Donnell *et al.* (2010), presented the highest levels of cell proliferation had a substitution of calcium by strontium of only 10%, suggesting that there may be a particular ratio in calcium and strontium content in the bioactive glass composition which may present the most enhancing effects.

Finally, an amount of 20 mg was selected to perform the study of the osteogenic effect of the glasses on MSCs, as this amount did not induce a statistically significant detrimental effect on MSCs in the case of Sr0 and Sr50 bioactive glasses, and it was the smallest amount that induced a significant detrimental effect in the case of Sr100.

6.3.3 Total RNA isolation from rat MSCs

The complete RNA content from MSCs cultured in monolayer and exposed to the dissolution products from 20 mg of Sr0, Sr50 and Sr100 bioactive glasses was isolated and measured (Figure 5.30).

The general increase in isolated total RNA observed from day 1 to day 14 may be associated with an increase in cell numbers due to proliferation. Although the generally lower amounts of total RNA isolated from the cells exposed to bioactive glass may be associated to the cytotoxic effect of glass dissolution, it was observed that the amount of RNA isolated at day 1 from all the samples treated with glass powders were similar to the control and then were lower than the control from day 3 onwards. As the glasses used in this study were not pre-incubated, it may be expected that the main cytotoxic effect will occur during the initial 24 hours. However, it is possible that the change in pH in the conditions used in this study may have longer term effects on the cells, slowing down cell proliferation rather than killing the cells. Additionally, the amounts of RNA obtained from the samples treated with the glass powders at day 14 increased as the substitution of calcium by strontium in the glass increased. This suggested that the presence of the strontium-substituted glass may have had a stimulatory effect on the MSCs rather than a deleterious effect.

In the case of the samples cultured in osteogenic medium conditions, the increase of total RNA isolated from MSCs from day 1 to day 6 may also be associated with cell proliferation. Also, the samples treated with bioactive glasses generally produced lower amounts of RNA than the control samples, cultured without any glass. In general, the samples appeared to show a different pattern to what was observed in the samples cultured in standard cell culture medium. The total amount of RNA obtained from the control samples at day 14 was generally lower than at day 6, suggesting that a particular change occurred to the cells between those two time points, slowing down their proliferation and even decreasing their numbers. Additionally, these results did not suggest a stimulatory effect of strontium on the proliferation of MSCs, as the amount of RNA obtained at day 14 in the

samples treated with Sr100 was lower than in the samples treated with Sr50. Finally, the samples treated with Sr0 at day 14 had reduced significantly in cell number and did not produce enough RNA.

Huang *et al*. (2007) suggested that three stages can be observed in the growth of osteoprogenitor cells *in vitro*. Cell proliferation occurs mainly from day 1 to day 4 of exposition to osteogenic cell culture medium. Early differentiation into osteoblasts then occurs from day 5 to day 14, followed by terminal differentiation and maturation of bone matrix from day 15 to day 28. They reported an increase of isolated DNA from murine MSCs during the first 4 days of culture followed by a gradual reduction until day 28. Although it may be difficult to determine a direct relationship between isolated RNA and cell numbers in a similar manner, the increase of isolated RNA in the control samples cultured in osteogenic cell culture medium between day 1 and 6 may suggest the occurrence of the proliferation stage as defined by Huang *et al*. (2007), and the decrease observed at day 14 may then be associated with the early differentiation stage. It is possible that the presence of both the osteogenic cell culture medium and the dissolution products of bioactive glasses may have affected the pattern of growth in osteoprogenitor cells, potentially inducing their differentiation.

6.3.4 Analysis of RT-qPCR data

Abundant research work has been published about the stimulatory effect of bioactive glasses on bone formation using various biological indicators of osteogenesis, demonstrating that there is a growing body of evidence supporting their potential use in bone regeneration applications.

Xynos *et al*. (2000a) reported higher levels of alkaline phosphatase activity and osteocalcin synthesis on human osteoblasts cultured directly on discs of 45S5 bioglass, suggesting that the ionic dissolution products released by the material may be able to influence cell cycle and control the differentiated cell population. Cells that were not capable of achieving a completely differentiated osteocyte phenotype were eliminated by apoptosis. The shift in cell population observed by Xynos *et al*. (2000a) toward mature osteoblasts occurred in a few hours and led to the formation of mineralised bone nodules

without the addition of bone growth factors. Xynos *et al.* (2000b) also reported a significant increase in the production of insulin-like growth factor II (IGF-II) by human osteoblasts after their exposure to dissolution products of 45S5 bioglass. IGF-II is a potent growth factor, very abundant in bone, which induces osteoblast proliferation. Therefore, it was suggested that the stimulatory effect of bioactive glass dissolution products on osteoblast proliferation may have been mediated by IGF-II. Later work by Xynos *et al*. (2001) also led to the discovery that critical concentrations of soluble silica and calcium cations were able to activate or up-regulate seven families of genes in human osteoblasts involved in proliferation and differentiation. Various studies have been performed investigating this topic, as reviewed by Hench (2009), confirming the results of Xynos *et al*. (2001) in cells from several sources (i.e. embryonic stem cells, foetal cells and adult primary cells).

Regarding the study of the osteogenic effect on rat MSCs, Radin *et al*. (2005) reported that the presence of 45S5 bioglass resulted in increased levels of alkaline phosphatase activity cultured both in direct contact with the samples and apart from them, suggesting that the glasses had a stimulatory effect on the osteoblastic differentiation of the cells. Yao *et al.* (2005) also reported an increased expression of alkaline phosphatase, osteocalcin and bone sialoprotein in RNA extracted from rat MSCs exposed to the dissolution products released from poly(lactide-co-glycolide) microspheres containing 45S5 bioglass particles. Reilly *et al.* (2007) compared the effect of bioactive glasses on both human and rat MSCs, and reported that human MSCs generally produced significantly lower levels of alkaline phosphatase activity than rat MSCs when exposed to bioactive glasses. No differences were observed in human MSCs cultured in 45S5 bioglass and cell culture plastic and no consistent effects were observed in response to bioactive glass dissolution, suggesting that the beneficial effects of bioactive glass on bone regeneration may not be mediated by an accelerated differentiation of MSCs. Alkaline phosphatase activity was also reported by Gentleman *et al*. (2010), observing that it increased in a human osteosarcoma cell line in response to their exposition to strontium-substituted bioactive glasses.

The differentiation of MSCs into osteoblasts is initially characterised by the expression of different osteospecific genes. The genes selected for this study were: runt-related transcription factor 2 gene (*Runx2*), alkaline phosphatase gene (*Alpl*), Type I collagen gene (*Col1a1*), bone gamma-carboxyglutamate (gla) protein gene (*Bglap*), secreted phosphoprotein 1 gene (*Spp1*) and bone morphogenetic protein 2 gene (*Bmp2*). Alkaline phosphatase activity has usually been considered as one the early markers of osteogenesis and was one of the first to be identified. *Runx2* has been identified as the major transcription factor controlling osteoblast commitment and differentiation, being expressed by MSCs at the onset of skeletal development and by osteoblasts during their differentiation. It regulates the expression of other genes such as *Col1a1*, *Spp1* and *Bglap*. Finally, *Bmp2* promotes *Runx2* expression in mesenchymal osteoprogenitor and osteoblastic cells. (Marie, 2008). Therefore, it is possible to establish the sequence of genetic events in which these genes are involved during the osteoblast differentiation of MSCs, as shown in Figure 6.2.

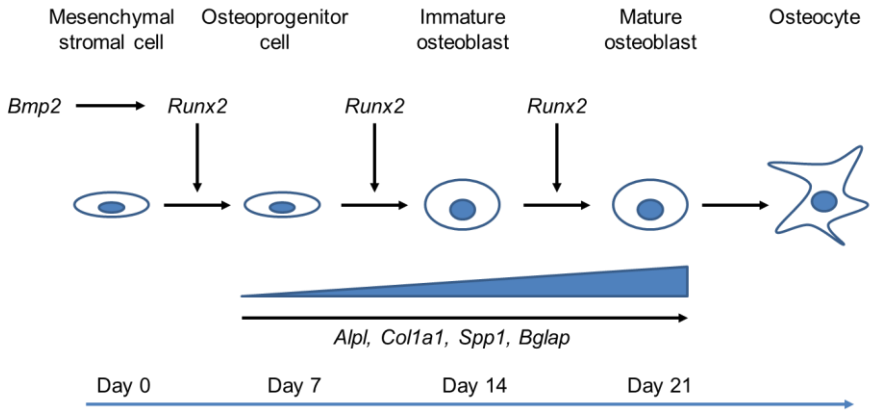

Figure 6.2. Schematic diagram representing the sequence of genetic events in the osteoblast differentiation of mesenchymal stromal cells, involving the genes *Bmp2*, *Runx2*, *Alpl*, *Col1a1*, *Spp1* and *Bglap*. Adapted from Marie (2008) and Safadi *et al*. (2009).

Results from the real-time quantitative PCR analyses (Figure 5.31 to Figure 5.36) suggested that the dissolution of bioactive glass particles stimulated the up-regulation of six genes involved in the osteogenic differentiation of MSCs. The expression of *Bmp2* increased in the presence of bioactive glass from day 1 in both standard cell culture medium and osteogenic cell culture medium conditions, suggesting that the presence of bioactive glass and the

ionic dissolution products stimulated the sequence of events shown above from the beginning point. The expression of *Runx2* was also up-regulated from day 1 in both media conditions, increasing gradually until it peaked at day 6. This occurred as expected for this gene if the process of osteoblast differentiation had already started, suggesting that the gene was stimulated due to the higher expression of *Bmp2*.

The study of *Alpl*, *Col1a1*, *Spp1* and *Bglap* showed that the expression of these genes was up-regulated from day 1 and generally increased their levels of expression with time, as expected to occur. However, there were differences between the two media conditions. The results suggested that the presence of both the osteogenic factors and the bioactive glasses had a more pronounced effect on the expression than the glasses on their own. *Alpl*, *Col1a1* and *Bglap* peaked at an earlier time point in osteogenic medium, and *Spp1* showed more consistently higher levels of expression from day 1. The general decline observed in all genes at day 14 may be due to the lower concentrations of the cations in dissolution as the glass powders were depleted after several cycles of media change. Although the addition of new bioactive glass particles to the samples may have resulted in generally higher levels of expression and it may be an interesting study to perform, it was considered that this experimental arrangement was appropriate as it was more similar to the potential conditions *in vivo*. It would not be generally feasible to introduce fresh bioactive glass to a scaffold after implantation *in vivo*.

These results also suggested that the strontium-substituted glasses may not always have a clear enhancing effect over the stimulation already induced by the unmodified glass. Statistically significant differences between Sr0 and Sr50 or between Sr0 and Sr100 bioactive glasses were observed for all the genes at different time points in both cell culture medium conditions, with the largest number of significant differences observed for Sr0 vs. Sr100. Although this may imply a potential stimulatory effect of strontium, the results were not consistent throughout the whole study and it is difficult to draw clear conclusions from this. The greatest stimulating effect of strontium appeared to be on *Col1a1, Alpl* and *Bglap* genes, while in other cases the levels of

expression were similar for the three glasses or, even, Sr0 was more stimulating than Sr50 or Sr100.

Isaac *et al*. (2011) reported the up-regulation of various osteoblast genetic markers in foetal calvarial bone cells exposed to strontium-substituted bioactive glasses fabricated through the sol-gel route, some of which were the same as those analysed in this study. The expression of genes related to extracellular bone matrix proteins (i.e. *Col1a1*, *Alpl*, *Bglap*) and osteoblastic transcription factors (i.e. *Runx2*) were observed to increase in both studies, suggesting a stimulatory effect of the bioactive glasses. Additionally, *Col1a1*, *Alpl* and *Bglap* showed a clearer up-regulation in the case of samples exposed to bioactive glass compositions with greater proportions of strontium substitution. However, there are significant differences between the work of Isaac *et al*. (2011) and this study that need to be discussed, as they may have a considerable impact in the results. Issac *et al*. (2011) used osteoblastic cells obtained from calvarial bones of mouse foetuses, which were cultured in osteogenic cell culture medium from the time of isolation. It is reasonable to presume that the pattern of genetic expression in response to external stimuli may not be the same in undifferentiated primary cells isolated from adult animals than in differentiated osteoblasts obtained from foetuses. Furthermore, the particles of strontium-substituted bioactive glass used were pre-incubated, a step which may potentially reduce its effect on the cells compared with non-pre-incubated particles. As previously discussed, pre-incubation of bioactive glasses may be used to reduce their potential cytotoxicity as the initial dissolution and change in pH will occur before exposure to cells. Additionally, pre-incubation in fully supplemented cell culture medium will result in the adsorption of proteins on the glass surface, forming a layer which is important to allow adequate cell attachment, proliferation and differentiation on the material. This was an understandable step in the case of Isaac *et al.* (2011), as the cells were cultured in direct contact with the glass particles. However, in this study the cells were exposed to the dissolution products and this step was not considered as required. The substitution of calcium by strontium in the glasses used by Isaac *et al.* (2011) was also performed on a weight basis rather than on a

molar basis, which may have resulted in reduced glass solubility and bioactivity.

More recently, Zhang *et al.* (2013) investigated the effect of the dissolution products of strontium-incorporated mesoporous bioactive glass scaffolds on the differentiation of rat bone marrow MSCs. The cell culture medium used was similar to one of the culture conditions in this study, which did not include any osteogenic factors such as ascorbic acid. The expression of *Runx2*, *Alpl*, *Bglap* and *Col1a1* genes was up-regulated in comparison with the control samples, which were MSCs exposed to the dissolution products of bioactive glass with no strontium. Additionally, the expression of *Runx2*, *Bglap* and *Col1a1* increased from day 7 to day 14, while the levels of *Alpl* decreased. In the study discussed in this report it was observed that the expression of these genes in standard cell culture conditions peaked at day 6 and decreased by day 14. However, as previously mentioned, the content of strontium in the media was not regularly replenished, so it may be expected to observe a reduced effect. Finally, the presence of strontium resulted in greater expression levels in *Alpl*, *Col1a1* and *Bglap*, but not in *Runx2*.

In conclusion, results from this study suggested an enhancing effect of strontium cations released by the dissolution of bioactive glasses on the expression of *Alpl*, *Col1a1* and *Bglap* genes. This is supported by results reported by Isaac *et al.* (2011) and Zhang *et al*. (2013), and may result in the stimulation of the differentiation of rat bone marrow MSCs into osteoblasts. The response of human MSCs should also be investigated, since it has been shown that bioactive glasses may have a decreased effect compared to rat MSCs (Reilly *et al.*, 2007).

Interestingly, when the expression levels in the osteogenic cell culture medium conditions were represented in relation to the expression levels in the control samples in the standard cell culture medium conditions (Figure 5.37, Figure 5.38 and Figure 5.39), two distinct patterns of expression could be identified: firstly, the expression of *Runx2, Alpl*, *Bglap* and *Bmp2* gradually increased through time, peaking at day 14; and secondly, *Col1a1* and *Spp1* presented two peaks of expression, at day 1 and 6. This may potentially be

associated with the time sequence of gene expression in the process of osteoblast differentiation and with the way in which the proteins derived from the genes are used by the cell.

Finally, it is significant to consider that, although the measurement of the variation of mRNA expression is an important indicator of cell differentiation, this is not the definitive approach to show how the process is operating. For example, a study of the osteoblast differentiation of human MSCs by Foster *et al*. (2005) did not show any clear concordance between the changes in the levels of gene expression and protein expression, except for alkaline phosphatase. Therefore, it may be recommendable to combine the mRNA isolation and analysis with proteomic techniques that may help to develop a clearer image of the mechanisms of cellular response to bioactive glass.

6.3.5 Conclusions from the study of osteogenic effect of strontium-substituted bioactive glass

The population of rat MSCs used in the study was first characterised by detecting the expression of molecular surface markers CD44, CD45 and CD90 using FACS analysis. The results suggested that 29.2% of the whole population of cells were actual multipotent MSCs, expressing both CD44 and CD90, and not expressing CD45. However, a literature survey showed that CD44 may not be the most appropriate marker as it has shown varying levels of expression in different experiments and is expressed in several other cell types. Therefore, it was recommended to select an alternative surface molecular marker in the identification of a population of rat MSCs.

The cytotoxicity of the dissolution of Sr0, Sr50 and Sr100 bioactive glasses on MSCs generally increased with the amount of glass powder used and with the proportion of strontium substitution in the glass composition, potentially due to a more severe effect on pH variation caused by the increased solubility of the glasses. However, Sr50 bioactive glass showed a less marked cytotoxic effect than Sr0 bioactive glass, suggesting a potential stimulatory effect of strontium on the MSCs that may be sufficient to neutralise the detrimental effect caused by the increased solubility of the glass.

Six genes associated with the process of osteoblastic differentiation of MSCs were up-regulated in response to the dissolution of Sr0, Sr50 and Sr100 bioactive glass powders, both in standard cell culture medium and osteogenic cell culture medium conditions. The level of expression of the genes generally increased with time, displaying different patterns depending on the time sequence of gene expression in the process of osteoblastic differentiation. The final decrease observed at day 14 may be due to a severely reduced concentration of the cations in dissolution due to the depletion of the glasses after several cycles of media change.

The strontium-substituted bioactive glasses generally stimulated gene expression up to levels similar to the unmodified glass. Greater stimulation was only observed at some time points and for some genes, mainly *Col1a1, Alpl* and *Bglap*. The results were not consistent throughout the whole study and, therefore, no definitive conclusions may be drawn on the reportedly superior ability of strontium-substituted bioactive glasses to enhance new bone formation compared with the unmodified parent compositions at this moment.

In conclusion, the results suggested that the particles of non-pre-incubated bioactive glass are able to stimulate the osteoblast differentiation of MSCs by up-regulating the expression of genes involved in the differentiation process, implying their potential to promote bone tissue formation and to be used as part of a novel electrospun composite material in bone tissue engineering applications.

7 Conclusions

The aim of this project was to design and fabricate an electrospun composite material combining PCL and particles of strontium-substituted bioactive glass and to evaluate its potential use as a scaffold for bone tissue engineering. To fulfil this purpose a series of objectives were established (See Aim and objectives) and a full programme of experimental work was planned and performed.

The conclusions of that work are as follow:

1) Three bioactive glass compositions, in which calcium was substituted by strontium in proportions of 0, 50 and 100% on a molar basis, were successfully fabricated. The characterisation of the bioactive glasses demonstrated that the strontium substitution had a well-defined effect on several material properties. These variations affect the way the glass works as a component of a composite material and the interactions of the composite material with cells and tissues *in vitro* and, potentially, *in vivo*. Increasing the content of strontium in the glass composition resulted in:
    a. An expansion of the glass network due to the larger strontium cation, which was observed as a progressive movement of the broad peak in the XRD spectra toward smaller values of angle 2θ.
    b. A reduction in glass transition temperature due to the expansion and weakening of the glass network, resulting in an increase of the working range of the glasses. This suggested a potential use of strontium-substituted glasses in applications that require the shaping and sintering of the glasses through a viscous flow process and where the unmodified glasses are not adequate due to crystallisation.
    c. A linear increase of glass density due to the greater mass of the strontium cation, and a linear decrease of oxygen density due to the expanded and less rigidly bonded glass network in the modified glasses.

   d. A linear increase of glass solubility due to the expansion of the glass network, potentially increasing glass bioactivity.

2) Glass dissolution began on the surface of the material, as demonstrated through SEM and EDS studies, resulting in compositional changes in agreement with what is expected from bioactive glasses.
3) Electrospun composite materials made of PCL and particles of strontium-substituted bioactive glass were successfully fabricated. The solution of 10 wt% PCL dissolved in a blend of DCM and DMF with ratio 90:10 v/v and with glass particles added following a 10:1 PCL:glass weight ratio produced the most regular fibres and the smallest amount of detectable defects in the electrospun materials. The composite fibres exhibited regions with irregular morphologies and expanded diameters where the bioactive glass particles were incorporated within the polymeric fibres, as demonstrated by EDS analysis. The surface of the fibres was porous, suggesting an increased surface area and, consequently, an improved capability to absorb water and to release the ionic dissolution products to the environment.
4) The dissolution of the bioactive glass particles and the subsequent release of their ionic dissolution products occurred rapidly after immersion in aqueous media, as demonstrated by rapid increases in environmental pH.
5) Interactions between PCL and bioactive glass particles in the composite materials may occur as a consequence of glass dissolution, resulting in a faster stabilisation of environmental pH around neutral values. A potential mechanism for this effect may be associated with an accelerated degradation of PCL due to the severe alkalinisation created by the dissolution of the bioactive glass particles and the subsequent release of the acidic degradation products. It is suggested that this effect may be used to regulate the initial increase of pH induced by glass dissolution, which may be harmful to cells and tissues after implantation.

6) Two methods to add bioactive glass particles on the surface of the electrospun fibres were developed and tested. The 'filtering method' proved to be the most effective, achieving efficiencies between 80% and 90% when using suspensions of glass particles of concentration 0.25% w/v and higher.
7) The electrospun composite materials generally presented good levels of *in vitro* biocompatibility, comparable to materials made of only electrospun PCL. However, the addition of more than 0.05 mg of additional surface bioactive glass particles using the 'filtering method' resulted in a significant increase of material cytotoxicity.
8) The dissolution of strontium-substituted bioactive glass powders exhibited a cytotoxic effect on rat MSCs. Amounts larger than 20 mg were considered as cytotoxic, inducing a significantly negative effect on cell viability. Sr50 was the least cytotoxic bioactive glass composition, possibly caused by the potentially stimulatory effect of MSCs by strontium which balanced the detrimental effect of the increased glass solubility. This also suggested that bioactive glass compositions containing both calcium and strontium may be more effective stimulating osteoprogenitor cells than glasses containing only calcium or strontium.
9) The dissolution of strontium-substituted bioactive glass particles resulted in the up-regulation of six genes associated with the process of osteoblastic differentiation of rat MSCs in both standard and osteogenic cell culture medium conditions, suggesting a stimulatory effect of strontium in the differentiation process and in the formation of new bone tissue. This also implied the potential of these glass compositions to be used as part of composite materials for bone tissue regeneration.
10) Strontium-substituted bioactive glasses generally stimulated gene expression at levels which were similar to those stimulated by the unmodified glass composition. In some cases (i.e. *Col1a1, Alpl* and *Bglap* genes) significantly higher levels of expression were observed. However, it is not possible to draw definitive conclusions about the

enhancing effect of strontium at this point as the results were not consistent throughout the whole study.

To summarise, electrospun composite materials made of PCL and particles of strontium-substituted bioactive glass were successfully designed and fabricated, exhibiting good *in vitro* biocompatibility and the release of glass dissolution products to the surrounding environment. The observed stimulatory effect of strontium-substituted bioactive glass dissolution on MSCs showed that these glasses are promising materials for bone tissue regeneration applications, potentially encouraging the formation of new bone tissue. Hence, the potential of the electrospun composite materials to be used as scaffolds in bone tissue engineering applications was confirmed.

8 Further work

The data presented in this report have demonstrated the potential of electrospun composite materials made of PCL and strontium-substituted bioactive glass to be used as scaffolds in bone tissue engineering. However, additional work needs to be done to expand our knowledge regarding the manufacturing process, the properties of the materials and the response of cells and tissues.

The following research activities are suggested as a continuation of the work presented in this thesis:

1) The manufacturing of the electrospun materials may be further improved by controlling important environmental parameters such as the temperature and the atmospheric humidity at which the process is performed. Noteworthy differences were sometimes observed as the temperature in the laboratory varied between seasons, and although it was possible to keep the temperature in the laboratory relatively constant using central heating and air conditioning, it did not allow for a fine control. This may be achieved by designing a special chamber which isolates the syringe and collecting plate from the external environment and which possesses systems that regulate these parameters within the enclosed space. It is expected that this work may require considerable effort and repeating the optimisation study of the electrospinning parameters will be necessary.
2) Based on reports by O'Donnell *et al.* (2010), a bioactive glass composition exhibiting a 10% substitution of calcium by strontium (i.e. 46.13 mol% SiO_2 – 24.35 mol% Na_2O – 24.22 mol% CaO – 2.69 mol% SrO – 2.60 mol% P_2O_5) presented the highest levels of cell proliferation after human osteosarcoma cells were exposed to their dissolution products. It would be interesting to study the cytotoxic and osteogenic effect of this glass composition on MSCs, as a previous step considering its inclusion in the electrospun composite materials.
3) The solubility studies of electrospun composite materials may be repeated under different experimental conditions to study the potential

interaction between the bioactive glass particles and the polymer. The samples may be immersed in simulated body fluids to expose them to a medium more similar to physiological conditions. The content of bioactive glass particles in the samples may also be increased to observe if it results in larger variations of pH and to study how the composite materials respond. The release of ions in dissolution over time may be studied using techniques such as inductively coupled plasma optical emission spectroscopy.

4) The 'filtering' method to add glass particles on the surface of the electrospun samples may benefit from further optimisation to increase particle attachment to the fibres. For example, this may be achieved by modifying the polymeric surface using plasma treatment. This would induce the creation of carboxyl groups on the surface of PCL, leading to increased hydrophilicity and the potential formation of electrostatic bonds with cationic groups on the particles of bioactive glass (i.e. Ca^{2+}, Sr^{2+}).
5) The growth of HA crystals on the electrospun samples may be studied by immersion in simulated body fluids over a period of several weeks, to observe its effect in the structure of the material, its degradation and its cytotoxicity.
6) The concentrations of the ions released in the dissolution of the bioactive glass powders used in the study of MSCs viability could be measured. Then, solutions of cell culture medium containing those concentrations could be prepared and tested on the cells in order to see if they would induce a similar cytotoxic effect.
7) The study of the effect of strontium-substituted bioactive glass on the osteoblastic differentiation of MSCs may be repeated to see if the results are similar to what has already been reported. Additionally, it would be interesting to extract the protein content from the cells to establish if the gene up-regulation can be linked to an increased synthesis of the associated proteins and enzymes.
8) Finally, MSCs may be cultured directly on samples of the electrospun composite materials over a period of several weeks to study cellular differentiation and the production of extracellular matrix using diverse

biochemical and histological methods. For example, an alkaline phosphatase assay may be used to measure its activity in the samples and alizarin red staining may be used to assess calcium deposition.

9 References

Azevedo, H.S., Reis, R.L. (2004) Understanding the enzymatic degradation of biodegradable polymers and strategies to control their degradation rate. In: R.L. Reis, J. San Roman (eds). *Biodegradable systems in tissue engineering and regenerative medicine*. Boca Raton, CRC Press. 177-201.

Baiguera, S., Jungebluth, P., Burns, A., Mavilia, C., Haag, J., De Coppi, P., Macchiriani, P. (2010) Tissue engineered human tracheas for in vivo implantation. *Biomaterials*, 31(34), 8931-8938.

Baji, A., Mai, Y.W., Wong, S.C., Abtahi, M., Chen, P. (2010) Electrospinning of polymer nanofibers: Effects on oriented morphology, structures and tensile properties. *Composites Science and Technology*, 70(5), 703-718.

Barone, D.T.J., Raquez, J.M., Dubois, P. (2010) Bone-guided regeneration: from inert biomaterials to bioactive polymer (nano) composites. *Polymers for Advanced Technologies*, 22(5), 463-475.

Barzilay, R., Sadan, O., Melamed, E., Offen, D. (2009) Comparative characterization of bone marrow-derived mesenchymal stromal cells from four different rat strains. *Cytotherapy*, 11(4), 435-442.

Beranova, M., Wasserbauer, R., Vancurova, D., Stifter, M., Ocenaskova, J. & Mara, M. (1990) effect of cytochrome-p-450 inhibition and stimulation on intensity of polyethylene degradation in microsomal fraction of mouse and rat livers. *Biomaterials*, 11(7), 521-524.

Boccaccini, A.R., Maquet, V. (2003) Bioresorbable and bioactive polymer/Bioglass® composites with tailored pore structure for tissue engineering applications. *Composites Science and Technology*, 63(16), 2417-2429.

Bognitzki, M., Czado, W., Frese, T., Schaper, A., Hellwig, M., Steinhart, M., Greiner, A., Wendorff, J.H. (2001). Nanostructured fibers via electrospinning. *Advanced Materials*, 13(1), 70-72.

Bohner, M. (2010) Resorbable biomaterials as bone graft substitutes. *Materials Today*, 13(1-2), 24-30.

Bonfield, W. (1988). Hydroxyapatite-reinforced polyethylene as an analogous material for bone replacement. *Annals of the New York Academy of Sciences*, 523, 173-177.

Bosetti, M., Cannas, M. (2005). The effect of bioactive glasses on bone marrow stromal cells differentiation. *Biomaterials*, 26(18), 3873-3879.

Boskey, A.L. (2005). The organic and inorganic matrices. In: J.O. Hollinger, B.A. Doll, C. Sfeir (eds). *Bone tissue engineering*. Boca Raton, CRC Press. 92-113.

Bottino, M.C., Thomas, V., Janowski, G.M. (2011). A novel spatially designed and functionally graded electrospun membrane for periodontal regeneration. *Acta Biomaterialia*, 7(1), 216-224.

Boxall, S.A., Jones, E. (2012) Markers for characterization of bone marrow multipotential stromal cells. *Stem Cells International* [online], Article ID 975871, DOI:10.1155/2012/975871. Available at: <http://www.hindawi.com/journals/sci/2012/975871/> [Accessed 20 August 2013]

Bueno, E.M., Glowacki, J. (2011) Biologic foundations for skeletal tissue engineering. In: K.A. Athanasiou (ed). *Synthesis lectures on tissue engineering*. San Rafael, Morgan & Claypool. DOI:10.2200/S00329ED1V01Y201101TIS007.

Burr, D.B. (2002) Targeted and nontargeted remodeling. *Bone*, 30(1), 2-4.

Chakrapani, V.Y., Gnanamani, A., Giridev, V.R., Madhusoothanan, M., Sekaran, G. (2012) Electrospinning of type I collagen and PCL nanofibers using acetic acid. *Journal of Applied Polymer Science*, 125(4), 3221-3227.

Chan, B.P., Leong, K.W. (2008) Scaffolding in tissue engineering: general approaches and tissue-specific considerations. *European Spine Journal*, 17(Suppl 4), 467-479.

Cipitria, A., Skelton, A., Dargaville, T.R., Dalton, P.D., Hutmacher, D.W. (2011) Design, fabrication and characterization of PCL electrospun scaffolds-a review. *Journal of Materials Chemistry*, 21(26), 9419-9453.

Clupper, D.C., Hench, L.L. (2003) Crystallization kinetics of tape cast bioactive glass 45S5. *Journal of Non-Crystalline Solids*, 318(1-2), 43-48.

Currey, J. (2009) Measurement of the Mechanical Properties of Bone: A Recent History. *Clinical Orthopaedics and Related Research*, 467(8), 1948-1954.

De Aza, P.N., De Aza, A.H., Pena, P., De Aza, S. (2007) Bioactive glasses and glass-ceramics. *Boletin de la Sociedad Española de Ceramica y Vidrio*, 46(2), 45-55.

Desai, K., Kit, K., Li, J., Zivanovic, S. (2008) Morphological and surface properties of electrospun chitosan nanofibers. *Biomacromolecules*, 9(3), 1000-1006.

Dinarvand, P., Seyedjafari, E., Shaifee, A., Jandaghi, A.B., Doostmohammadi, A., Fathi, M.H., Farhadian, S., Soleimani, M. (2011) New approach to bone tissue engineering: simultaneous applications of hydroxyapatite and bioactive glass coated on a poly(L-lactic acid) scaffold. *ACS Applied Materials & Interfaces*, 3(11), 4518-24.

Discher, D.E., Janmey, P., Wang, Y.L. (2005) Tissue cells feel and respond to the stiffness of their substrate. *Science*, 310(5751), 1139-1143.

Dong, Z.X., Kennedy, S.J., Wu, Y.Q. (2011) Electrospinning materials for energy-related applications and devices. *Journal of Power Sources*, 196(11), 4886-4904.

Doshi, J., Reneker, D.H. (1995) Electrospinning process and applications of electrospun fibers. *Journal of Electrostatics*, 35(2-3), 151-160.

Doweidar, H. (1996) The density of alkali silicate glasses in relation to the microstructure. *Journal of Non-Crystalline Solids*, 194(1-2), 155-162.

Doweidar, H. (1999) Density-structure correlations in silicate glasses. *Journal of Non-Crystalline Solids*, 249(2-3), 194-200.

Du, J.C., Xiang, Y. (2012) Effect of strontium substitution on the structure, ionic diffusion and dynamic properties of 45S5 Bioactive glasses. *Journal of Non-Crystalline Solids*, 358(8), 1059-1071.

Ducheyne, P., Qiu, Q. (1999) Bioactive ceramics: the effect of surface reactivity on bone formation and bone cell function. *Biomaterials*, 20(23-24), 2287-2303.

Eden, M., (2011) The split network analysis for exploring composition-structure correlations in multi-component glasses: 1. Rationalizing bioactivity-composition trends of bioglasses. *Journal of Non-Crystalline Solids*, 357(6-7), 1595-1602.

El-Ghannam, A., Ducheyne, P., Shapiro, I.M. (1999) Effect of serum proteins on osteoblast adhesion to surface-modified bioactive glass and hydroxyapatite. *Journal of Orthopaedic Research*, 17(3), 340-345.

Elgayar, I., Aliev, A.E., Boccaccini, A.R., Hill, R.G. (2005) Structural analysis of bioactive glasses. *Journal of Non-Crystalline Solids*, 351(2), 173-183.

Engler, A.J., Sen, S., Sweeney, H.L., Discher, D.E. (2006) matrix elasticity directs stem cell lineage specification. *Cell*, 126(4), 677-689.

Fabbri, P., Cannillo, V., Sola, A., Dorigato, A., Chiellini, F. (2010) Highly porous poly(caprolactone)-45S5 Bioglass (R) scaffolds for bone tissue engineering. *Composites Science and Technology*, 70(13), 1869-1878.

Finkemeier, C.G. (2002) Bone-grafting and bone-graft substitutes. *The Journal of Bone and Joint Surgery*. 84A(3), 454-464.

Foster, L.J., Zeemann, P.A., Li, C., Mann, M., Jensen, O.N., Kassem, M. (2005) Differential expression profiling of membrane proteins by quantitative proteomics in a human mesenchymal stem cell line undergoing osteoblast differentiation. *Stem Cells*, 23(9), 1367-1377.

Fredholm, Y.C., Karpukhina, N., Law, R.V., Hill, R.G. (2010) Strontium containing bioactive glass: glass structure and physical properties. *Journal of Non-Crystalline Solids*, 356(44-49), 2546-2551.

Fredholm, Y.C., Karpukhina, N., Brauer, D.S., Jones, J.R., Law, R.V., Hill, R.G. (2012) Influence of strontium for calcium substitution in bioactive

glasses on degradation, ion release and apatite formation. *Journal of the Royal Society Interface*, 9(70), 880-889.

Fujihara, K., Kotaki, M., Ramakrishna, S. (2005) Guided bone regeneration membrane made of poly(caprolactone)/calcium carbonate composite nano-fibers. *Biomaterials*, 26(19), 4139-4147.

Gao, C.X., Gao, Q., Li, Y.D., Rahaman, M.N., Teramoto, A., Abe, K. (2013) In Vitro Evaluation of Electrospun Gelatin-Bioactive Glass Hybrid Scaffolds for Bone Regeneration. *Journal of Applied Polymer Science*, 127(4), 2588-2599.

Gauthier, O., Bouler, J.M., Aguado, E., Pilet, P., Daculsi, G. (1998) Macroporous biphasic calcium phosphate ceramics: influence of macropore diameter and macroporosity percentage on bone ingrowth. *Biomaterials*, 19(1-3), 133-139.

Gentleman, E., Fredholm, Y.C., Jell, G., Loftibakhshaiesh, N., O'Donnell, M.D., Hill, R.G., Stevens, M.M. (2010) The effects of strontium-substituted bioactive glasses on osteoblasts and osteoclasts *in vitro*. *Biomaterials*, 31(14), 3949-3956.

Goh, Y.F., Shakir, I., Hussain, R. (2013) Electrospun fibers for tissue engineering, drug delivery, and wound dressing. *Journal of Materials Science*, 48(8), 3027-3054.

Gopferich, A. (1996) Mechanisms of polymer degradation and erosion. *Biomaterials*, 17(2), 103-114.

Gorustovich, A.A., Steimetz, T., Cabrini, R.L., Lopez, J.M.P. (2010) Osteoconductivity of strontium-doped bioactive glass particles: A histomorphometric study in rats. *Journal of Biomedical Materials Research Part A*, 92A(1), 232-237.

Hartman, O., Zhang, C., Adams, E.L., Farach-Carson, M.C., Petrelli, N.J., Chase, B.D., Rabolt, J.E. (2010) Biofunctionalization of electrospun PCL-based scaffolds with perlecan domain IV peptide to create a 3-D pharmacokinetic cancer model. *Biomaterials*, 31(21), 5700-5718.

Hass, R., Kasper, C., Bohm, S., Jacobs, R. (2011) Different populations and sources of human mesenchymal stem cells (MSC): A comparison of adult and neonatal tissue-derived MSC. *Cell Communication and Signaling*, 9,12.

Hench, L.L. (1998) Bioceramics. *Journal of the American Ceramic Society*, 81(7), 1705-1728.

Hench, L.L (2006) The story of Bioglass®. *Journal of Materials Science – Materials in Medicine*, 17(11), 967-978.

Hench, L.L. (2009) Genetic design of bioactive glass. *Journal of the European Ceramic Society*, 29(7), 1257-1265.

Hench, L.L., Andersson, O. (1993) Bioactive Glasses. In: Hench, L.L., Wilson, J. (eds). *An Introduction to Bioceramics*. Singapore, World Scientific, 41-62.

Hench, L.L., Best, S.M. (2013) Ceramics, glasses and glass-ceramics: basic principles. In: B.D. Ratner, A.S. Hoffman, F.J. Schoen, J.E. Lemons (eds). *Biomaterials science: An introduction to materials in medicine*. London, Elsevier Science and Technology Books, 128-165.

Hench, L.L., Polak, J.M. (2002) Third-generation biomedical materials. *Science*, 295(5557), 1014-1017.

Hench, L.L., Thompson, I. (2010) Twenty-first century challenges for biomaterials. *Journal of the Royal Society Interface*, 7, S379-S391.

Hench, L.L., Wilson, J. (1984) Surface-active biomaterials. *Science*, 226, 630-636.

Hill, R.G. (1996) An alternative view of the degradation of bioglass. *Journal of Materials Science Letters*, 15(13), 1122-1125.

Hill, R.G., Brauer, D.S. (2011) Predicting the bioactivity of glasses using the network connectivity or split network models. *Journal of Non-Crystalline Solids*, 357(24), 3884-3887.

Holzwarth, J.M., Ma, P.X. (2011) Biomimetic nanofibrous scaffolds for bone tissue engineering. *Biomaterials*, 32(36), 9622-9629.

Huang, Z.M., Zhang, Y.Z., Kotaki, M., Ramakrishna, S. (2003) A review on polymer nanofibers by electrospinning and their applications in nanocomposites. *Composites Science and Technology*, 63(15), 2223-2253.

Huang, Z.N., Nelson, E.R., Smith, R.L., Goodman, S.B. (2007) The sequential expression profiles of growth factors from osteroprogenitors to osteoblasts In vitro. *Tissue Engineering*, 13(9), 2311-2320.

Huppa, L., Yli-Urpo, A. (2012) Dental applications of glasses. In: J. Jones, A. Clare (eds). *Bio-Glasses: An Introduction*. Chichester, John Wiley and Sons Ltd., 159-176.

Ikada, Y. (2006) Challenges in tissue engineering. In: *Tissue Engineering: Fundamentals and Applications*. Oxford, Elsevier Ltd., 423-462.

International Standards Office (2008) ISO 6872 Dentistry – Ceramic Materials. Geneva, ISO.

Isaac, J., Nohra, J., Lao, J., Jallot, E., Nedelec, J.M., Berdal, A., Sautier, J.M. (2011) Effects of strontium-doped bioactive glass on the differentiation of cultured osteogenic cells. *European Cells and Materials*, 21, 130-143.

Jang, J.H., Castano, O., Kim, H.W. (2009) Electrospun materials as potential platforms for bone tissue engineering. *Advanced drug delivery reviews*, 61(12), 1065-1083.

Jha, B.S., Ayres, C.E., Bowman, J.R., Telemeco, T.A., Sell, S.A., Bowlin, G.L., Simpson, D.G. (2011) Electrospun collagen: A tissue engineering scaffold with unique functional properties in a wide variety of applications. *Journal of Nanomaterials* [online], Article ID 348268, DOI:10.1155/2011/348268. Available at: <http://www.hindawi.com/journals/jnm/2011/348268/> [Accessed 27 July 2013].

Jones, J.R. (2011) Hierarchical porous scaffolds for bone regeneration. In: L.L. Hench, J.R. Jones, M.B. Fenn (eds) *New materials and technologies for healthcare*. London, Imperial College Press, 107-130.

Jones, J.R. (2013) Review of bioactive glass: From Hench to hybrids. *Acta Biomaterialia*. 9(1), 4457-4486.

Jones, J.R., Hench, L.L. (2004) Factors affecting the structure and properties of bioactive foam scaffolds for tissue engineering. *Journal of Biomedical Materials Research Part B-Applied Biomaterials*, 68B(1), 36-44.

Kakar, S., Einhorn, T.A. (2005) Tissue engineering of bone. In: J.O. Hollinger, B.A. Doll, C. Sfeir (eds). *Bone tissue engineering*. Boca Raton, CRC Press, 284-309.

Karpov, M., Laczka, M., Leboy, P.S., Osyczka, A.M. (2008) Sol-gel bioactive glasses support both osteoblast and osteoclast formation from human bone marrow cells. *Journal of Biomedical Materials Research Part A*, 84A(3), 718-726.

Katsanevakis, E., Wen, X.J., Zhang, N. (2012) Creating Electrospun Nanofiber-Based Biomimetic Scaffolds for Bone Regeneration. In: R. Jayakumar, S. Nair (eds). *Biomedical Applications of Polymeric Nanofibers*. Berlin, Springer Berlin Heidelberg, 63-100.

Khang, G. (2012) Biomaterials and manufacturing methods for scaffold in regenerative medicine. In: G. Khang (ed). *Handbook of intelligent scaffolds for tissue engineering and regenerative medicine*. Singapore, CRC Press, 3-50.

Kim, H.W., Lee, H.H., Chun, G.S. (2008) Bioactivity and osteoblast responses of novel biomedical nanocomposites of bioactive glass nanofiber filled poly(lactic acid). *Journal of Biomedical Materials Research Part A*, 85A(3), 651-663.

Kim, I.A., Rhee, S.H. (2010) Effects of poly(lactic-co-glycolic acid) (PLGA) degradability on the apatite-forming capacity of electrospun PLGA/SiO2-CaO nonwoven composite fabrics. *Journal of Biomedical Materials Research Part B-Applied Biomaterials*, 93B(1), 218-226.

Kim, N.K., Choi, B.H., Kim, K.H., Park, H.S., Park, S.R., Min, B.H. (2010) Changes in the expression pattern of stem cell markers in rat bone marrow mononuclear cells during primary culture. *Tissue Engineering and Regenerative Medicine*, 7(3), 344-349.

Kwon, I.K., Kidoaki, S., Matsuda, T. (2005) Electrospun nano- to microfiber fabrics made of biodegradable copolyesters: structural characteristics, mechanical properties and cell adhesion potential. *Biomaterials*, 26(18), 3929-3939.

Labet, M., Thielemans, W. (2009) Synthesis of polycaprolactone: a review. *Chemical Society Reviews*, 38(12), 3484-3504.

Labow, R.S., Meek, E., Santerre, P. (1999) The biodegradation of poly(urethane)s by the esterolytic activity of serine proteases and oxidative enzyme systems. *Journal of Biomaterials Science-Polymer Edition*, 10(7), 699-713.

Lam, C.X.F., Savalani, M.M., Teoh, S.H., Hutmacher, D.W. (2008) Dynamics of in vitro polymer degradation of poly(caprolactone)-based scaffolds: accelerated versus simulated physiological conditions. *Biomedical Materials*, 3(3), 1-15.

Langer, R., Vacanti, J.P. (1993) Tissue engineering. *Science*, 260(5110), 920-926.

Lao, J., Nedelec, J.M., Jallot, E. (2009) New strontium-based bioactive glasses: physicochemical reactivity and delivering capability of biologically active dissolution products. *Journal of Materials Chemistry*, 19(19), 2940-2949.

Le Blanc, K., Tammik, C., Rosendahl, K., Zetterberg, E., Ringden, O. (2003) HLA expression and immunologic properties of differentiated and undifferentiated mesenchymal stem cells. *Experimental Hematology*, 31(10), 890-896.

Lee, K.H., Kim, H.Y., Khil, M.S., Ra, Y.M., Lee, D.R. (2003) Characterization of nano-structured poly(epsilon-caprolactone) nonwoven mats via electrospinning. *Polymer*, 44(4), 1287-1294.

Li, A., Wang, D., Xiang, J., Newport, R.J., Reinholdt, M.X., Mutin, P.H., Vantelon, D., Bonhomme, C., Smith, M.E., Laurencin, D., Qiu, D. (2011) Insights into new calcium phosphosilicate xerogels using an advanced characterization methodology. *Journal of Non-Crystalline Solids*, 357(19-20), 3548-3555.

Li, K.N., Wang, J.N., Liu, X.Q., Xiong, X.P., Liu, H.Q. (2012) Biomimetic growth of hydroxyapatite on phosphorylated electrospun cellulose nanofibers. *Carbohydrate Polymers*, 90(4), 1573-1581.

Li, S.M., Garreau, H., Vert, M. (1990) Structure property relationships in the case of the degradation of massive aliphatic poly-(alpha-hydroxy acids) in aqueous-media .1. Poly(dl-lactic acid). *Journal of Materials Science-Materials in Medicine*, 1(3), 123-130.

Li, W.J., Cooper, J.A., Mauck, R.L., Tuan, R.S. (2006) Fabrication and characterization of six electrospun poly(alpha-hydroxy ester)-based fibrous

scaffolds for tissue engineering applications. *Acta Biomaterialia*, 2(4), 377-385.

Li, Y., Li, J., Zhu, S., Luo, E., Feng, G., Chen, Q., Hu, J. (2012) Effects of strontium on proliferation and differentiation of rat bone marrow mesenchymal stem cells. *Biochemical and Biophysical Research Communications*, 418(4), 725-730.

Liao, S., Murugan, R., Chan, C.K., Ramakrishna, S. (2008) Processing nanoengineered scaffolds through electrospinning and mineralization, suitable for biomimetic bone tissue engineering. *Journal of the Mechanical Behavior of Biomedical Materials*, 1(3), 252-260.

Lin, J.Y., Shang, Y.W., Ding, B., Yang, J.M., Yu, J.Y., Al-Deyab, S.S. (2012) Nanoporous polystyrene fibers for oil spill cleanup. *Marine Pollution Bulletin*, 64(2), 347-352.

Lin, P., Chan, W.C.W., Badylak, S.F., Bhatia, S.N. (2004) Assessing porcine liver-derived biomatrix for hepatic tissue engineering. *Tissue Engineering*, 10(7-8), 1046-1053.

Lu, H., Zhang, T., Wang, X.P., Fang, Q.F. (2009) Electrospun submicron bioactive glass fibers for bone tissue scaffold. *Journal of Materials Science-Materials in Medicine*, 20(3), 793-798.

Lu, H.H., El-Amin, S.F., Scott, K.D., Laurencin, C.T. (2003) Three-dimensional, bioactive, biodegradable, polymer-bioactive glass composite scaffolds with improved mechanical properties support collagen synthesis and mineralization of human osteoblast-like cells in vitro. *Journal of Biomedical Materials Research Part A*, 64A(3), 465-474.

Lu, X.Q., Zhai, W.Y., Zhou, Y.L., Zhou, Y., Zhang, H.F., Chang, J. (2010) Crosslinking effect of Nordihydroguaiaretic acid (NDGA) on decellularized heart valve scaffold for tissue engineering. *Journal of Materials Science-Materials in Medicine*, 21(2), 473-480.

Maniatopoulos, C., Sodek, J., Melcher, A.H. (1988) Bone formation in vitro by stromal cells obtained from bone marrow of young adult rats. *Cell and Tissue Research*, 254(2), 317-330.

Marie P.J., Ammann, P., Boivin, G., Rey, C. (2001) Mechanisms of action and therapeutic potential of strontium in bone. *Calcified Tissue International*, 69(3), 121-129.

Marie, P.J. (2005) Strontium as therapy for osteoporosis. *Current Opinion in Pharmacology*, 5(6), 633-636.

Marie, P.J. (2008) Transcription factors controlling osteoblastogenesis. *Archives of Biochemistry and Biophysics*, 473(2), 98-105.

Martins, A., Reis, R.L., Neves, N.M. (2008) Electrospinning: processing technique for tissue engineering scaffolding. *International Materials Reviews*, 53(5), 257-274.

Mashiba, T., Turner, C.H., Hirano, T., Forwood, M.R., Johnston, C.C., Burr, D.B. (2001) Effects of suppressed bone turnover by bisphosphonates on microdamage accumulation and biomechanical properties in clinically relevant skeletal sites in beagles. *Bone*, 28(5), 524-531.

Mathew, R., Stevensson, B., Tilocca, A. Edén, M. (2013) Toward a Rational Design of Bioactive Glasses with Optimal Structural Features: Composition–Structure Correlations Unveiled by Solid-State NMR and MD Simulations. *The Journal of Physical Chemistry B*, 118(3), 833-844.

Matthews, J.A., Wnek, G.E., Simpson, D.G., Bowlin, G.L. (2002) Electrospinning of collagen nanofibers. *Biomacromolecules*, 3(2), 232-238.

McRae, R., Esser, M. (2008) Pathology and healing of fractures. In: *Practical fracture treatment*. London, Elsevier Health Sciences, 3-24

Mercier, C., Follet-Houttemanne, C., Pardini, A., Revel, B. (2011) Influence of P2O5 content on the structure of SiO2-Na2O-CaO-P2O5 bioglasses by Si-29 and P-31 MAS-NMR. *Journal of Non-Crystalline Solids*, 357(24), 3901-3909.

Megelski, S., Stephens, J.S., Chase, D.B., Rabolt, J.F. (2002) Micro- and nanostructured surface morphology on electrospun polymer fibers. *Macromolecules*, 35(22), 8456-8466.

Miao, J.J., Miyauchi, M., Simmons, T.J., Dordick, J.S., Linhardt, R.J. (2010) Electrospinning of Nanomaterials and Applications in Electronic Components and Devices. *Journal of Nanoscience and Nanotechnology*, 10(9), 5507-5519.

Middleton, J.C., Tipton, A.J. (2000) Synthetic biodegradable polymers as orthopaedic devices. *Biomaterials*, 21(23), 2335-2346.

Migliaresi, C., Ruffo, G.A., Volpato, F.Z., Zeni, D. (2012) Advanced electrospinning setups and special fibre and mesh morphologies. In: N.M. Neves (ed). *Electrospinning for advanced biomedical applications and therapies*. Portland, Smithers Rapra, 23-68.

Moore, W.R., Graves, S.E., Bain, G.I. (2001) Synthetic bone graft substitutes. *ANZ Journal of Surgery*, 71(6), 354-361.

Moroni, L., De Wijn, J.R., Van Blitterswijk, C.A. (2008) Integrating novel technologies to fabricate smart scaffolds. *Journal of Biomaterials Science-Polymer Edition*, 19(5), 543-572.

Myeroff, C., Archdeacon, M. (2011) Autogenous Bone Graft: Donor Sites and Techniques. *Journal of Bone and Joint Surgery-American Volume*, 93A(23), 2227-2236.

Ngiam, M., Liao, S., Patil, A.J., Cheng, Z.Y., Yang, F.Y., Gubler, M.J., Ramakrishna, S., Chan, C.K. (2009) Fabrication of Mineralized Polymeric Nanofibrous Composites for Bone Graft Materials. *Tissue Engineering Part A*, 15(3), 535-546.

Nielsen, S.P. (2004) The biological role of strontium. *Bone*, 35(3), 583-588.

O'Donnell, M.D., Candarlioglu, P.L., Miller, C.A., Stevens, M.M. (2010) Materials characterisation and cytotoxic assessment of strontium-substituted bioactive glasses for bone regeneration. *Journal of Materials Chemistry*, 20(40), 8934-41.

O'Donnell, M.D., Hill, R.G. (2010) Influence of strontium and the importance of glass chemistry and structure when designing bioactive glasses for bone regeneration. *Acta Biomaterialia*, 6(7), 2382-2385.

Oudadesse, H., Dietrich, E., Gal, Y.L., Pellen, P., Bureau, B., Mostafa, A.A., Cathelineau, G. (2011) Apatite forming ability and cytocompatibility of pure and Zn-doped bioactive glasses. *Biomedical Materials*, 6(3). DOI:10.1088/1748-6041/6/3/035006.

Papenburg, B.J., Vogelaar, L., Bolhuis-Versteeg, L.A.M., Lammertink, R.G.H., Stamatialis, D., Wessling, M. (2007) One-step fabrication of porous micropatterned scaffolds to control cell behaviour. *Biomaterials*, 28(11), 1998-2009.

Park, S.Y., Ki, C.S., Park, Y.H., Jung, H.M., Woo, K.M., Kim, H.J. (2010) Electrospun silk fibroin scaffolds with macropores for bone regeneration: an in vitro and in vivo study. *Tissue Engineering Part A*, 16(4), 1271-1279.

Patlolla, A., Collins, G., Arinzeh, T.L. (2010) Solvent-dependent properties of electrospun fibrous composites for bone tissue regeneration. *Acta Biomaterialia*, 6(1), 90-101.

Pedone, A., Charpentier, T., Malavasi, G., Menziani, M.C. (2010) New insights into the atomic structure of 45S5 bioglass by means of solid-state NMR spectroscopy and accurate first-principles simulations. *Chemistry of Materials*, 22(19), 5644-5652.

Pittenger, M.F., Mackay, A.M., Beck, S.C., Jaiswal, R.K., Douglas, R., Mosca, J.D., Moorman, M.A., Simonetti, D.W., Craig, S., Marshak, D.R. (1999) Multilineage potential of adult human mesenchymal stem cells. *Science*, 284(5411), 143-147.

Pountos, I., Corscadden, D., Emery, P., Giannoudis, P.V. (2007) Mesenchymal stem cell tissue engineering: Techniques for isolation, expansion and application. *Injury-International Journal of the Care of the Injured*, 38, S23-S33.

Prabhakaran, M.P., Venugopal, J., Ramakrishna, S. (2009) Electrospun nanostructured scaffolds for bone tissue engineering. *Acta Biomaterialia*, 5(8), 2884-2893.

Pulapura, S., Kohn, J. (1992) Trends in the development of bioresorbable polymers for medical applications. *Journal of biomaterials applications*, 6(3), 216-250.

Raggatt, L.J., Partridge, N.C. (2010) Cellular and molecular mechanisms of bone remodelling. *The Journal of Biological Chemistry*, 285(33), 25103-25108.

Rasband, W.S., ImageJ, U.S. National Institutes of Health, Bethesda, Maryland, USA, http://rsb.info.nih. Gov/ij/, 1997-2008.

Radin, S., Reilly, G., Bhargave, G., Leboy, P.S., Ducheyne, P. (2005) Osteogenic effects of bioactive glass on bone marrow stromal cells. *Journal of Biomedical Materials Research Part A*, 73A(1), 21-29.

Ratner, B.D. (2013) A history of biomaterials. In: B.D. Ratner, A.S. Hoffman, F.J. Schoen, J.E. Lemons (eds). *Biomaterials science: An introduction to materials in medicine*. London, Elsevier Science and Technology Books, xli-liii.

Ratner, B.D., Hoffman, A.S., Schoen, F.J., Lemons, J.E. (2013) Biomaterials science: an evolving, multidisciplinary endeavour. In: B.D. Ratner, A.S. Hoffman, F.J. Schoen, J.E. Lemons (eds). *Biomaterials science: An introduction to materials in medicine*. London, Elsevier Science and Technology Books, XXV-XXXIX.

Ray, N.H. (1974) Composition – property relationships in inorganic oxide glasses. *Journal of Non-Crystalline Solids*, 15(3), 423-434.

Reilly, G., Radin, S., Chen, A.T., Ducheyne, P. (2007) Differential alkaline phosphatase responses of rat and human bone marrow derived mesenchymal stem cells to 45S5 bloactive glass. *Biomaterials*, 28(28), 4091-4097.

Remlinger, N.T., Czajka, C.A., Juhas, M.E., Vorp, D.A., Stolz, D.B., Badylak, S.F., Gilbert, S., Gilbert, T.W. (2010) Hydrated xenogeneic decellularized tracheal matrix as a scaffold for tracheal reconstruction. *Biomaterials*, 31(13), 3520-3526.

Reneker, D.H., Kataphinan, W., Theron, A., Zussman, E., Yarin, A.L. (2002) Nanofiber garlands of poly(caprolactone) by electrospinning. *Polymer*, 43(25), 6785-6794.

Reneker, D.H., Yarin, A.L. (2008) Electrospinning jets and polymer nanofibers. *Polymer*, 49(10), 2387-2425.

Rezwan, K., Chen, Q.Z., Blaker, J.J. Boccaccini, A.R. (2006) Biodegradable and bioactive porous polymer/inorganic composite scaffolds for bone tissue engineering. *Biomaterials*, 27(18), 3413-3431.

Rho, J.Y., Kuhn-Spearing, L., Zioupos, P. (1998) Mechanical properties and the hierarchical structure of bone. *Medical Engineering & Physics*, 20(2), 92-102.

Safadi, F.F., Barbe, M.F., Abdelmagid, S.M., Rico, C.M., Aswad, R.A., Litvin, J., Popoff, S.N. (2009) Bone structure, development and bone biology. In: J.S. Khurana (ed). *Bone pathology*. New York, Humana Press, 1-50.

Saidak, Z., Marie, P.J. (2012) Strontium signaling: molecular mechanisms and therapeutic implications in osteoporosis. *Pharmacology and Therapeutics*, 136(2), 216-226.

Sakai, S., Yamada, Y., Yamaguchi, T., Kawakami, K. (2006) Prospective use of electrospun ultra-fine silicate fibers for bone tissue engineering. *Biotechnology Journal*, 1(9), 958-962.

Saltzman, W.M., Kyriakides, T.R. (2007) Cell interactions with polymers. In: R. Lanza, R. Langer, J. Vacanti (eds). *Principles of tissue engineering*. Burlington, Elsevier Academic Press, 279-296.

Santos Jr, A.R. (2010) Bioresorbable polymers for tissue engineering. In: D. Eberli (ed). 2010. *Tissue engineering* [e-book]. InTech, DOI: 10.5772/8580. Available at: <http://www.intechopen.com/books/tissue-engineering/bioresorbable-polymers-for-tissue-engineering> [Accessed 15 July 2013]

Santerre, J.P., Labow, R S., Duguay, D.G., Erfle, D., Adams, G.A. (1994) biodegradation evaluation of polyether and polyester-urethanes with oxidative and hydrolytic enzymes. *Journal of Biomedical Materials Research*, 28(10), 1187-1199.

Schaffler, M.B. (2003) Role of bone turnover in microdamage. *Osteoporosis International*, 14, S73-S77.

Schaner, P.J., Martin, N.D., Tulenko, T.N., Shapiro, I.M., Tarola, N.A., Leichter, R.F., Carabasi, R.F., Dimuzio, P.J. (2004) Decellularized vein as a potential scaffold for vascular tissue engineering. *Journal of Vascular Surgery*, 40(1), 146-153.

Schneider, O.D., Loher, S., Brunner, T.J., Uebersax, L., Simonet, M., Grass, R.N., Merkle, H.P., Stark, W.J. (2008) Cotton wool-like nanocomposite biomaterials prepared by electrospinning: In vitro bioactivity and osteogenic differentiation of human mesenchymal stem cells. *Journal of Biomedical Materials Research Part B-Applied Biomaterials*, 84B(2), 350-362.

Schofer, M.D., Fuchs-Winkelmann, S., Grabedunkel, C., Wack, C., Dersch, R., Rudisile, M., Wendorff, J.H., Greiner, A., Paletta, J.R.J., Boudriot, U. (2008) Influence of poly(L-Lactic Acid) nanofibers and BMP-2-containing poly(L-Lactic Acid) nanofibers on growth and osteogenic differentiation of human mesenchymal stem cells. *The Scientific World Journal*, 8, 1269-1279.

Seitz, H., Rieder, W., Irsen, S., Leukers, B., Tille, C. (2005) Three-dimensional printing of porous ceramic scaffolds for bone tissue engineering. *Journal of Biomedical Materials Research Part B-Applied Biomaterials*, 74B(2), 782-788.

Sellgren, K.L., Ma, T. (2012) Perfusion conditioning of hydroxyapatite-chitosan-gelatin scaffolds for bone tissue regeneration from human mesenchymal stem cells. *Journal of Tissue Engineering and Regenerative Medicine*, 6(1), 49-59.

Seol, Y.J., Park, D.Y., Park, J.Y., Kim, S.W., Park, S.J., Cho, D.W. (2013) A new method of fabricating robust freeform 3D ceramic scaffolds for bone tissue regeneration. *Biotechnology and Bioengineering*, 110(5), 1444-1455.

Sepulveda, P., Jones, J.R., Hench, L.L. (2001) Characterization of melt-derived 45S5 and sol-gel–derived 58S bioactive glasses. *Journal of Biomedical Materials Research*, 58(6), 734-740.

Sepulveda, P., Jones, J.R., Hench, L.L. (2002) Bioactive sol-gel foams for tissue repair. *Journal of Biomedical Materials Research*, 59(2), 340-348.

Shih, Y.R.V., Chen, C.N., Tsai, S.W., Wang, Y.J., Lee, O.K. (2006) Growth of mesenchymal stem cells on electrospun type I collagen nanofibers. *Stem Cells*, 24(11), 2391-2397.

Shin, S.Y., Park, H.N., Kim, K.H., Lee, M.H., Choi, Y.S., Park, Y.J., Lee, Y.M., Ku, Y., Rhyu, I.C., Han, S.B., Lee, S.J., Chung, C.P. (2005) Biological evaluation of chitosan nanofiber membrane for guided bone regeneration. *Journal of Periodontology*, 76(10), 1778-1784.

Shin, S.-H., Purevdorj, O., Castano, O., Planell, J.A., Kim, H.-W. (2012) A short review: Recent advances in electrospinning for bone tissue regeneration. *Journal of tissue engineering*, 3(1), DOI: 10.1177/2041731412443530.

Shirakigawa, N., Ijima, H., Takei, T. (2012) Decellularized liver as a practical scaffold with a vascular network template for liver tissue engineering. *Journal of Bioscience and Bioengineering*, 114(5), 545-551.

Sila-Asna, M., Bunyaratvej, A., Maeda, S., Kitaguchi, H., Bunyaratavej, N. (2007) Osteoblast differentiation and bone formation gene expression in strontium-inducing bone marrow mesenchymal stem cell. *The Kobe Journal of Medical Sciences*, 53(1-2), 25-35.

Sill, T.J., von Recum, H.A. (2008) Electro spinning: Applications in drug delivery and tissue engineering. *Biomaterials*, 29(13), 1989-2006.

Sreerekha, P.R., Menon, D., Nair, S.V., Chennazhi, K.P. (2013) Fabrication of Fibrin Based Electrospun Multiscale Composite Scaffold for Tissue Engineering Applications. *Journal of Biomedical Nanotechnology*, 9(5), 790-800.

Srinivasarao, M., Collings, D., Philips, A., Patel, S. (2001) Three-dimensionally ordered array of air bubbles in a polymer film. *Science*, 292(5514), 79-83.

Stamboulis, A.G., Hench, L.L., Boccaccini, A.R. (2002) Mechanical properties of biodegradable polymer sutures coated with bioactive glass. *Journal of Materials Science: Materials in Medicine*, 13(9), 843-848.

Suggs, L.J., Moore, S.A., Mikos, A.G. (2007) Synthetic biodegradable polymers for medical applications. In: J.E. Mark (ed). *Physical properties of polymers handbook*. New York, Springer, 939-949.

Supaphol, P., Suwantong, O., Sangsanoh, P., Srinivasan, S., Jayakumar, R., Nair, S. V. (2012) Electrospinning of biocompatible polymers and their potentials in biomedical applications. In: R. Jayakumar, S. Nair (eds) *Biomedical Applications of Polymeric Nanofibers*. Berlin, Springer Berlin Heidelberg, 213-239.

Tedder, M.E., Liao, J., Weed, B., Stabler, C., Zhang, H., Simionescu, A., Simionescu, D. T. (2009) Stabilized Collagen Scaffolds for Heart Valve Tissue Engineering. *Tissue Engineering Part A*, 15(6), 1257-1268.

Tesavibul, P., Felzmann, R., Gruber, S., Liska, R., Thompson, I., Boccaccini, A.R., Stampfl, J. (2012) Processing of 45S5 Bioglass (R) by lithography-based additive manufacturing. *Materials Letters*, 74, 81-84.

Therin, M., Christel, P., Li, S.M., Garreau, H., Vert, M. (1992) In vivo degradation of massive poly(alpha-hydroxy acids) - validation of in vitro findings. *Biomaterials*, 13(9), 594-600.

Toskas, G., Cherif, C., Hund, R.D., Laourine, E., Fahmi, A., Mahltig, B. (2011) Inorganic/organic (SiO2)/PEO hybrid electrospun nanofibers produced from a modified sol and their surface modification possibilities. *Acs Applied Materials & Interfaces*, 3(9), 3673-3681.

Treiser, M., Abramson, S., Langer, R., Kohn, J. (2013) Degradable and resorbable biomaterials. In: B.D. Ratner, A.S. Hoffman, F.J. Schoen, J.E. Lemons (eds). *Biomaterials science: An introduction to materials in medicine*. London, Elsevier Science and Technology Books, 179-195.

Tripatanasuwan, S., Zhong, Z.X., Reneker, D.H. (2007) Effect of evaporation and solidification of the charged jet in electrospinning of poly(ethylene oxide) aqueous solution. *Polymer*, 48(19), 5742-5746.

Tucker, N., Stanger, J.J., Staiger, M.P., Razzaq, H., Hofman, K. (2012) The history of the science and technology of electrospinning from 1600 to 1995. *Journal of Engineered Fibers and Fabrics*, 7, 63-73.

Vallet-Regi, M. (2001) Ceramics for medical applications. *Journal of the Chemical Society – Dalton Transactions*, 2, 97-108.

Verborgt, O., Gibson, G.J., Schaffler, M.B. (2000) Loss of osteocyte integrity in association with microdamage and bone remodeling after fatigue in vivo. *Journal of Bone and Mineral Research*, 15(1), 60-67.

Vert, M., Li, S.M., Spenlehauer, G., Guerin, P. (1992) Bioresorbability and biocompatibility of aliphatic polyesters. *Journal of Materials Science-Materials in Medicine*, 3(6), 432-446.

Von burkersroda, F., Schedl, L., Gopferich, A. (2002) Why degradable polymers undergo surface erosion or bulk erosion. *Biomaterials*, 23(21), 4221-4231.

Wang, X., Nyman, J.S., Dong, X., Leng, H., Reyes, M. (2010) Fundamental biomechanics in bone tissue engineering. In: K.A. Athanasiou, (ed).

Synthesis lectures on tissue engineering. San Rafael, Morgan & Claypool. DOI 10.2200/S00246ED1V01Y200912TIS004.

Williams, D.F., Zhong, S.P. (1991) Talking point. Are free radicals involved in biodegradation of implanted polymers? *Advanced Materials*, 3, 623-626.

Williams, D.F., Zhong, S.P. (1994) Biodeterioration/biodegradation of polymeric medical devices in situ. *International Biodeterioration & Biodegradation*, 34, 95-130.

Wilson, C.E., Van Blitterswijk, C.A., Verbout, A.J., Dhert, W.J.A., De Bruijn, J.D. (2011) Scaffolds with a standardized macro-architecture fabricated from several calcium phosphate ceramics using an indirect rapid prototyping technique. *Journal of Materials Science-Materials in Medicine*, 22(1), 97-105.

Woesz, A., Best, S.M. (2008) Cellular response to bioceramics. In: L. DiSilvio (ed). *Cellular response to biomaterials*. London, CRC Press, 136-155.

Woodruff, M.A., Hutmacher, D.W. (2010) The return of a forgotten polymer-Poly(caprolactone) in the 21st century. *Progress in Polymer Science*, 35(10), 1217-1256.

Wutticharoenmongkol, P., Sanchavanakit, N., Pavasant, P., Supaphol, P. (2006) Preparation and characterization of novel bone scaffolds based on electrospun poly(caprolactone) fibers filled with nanoparticles. *Macromolecular Bioscience*, 6(1), 70-77.

Xiang, Y., Du, J.C. (2011) Effect of strontium substitution on the structure of 45S5 bioglasses. *Chemistry of Materials*, 23(11), 2703-2717.

Xin, X.J., Hussain, M., Mao, J.J. (2007) Continuing differentiation of human mesenchymal stem cells and induced chondrogenic and osteogenic lineages in electrospun PLGA nanofiber scaffold. *Biomaterials*, 28(2), 316-325.

Xynos, I.D., Hukkanen, M.V.J., Batten, J.J., Buttery, L.D., Hench, L.L., Polak, J.M. (2000a) Bioglass (R) 45S5 stimulates osteoblast turnover and enhances bone formation in vitro: Implications and applications for bone tissue engineering. *Calcified Tissue International*, 67(4), 321-329.

Xynos, I.D., Edgar, A.J., Buttery, L.D.K., Hench, L.L., Polak, J. M. (2000b) Ionic products of bioactive glass dissolution increase proliferation of human osteoblasts and induce insulin-like growth factor II mRNA expression and protein synthesis. *Biochemical and Biophysical Research Communications*, 276(2), 461-465.

Xynos, I.D., Edgar, A.J., Buttery, L.D.K., Hench, L.L., Polak, J.M. (2001) Gene-expression profiling of human osteoblasts following treatment with the ionic products of Bioglass (R) 45S5 dissolution. *Journal of Biomedical Materials Research*, 55(2), 151-157.

Yamaguchi, T., Sakai, S., Watanabe, R., Tarao, T., Kawakami, K. (2010) Heat treatment of electrospun silicate fiber substrates enhances cellular

adhesion and proliferation. *Journal of Bioscience and Bioengineering*, 109(3), 304-306.

Yang, F., Both, S.K., Yang, X.C., Walboomers, X.F., Jansen, J.A. (2009) Development of an electrospun nano-apatite/PCL composite membrane for GTR/GBR application. *Acta Biomaterialia*, 5(9), 3295-3304.

Yang, S.F., Leong, K.F., Du, Z.H., Chua, C.K. (2001) The design of scaffolds for use in tissue engineering. Part 1. Traditional factors. *Tissue Engineering*, 7(6), 679-689.

Yao, J., Radin, S., Reilly, G., Leboy, P.S., Ducheyne, P. (2005) Solution-mediated effect of bioactive glass in poly (lactic-co-glycolic acid)-bioactive glass composites on osteogenesis of marrow stromal cells. *Journal of Biomedical Materials Research Part A*, 75A(4), 794-801.

Yoshimoto, H., Shin, Y.M., Terai, H., Vacanti, J.P. (2003) A biodegradable nanofiber scaffold by electrospinning and its potential for bone tissue engineering. *Biomaterials*, 24(12), 2077-2082.

Yuan, J.S., Reed, A., Chen, F., Stewart Jr, C.N (2006) Statistical analysis of real-time PCR data. *BMC Bioinformatics*, 7(85), [Online] Available at: <http://www.biomedcentral.com/1471-2105/7/85> [Accessed 25 March 2013].

Yue, W.M., Liu, W., Bi, Y.W., He, X.P., Sun, W.Y., Pang, X.Y., Gu, X.H., Wang, X.P. (2008) Mesenchymal stem cells differentiate into an endothelial phenotype, reduce neointimal formation, and enhance endothelial function in a rat vein grafting model. *Stem Cells and Development*, 17(4), 785-793.

Yunos, D.M., Bretcanu, O., Boccaccini, A.R. (2008) Polymer-bioceramic composites for tissue engineering scaffolds. *Journal of Materials Science*, 43(13), 4433-4442.

Zachariasen, W.H. (1932) The atomic arrangement in glass. *Journal of the American Chemical Society*, 54, 3841-3851.

Zhang, Y.Z., Ouyang, H.W., Lim, C.T., Ramakrishna, S., Huang, Z.M. (2005) Electrospinning of gelatin fibers and gelatin/PCL composite fibrous scaffolds. *Journal of Biomedical Materials Research Part B-Applied Biomaterials*, 72B(1), 156-165.

Zhang, Y., Wei, L., Chang, J., Miron, R J., Shi, B., Yi, S., Wu, C. (2013) Strontium-incorporated mesoporous bioactive glass scaffolds stimulating in vitro proliferation and differentiation of bone marrow stromal cells and in vivo regeneration of osteoporotic bone defects. *Journal of Materials Chemistry B*, 1(41), 5711-5722.

Zhao, Y.L., Zhang, Z.G., Wang, J.L., Yin, P., Wang, Y., Yin, Z.Y., Zhou, J.Y., Xu, G., Liu, Y., Deng, Z.G., Zhen, M.C., Cui, W.G., Liu, Z.C. (2011) Preparation of decellularized and crosslinked artery patch for vascular tissue-engineering application. *Journal of Materials Science-Materials in Medicine*, 22(6), 1407-1417.